Iterative Global-local Methods to Consider the Local Deformation Effects in the Analysis of Thin-walled Beams

By

Ashkan Afnani

A Thesis submitted to
the Graduate Research School
in partial fulfilment of the
requirement for the degree of

DOCTOR OF PHILOSOPHY
In Engineering

Faculty of Engineering & IT
University of Technology Sydney
Sydney, Australia

October 2016

Certificate of authorship and originality

I certify that the work in this thesis has not previously been submitted for a degree nor has it been submitted as part of requirements for a degree except as fully acknowledged within the text.

I also certify that the thesis has been written by me. Any help that I have received in my research work and the preparation of the thesis itself has been acknowledged. In addition, I certify that all information sources and literature used are indicated in the thesis.

Ashkan Afnani Esfandabadi

To Vida

Acknowledgements

I would like to express my sincere gratitude to my supervisor Dr. R. Emre Erkmen for his continuous support and encouragement throughout my PhD studies. His very broad technical knowledge along with his engaging personality created an ideal atmosphere for doing research.

I would like to thank Professor Bijan Samali, who has been an invaluable source of inspiration during my studies. Without his kind presence, it would have been difficult to imagine my starting a PhD in Australia.

I would like to express my happiness for having Vida Niki as my wife, companion and colleague. She has been a major source of motivation from the start of my tertiary education.

Finally, I am grateful for the continual encouragement of my wonderful parents, Rahbar and Nadia, who taught me from my early days not to settle for less than perfection

Abstract

Thin walled members are one of the most widely used structural elements in modern structures. Beam-type finite elements, which are conventionally used to model these members, cannot capture cross-sectional deformation. On the other hand, the use of two-dimensional shell-type elements leads to computationally uneconomical models that cannot be adopted for common engineering practice.

The aim of this study is to develop a numerical method to incorporate the effect of local deformation on the global response of a thin-walled beam. For this purpose, the Iterative Global-local Method is developed in which beam elements are used as the global model while two-dimensional shell elements are placed at critical regions to constitute the local model. The two models are synchronised within each computational iteration via a kinematically appropriate mathematical link.

The Iterative Global-local Method is developed for elastic and elasto-plastic material response, for fibre-reinforced composite laminates, for pipes and curved thin-walled members. The accuracy and efficiency verification of the method is verified through comparisons with detailed finite element modelling and test data from the literature.

Table of Contents

Chapter 1: Introduction and Summary

1.1. Introduction

Thin walled members are one of the most widely used structural elements in modern structures. Since these elements are commonly built in beam-type shapes (i.e. long span in comparison with cross-sectional dimensions), they are conventionally modelled by one-dimensional finite elements (i.e. beam-type elements) which are computationally economical and also accurate in most cases. The formulation of this class of elements is based on the assumption that the cross-section remains rigid after the deformation and consequently, the deformations of the cross-sectional (i.e. local deformations) cannot be captured by these elements. However, cross-sectional deformations such as local buckling of webs and flanges and distortional buckling can have detrimental effects on the global behaviour of the structure, which leads to the need for a more accurate technique. If one is interested in capturing the deformations more accurately, two-dimensional shell-type elements are available that can be used to model each segment of the elements by a number of shell finite elements. However, the use of shell elements may lead to excessively large models for practical cases, which are computationally uneconomical and are mostly avoided by engineers.

In order to make use of the advantages of both approaches discussed above, the *Iterative Global-local Method* can be used. In this method, the structure is modelled by simple beam-type elements while allowing the introduction of shell-type elements at critical locations to capture the local deformation modes such as local buckling. The critical locations may be places where large local loads exist, the locations of cracks, defects or holes and generally wherever a closer view of the stress distribution or deformations is required. The primary benefit of this method is that it allows the identification of the effect of local deformations on the global response of the member without necessitating the use of two-dimensional shell-type elements throughout the domain of the member.

1.2. Objectives

The objective of the current thesis is to develop iterative global-local finite element methods to consider the effect of localised behaviour on the global response of various types of thin-walled members. Such effects can be defined as any changes in the global response of the member that is caused by forces, deformational modes or stresses that cannot be described in the formulation of the global model (e.g. local buckling in thin-walled members).

The finite element formulations can be divided into three main categories: the displacement-based formulations, the force-based formulations and the mixed (hybrid) formulations. In this study, the displacement-based formulation is adopted as the main framework, mainly due to the availability of displacement-based numerical models for thin-walled members in the literature.

In order to develop the multi-scale technique, two levels of idealisation of the structural elements are required. In this study, a one-dimensional beam-type finite element model

is adopted as the global structural model while a two-dimensional shell-type finite element is used as the local structural model. The details of the adopted formulations are presented in the subsequent chapters.

The developed formulations are implemented in FORTRAN programming language, and their accuracy, efficiency and applicability are assessed through several numerical examples. Result from literature and full shell-type models are used as benchmarks for comparison.

1.3. Contents of the thesis

Chapter 2 starts with a literature review of different methods used for the analysis of a thin-walled member, considering different modes of instabilities, followed by an introduction to the Iterative Global-local Method. Then, the suitability of the later for capturing the effect of local buckling in a thin-walled member is discussed. The beam and shell elements that are used for the global and local models are presented in details, and the overlapping domain decomposition operator – that works as a link between the two models – is introduced. Later, the required modifications are applied to the original formulation to make it applicable to beams under general loading conditions and finally, numerical examples are presented to demonstrate the accuracy of the proposed method.

Chapter 3 includes the development of the Iterative Global-local Method for the analysis of thin-walled beams made of fibre-reinforced polymer composite laminates. For that purpose, proper modifications are applied to the global and local models to accommodate elements composed of several layers with various orientations of the fibres. Numerical examples are presented later in the chapter.

The development of the proposed method for closed thin-walled members with circular cross-section is presented in Chapter 4. The appropriate beam element based on the Euler-Bernoulli beam theory is employed for the global model while a curved shell is developed for the local model. Since pipes commonly exhibit elasto-plastic behaviour, the constitutive relations in the local model are modified in order to capture elastic perfectly-plastic response. The accuracy of the developed shell element is verified through comparisons with results from the literature, followed by verification of the iterative global-local procedure in capturing the ovalisation and local buckling effects in the pipes.

Up to this stage, the beam is assumed to be straight. In order to generalise the method to include curved structural elements such as arches and in-plan curved beams, an exact thin-walled curved beam formulation is developed in Chapter 5. The main characteristic of the introduced element is its superiority in modelling beams with medium to high curvature values. This element is utilised in Chapter 6 as the global element for the Iterative Global-local Method for the analysis of curved thin-walled members. The local shell element is also modified to have the capability to form a curved beam element. Subsequently, the decomposition operator is changed to accommodate the curved beam.

In chapter 7, the primary findings of the thesis are summarised and recommendations for further research in the field are made.

Chapter 2: Preliminaries to the Iterative Global-local Method

2.1. Introduction

The Iterative Global-Local Method (IGLM) is introduced in this chapter as a powerful tool for capturing the effect of localised deformation on the global response of thin-walled structural members. In order to demonstrate the need for a mathematically legitimate and computationally efficient method for the analysis of thin-walled members, a literature review is presented first that introduces the current methodologies for the analysis of thin-walled beams. Then, the main concept and the three components of the Iterative Global-Local Method are presented in detail, followed by the solution algorithm of the method. Later, the kinematic assumptions of the original IGLM are modified to make the method applicable for general loading conditions. Finally, Numerical examples are presented to demonstrate the efficiency and accuracy of the proposed method.

2.2. Literature review

2.2.1. Vlasov Theory for thin-walled beams

Vlasov (1961) proposed a theory for the analysis of thin-walled beams (TWB). The main assumptions of Vlasov theory are:

- Distortions in the cross-section are assumed to be negligible during deformations (i.e. rigid cross-section assumption). However, warping due to the bending of flanges is allowed,
- The shear strains at mid-surface of the section are considered to be negligible,
- Normal stresses perpendicular to the centre line of the section are negligible compared to the stresses in the other two directions.

In TWBs, Bernoulli's assumption that plane sections prior to the application of the load remain plane is not applicable, which is due to the warping displacements common in thin-walled beams. ***Bimoment***, which is the loading responsible for warping deformations, can be defined as a set of loadings resulting in two couples acting at two separate planes as shown in Figure 2.1.

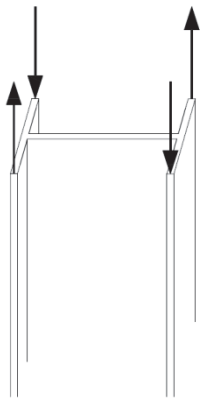

Figure 2.1: Load set resulting in a bimoment

According to the classical beam theory, the four loads in the figure cancel each other without any effect. Nevertheless, the aforementioned load system has a significant effect on the deformations of the TWB, neglecting which can result in a considerable error. Therefore, bimoments lead to the new stress resultant to be considered in the stress state of a member.

According to the Vlasov's first assumption, the displacements of the cross-section parallel to its plane are the same as in rigid body motion; therefore, the horizontal and the vertical components of displacement $u(\mathrm{s},z)$ and $v(s,z)$ of an arbitrary point P on the mid-surface of the cross-section can be expressed in terms of the horizontal and vertical displacement components $u(z)$ and $v(z)$ of a pole $A\left(a_x,a_y\right)$ and the angle of rotation $\phi(z)$ of the cross-section.

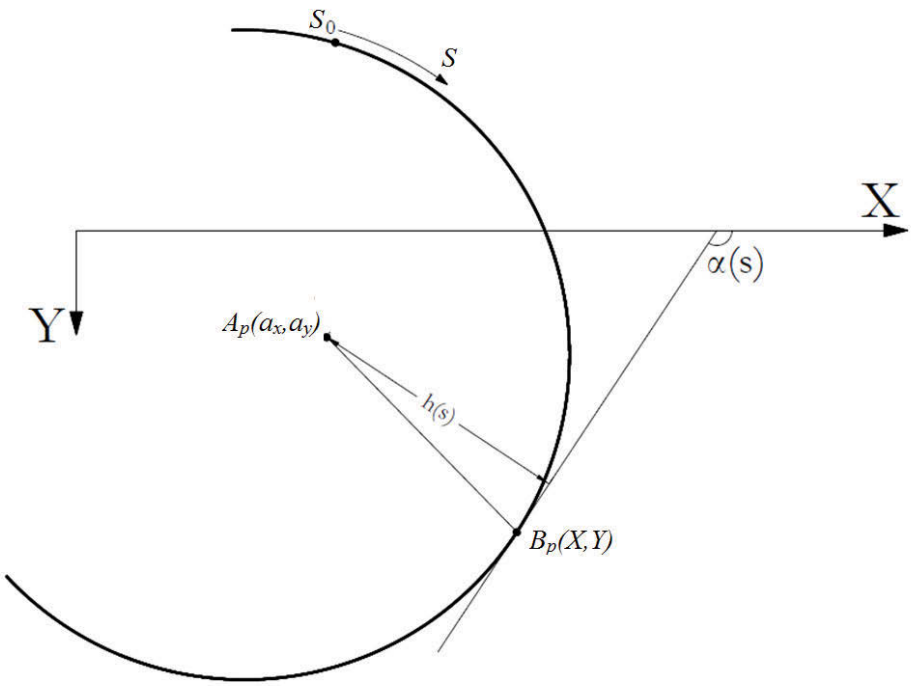

Figure 2.2: Sectorial coordinate in Vlasov thin-walled theory

It should be noted that coordinate s is defined as a sectorial coordinate and is measured from a sectorial origin S_0 located on the mid-surface of the cross-section (Figure 2.2). So that the arbitrary point P can be identified to have coordinates $x(s)$ and y(s) and we can write the definition of the displacement components as follows:

$$u(s,\mathrm{z}) = u(\mathrm{z}) - \left[y(s) - a_y \right] \phi(z) \tag{2.1}$$

$$v(s,\mathrm{z}) = v(\mathrm{z}) + \left[x(s) - a_x \right] \phi(z) \tag{2.2}$$

The second of the aforementioned assumptions requires the shear strain at the mid-surface to vanish

$$\gamma_{z\eta} = \frac{\partial w}{\partial s} + \frac{\partial \eta}{\partial z} = 0 \tag{2.3}$$

where η is the component of displacement in the tangential direction of the mid-surface. So we need an expression for η in terms of the horizontal and vertical displacement components, which can be easily found by projecting u and v on the tangential unit vector $\vec{t} = \left[\cos\alpha(s), \sin\alpha(s)\right]$ at point P. It should be noted that $\alpha(s)$ is the angle between the tangent at point P and the x-axis (Figure 2.2). We have

$$\eta(s,z) = u(\mathrm{s})\cos\alpha(\mathrm{s}) + v(\mathrm{s})\sin\alpha(\mathrm{s}) \tag{2.4}$$

Substituting Eqs. (2.1) and (2.2) into Eq. (2.3)

$$w(s,\mathrm{z}) = \int \left(\left[u'(z) - (y - a_y)\phi'(z) \right] \cos\alpha(\mathrm{s}) + \left[v'(z) + (x - a_x)\phi'(z) \right] \sin\alpha(\mathrm{s}) \right) ds \tag{2.5}$$

Where $(\ )'$ denotes the derivative with respect to z. By performing the required integration and defining the normal distance from the pole A to point P as

$h(s) = (x - a_x)\sin\alpha(\mathrm{s}) - (y - a_y)\cos\alpha(\mathrm{s})$, defining the sectorial coordinate ω such that $d\omega(s) = h(s)ds$, and considering that $dx = ds\cos\alpha(\mathrm{s})$ and $dy = ds\sin\alpha(\mathrm{s})$, Eq. (2.5) will change to

$$w(s,\mathrm{z}) = w(z) - x(s)u'(z) - y(s)v'(z) - \omega(s)\phi'(z) \tag{2.6}$$

The normal stress in the longitudinal direction can be found by differentiating Eq. (2.6) with respect to *z* to obtain

$$\varepsilon_{zz} = w'(z) - x(s)u''(z) - y(s)v''(z) - \omega(s)\phi''(z) \tag{2.7}$$

Based on Vlasov (1961), the normal stress acting in the tangential direction σ_{ss} is neglected, which results in an approximate constitutive relation of $\varepsilon_{zz} = \frac{\sigma_{zz}}{E}$. The normal stresses are assumed to be constant throughout the thickness while a linear gradient for shear stresses is considered in the theory.

2.2.2. Instability of thin-walled members

Buckling can be defined as the stage when an ideal structural member under compression reaches a stage of neutral equilibrium, which is if disturbed from the equilibrium position, it neither continues to displace more nor returns to the initial position. It is at this point that the structure is unstable, as is common in relatively slender structural members. Buckling can be classified as global, local and distortional, where global buckling is the instability of the whole member (i.e. a column), local buckling is the buckling of a sub-element (i.e. the buckling of a flange or web of a column cross section) over a limited domain, and distortional buckling. This review will start from instability of isolated plate elements; will discuss the instability of plate

assemblies, and the effect of local buckling on other modes of instability, while covering the main modes of global buckling in beams and common methodologies to assess the buckling loads in different cases.

2.2.2.1. Instability of Plates

Saint-Venant (1883) was the first one to obtain the general differential equation of the plate buckling problem for elastic plates loaded in-plane (Figure 2.3).

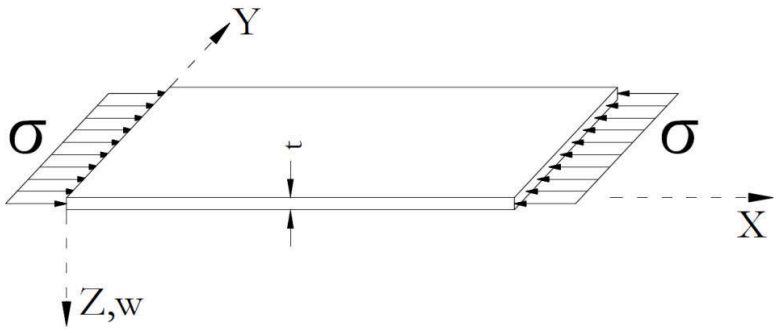

Figure 2.3: St. Venant Plate buckling

If a compressive stress σ is applied in the longitudinal direction, the differential equation will be:

$$\frac{\partial^4 w}{\partial x^4} + 2\frac{\partial^4 w}{\partial x^2 \partial y^2} + \frac{\partial^4 w}{\partial y^4} + \frac{\sigma t}{D}\frac{\partial^2 w}{\partial x^2} = 0 \qquad (2.8)$$

where t is the plate thickness, w is the deflection of the plate and D is the flexural rigidity. Bryan (1891) solved the differential equations for simply supported edges, focusing on ship plates. The problem was solved for several other boundary conditions by Timoshenko (1910). von Kármán (1910) obtained nonlinear equations for post-buckling behaviour of perfect plates and Marguerre (1939) generalized the theory to include initial imperfections in the calculations. Several researchers tried approximate solutions to Marguerre's equations (e.g. Timoshenko & Gere (1961)).

However, in reality the problem is finding the buckling load of an assembly of plate elements rather than a solo plate. To tackle the problem, different methodologies have been proposed in the literature. One of the earliest techniques was proposed by Lundquist et al. (1943), who used the moment distribution method for assemblies subjected to uniform compressive stresses. A different method was utilized by Bleich (1952) and Bulson (1967). They solved the differential equation for each plate segment while satisfying static and kinematic continuity at plate junctions.

One of the popular methods for prediction of the buckling load of structural members is the ***Finite Strip Method (FSM)***, which was developed as an alternative method to finite element for the stability analysis of thin-walled members. It was used by several researchers such as Przemieniecki (1973), Plank & Wittrick (1974) and Cheung (1976). In this method, the structural members such as I-section columns are modelled by a series of connected narrow longitudinal elements (called strips) spanning over the entire length of the member, resulting in considerable reduction in computational cost compared to the finite elements method. Conventionally, polynomial displacement functions were used in the transverse direction and Fourier series displacement functions in the longitudinal direction. It was observed later by Mahendran & Murray (1986) that some problems arose in the presence of shear forces. In order to solve this problem, Fourier functions were replaced by B-spline displacement functions (Fan & Cheung 1983; Lau & Hancock 1986; Van Erp & Menken 1990). Although efficient in most practical cases, the finite strip method cannot be easily used to model cases with complex geometry or boundary conditions. In these cases, the finite element method, which is discussed in the following sections, can be used efficiently.

2.2.2.2. Instabilities of thin-walled members

Lateral-torsional buckling is defined by the American Institute of Steel Construction (AISC) as a "buckling mode of the flexural member involving deflection out of the plane of bending occurring simultaneously with a twist about the shear centre of the cross-section", which is commonly the determining buckling mode in laterally unsupported long beams.

The closed form of the equation of lateral-torsional buckling of thin-walled members is available for limited loading (uniform bending) and boundary conditions, which is the result of the work of several researchers in 1960s, e.g. (Chajes & Winter 1965; Timoshenko & Gere 1961). These closed form formulations are based on the Vlasov thin-walled theory and consequently neglect the effect of web distortions on the lateral-torsional resistance of the member, as one of the assumptions of Vlasov is that the cross-sections remain rigid during the deformations. Hancock et al. (1980) generalized the theory by including the effect of web distortions in the critical load.

The effect of non-uniformity of internal moment on the lateral-torsional buckling load is normally determined through a correcting multiplier called *moment gradient factor* and is the result of studies by numerous researchers starting from the early work of Salvadori (1955), who offered moment gradient factor for linear bending moment gradient, to more comprehensive studies with the aid of finite element method (Grenier et al. 1999; Lim et al. 2003; Serna et al. 2006; Wong & Driver 2010).

2.2.3. Buckling vs. post-buckling

When the compressive load reaches its critical value, the structure will undergo a large sudden displacement. At the same time, the load may decrease, remain constant or increase. For the first two cases, the maximum load that the structure can carry is the critical (i.e. buckling) load. On the other hand, if there is an increase in the load beyond the buckling load, we say that the structure has a *post-buckling* strength. Post-buckling is mostly common in the buckling of plates, where the local buckling in a segment of a plate may not lead to failure, and it can withstand loads larger than its initial buckling load.

Post-buckling is a highly nonlinear phenomenon. Firstly, the stress-strain curve may be nonlinear due to inelastic behaviour of the material. Secondly, geometric nonlinearity exists due to the large displacements undergone in the initial buckling and finally, boundary conditions may change due to a change in contact situation.

2.2.3.1. The Effective width method

von Karman et al. (1932) proposed the *Effective width method*, which is still the most commonly used method for design purposes. The method is based on the fact that the local buckling in plates occurs in regions away from the supports. As a result, it is assumed in the effective width method that a portion of the plate, located close to the supports, is carrying the total load with a uniform stress distribution, while the stresses in the buckled region are ignored.

This method is currently used in most codes of practice as the primary method to deal with the local buckling of thin-walled steel sections. Although conceptually straightforward, the effective width method may be cumbersome to apply to members

with complex cross-sectional geometry because the effective width for each segment of the cross-section needs to be calculated separately and the results need to be used to find sectional and sectorial properties. Apart from that, the stress distribution used in the calculation of the effective width is the average of longitudinal membrane stress and the variation of stresses through the thickness and along the length of the plate is ignored. In other words, the real effective width is more complicated than that which is assumed (Schafer 2008). Lastly, the inter-element (e.g. between the flange and web) equilibrium and compatibility is ignored.

2.2.3.2. Direct strength method

Direct strength method (DSM) is a simple design approach, in which the strength of a member can be determined based on elastic instabilities of the section, namely local, distortional and global buckling, in combination with yield stress of the material. The buckling load according to each instability mode can be calculated by analytical or numerical (e.g. finite strip method) procedures. The main advantage of the DSM over the effective width method is simplicity (compared to the aforementioned difficulty in calculating effective width for sections comprising of several plate elements). Apart from that, unlike the effective width approach, compatibility and equilibrium are satisfied between segments of cross-section. The method has gained more popularity in recent years and has been accepted by several codes of practice as an acceptable alternative to the effective width method.

The origin of the direct strength method for columns starts from works by Hancock and his colleagues on distortional buckling of channel sections (Kwon & Hancock 1991; Lau & Hancock 1987). Hancock et al. (1994) performed tests on thin-walled members and could correlate the distortional buckling strength with slenderness determined based

on distortional buckling stresses and proposed design curves accordingly. Schafer & Pekoz (1998) performed tests on a large variety of cold-formed sections and using the results, taking all buckling modes (local, distortional and global) into account.

Rusch & Lindner (2001) performed experiments on cold-formed I-section to compare the direct strength method to the effective width method and concluded that the use of direct strength method may lead to overestimation of the buckling load. They stated that the shift in the neutral axis of the section due to the local buckling is ignored in the direct strength method. Therefore, the additional bending moment caused by the aforementioned shift is ignored, resulting in overestimation of the buckling load. Comparing test results with the results of the two methods, they concluded that the effective width approach is more accurate than the direct strength method.

2.2.4. Distortional buckling

Distortional buckling can be considered as a combination of two primary modes of instability of thin-walled steel members: the local and the lateral (or flexural-torsional buckling). In local buckling, an element of the cross-section (i.e. web or flange) buckles locally without any lateral displacement, spanning over a relatively short domain of the member. However, in the global buckling, the member buckles by the lateral deformation or/and the twist of the cross-section without any change in the cross-sectional geometry. The former is common in short-length members and the latter in long ones, but in intermediate lengths, distortional buckling occurs, in which the lateral deformations and the distortion of the cross-section occur simultaneously.

Closed form solutions for distortional buckling were derived by several researchers (Bradford 1994; Hancock et al. 1980). Jönsson (1999) proposed a distortional theory for

thin-walled beams by embedding distortional displacement mode into the kinematic assumptions of the classic Vlasov theory. The applicability of analytical models is limited to cases with simple geometry and boundary conditions. On the other hand, numerical methods have gained popularity in the last few decades.

One of the first models was proposed by Bradford & Trahair (1981), who introduced a finite element with 12 degrees of freedom, in which the flanges were modelled by beam elements and the web as a plate that can distort in the plane of its cross-section.

Roberts & Jhita (1983) used energy methods to analyse local, lateral and distortional buckling of I-section beams. It was observed that distortional buckling was critical in slender beams.

Bradford (1994) observed that the distortional buckling of short beams with slender webs occur at significantly lower load compared to lateral buckling. It was also seen that, in a continuously restrained beam, the main buckling mode is distortional.

Ma & Hughes (1996) developed an energy method that included the effect of web distortion on the lateral buckling of mono-symmetric beams and observed that the exclusion of web distortion (rigid-web assumption) overestimates the lateral-torsional buckling load.

Petrolito (1995) and Eisenberger (2003) included higher order terms by assigning a cubic variation for the axial displacement over the cross-section while keeping the lateral displacement constant, and the significant effect of the higher order terms for short beams was confirmed.

Dekker & Kemp (1998) used an equivalent spring system in order to model the relative stiffness of the web and the flanges of doubly symmetric I-sections. The model correlated well with the results from Bradford & Trahair (1981) for elastic buckling.

In order to increase the accuracy of the model by Bradford & Trahair (1981), Bradford & Ronagh (1997) increased the degrees of freedom to 16. Later on, Poon & Ronagh (2004) increased the accuracy of the model by proposing a 5^{th} order polynomial for web displacements instead of the commonly used cubic polynomial. They also observed that the distortional buckling was more significant when the flanges are relatively large or the beam has a short length, which was the case where the difference between the 5^{th} order and the cubic polynomial became more pronounced.

2.2.5. Evaluating the effect of local buckling on the global behavior

As a result of local buckling, the behaviour of the member may change significantly. van der Neut (1969) investigated the interaction of local and global buckling of an idealized column made of elastic material. It was observed that, for long columns, the failure was purely due to the overall (Euler) buckling of the column. On the other hand, for columns shorter than a specific length, local buckling occurs prior to the Euler buckling. For evaluating the post-buckling behaviour of the column, he reduced the bending stiffness by a reduction factor η, which was assumed to remain constant and was taken as 0.4083.

A number of methodologies have been developed to assess the reduction in the stiffness of columns due to local buckling. For example, Bijlaard & Fisher (1953) used the split rigidities method, which is finding rigidities based on the deformations of the section in a mode which is the result of the additional local buckling deformation due to the

interaction of local and overall buckling modes. DeWolf et al. (1974) found the flexural rigidities by the use of the effective width concept while Hancock (1981) used the finite-strip post buckling analysis to calculate rigidities of locally buckled I-sections. Wang et al. (1977) and Wang & Pao (1980) introduced a finite element which included the effect of local buckling on the overall buckling load by decreasing the stiffness of the section according to the effective width method. The problem is nonlinear due to the following reasons:

- The stiffness of the column in the post-buckling range depends on the effective widths of the buckled plates, and
- The applied load and the effective widths of the plates are interdependent.

Therefore an iterative approach was adopted. However, even the iterative effective width method is approximate as it relies on semi-empirical formulas to determine the extent of the buckled plate regions and does not incorporate the actual stresses in the analysis.

In beam-columns (or eccentrically loaded columns), the reduction in section stiffness due to the local buckling results in an increase in the lateral displacement of the member, which causes a further reduction in the load-carrying capacity of the member. Rhodes & Harvey (1971) studied the effect of local buckling on the behaviour of a beam-column with channel cross-section. To this end, they used differential equations of an eccentrically loaded pin-column. The use of the proposed method is limited because the flexural rigidity was assumed to be constant, and it was only applicable to pinned columns. To overcome these problems, Davids & Hancock (1987) developed a theory by combining the finite strip method of nonlinear elastic analysis of locally buckled thin-walled sections with the influence coefficient method of analysis of beam-

columns. The advantage of the theory was that it allowed the inclusion of the effect of initial imperfections, general loading and boundary conditions and residual strains.

Rasmussen (1997) used the variational principles to obtain the differential equations and the boundary conditions of the global buckling of locally buckled thin-walled members. The method was applicable to arbitrary cross-sections and boundary conditions, for the members in compression, bending and combined compression and bending. The method was applied to doubly-symmetric sections in compression and combined bending and compression. Later, Young & Rasmussen (1997) applied the method to singly-symmetric sections in compression.

2.2.6. Generalized beam theory

Generalized beam theory (GBT), which was developed originally by Schardt (1989), is a method for buckling problems of thin-walled prismatic members. In this method, the mechanical behavior of the member is described by ordinary differential equations, where the displacement resultants are similar to individual buckling modes. In other words, the problem is solved in a modal basis, where the degrees of freedom are the predefined possible buckling modes of the member, instead of conventional nodal degrees of freedom. GBT was used to implement beam theories including in-plane deformations of the cross-section and good results were obtained by appropriate selection of shape-functions for the deformations of the cross-section.

The theory proposed by Schardt (1989) was applicable to linear problems only. Schardt (1994) stated that second order effects can arise due to normal or shear stresses and developed 2nd order GBT, which focused on the effect of longitudinal stresses because they have the most important effect in practical problems. So far, the method was

applicable to elastic buckling analysis of thin-walled members with "unbranched" open cross-sections, but Silvestre & Camotim (2003) and Dinis et al. (2006) introduced formulations to include open branched and closed sections and Silvestre (2007) extended the theory to analyze the buckling of circular cylindrical cross-sections. Rendek & Baláž (2004) used GBT for the static analysis of thin-walled beams and provided a comparison with experimental results and Bebiano et al. (2007) made the GBT applicable to thin-walled members under non-uniform bending by including terms to account for longitudinal stress gradient and corresponding shear stresses.

Carrera & Petrolo (2012) used Lagrange polynomials to define the displacement field above the cross-section of the beam for the so-called Lagrange points on the cross-section. The formulation used displacement degrees of freedom, and showed good results when compared to solid finite elements for several examples.

2.2.7. Iterative Global-local Method

Accurate modelling of regions with steep stress gradient without overcomplicating the finite element model has been a challenge in the finite element procedure for several decades, especially in the aircraft industry. A popular example in the literature concerns modelling of a stiffened panel with circular central cut-out (Figure 2.4). The problem with this example is that the high stress-concentration around the hole requires a detailed analysis while a simple model can be reasonably considered adequate for the rest of the structure. Consequently, performing a highly-detailed analysis of the whole structure would be computationally inefficient while a coarse model is not sufficient for accurate modelling of the critical regions around the cut-out. The family of global-local procedures attempt to address this issue by proposing alternative analysis procedures (Noor 1986).

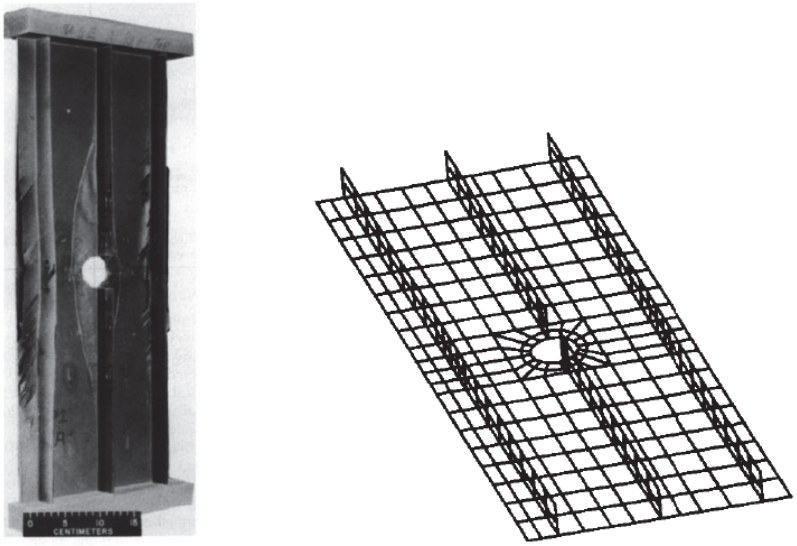

Figure 2.4: Stiffened panel with circular hole, after Knight Jr et al. (1991)

"Hybrid Method" is a type of global-local method in which a classical variational procedure (e.g. conventional Ritz Method) is used for the global analysis of the structure while a discretised solution method such as the finite element form of the Ritz method is adopted for the local regions, e.g. (Mote 1971; Noor & Peters 1983).

"Zooming Method" is the second type of global-local method discussed here. It is based on adopting a coarse mesh for the whole structure and a refined mesh for the area of expected high stress-gradient (Hirai et al. 1985; Sun & Mao 1988). In this method, the global model is initially solved, and the resulting displacements are used as boundary conditions for the local/refined model. This method requires careful treatment of the interface between the local and global models to minimise the error on the boundaries.

Another attempt has been modelling the critical local region with different mathematical models and hence, creating a hierarchy of the mathematical models (Noor 1986). An example of such procedure is shown in Figure 2.5 for the analysis of a stiffened panel with cut-out. The body of the panel far from the cut-out is modelled by shell elements based on classical shell theory while the area adjacent to the cut-out is formulated by

boundary layer theory, and the intermediate area between the two is modelled according to the shear deformation theory. Similarly, the mathematical models for analysing the stiffening plates are different according to the position of the plate with respect to the cut-out: the stiffeners close to the cut-out are modelled by plate theory while the model is changed to thin-walled and classical Euler-Bernoulli beam theories when farther from the location with high stress concentration.

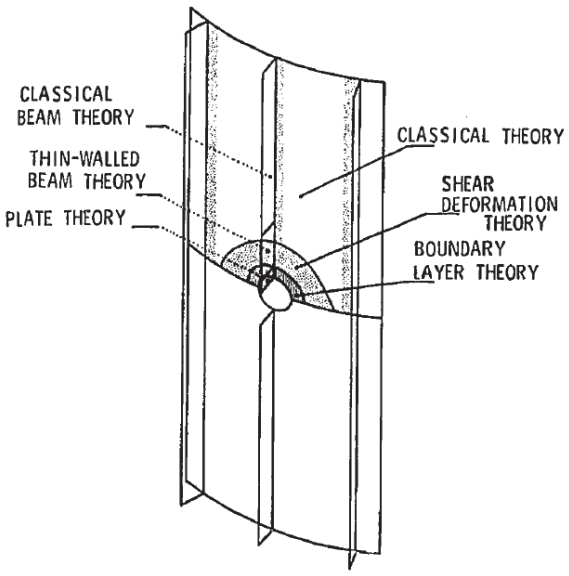

Figure 2.5: Hierarchy of mathematical model for the stiffened panel, after (Noor 1986)

Whitcomb (1991) introduced the ***iterative*** global/local method to consider the effect of stress concentration in a locally refined area on the global model. For that purpose, a coarse mesh was used in the global model with a dense mesh around a cut-out. The effect of the presence of the cut-out on the global model was considered by ensuring that the stresses on the boundaries of the two models are balanced. For that purpose, a modified Newton-Raphson iterative procedure was used to ensure that the unbalanced forces between the local and the global model vanish. The application of the model was later generalised for defects in bonded joints and geometric nonlinearities in subsequent studies (Whitcomb & Woo 1993a, 1993b).

Gendre et al. (2009) developed a ***non-intrusive*** iterative global-local computational method to solve the problem where nonlinearity is limited in a small subdomain of the structure. "Non-intrusive" means that it does not introduce any additional error based on the approximate assumptions of the boundaries and can be entirely addressed based on the standard finite element formulations. Therefore, it can be easily implemented in the commercial finite element codes. They used linear finite element models (shell and solid elements) for the total domain while a nonlinear local model was employed in the area of nonlinearity. The primary source of nonlinearity in this study was inelastic behaviour, so they used different constitutive relations for the local region than the simple linear-elastic behaviour of the global structure. The limitation of this procedure was that the boundaries of the global and local models are assumed to be matching. Liu et al. (2014) introduced a non-intrusive Iterative Global-local Method for non-matching interface between the local and global model (Figure 2.6)

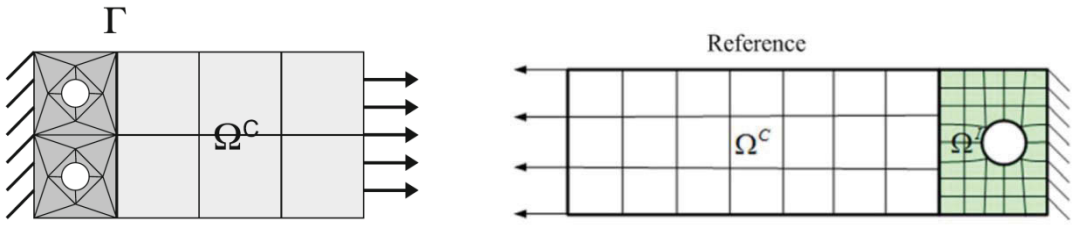

(a) Matching interface(Gendre et al. 2009) (b) Non-Matching interface (Liu et al. 2014)

Figure 2.6: Matching and non-matching interface between the global and local regions

It should be noted that in all of the studies mentioned here, the type of the element is assumed to be the same for the global and local regions (e.g. shell elements). However, it will be shown in the following sections that the method developed in the current study is based on adopting different finite elements for the global and local models.

2.3 Motivation for the Iterative Global-local Method

2.3.1. Introduction

As discussed in the previous sections, different methodologies have been proposed for the analysis of thin-walled beams. Especially, when local buckling of section elements (such as web and flanges) occurs, even the numerical methods discussed so far depend on empirical/semi-empirical methods like the effective width method. In other words, if one is to capture the local buckling of a thin-walled beam rigorously, one has to model the whole domain of the beam by detailed finite elements such as shell elements. The latter method results in overly huge-sized computational models that are not applicable in everyday analysis and design of thin-walled beams.

"Sub-structuring" technique is a method that has been tried to overcome such difficulty, e.g. (Yamao & Sakimoto 1986). In this method, elements with two degrees of accuracy are used. Less detailed elements (i.e. beam element) are used in regions that are not likely to undergo local buckling behaviour while more accurate elements (i.e. shell elements) are used in places susceptible to local buckling or other cross-sectional related deformations. In order to connect the shell elements to the beam elements, the nodes of the shell elements at the place of the intersection are tied together by means of a constraint. This method allows the incorporation of cross-sectional related deformations without necessitating large computational models; however, applying changes to the critical region (i.e. the region which is modelled by the more-detailed shell-elements) requires a complete change in the model. In other words, in the case in which the predefined susceptible region is found to be insufficient in capturing the

deformations of the beam, it needs to be extended to a larger domain, which means changing the numerical model.

Alternatively, the Iterative Global-Local Method (IGLM) can be used, which allows the application of more detailed finite elements (e.g. shell-type elements) in critical regions on top of an existing less detailed element (e.g. beam-type elements), a practice that allows the rigorous finite element modelling of local buckling while keeping the model computationally economical. Unlike the sub-structuring technique, applying changes to the critical regions in the Iterative Global-local Method is quite simple because the local model does not interrupt the global model; therefore, a change in the critical region does not change the global model of the structure.

2.3.2. Background

New challenges in computational mechanics such as large deformations in manufacturing processes and crack propagations has made the conventional numerical techniques unsuitable and is some cases useless. To overcome this difficulty, current research focus in computational mechanics has been placed on adaptive numerical techniques,

The iterative global-local (or multi-scale) method, which is the focus of this thesis, is based on the hierarchy at the level of solution (Feyel 2003; Fish et al. 1994; Geers et al. 2010; Hughes & Sangalli 2007; Liu et al. 2000). To be more precise, the Iterative Global-local Method allows the application of more detailed and more precise elements at the critical places only without necessitating any change in the neighbouring regions. The interaction of local buckling of a thin-walled member and the global modes is a problem with deformation fields of different scales. In order to incorporate the effect of

local buckling on the global behaviour of a thin-walled beam, Erkmen (2013) developed a numerical method which can be considered as an Iterative Global-local Method. In this method, the local and global aspects of the thin-walled beam are modelled by using two different kinematical assumptions. That is, simple beam-type finite elements were used for the global response of the structure while more sophisticated and more detailed shell-type finite elements were utilized to demonstrate the local behaviour of the thin-walled member. In other words, the beam-type elements were used to cover the total domain of the problem while the shell elements were placed in a subset of the whole domain where it was thought to be critical (i.e. where large local loading exists or where the beam was thought to be susceptible to local buckling or large local deformations). A layout of the model showing the decomposition of the domain is shown in Figure 2.7.

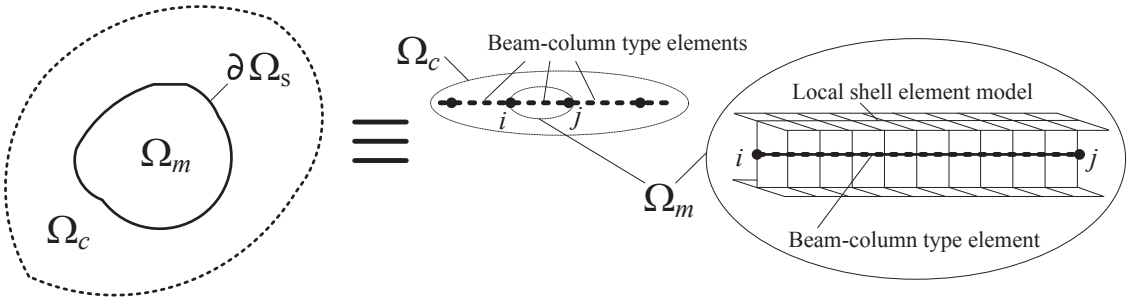

Figure 2.7: Domain decomposition of the thin-walled member using the Iterative Global-local Method (After Erkmen 2013)

In order to synchronize the two models, a specific operator was developed that projected the displacement field of the shell elements on the corresponding degrees of freedom of the coarse-scale model (the beam element). Due to the specific kinematic assumptions in the development of the aforementioned operator, the method was applicable to cases with uniform bending moment conditions only.

2.4. The beam element

The beam element used as the global/coarse-scale model of the Iterative Global-local Method is developed based on the classical thin-walled beam theory (discussed in Section 2.2.1). The strain vector of such element can be written in terms of the displacements parallel to $\bar{x}$, $\bar{y}$ and $\bar{z}$ directions, i.e. $\bar{u}(\bar{z})$, $\bar{v}(\bar{z})$ and $\bar{w}(\bar{z})$, respectively, the angle of twist of the cross-section ϕ, and their derivatives (Figure 2.8).

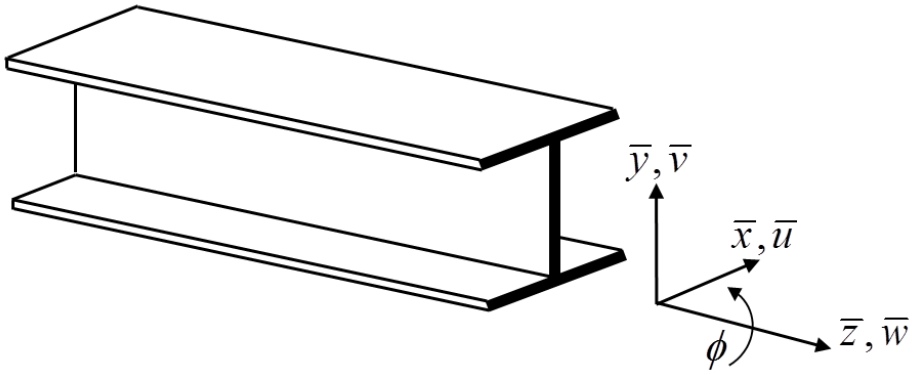

Figure 2.8: Directions of the beam element

The strain vector can be decomposed into linear and nonlinear components, i.e. $\bar{\boldsymbol{\varepsilon}} = \bar{\boldsymbol{\varepsilon}}_L + \bar{\boldsymbol{\varepsilon}}_N$. Each part can be obtained by multiplying the matrix of cross-sectional coordinates *S* by linear and nonlinear vectors including displacement components.

$$\bar{\boldsymbol{\varepsilon}}_L = \begin{langle} \bar{\varepsilon}_L & 0 & \bar{\gamma}_L & 0 \end{rangle}^T = \bar{\mathbf{S}}\bar{\boldsymbol{\chi}}_L \tag{2.9}$$

$$\bar{\boldsymbol{\varepsilon}}_N = \begin{langle} \bar{\varepsilon}_N & 0 & \bar{\gamma}_N & 0 \end{rangle}^T = \bar{\mathbf{S}}\bar{\boldsymbol{\chi}}_N \tag{2.10}$$

where

$$\bar{\mathbf{S}} = \begin{bmatrix} 1 & -\bar{x} & -\bar{y} & -\bar{\omega} & \bar{x}^2+\bar{y}^2 & 0 \\ 0 & 0 & 0 & 0 & 0 & 0 \\ 0 & 0 & 0 & 0 & 0 & -2\bar{r} \\ 0 & 0 & 0 & 0 & 0 & 0 \end{bmatrix} \tag{2.11}$$

The vector of linear derivatives of the displacement is

$$\bar{\boldsymbol{\chi}}_L{}^T = \left\langle \bar{w}' \quad \bar{u}'' \quad \bar{v}'' \quad \bar{\phi}'' \quad 0 \quad \bar{\phi}' \right\rangle^T \tag{2.12}$$

while the nonlinear displacement vector can be considered as follows based on Trahair (1993)

$$\bar{\boldsymbol{\chi}}_N{}^T = \left\langle \frac{1}{2}\left(\bar{u}'^2+\bar{v}'^2\right) - a_x\bar{v}'\bar{\phi}' + a_y\bar{u}'\bar{\phi}' + \frac{1}{2}\left(a_x{}^2+a_y{}^2\right)\bar{\phi}'^2 \quad -\bar{v}'\bar{\phi}' + a_x\bar{\phi}'^2 \quad \bar{u}'\bar{\phi}' + a_y\bar{\phi}'^2 \quad 0 \quad \frac{1}{2}\bar{\phi}'^2 \quad 0 \right\rangle \tag{2.13}$$

In Eq. (2.11), $\bar{x}$ and $\bar{y}$ denote the coordinates of a point on the cross-section, $\bar{r}$ is the normal distance from the mid-surface, a_x and a_y refer to the coordinates of the pole, and $\bar{\omega}$ is the sectorial coordinate according to Vlasov thin-walled theory.

The beam finite element is formulated by assuming a linear interpolation for $\bar{w}$ and cubic interpolations for $\bar{u}$, $\bar{v}$ and $\bar{\phi}$. As a result, the interpolation matrix $\bar{\mathbf{X}}_a$ can be formed to relate the displacement vector at an arbitrary point inside the element ($\bar{\mathbf{u}}_a$) to the nodal displacement vector $\bar{\mathbf{d}}$ by the following equation:

$$\bar{\mathbf{u}}_a = \bar{\mathbf{X}}_a\bar{\mathbf{d}} \tag{2.14}$$

where

$$\bar{\mathbf{u}}_a = \left\langle \bar{w} \quad \bar{u} \quad \bar{v} \quad \bar{\phi} \right\rangle^{\mathrm{T}} \tag{2.15}$$

$$\bar{\mathbf{X}}_a = \begin{bmatrix} \mathbf{L}^{\mathrm{T}} & \mathbf{0} & \mathbf{0} & \mathbf{0} \\ \mathbf{0} & \mathbf{H}^{\mathrm{T}} & \mathbf{0} & \mathbf{0} \\ \mathbf{0} & \mathbf{0} & \mathbf{H}^{\mathrm{T}} & \mathbf{0} \\ \mathbf{0} & \mathbf{0} & \mathbf{0} & \mathbf{H}^{\mathrm{T}} \end{bmatrix} \tag{2.16}$$

in which

$$\mathbf{L} = \left\langle 1 - \frac{\bar{z}}{L} \quad \frac{\bar{z}}{L} \right\rangle^{\mathrm{T}} \tag{2.17}$$

and

$$\mathbf{H} = \left\langle 1 - \frac{3\bar{z}^2}{L^2} + \frac{2\bar{z}^3}{L^3} \quad \bar{z} - \frac{2\bar{z}^2}{L} + \frac{\bar{z}^3}{L^2} \quad \frac{3\bar{z}^2}{L^2} - \frac{2\bar{z}^3}{L^3} \quad -\frac{\bar{z}^2}{L} + \frac{\bar{z}^3}{L^2} \right\rangle^{\mathrm{T}} \tag{2.18}$$

The nodal displacement vector $\bar{\mathbf{d}}$ is shown in Eq. (2.19)

$$\bar{\mathbf{d}} = \left\langle \bar{w}_1 \quad \bar{w}_2 \quad \bar{u}_1 \quad \bar{\theta}_{x1} \quad \bar{u}_2 \quad \bar{\theta}_{x2} \quad \bar{v}_1 \quad \bar{\theta}_{y1} \quad \bar{v}_2 \quad \bar{\theta}_{y2} \quad \bar{\phi}_1 \quad \bar{\varphi}_1 \quad \bar{\phi}_2 \quad \bar{\varphi}_2 \right\rangle^{\mathrm{T}} \tag{2.19}$$

in which subscripts 1 and 2 refer to the starting and the ending nodes of the beam element respectively, $\bar{\theta}_x$ and $\bar{\theta}_y$ are the rotations in $\bar{z}$–$\bar{x}$ and $\bar{z}$–$\bar{y}$ planes respectively, and $\bar{\varphi}$ is associated with the warping deformations of the cross-section.

The displacement of a point on the cross-section $\bar{\mathbf{u}}$ can be expressed in terms of the vector of nodal displacements $\bar{\mathbf{d}}$ by using the decomposition matrix $\mathbf{N}$ (Trahair 1993). The decomposition matrix $\mathbf{N}$ can be written as the product of the multiplication of an interpolation matrix $\mathbf{Z}$ and a second matrix $\mathbf{Y}$ (i.e. $\mathbf{N} = \mathbf{YZ}$). The first matrix $\mathbf{Z}$ contains the interpolation functions that are used to calculate the displacements of any

point on the axis of the beam from the nodal displacements while the second matrix **Y** determines the displacements of any point of the cross-section from the displacement of the axis according to the kinematic assumptions of the classical thin-walled beam theory Vlasov (1961). These matrices are shown explicitly in Eqs. (2.20), (2.21) and (2.22).

$$\bar{\mathbf{u}} = \left\langle \bar{w}_\alpha \quad \bar{u}_\alpha \quad \bar{u}'_\alpha \quad \bar{v}_\alpha \quad \bar{v}'_\alpha \quad \bar{\phi}_\alpha \right\rangle^{\mathrm{T}} \tag{2.20}$$

$$\mathbf{Z} = \begin{bmatrix} \mathbf{L}^{\mathrm{T}} & \mathbf{0} & \mathbf{0} & \mathbf{0} \\ \mathbf{0} & \mathbf{H}^{\mathrm{T}} & \mathbf{0} & \mathbf{0} \\ \mathbf{0} & \mathbf{0} & \mathbf{H}^{\mathrm{T}} & \mathbf{0} \\ \mathbf{0} & \mathbf{0} & \mathbf{0} & \mathbf{H}^{\mathrm{T}} \\ \mathbf{0} & \dfrac{\mathrm{d}\mathbf{H}^{\mathrm{T}}}{\mathrm{d}\bar{z}} & \mathbf{0} & \mathbf{0} \\ \mathbf{0} & \mathbf{0} & \dfrac{\mathrm{d}\mathbf{H}^{\mathrm{T}}}{\mathrm{d}\bar{z}} & \mathbf{0} \\ \mathbf{0} & \mathbf{0} & \mathbf{0} & \dfrac{\mathrm{d}\mathbf{H}^{\mathrm{T}}}{\mathrm{d}\bar{z}} \end{bmatrix} \tag{2.21}$$

$$\mathbf{Y} = \begin{bmatrix} 1 & 0 & 0 & 0 & -\bar{x} & -\bar{y} & -\bar{\omega} \\ 0 & 1 & 0 & -\left(\bar{y} - a_y\right) & 0 & 0 & 0 \\ 0 & 0 & 0 & 0 & 1 & 0 & -\left(\bar{y} - a_y\right) \\ 0 & 0 & 1 & \left(\bar{x} - a_x\right) & 0 & 0 & 0 \\ 0 & 0 & 0 & 0 & 0 & -1 & -\left(\bar{x} - a_x\right) \\ 0 & 0 & 0 & -1 & 0 & 0 & 0 \end{bmatrix} \tag{2.22}$$

Assuming elastic material behaviour, we can write the stress vector as

$$\bar{\boldsymbol{\sigma}} = \left\langle \bar{\sigma} \quad 0 \quad \bar{\tau} \quad 0 \right\rangle^{\mathrm{T}} \tag{2.23}$$

And the material properties matrix would be

$$\bar{\mathbf{E}} = \left[\begin{array}{ccc:c} E & 0 & 0 & 0 \\ 0 & 0 & 0 & 0 \\ 0 & 0 & \dfrac{E}{2(1+\nu)} & 0 \\ \hdashline 0 & 0 & 0 & 0 \end{array}\right] \tag{2.24}$$

We should note that the constitutive matrix $\bar{\mathbf{E}}$ used here is different from the one used for the shell element is Section 2.5, in order to satisfy the second and third postulate of the beam theory. Because of the rigid cross-sectional assumption of the thin-walled beam theory, Poisson ratio effects would cause the element to behave overly stiff. By adopting the constitutive matrix of Eq. (2.24), additional strain would be produced within the cross-sectional plane of the beam, which eliminates the stresses in the cross-sectional plane. Consequently, the third postulate of the beam theory – that is, normal stresses within the cross-sectional plane are zero – would be satisfied.

Based on the above derivations, the variational formulation can be written down to obtain the equilibrium equation:

$$\delta\bar{\Pi} = \int_L \int_A \delta\bar{\boldsymbol{\varepsilon}}^{\mathrm{T}} \bar{\boldsymbol{\sigma}} \mathrm{d}A\, \mathrm{d}\bar{z} - \delta\bar{\mathbf{d}}^{\mathrm{T}} \bar{\mathbf{f}} = 0 \tag{2.25}$$

where A is the cross-sectional area, L is the length of the element and $\bar{\mathbf{f}}$ is the external load vector. The variation of the strain vector $\delta\bar{\boldsymbol{\varepsilon}}$ of the beam element can be written as

$$\delta\bar{\boldsymbol{\varepsilon}} = \bar{\mathbf{S}}\bar{\mathbf{B}}\delta\bar{\mathbf{d}} \tag{2.26}$$

where $\bar{\mathbf{S}}$ is given in Eq. (2.11) and $\bar{\mathbf{B}}$ is found according to

$$\bar{\mathbf{B}}=\begin{bmatrix} 1 & \bar{u}'+a_y\bar{\phi}' & 0 & \bar{v}'-a_x\bar{\phi}' & 0 & 0 & a_y\bar{u}'-a_x\bar{v}'+\left(a_x{}^2+a_y{}^2\right)\bar{\phi}' & 0 \\ 0 & 0 & 1 & 0 & \bar{\phi} & \bar{v}'' & 2a_x\bar{\phi}' & 0 \\ 0 & 0 & -\bar{\phi} & 0 & 1 & -\bar{u}'' & 2a_y\bar{\phi}' & 0 \\ 0 & 0 & 0 & 0 & 0 & 0 & 0 & 1 \\ 0 & 0 & 0 & 0 & 0 & 0 & \bar{\phi}' & 0 \\ 0 & 0 & 0 & 0 & 0 & 0 & 1 & 0 \end{bmatrix}\nabla\bar{\mathbf{X}}_a \tag{2.27}$$

$\bar{\mathbf{X}}_a$ in Eq. (2.27) is specified in Eq. (2.16), and ∇ is a differential operator as in Eq. (2.28)

$$\nabla=\begin{bmatrix} \frac{\mathrm{d}}{\mathrm{d}z} & 0 & 0 & 0 & 0 & 0 & 0 & 0 \\ 0 & \frac{\mathrm{d}}{\mathrm{d}z} & \frac{\mathrm{d}^2}{\mathrm{d}z^2} & 0 & 0 & 0 & 0 & 0 \\ 0 & 0 & 0 & \frac{\mathrm{d}}{\mathrm{d}z} & \frac{\mathrm{d}^2}{\mathrm{d}z^2} & 0 & 0 & 0 \\ 0 & 0 & 0 & 0 & 0 & 1 & \frac{\mathrm{d}}{\mathrm{d}z} & \frac{\mathrm{d}^2}{\mathrm{d}z^2} \end{bmatrix}^{\mathrm{T}} \tag{2.28}$$

The incremental equilibrium equation can be obtained by subtracting the equilibrium equations of two neighbouring equilibrium positions. The result is then linearized by ignoring second- and higher-order terms. It should be noted that Eq. (2.26) is substituted in the variational equation (Eq. (2.25)) to obtain the result. We have

$$\delta\left(\delta\bar{\Pi}\right)\approx\delta\bar{\mathbf{d}}^{\mathrm{T}}\bar{\mathbf{K}}\delta\bar{\mathbf{d}}-\delta\bar{\mathbf{d}}^{\mathrm{T}}\delta\bar{\mathbf{f}}=0 \tag{2.29}$$

where $\bar{\mathbf{K}}$ is the stiffness matrix, and can be found from the following equations

$$\bar{\mathbf{K}}=\int_L\int_A\bar{\mathbf{B}}^{\mathrm{T}}\bar{\mathbf{S}}^{\mathrm{T}}\bar{\mathbf{E}}\bar{\mathbf{S}}\bar{\mathbf{B}}\mathrm{d}A\mathrm{d}\bar{z}+\int_L\bar{\mathbf{M}}_\sigma\mathrm{d}\bar{z} \tag{2.30}$$

in which $\bar{\mathbf{M}}_\sigma\delta\bar{\mathbf{d}}=\delta\bar{\mathbf{B}}^{\mathrm{T}}\int_A\bar{\mathbf{S}}^{\mathrm{T}}\bar{\boldsymbol{\sigma}}\mathrm{d}A$.

2.5. The shell element

2.5.1. Introduction

As discussed in Section 2.3, a more detailed structural element is required to serve as the local model in the Iterative Global-local Method. For a thin-walled member, a shell-type finite element is the most suitable to capture the localized behaviour such as local buckling of web and flanges. The shell element used in this study is a 4-node element with 6 degrees of freedom per node. The plate bending component of the element is formulated based on Discrete Kirchhoff Quadrilateral (DKQ) according to Batoz & Tahar (1982). In this technique, the element is produced based on Kirchhoff's classical theory for thin plates, which assumes negligible shear deformation effects across the thickness of the plate element. The degrees of freedom associated to DKQ are the vertical displacement (w) of the nodes plus two bending rotations ($\hat{\theta}_x$) and ($\hat{\theta}_y$), as shown in Figure 2.9.

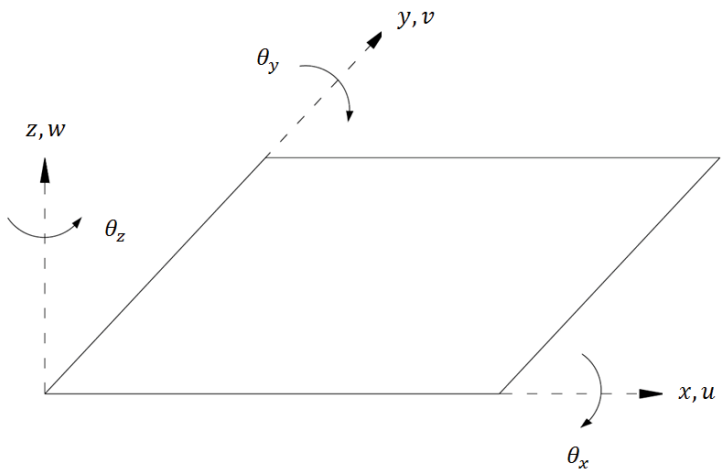

Figure 2.9: Shell element degrees of freedom

The membrane component of the element is obtained according to the model proposed by Ibrahimbegovic et al. (1990), which employs the drilling degree of freedom (i.e. rotation around the out-of-plane axis). Consequently, the degrees of freedom from the membrane component consist of two displacements in the direction of x and y axes (along the plate) and the drilling rotation $\hat{\theta}_z$, which constitutes 6 degrees of freedom in total. Details of the membrane and bending components of the shell element are discussed in the following sections.

2.5.2. The membrane component of the shell element

The in-plane (membrane) behaviour of shell elements is classically modelled by elements with in-plane translational degrees of freedom only, i.e. u and v in Figure 2.9 without considering the rotational degree of freedom θ_z, referred to as the drilling degree of freedom (Zienkiewicz 1977). By considering the bending behaviour of the shell element with 3 out-of-plane displacement components (w, θ_x and θ_y in Figure 2.9), the element would have 5 degrees of freedom per node. Although such an element is theoretically sound, some modelling and numerical problems may arise due to the lack of the drilling degree of freedom (Frey 1989); namely,

- If the shell element is connected to an out-of-plane beam-type element (e.g. modelling floor slabs connected to columns), the torsional degree of freedom of the column does not have any counterpart in the shell element and hence they cannot be connected.
- If the shell elements that are connected to each other are non-coplanar (i.e. the local and global coordinate directions are different), the transformation would lead to singularity in the global stiffness matrix. For example, considering the

two elements shown in Figure 2.10, the bending rotation of element 1 at edge AB is equivalent to the drilling d.o.f. of element 2, and vice versa. Therefore existence of such d.o.f is essential in the assemblage of these elements.

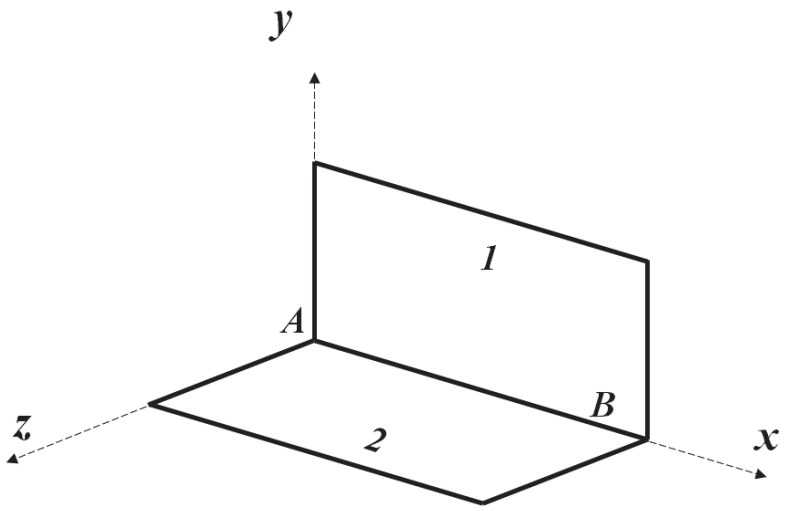

Figure 2.10: Assemblage of non-coplanar shell elements

Allman (1984) introduced "vertex rotations" ω which were defined based on the transverse displacement of the middle of the element side (u_{n12} in Figure 2.11).

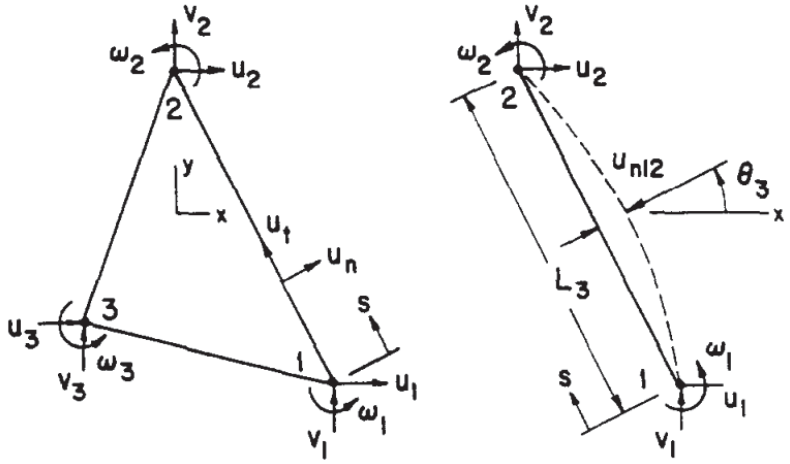

Figure 2.11: Vertex rotations in a triangular membrane element, after Cook (1986)

He assumed that the normal and tangential components of displacement (i.e. u_n and u_t) along a side of the element can be interpolated with cubic and linear interpolations, respectively from the nodal values, i.e.,

$$u_n = a_1 + a_2 s + a_3 s^2 \tag{2.31}$$

$$u_t = a_4 + a_5 s \tag{2.32}$$

where the coordinate s is measured from one end of the side to the other, and the constants a_1 to a_5 are found based on the nodal values of the normal and tangential displacement components u_{n1}, u_{n2}, v_{n1} and v_{n2}, which are in turn calculated from the nodal values of u and v.

$$u_{n1} = u_1 \cos\theta_3 + v_1 \sin\theta_3 \tag{2.33}$$

$$u_{t1} = -u_1 \sin\theta_3 + v_1 \cos\theta_3 \tag{2.34}$$

where θ_3 is the angle between the element side in consideration and the x axis. So far 4 equations are presented for the 5 unknowns. The 5th boundary condition is found based on the difference of the vertex rotations as

$$\left(\frac{\partial u_n}{\partial s}\right)_2 - \left(\frac{\partial u_n}{\partial s}\right)_1 = -\omega_2 + \omega_1 \tag{2.35}$$

Consequently, Eqs. (2.31) and (2.32) can be written as (Cook 1986)

$$u_n = \left(1 - \frac{s}{L_3}\right) u_{n1} + \frac{s}{L_3} u_{n2} + \frac{4s}{L_3}\left(1 - \frac{s}{L_3}\right) u_{n12} \tag{2.36}$$

$$u_t = \left(1 - \frac{s}{L_3}\right) u_{t1} + \frac{s}{L_3} u_{t2} \tag{2.37}$$

u_{n12} in Eq. (2.36) is the transverse displacement of the mid-side (Figure 2.11), and can be written in terms of the vertex displacements as

$$u_{n12} = \frac{L_3}{8}\left(\omega_2 - \omega_1\right) \tag{2.38}$$

which can be replaced in Eq. (2.36) to obtain (Jin 1994)

$$u_n = \left(1 - \frac{s}{L_3}\right) u_{n1} + \frac{s}{L_3} u_{n2} - \frac{s}{2}\left(1 - \frac{s}{L_3}\right)\left(\omega_1 - \omega_2\right) \tag{2.39}$$

The above equations can be used to obtain the interpolation functions within the triangular element. Similar equations can be derived for quadrilateral elements to obtain the displacement field *u* and *v* as

$$u = \sum_{i=1}^{8} N_i\left(\xi, \eta\right) u_i \tag{2.40}$$

$$v = \sum_{i=1}^{8} N_i\left(\xi, \eta\right) v_i \tag{2.41}$$

where ξ and η are natural coordinates and N_i are the shape functions (Zienkiewicz & Taylor 2005)

$$N_i = \tfrac{1}{2}\left(1 - \xi^2\right)\left(1 + \eta_i \eta\right) \quad i = 5, 7 \tag{2.42}$$

$$N_i = \tfrac{1}{2}\left(1 - \eta^2\right)\left(1 + \xi_i \xi\right) \quad i = 6, 8 \tag{2.43}$$

$$N_i = \tfrac{1}{4}(1+\xi_i\xi)(1+\eta_i\eta) - \tfrac{1}{2}N_m - \tfrac{1}{2}N_n \quad i = 6,8$$
$$i = 1,2,3,4 \quad m,n = 8,5;5,6;6,7;7,8. \tag{2.44}$$

in which $i = 1,2,3,4$ refers to the nodal values while $i = 5,6,7,8$ represent the displacement values at the middle of the element sides as in Figure 2.12.

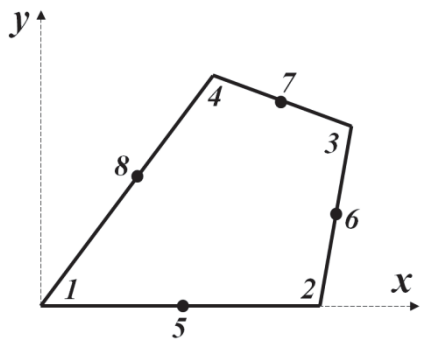

Figure 2.12: Nodes of a membrane element

It should be noted that the vertex rotations ω_i are not the true rotations of the nodes. The true rotation (i.e. the drilling rotations) can be written in terms of the in-plane translations as

$$\Omega = \tfrac{1}{2}\left(\frac{\partial v}{\partial x} - \frac{\partial u}{\partial y}\right) \tag{2.45}$$

Hughes & Brezzi (1989) described the boundary value problem as

$$div\ \sigma + f = 0 \tag{2.46}$$

$$skew\ \sigma = 0 \tag{2.47}$$

$$\Omega = skew\ (\nabla\ u) \tag{2.48}$$

$$symm\ \sigma = C\ symm\ (\nabla u) \tag{2.49}$$

where Eqs. (2.46) to (2.49) define the equilibrium equation, the symmetry of the stress tensor, the drilling rotation and the constitutive equation, respectively. It should be noted that *skew* in the above refers to the skew-symmetric part of the corresponding tensor while *symm* denotes the symmetric part, i.e.

$$skew\ \sigma = \tfrac{1}{2}\left(\sigma - \sigma^T\right) \tag{2.50}$$

$$symm\ \sigma = \tfrac{1}{2}\left(\sigma + \sigma^T\right) \tag{2.51}$$

Hughes & Brezzi (1989) developed the variational formulation as

$$\int symm(\nabla u).C.symm(\nabla u)\,dV + \rho\int\left(skew(\nabla u)-\Omega\right)^T\left(skew(\nabla u)-\Omega\right)dV - \int u.f dV = 0 \tag{2.52}$$

where ρ is a penalty term. The second term in Eq. (2.52) denotes that the skew symmetric part of the displacement gradient is enforced as a Lagrange multiplier to ensure that the drilling rotation is compatible with the skew part of the displacement gradient. Ibrahimbegovic et al. (1990) combined the Allman's interpolations with the independent treatment of the drilling degree of freedom. For that purpose, the drilling rotation is interpolated using the standard bilinear shape functions, i.e.

$$\Omega = \sum_{i=1}^{4} N_i(\xi,\eta)\Omega_i \tag{2.53}$$

where $N_i = \tfrac{1}{4}(1+\xi_i\xi)(1+\eta_i\eta) \quad i = 1,2,3,4$. The in-plane translation components *u* and *v* are interpolated using the Allman-type interpolations.

2.5.3. The bending component of the shell element

The local coordinate system of the flat shell element is normally chosen according to Figure 2.13, i.e. the shell is placed in the *x*-*y* plane, and the origin is placed at the mid-plane (Cook et al. 2002; Timoshenko & Woinowsky-Krieger 1959).

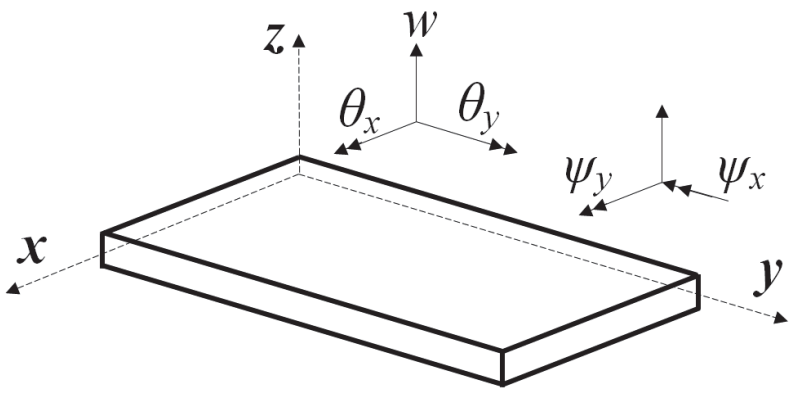

Figure 2.13: Plate bending degrees of freedom

It is assumed that if the element is subjected to bending action only (i.e. in-plane loading is not present), the mid-plane would be stress free and act as the neutral surface; that is, $\varepsilon_{xx} = \varepsilon_{xy} = \gamma_{xy} = 0$ at $z = 0$. Furthermore, a straight line perpendicular to the mid-plane is assumed to remain straight after the deformation. The in-plane displacement fields *u* and *v* can be written as

$$u = -z\psi_x \tag{2.54}$$

$$v = -z\psi_y \tag{2.55}$$

where z is the distance from the mid-plane, and ψ_x and ψ_y are the rotation components of a straight line normal to the mid-plane (Figure 2.13). Accordingly, the strain components can be calculated as

$$\varepsilon_{xx} = -z\frac{\partial \psi_x}{\partial x} \tag{2.56}$$

$$\varepsilon_{yy} = -z\frac{\partial \psi_y}{\partial y} \tag{2.57}$$

$$\gamma_{xy} = -z\left(\frac{\partial \psi_x}{\partial y} + \frac{\partial \psi_y}{\partial x}\right) \tag{2.58}$$

$$\gamma_{yz} = \frac{\partial w}{\partial y} - \psi_y \tag{2.59}$$

$$\gamma_{xz} = \frac{\partial w}{\partial x} - \psi_x \tag{2.60}$$

The following stress resultants can be defined.

$$M_x = \int_{-\frac{t}{2}}^{\frac{t}{2}} \sigma_{xx} z dz \tag{2.61}$$

$$M_y = \int_{-\frac{t}{2}}^{\frac{t}{2}} \sigma_{yy} z dz \tag{2.62}$$

$$M_{xy} = \int_{-\frac{t}{2}}^{\frac{t}{2}} \tau_{xy} z dz \tag{2.63}$$

$$Q_x = \int_{-\frac{t}{2}}^{\frac{t}{2}} \tau_{xz} dz \tag{2.64}$$

$$Q_y = \int_{-\frac{t}{2}}^{\frac{t}{2}} \tau_{yz} dz \tag{2.65}$$

Depending on the orientation of the normal to the mid-plane in the deformed configuration, two theories can be developed; namely the Kirchhoff Plate Theory and the Mindlin-Reissner Plate theory.

2.5.3.1. Kirchhoff Plate Theory

In Kirchhoff Plate Theory it is assumed that a straight line perpendicular to the mid-plane in the undeformed shape remains straight and perpendicular to the mid-plane after the deformation. In other words, the rotation of the perpendicular line to the mid-plane would be equal to the slope of the deformed plate, i.e. $\psi_y = \frac{\partial w}{\partial y}$ and $\psi_x = \frac{\partial w}{\partial x}$. Consequently, the out-of-plane shear strain components γ_{yz} and γ_{xz} would be equal to zero (Eqs. (2.59), (2.60)). The shear deformations are therefore neglected in the kinematics of the Kirchhoff theory, which makes it analogous to the Euler-Bernoulli theory for beams. The remaining strain terms can be written as

$$\varepsilon_{xx} = -z\frac{\partial^2 w}{\partial x^2} \tag{2.66}$$

$$\varepsilon_{yy} = -z\frac{\partial^2 w}{\partial y^2} \tag{2.67}$$

$$\gamma_{xy} = -2z\frac{\partial^2 w}{\partial x \partial y} \tag{2.68}$$

Considering that the normal strain along the z direction is negligible, the moment-curvature relation can be written as

$$\{\mathbf{M}\} = -[\mathbf{D}]\{\boldsymbol{\chi}\}$$

$$\begin{Bmatrix} M_x \\ M_y \\ M_{xy} \end{Bmatrix} = \frac{-Eh^3}{12\left(1-\upsilon^2\right)} \begin{bmatrix} 1 & \upsilon & 0 \\ \upsilon & 1 & 0 \\ 0 & 0 & \frac{1-\upsilon}{2} \end{bmatrix} \begin{Bmatrix} \frac{\partial^2 w}{\partial x^2} \\ \frac{\partial^2 w}{\partial y^2} \\ \frac{\partial^2 w}{\partial x \partial y} \end{Bmatrix} \tag{2.69}$$

Plate elements based on Kirchhoff Theory were initially developed by adopting different interpolation functions for the out-of-plane displacement *w* throughout the element (Cook et al. 2002; MacNeal 1994). These elements can be called "strict Kirchhoff" elements since the transverse shear strain is zero throughout the element, as opposed to "Kirchhoff elements" in which the vanishing of the transverse shear strain is imposed as a constraint at certain locations of the element only. The most widely used discrete Kirchhoff elements are the "Discrete Kirchhoff Triangle DKT" (Batoz et al. 1980) and the "Discrete Kirchhoff Quadrilateral DKQ" (Batoz & Tahar 1982). The Discrete Kirchhoff Quadrilateral, which is used as the bending part of the shell element in this chapter, is discussed in more detail.

The strain energy of the Kirchhoff element can be written as

$$U = \tfrac{1}{2}\int \{\boldsymbol{\varepsilon}\}^{\mathrm{T}} [\mathbf{E}] \{\boldsymbol{\varepsilon}\}\, dV = \int \{\boldsymbol{\chi}\}^{\mathrm{T}} [\mathbf{D}] \{\boldsymbol{\chi}\}\, dA \tag{2.70}$$

where $\boldsymbol{\chi}$ and $\mathbf{D}$ are defined in Eq. (2.69). In the development of the DKQ, initially the rotation of the normal to the undeformed mid-plane (ψ_x and ψ_y) and the slope of the deformed shell ($\frac{\partial w}{\partial x}$ and $\frac{\partial w}{\partial y}$) are treated as different parameters (Batoz & Tahar 1982). For that purpose, 4 nodes in the centre of the sides of the element are added to the vertex node to form an 8-node element (Figure 2.14), which is later going to be reduced to a 4-node quadrilateral.

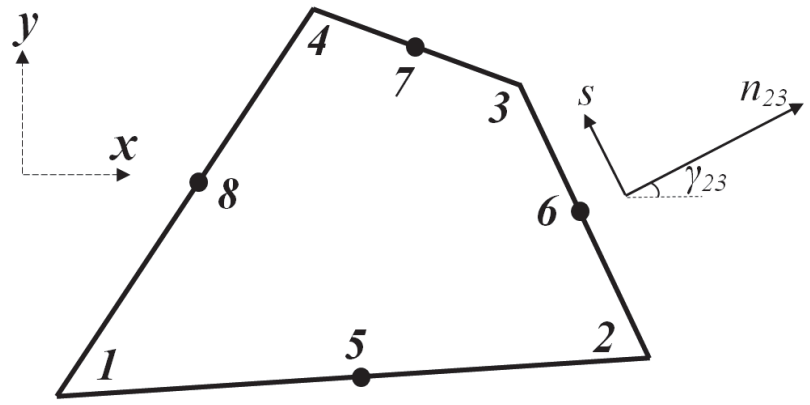

Figure 2.14: Discrete Kirchhoff Quadrilateral

The rotation components are interpolated using all the nodes as

$$\psi_x = \sum_{i=1}^{8} N_i \psi_{xi} \tag{2.71}$$

$$\psi_y = \sum_{i=1}^{8} N_i \psi_{yi} \tag{2.72}$$

The lateral deflection w is defined only at the boundaries of the element based on the nodal values at the vertex of the element, i.e. nodes 1 to 4 in Figure 2.14. The derivative of w with respect to s at the mid-side node $w_{,s5}$ can be interpolated from the vertex nodal displacement. For example, for node 5 we have

$$w_{,s5} = -\frac{3}{2L_{23}}\left(w_2 - w_3\right) - \frac{1}{4}\left(w_{,s2} - w_{,s3}\right) \tag{2.73}$$

where $w_{,s}$ can be calculated in terms of $w_{,x}$ and $w_{,y}$ as

$$w_{,s} = -w_{,x}\sin\gamma + w_{,y}\cos\gamma \tag{2.74}$$

It should be noted that 28 degrees of freedom are introduced, which are the rotation components for 8 nodes (16 DOFs) and the lateral displacement w and slopes $w_{,x}$ and

$w_{,y}$ at 4 nodes (12 DOFs). These degrees of freedom are reduced to the anticipated 12 degrees of freedom by applying 14 constraints as the following:

- The out-of-plane shear strain values should be zero according to the Kirchhoff Plate Theory (i.e. $w_{,x} = \psi_x$ and $w_{,y} = \psi_y$). This condition is imposed on the vertex nodes, which introduces 8 constraints. Additionally, the transverse shear strain at the mid-side nodes γ_{sz} is set to zero, which adds 4 constraints.
- The normal slopes are assumed to vary linearly along the element sides. For example for node 5 we can write

$$\psi_{n5} = \frac{1}{2}\left(w_{,n2} + w_{,n3}\right), \tag{2.75}$$

which adds 4 remaining constraints.

Consequently, the rotational degrees of freedom in Eqs. (2.70) and (2.71) can be written in terms of the vertex lateral displacements and slopes. The interpolation functions obtained from this procedure are presented explicitly in Appendix 2.A.

2.5.3.2. Mindlin-Reissner Plate Theory

In Mindlin-Reissner Theory, the straight lines perpendicular to the mid-plane before the deformation are assumed to remain straight, but not necessarily normal to the mid-plane during deformation. Consequently, apart from the lateral displacement *w*, two extra displacement fields; namely the components of rotation of the normal to the plane ψ_x and ψ_y, are required to determine the deformation of a Mindlin-Reissner plate. Since this theory takes the shear deformation effect into account, it is suitable for relatively thick plates or plates made of material with low shear modulus. The Mindlin-Reissner

theory is analogous to the Timoshenko theory for beams. For an isotropic, linearly elastic material, the displacement-stress resultant relationship can be written as

$$\{\mathbf{M}\} = -[\mathbf{D}_M]\{\chi\}$$

$$\begin{Bmatrix} M_x \\ M_y \\ M_{xy} \\ Q_x \\ Q_y \end{Bmatrix} = - \begin{bmatrix} D & D\upsilon & 0 & 0 & 0 \\ D\upsilon & D & 0 & 0 & 0 \\ 0 & 0 & D\dfrac{1-\upsilon}{2} & 0 & 0 \\ 0 & 0 & 0 & kGt & 0 \\ 0 & 0 & 0 & 0 & kGt \end{bmatrix} \begin{Bmatrix} \psi_{x,x} \\ \psi_{y,y} \\ \psi_{x,y} + \psi_{x,y} \\ \psi_x - w_{,x} \\ \psi_y - w_{,y} \end{Bmatrix} \tag{2.76}$$

where $D = \dfrac{Eh^3}{12\left(1-\upsilon^2\right)}$, in which h is the thickness of the plate. k is used to account for parabolic variation of transverse shear stress, and kt is the effective thickness for shear deformation. For homogenous plates, k is taken as $k = \frac{5}{6}$.

2.5.4. Formulation of the shell element used in the Iterative Global-local Method

As discussed in Section 2.5.1, the shell element is composed of a membrane element with drilling degree of freedom for the in-plane behaviour and a Discrete Kirchhoff Quadrilateral for the plate bending deformations. Accordingly, the nodal displacements are collected as

$$\hat{\mathbf{d}} = \left\langle \hat{u}_1 \quad \hat{v}_1 \quad \hat{\theta}_{z1} \quad \hat{w}_1 \quad \hat{\theta}_{x1} \quad \hat{\theta}_{y1} \quad \hat{u}_2 \quad \ldots \quad \hat{u}_4 \quad \hat{v}_4 \quad \hat{\theta}_{z4} \quad \hat{w}_4 \quad \hat{\theta}_{x4} \quad \hat{\theta}_{y4} \right\rangle^{\mathrm{T}} \tag{2.77}$$

where subscripts 1 to 4 refer to the four nodes of the quadrilateral element. The interpolation matrix $\hat{\mathbf{X}}$ can be used to obtain the displacement vector $\hat{\mathbf{u}}$ of any point of the shell as

$$\hat{\mathbf{u}} = \hat{\mathbf{X}}\hat{\mathbf{d}} \tag{2.78}$$

where

$$\hat{\mathbf{u}} = \left\langle \hat{u}_0 \quad \hat{v}_0 \quad \hat{\theta}_z \quad \hat{w}_0 \quad \hat{\theta}_x \quad \hat{\theta}_y \right\rangle^{\mathrm{T}} \tag{2.79}$$

The out of plane deflection $\hat{w}$ is interpolated linearly, while the standard bilinear interpolation is used for the independent drilling rotation $\hat{\theta}_z$, and the Allman-type interpolation functions are used for the in-plane displacements $\hat{u}_0$ and $\hat{v}_0$ according to Ibrahimbegovic et al. (1990). The components of interpolation matrix $\hat{\mathbf{X}}$ are given explicitly in Appendix 2.A.

The equilibrium equations of the shell model are obtained in the variational form as

$$\delta\hat{\Pi} = \int_L \int_A \delta\hat{\boldsymbol{\varepsilon}}^{\mathrm{T}} \hat{\boldsymbol{\sigma}} \mathrm{d}A\mathrm{d}z - \delta\hat{\mathbf{d}}^{\mathrm{T}} \hat{\mathbf{f}} = 0 \tag{2.80}$$

where $\hat{\boldsymbol{\varepsilon}}$ represents the strain vector of the shell element, which can be composed of strains due to plate bending $\hat{\boldsymbol{\varepsilon}}_b$, membrane action $\hat{\boldsymbol{\varepsilon}}_{mm}$, and strains due to second order membrane and plate bending action $\hat{\boldsymbol{\varepsilon}}_N$, i.e.

$$\hat{\boldsymbol{\varepsilon}} = \hat{\boldsymbol{\varepsilon}}_b + \hat{\boldsymbol{\varepsilon}}_{mm} + \hat{\boldsymbol{\varepsilon}}_N \tag{2.81}$$

The plate bending portion of the strain can be written as

$$\hat{\boldsymbol{\varepsilon}}_b = -z \begin{Bmatrix} \dfrac{\partial \hat{\theta}_x}{\partial x} \\ \dfrac{\partial \hat{\theta}_y}{\partial y} \\ \dfrac{\partial \hat{\theta}_x}{\partial y} + \dfrac{\partial \hat{\theta}_y}{\partial x} \\ \hline 0 \end{Bmatrix} = -z \begin{Bmatrix} \hat{\boldsymbol{\chi}} \\ \hline 0 \end{Bmatrix} \tag{2.82}$$

in which $\hat{\boldsymbol{\chi}}$ is the curvature vector. The second term in Eq. (2.81) can be written as

$$\hat{\boldsymbol{\varepsilon}}_{mm} = -z \begin{Bmatrix} \dfrac{\partial \hat{u}_0}{\partial x} \\ \dfrac{\partial \hat{v}_0}{\partial y} \\ \dfrac{\partial \hat{u}_0}{\partial y} + \dfrac{\partial \hat{v}_0}{\partial x} \\ \hline \dfrac{1}{2}\left(\dfrac{\partial \hat{v}_0}{\partial x} - \dfrac{\partial \hat{u}_0}{\partial y} \right) - \hat{\theta}_z \end{Bmatrix} = \begin{Bmatrix} \hat{\boldsymbol{\varepsilon}}_m \\ \hline \dfrac{1}{2}\left(\dfrac{\partial \hat{v}_0}{\partial x} - \dfrac{\partial \hat{u}_0}{\partial y} \right) - \hat{\theta}_z \end{Bmatrix} \tag{2.83}$$

in which $\hat{\boldsymbol{\varepsilon}}_m$ is the vector of membrane strains and the last row in Eq. (2.83) contains the skew symmetric part of the membrane strains introduced to avoid numerical stability issues when drilling rotations $\hat{\theta}_z$ are used with Allman-type interpolations. The non-linear strain component can be written as

$$\hat{\boldsymbol{\varepsilon}}_N = \begin{Bmatrix} \dfrac{1}{2}\left(\dfrac{\partial \hat{w}_0}{\partial x} \right)^2 + \dfrac{1}{2}\left(\dfrac{\partial \hat{v}_0}{\partial x} \right)^2 \\ \dfrac{1}{2}\left(\dfrac{\partial \hat{w}_0}{\partial y} \right)^2 \\ 0 \\ \hline 0 \end{Bmatrix} \tag{2.84}$$

The stress vector $\hat{\boldsymbol{\sigma}}$ can be obtained from the strain field by assuming a linear elastic behaviour, i.e. $\hat{\boldsymbol{\sigma}} = \hat{\mathbf{E}}\hat{\boldsymbol{\varepsilon}}$. The constitutive matrix $\hat{\mathbf{E}}$ can be written as

$$\hat{\mathbf{E}} = \frac{E}{1-\nu^2}\left[\begin{array}{ccc:c} 1 & \nu & 0 & 0 \\ \nu & 1 & 0 & 0 \\ 0 & 0 & \frac{1-\nu}{2} & 0 \\ \hdashline 0 & 0 & 0 & \frac{1-\nu}{2} \end{array}\right] \tag{2.85}$$

Similar to the beam element, the variation of the strain vector for the shell element can be expressed as

$$\delta\hat{\boldsymbol{\varepsilon}} = \hat{\mathbf{S}}\hat{\mathbf{B}}\delta\hat{\mathbf{d}} \tag{2.86}$$

The incremental equilibrium equation can be obtained in a similar way to the beam element formulation resulting in the following equilibrium equation

$$\delta\left(\delta\hat{\Pi}\right) \approx \delta\hat{\mathbf{d}}^{\mathrm{T}}\hat{\mathbf{K}}\delta\hat{\mathbf{d}} - \delta\hat{\mathbf{d}}^{\mathrm{T}}\delta\hat{\mathbf{f}} = 0 \tag{2.87}$$

where $\hat{\mathbf{K}}$ is the stiffness matrix of the shell element, and can be found from the following equations

$$\hat{\mathbf{K}} = \int_L \int_A \hat{\mathbf{B}}^{\mathrm{T}}\hat{\mathbf{S}}^{\mathrm{T}}\hat{\mathbf{E}}\hat{\mathbf{S}}\hat{\mathbf{B}}\,\mathrm{d}A\mathrm{d}\bar{z} + \int_L \hat{\mathbf{M}}_\sigma\,\mathrm{d}\bar{z} \tag{2.88}$$

in which $\hat{\mathbf{M}}_\sigma\delta\hat{\mathbf{d}} = \delta\hat{\mathbf{B}}^{\mathrm{T}}\int_A \hat{\mathbf{S}}^{\mathrm{T}}\hat{\boldsymbol{\sigma}}\,\mathrm{d}A$.

2.6. The Iterative Global-local Method

As discussed in the previous sections, in the Iterative Global-local Method, the total domain of the structure is primarily modelled by a less-detailed structural idealization (i.e. the coarse-scale model, which is the beam model discussed in section 2.4). The

fine-scale model (i.e. the shell element discussed in section 2.5) is placed in the critical regions, which are a subset of the total domain. The critical regions can be defined as places where large local deformation are anticipated, places where local defect exist, regions that seem to be susceptible to local buckling and where large concentrated loading exists. In other words, since the beam element used in the coarse-scale model is not capable of capturing deformations at the cross-sectional level due to the rigid-cross section assumption, the coarse-scale model needs to be placed anywhere that such assumption may be violated.

A schematic of the global-local analysis can be seen in Figure 2.15, where the total domain is shown by Ω_c and the critical part is depicted by Ω_m. The boundary between the two is $\partial\Omega_S$, or the points *i* and *j*. It should be noted that the two aforementioned models have an overlap throughout Ω_m, which is why the method is sometimes referred to as overlapping decomposition technique.

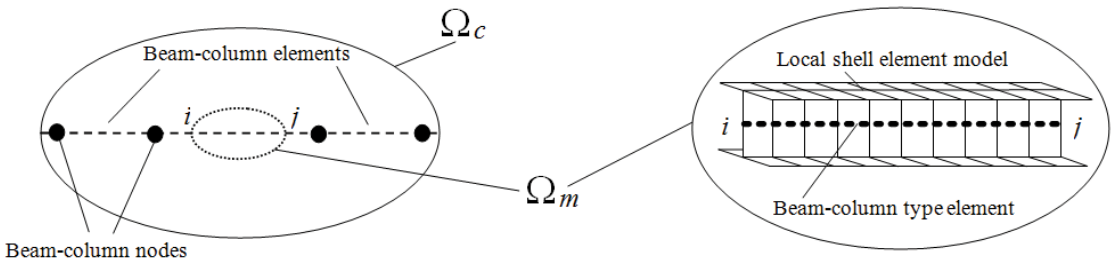

Figure 2.15: Decomposition of the analysis domain

Based on the Bridging multiscale approach proposed by Liu et al. (1997), the shell nodal displacement vector is decomposed into a global/coarse-scale component and a difference term. To this end, a decomposition matrix **N** is used, which projects the beam results onto the nodal points of the shell model, i.e. $\hat{\mathbf{d}} = \mathbf{N}\bar{\mathbf{d}} + \mathbf{d}'$. In other words,

the total displacement of a shell node is additively decomposed into the displacement analogous to the beam element displacements $\mathbf{N}\bar{\mathbf{d}}$ and a difference term $\mathbf{d}'$. The decomposition matrix $\mathbf{N}$ is obtained by multiplying $\mathbf{Y}$ and $\mathbf{Z}$ matrices in Eqs. (2.21) and (2.22) and is given in Eq. (2.89)

$$\mathbf{N}=\begin{bmatrix} \mathbf{L}^{\mathrm{T}} & -\bar{x}\dfrac{\mathrm{d}\mathbf{H}^{\mathrm{T}}}{\mathrm{d}\bar{z}} & -\bar{y}\dfrac{\mathrm{d}\mathbf{H}^{\mathrm{T}}}{\mathrm{d}\bar{z}} & -\bar{\omega}\dfrac{\mathrm{d}\mathbf{H}^{\mathrm{T}}}{\mathrm{d}\bar{z}} \\ \mathbf{0} & \mathbf{H}^{\mathrm{T}} & \mathbf{0} & -\left(\bar{y}-a_y\right)\mathbf{H}^{\mathrm{T}} \\ \mathbf{0} & \dfrac{\mathrm{d}\mathbf{H}^{\mathrm{T}}}{\mathrm{d}\bar{z}} & \mathbf{0} & -\left(\bar{y}-a_y\right)\dfrac{\mathrm{d}\mathbf{H}^{\mathrm{T}}}{\mathrm{d}\bar{z}} \\ \mathbf{0} & \mathbf{0} & \mathbf{H}^{\mathrm{T}} & \left(\bar{x}-a_x\right)\mathbf{H}^{\mathrm{T}} \\ \mathbf{0} & \mathbf{0} & -\dfrac{\mathrm{d}\mathbf{H}^{\mathrm{T}}}{\mathrm{d}\bar{z}} & -\left(\bar{x}-a_x\right)\dfrac{\mathrm{d}\mathbf{H}^{\mathrm{T}}}{\mathrm{d}\bar{z}} \\ \mathbf{0} & \mathbf{0} & \mathbf{0} & -\mathbf{H}^{\mathrm{T}} \end{bmatrix} \tag{2.89}$$

It should be noted that $\mathbf{N}$ is a linear operator and therefore, the variation of $\mathbf{N}$ is equal to zero. By this it is meant that there are no displacement terms present in $\mathbf{N}$ (i.e. this matrix can be constructed before the start of the analysis and need not be changed throughout the analysis procedure). Consequently, the variation of the displacement field, which is required for the equilibrium equation, can be written as:

$$\delta\hat{\mathbf{d}}=\mathbf{N}\delta\bar{\mathbf{d}}+\delta\mathbf{d}' \tag{2.90}$$

As a result, the strain vector of the shell model can be decomposed into two parts: $\hat{\boldsymbol{\varepsilon}}=\bar{\boldsymbol{\varepsilon}}+\boldsymbol{\varepsilon}'$, in which the term $\bar{\boldsymbol{\varepsilon}}$ refers to the strain due to the beam formulation and $\boldsymbol{\varepsilon}'$ is the difference between the results of the shell and beam element formulations. Using Eq. (2.90), the variation of the strain vector can be decomposed as

$$\delta\hat{\boldsymbol{\varepsilon}}=\hat{\mathbf{S}}\hat{\mathbf{B}}\delta\mathbf{d}=\hat{\mathbf{S}}\hat{\mathbf{B}}\left(\mathbf{N}\delta\bar{\mathbf{d}}+\delta\mathbf{d}'\right)=\hat{\mathbf{S}}\hat{\mathbf{B}}\mathbf{N}\delta\bar{\mathbf{d}}+\hat{\mathbf{S}}\hat{\mathbf{B}}\delta\mathbf{d}'=\delta\bar{\boldsymbol{\varepsilon}}+\delta\boldsymbol{\varepsilon}' \tag{2.91}$$

So that

$$\delta\bar{\boldsymbol{\varepsilon}} = \hat{\mathbf{S}}\hat{\mathbf{B}}\mathbf{N}\delta\bar{\mathbf{d}} \tag{2.92}$$

$$\delta\boldsymbol{\varepsilon}' = \hat{\mathbf{S}}\hat{\mathbf{B}}\delta\mathbf{d}' \tag{2.93}$$

The decomposition matrix $\mathbf{N}$ is constructed based on the kinematic assumptions of the thin-walled beam of Vlasov (1961). Thus, the use of $\mathbf{N}$ is equivalent to constraining the degrees of freedom of the shell element to obey the kinematics of the beam element at the boundaries (i.e. Vlasov kinematics). As a result, the first term in Eq. (2.91) (i.e. $\delta\bar{\boldsymbol{\varepsilon}}$) is actually the variation of the strain vector of the beam formulation, and the second term (i.e. $\delta\boldsymbol{\varepsilon}'$) is the difference between the two models.

Using the decomposition in the strain vector, the stress vector can also be decomposed as $\hat{\boldsymbol{\sigma}} = \bar{\boldsymbol{\sigma}} + \boldsymbol{\sigma}'$. By introducing these values into the variational form of the shell element i.e. Eq. (2.25), the equilibrium condition requires the simultaneous satisfaction of the two equations as

$$\delta\Pi_1 = \delta\bar{\mathbf{d}}^{\mathrm{T}}\mathbf{N}^{\mathrm{T}}\int_L\int_A \hat{\mathbf{B}}^{\mathrm{T}}\hat{\mathbf{S}}^{\mathrm{T}}\bar{\boldsymbol{\sigma}}\,\mathrm{d}A\mathrm{d}\bar{z} - \delta\bar{\mathbf{d}}^{\mathrm{T}}\mathbf{N}^{\mathrm{T}}\hat{\mathbf{f}} + \delta\bar{\mathbf{d}}^{\mathrm{T}}\mathbf{F} = 0 \tag{2.94}$$

$$\delta\Pi_2 = \delta\mathbf{d}'^{\mathrm{T}}\int_L\int_A \hat{\mathbf{B}}^{\mathrm{T}}\hat{\mathbf{S}}^{\mathrm{T}}\hat{\boldsymbol{\sigma}}\,\mathrm{d}A\mathrm{d}\bar{z} - \delta\mathbf{d}'^{\mathrm{T}}\,\mathbf{f} = 0 \tag{2.95}$$

where $\mathbf{F}$ is the complementary load vector due to the difference between beam and shell elements and can be expressed explicitly as

$$\mathbf{F} = \mathbf{N}^{\mathrm{T}}\int_L\int_A \hat{\mathbf{B}}^{\mathrm{T}}\hat{\mathbf{S}}^{\mathrm{T}}\left(\hat{\boldsymbol{\sigma}} - \bar{\boldsymbol{\sigma}}\right)\mathrm{d}A\mathrm{d}\bar{z} = \int_L\int_A \bar{\mathbf{B}}^{\mathrm{T}}\bar{\mathbf{S}}^{\mathrm{T}}\boldsymbol{\sigma}'\,\mathrm{d}A\mathrm{d}\bar{z} \tag{2.96}$$

2.6.1. Linearization of the equilibrium equations

The two equilibrium equations of the overlapping region have to be linearized, which can be done by taking the variation of each of the equations. The linearization of Eq. (2.94) results in

$$\delta\left(\delta\Pi_1\right)=\delta\left(\delta\bar{\mathbf{d}}^{\mathrm{T}}\mathbf{N}^{\mathrm{T}}\int_L\int_A\hat{\mathbf{B}}^{\mathrm{T}}\hat{\mathbf{S}}^{\mathrm{T}}\bar{\boldsymbol{\sigma}}\mathrm{d}A\mathrm{d}\bar{z}-\delta\bar{\mathbf{d}}^{\mathrm{T}}\mathbf{N}^{\mathrm{T}}\hat{\mathbf{f}}+\delta\bar{\mathbf{d}}^{\mathrm{T}}\mathbf{F}\right)=0 \tag{2.97}$$

In the first term on the right hand side of Eq. (2.97), only the terms $\hat{\mathbf{B}}$ and $\bar{\boldsymbol{\sigma}}$ have non-zero variations. It should be noted that the variation of the decomposition matrix $\mathbf{N}$ vanishes since it does not contain any displacement terms at its current form, i.e. Eq. (2.89), although it will be shown in Chapter 4 that for more general loading conditions, displacement terms enter the decomposition matrix and its variation would not vanish.

$$\delta\left(\delta\bar{\mathbf{d}}^{\mathrm{T}}\mathbf{N}^{\mathrm{T}}\int_L\int_A\hat{\mathbf{B}}^{\mathrm{T}}\hat{\mathbf{S}}^{\mathrm{T}}\bar{\boldsymbol{\sigma}}\mathrm{d}A\mathrm{d}\bar{z}\right)=\delta\bar{\mathbf{d}}^{\mathrm{T}}\mathbf{N}^{\mathrm{T}}\left(\int_L\int_A\hat{\mathbf{B}}^{\mathrm{T}}\hat{\mathbf{S}}^{\mathrm{T}}\delta\bar{\boldsymbol{\sigma}}\mathrm{d}A\mathrm{d}\bar{z}+\int_L\int_A\delta\hat{\mathbf{B}}^{\mathrm{T}}\hat{\mathbf{S}}^{\mathrm{T}}\bar{\boldsymbol{\sigma}}\mathrm{d}A\mathrm{d}\bar{z}\right) \tag{2.98}$$

From Eq. (2.92) $\delta\bar{\boldsymbol{\sigma}}$ can be written as

$$\delta\bar{\boldsymbol{\sigma}}=\bar{E}\delta\bar{\boldsymbol{\varepsilon}}=\bar{E}\hat{\mathbf{S}}\hat{\mathbf{B}}\mathbf{N}\delta\bar{\mathbf{d}}, \tag{2.99}$$

and by defining $\tilde{\mathbf{M}}_\sigma$ such that $\tilde{\mathbf{M}}_\sigma\delta\hat{\mathbf{d}}=\delta\hat{\mathbf{B}}^{\mathrm{T}}\int_A\hat{\mathbf{S}}^{\mathrm{T}}\bar{\boldsymbol{\sigma}}\mathrm{d}A$, Eq. (2.98) can be written as

$$\delta\left(\delta\bar{\mathbf{d}}^{\mathrm{T}}\mathbf{N}^{\mathrm{T}}\int_L\int_A\hat{\mathbf{B}}^{\mathrm{T}}\hat{\mathbf{S}}^{\mathrm{T}}\bar{\boldsymbol{\sigma}}\mathrm{d}A\mathrm{d}\bar{z}\right)=\delta\bar{\mathbf{d}}^{\mathrm{T}}\bar{\mathbf{K}}\delta\bar{\mathbf{d}} \tag{2.100}$$

where $\bar{\mathbf{K}} = \mathbf{N}^{\mathrm{T}}\left(\int_L\int_A \hat{\mathbf{B}}^{\mathrm{T}}\hat{\mathbf{S}}^{\mathrm{T}}\bar{E}\hat{\mathbf{S}}\hat{\mathbf{B}}\mathrm{d}A\mathrm{d}\bar{z} + \int_L \tilde{\mathbf{M}}_{\sigma}\mathrm{d}\bar{z}\right)\mathbf{N}$ and can be replaced by the beam stiffness matrix in Eq. (2.30). Consequently, the linearized form of the first equilibrium equation can be written as

$$\delta\left(\delta\Pi_1\right) = \delta\bar{\mathbf{d}}^{\mathrm{T}}\bar{\mathbf{K}}\delta\bar{\mathbf{d}} - \delta\bar{\mathbf{d}}^{\mathrm{T}}\delta\bar{\mathbf{f}} \tag{2.101}$$

Similarly, from the linearization of Eq. (2.95) we have

$$\delta\left(\delta\Pi_2\right) = \delta\mathbf{d}'^{\mathrm{T}}\hat{\mathbf{K}}\delta\hat{\mathbf{d}} - \delta\mathbf{d}'^{\mathrm{T}}\delta\hat{\mathbf{f}} = 0 \tag{2.102}$$

in which $\hat{\mathbf{K}}$ is the stiffness matrix of the shell element, and was defined in Eq. (2.88). Since the variation of the difference displacement term $\delta\mathbf{d}'$ is arbitrary, Eqs. (2.87) and (2.102) admit the same displacement solutions, which is the solution of the shell model. The main point of the Iterative Global-local Method is that this shell solution is sought after at critical regions only (i.e. the overlapping region) and avoided at other locations for the economy of the model.

2.6.2. Interface boundary conditions

Since the overlapping shell may lie at any location along the beam, its boundary conditions need to be clearly defined. For that purpose, the displacement of the global beam model at the boundaries of the fine-scale model is used as an interface boundary condition for the local shell model. To impose the displacement boundary conditions, we divide the displacement vector of the shell model into boundary and internal displacement vectors, which results in the partitioning of the stiffness matrix of the shell element as

$$\underbrace{\begin{bmatrix} \hat{\mathbf{K}}_a & \hat{\mathbf{K}}_b \\ \hat{\mathbf{K}}_b^{\mathrm{T}} & \hat{\mathbf{K}}_c \end{bmatrix}}_{\hat{\mathbf{K}}} \underbrace{\begin{Bmatrix} \boxed{\delta\hat{\mathbf{d}}_{i\&j}} \\ \delta\hat{\mathbf{d}}_{IN} \end{Bmatrix}}_{\delta\hat{\mathbf{d}}} = \underbrace{\begin{Bmatrix} \delta\hat{\mathbf{f}}_{i\&j} \\ \boxed{\delta\hat{\mathbf{f}}_s} \end{Bmatrix}}_{\delta\hat{\mathbf{f}}} \tag{2.103}$$

where $\hat{\mathbf{d}}_{i\&j}$ and $\delta\hat{\mathbf{d}}_{IN}$ are the displacement values at the boundary of the shell and internal degrees of freedom, respectively, $\hat{\mathbf{f}}_s$ is the vector of specified external loads that fall into the overlapping analysis domain, and $\hat{\mathbf{f}}_{i\&j}$ is the vector of tractions at the boundaries of the local shell model. The local shell stiffness matrix $\hat{\mathbf{K}}$ is partitioned according to the decomposition of the shell nodal displacements into boundary and internal. The specified displacement and loads in Eq. (2.103) are placed in the box symbol ($\boxed{\ }$). The displacement field $\hat{\mathbf{d}}_{i\&j}$ is calculated from the beam displacement fields at the boundaries of the local shell as

$$\hat{\mathbf{d}}_{i\&j} \approx \mathbf{N}\bar{\mathbf{d}}_{i\&j} + \tilde{\mathbf{d}}_{i\&j} \tag{2.104}$$

where $\mathbf{N}$ is the decomposition matrix and $\bar{\mathbf{d}}_{i\&j}$ is the beam displacement vector at the ends i and j of the local shell model. The additional displacement term $\tilde{\mathbf{d}}_{i\&j}$ in Eq. (2.104) is the displacement field in the fine-scale model due to the Poisson ratio effects, which is discussed in the following paragraph in more detail.

Even in the absence of local buckling, the Poisson ratio effect causes changes in the cross-sectional dimensions of a thin-walled beam. However, the rigid cross-sectional assumption of the beam theories does not allow this effect to be captured since it does not account for displacements in the cross-sectional plane. This issue was considered in the derivations of the beam element in Section 2.4 by using the constitutive equation modified according to Poisson ratio effects, i.e. Eq. (2.24). It would be equivalent to

considering an extra strain component, i.e. $\boldsymbol{\varepsilon}'=\langle 0 \quad -\nu\varepsilon \quad 0 \quad 0\rangle^{\mathrm{T}}$, in the coarse-scale/global analysis domain, which is required to be considered at the interface of the global-local model ($\partial\Omega_s$ in Figure 2.7). It should be noted that considering the Poisson ratio effect in the interface is necessary because the decomposition matrix **N** is developed based on the kinematics of the thin-walled beam theory, which is based on the rigid cross-sectional assumption. For that purpose, firstly the aforementioned strain component ($-\nu\varepsilon$) is numerically integrated over the cross-sectional contour at each end of the overlapping region. Then the rigid body motion is removed by imposing the condition that the summation of these displacements should be zero across the cross-section to obtain the desired displacement vector $\tilde{\mathbf{d}}_{i\&j}$ to be used in Eq. (2.104).

2.6.3. Algorithm for the solution procedure

The algorithm of the solution procedure of the Iterative Global-local Method is discussed herein. Firstly, the coarse-scale (i.e. the beam) model is solved while keeping the fine-scale (i.e. the shell) model fixed to obtain the global displacement field $\bar{\mathbf{d}}$. Then the results of the beam model at the boundaries of the local shell are imposed on the fine-scale model as the interface boundary conditions (Section 2.6.2), and along with the additional external loads at the overlapping region, the fine-scale model is solved to obtain the shell displacement values $\hat{\mathbf{d}}$. It should be noted that at this stage, the coarse-scale displacement values are kept unchanged and unaffected by the fine-scale results. In order to verify that the two models are synchronised, the stress vectors of the fine- and coarse-scale models are compared and any unbalanced stress values are again applied to the coarse-scale model. Based on the above description, two criteria

have to be met in order to terminate the iterations of each step and achieve convergence (Qian et al. 2004); namely,

- The equilibrium of the coarse-scale/beam model and the fine-scale/shell model has to be achieved,
- The difference in the stress vectors of the global and local models should be smaller than a tolerance, which is achieved through the complementary force introduced in Eq. (2.96).

A flowchart of the procedure is shown in Figure 2.16.

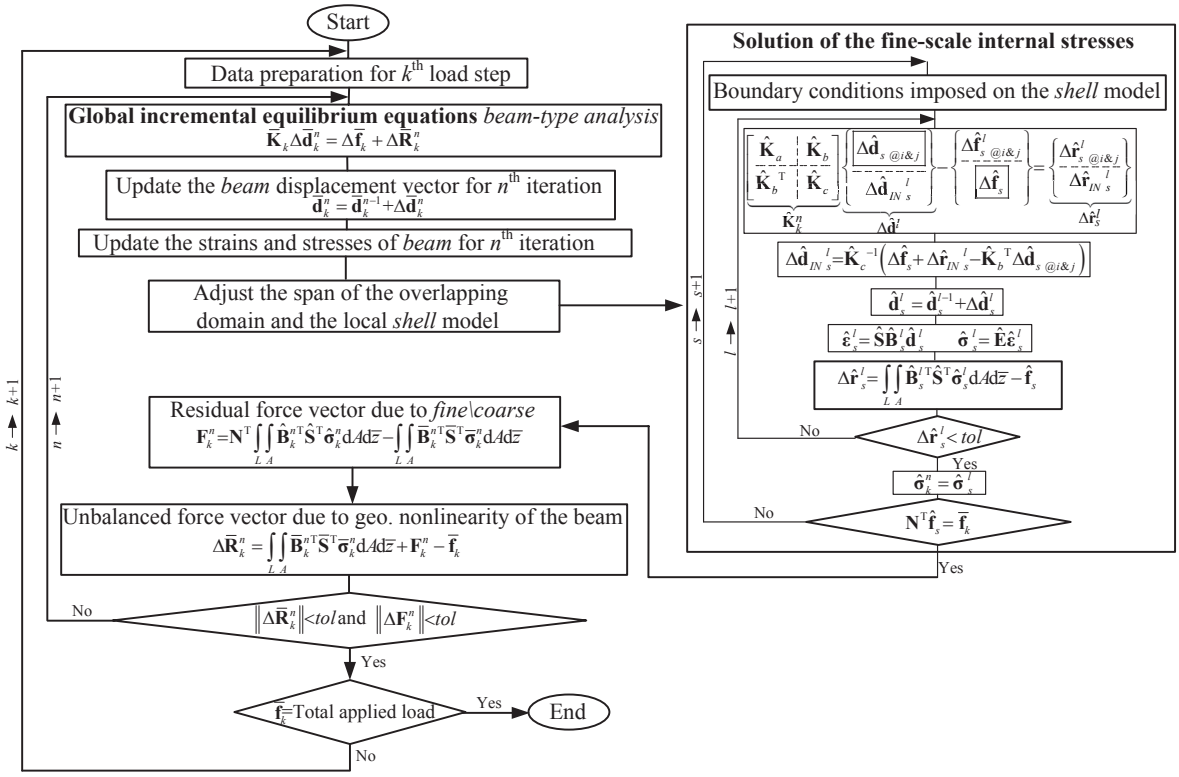

Figure 2.16: Flowchart of the iterative global-local algorithm

The global model is solved using a Newton-Raphson incremental-iterative approach with a step-by-step load control procedure, i.e.

$$\bar{\mathbf{K}}_k \Delta\bar{\mathbf{d}}_k^n = \Delta\bar{\mathbf{f}}_k + \Delta\bar{\mathbf{R}}_k^n \tag{2.105}$$

where $\bar{\mathbf{K}}_k$ is the tangent stiffness matrix of the coarse-scale/beam model at the beginning of each incremental step, $\Delta\bar{\mathbf{f}}_k$ is the external load increment, and $\Delta\bar{\mathbf{R}}_k^n$ is the unbalanced force at the n^{th} iteration of the k^{th} step, which can be obtained from Eq. (2.94) as

$$\Delta\bar{\mathbf{R}}_k^n = -\int_L \int_A \bar{\mathbf{B}}_k^{n\mathrm{T}} \bar{\mathbf{S}}^{\mathrm{T}} \bar{\boldsymbol{\sigma}}_k^n \mathrm{d}A\mathrm{d}\bar{z} - \mathbf{F}_k^n + \bar{\mathbf{f}}_k \tag{2.106}$$

We can solve Eq. (2.105) to get the incremental displacement values of the coarse-scale model, which can be used to find the total displacement values at the end of the n^{th} iteration, i.e. $\bar{\mathbf{d}}_k^n = \bar{\mathbf{d}}_k^{n-1} + \Delta\bar{\mathbf{d}}_k^n$. The calculated displacement vector is then used to update the strain vector $\bar{\boldsymbol{\varepsilon}}_k^n$ and the stress vector $\bar{\boldsymbol{\sigma}}_k^n$ of the global model.

Within each load step k of the coarse-scale model, the fine-scale model is solved by adopting an incremental-iterative step-by-step technique. The displacement boundary conditions (from the coarse-scale model) and the external loads in the overlapping region are imposed on the shell model in s steps, and the internal displacement values of the shell model (i.e. $\Delta\hat{\mathbf{d}}_{IN\,s}^{\,l}$) are obtained in l iterations. The second line of Eq. (2.103) can be used for that purpose as

$$\Delta\hat{\mathbf{d}}_{IN\,s}^{\,l} = \hat{\mathbf{K}}_c^{-1}\left(\Delta\hat{\mathbf{f}}_s + \Delta\hat{\mathbf{r}}_{IN\,s}^{\,l} - \hat{\mathbf{K}}_b^{\mathrm{T}} \Delta\hat{\mathbf{d}}_{s\,i\&j}\right) \tag{2.107}$$

where $\Delta\hat{\mathbf{d}}_{s\,i\&j}$ is the specified interface displacement at the boundaries of the local shell model, and $\Delta\hat{\mathbf{r}}_{IN\,s}^{\,l}$ is the unbalanced force vector that accounts for the geometric nonlinearities within the local shell model, which can be written as

$$\Delta\hat{\mathbf{r}}_s^l = -\int_L \int_A \hat{\mathbf{B}}_s^{l\mathrm{T}} \hat{\mathbf{S}}^{\mathrm{T}} \hat{\boldsymbol{\sigma}}_s^l \mathrm{d}A\mathrm{d}\bar{z} + \hat{\mathbf{f}}_s \tag{2.108}$$

The local incremental displacement values obtained from Eq. (2.107) are used to determine the displacement configuration of the fine-scale model at the current stage, i.e. $\hat{\mathbf{d}}_s^l = \hat{\mathbf{d}}_s^{l-1} + \Delta\hat{\mathbf{d}}_s^l$, which is used to update the internal strain field $\hat{\boldsymbol{\varepsilon}}_s^l$ and the stress field $\hat{\boldsymbol{\sigma}}_s^l$ of the shell model. If the local convergence criterion is satisfied, i.e. $\left\|\Delta\hat{\mathbf{r}}_s^l\right\| < \varepsilon_{tol}$ then $\hat{\boldsymbol{\sigma}}_k^n = \hat{\boldsymbol{\sigma}}_s^l$ is used for the complementary force calculations within the k^{th} step in n^{th} iteration, i.e. $\mathbf{F}_k^n = \mathbf{N}^{\mathrm{T}} \int_L \int_A \hat{\mathbf{B}}_k^{n\mathrm{T}} \hat{\mathbf{S}}^{\mathrm{T}} \hat{\boldsymbol{\sigma}}_k^n \mathrm{d}A\mathrm{d}\bar{z} - \int_L \int_A \bar{\mathbf{B}}_k^{n\mathrm{T}} \bar{\mathbf{S}}^{\mathrm{T}} \bar{\boldsymbol{\sigma}}_k^n \mathrm{d}A\mathrm{d}\bar{z}$.

It should be noted that although the equilibrium equation is satisfied at this stage, i.e. $\left\|\Delta\bar{\mathbf{R}}_k^n\right\| < \varepsilon_{tol}$, the results are not accepted unless the complementary force vector is smaller than a predefined tolerance, i.e. $\left\|\Delta\mathbf{F}_k^n\right\| < \varepsilon_{tol}$, which is the aforementioned second criterion of convergence.

2.7. The Iterative Global-local Method for non-uniform bending conditions

2.7.1. Introduction

The Iterative Global-local Method in its original formulation (Erkmen 2013) is applicable to elements under loading conditions that result in a uniform internal bending action only. In order to overcome this restriction and make the method applicable for general loading conditions, the kinematical assumptions of the problem are revisited in this section and required modifications are made by including higher order displacement

terms. Numerical examples are then presented in order to demonstrate the accuracy of the proposed formulation (Erkmen & Afnani 2014).

2.7.2. Formulation

In order to overcome the deficiency of the Iterative Global-local Method in dealing with cases with non-uniform internal bending conditions, the kinematic assumptions of the adopted thin-walled theory is modified to include second-order displacement terms according to Trahair (1993). The normal strain in an arbitrary point on the cross section can be obtained as

$$\varepsilon_p = w_p' + 0.5\left(u_p'^2 + v_p'^2\right) \tag{2.109}$$

where u_p, v_p and w_p are displacements of the point with respect to *x*, *y* and *z* axes, respectively, (Figure 2.8), and $\square'$ denotes the derivative with respect to the axis of the beam (i.e. z axis) . The displacement along the *z* axis was considered by Erkmen (2013) as

$$w_p = w - xu' - yv' - \omega\phi' \tag{2.110}$$

which included the first order terms only. The second-order terms can be added to obtain (Trahair 1993)

$$w_p = w - xu' - yv' - \omega\phi' + \left(-xv'\phi + yu'\phi\right) \tag{2.111}$$

The new identity for w_p is now replaced in Eq. (2.109) to obtain the normal strain. While the linear part of the strain vector (i.e. $\overline{\boldsymbol{\chi}}_L$, Eq. **(2.12)**) remains unchanged, two

elements in the nonlinear strain vector are affected by this modification, which change the $\bar{\boldsymbol{\chi}}_N$ vector to

$$\bar{\boldsymbol{\chi}}_N{}^{\mathrm{T}}=\left\langle \frac{1}{2}\left(\bar{u}'^2+\bar{v}'^2\right)-a_x\bar{v}'\bar{\phi}'+a_y\bar{u}'\bar{\phi}'+\frac{1}{2}\left(a_x{}^2+a_y{}^2\right)\bar{\phi}'^2 \quad \boxed{\bar{v}''\bar{\phi}}+a_x\bar{\phi}'^2 \quad \boxed{-\bar{u}''\bar{\phi}}+a_y\bar{\phi}'^2 \quad 0 \quad \frac{1}{2}\bar{\phi}'^2 \quad 0 \right\rangle \tag{2.112}$$

The difference between Eqs. (2.112) and (2.13) is in the 2nd and 3rd elements, where $-\bar{v}'\bar{\phi}'$ and $\bar{u}'\bar{\phi}'$ are replaced by $\bar{v}''\bar{\phi}$ and $-\bar{u}''\bar{\phi}$, respectively (placed in the box symbol $\square$). As a result, the formulation of the beam element, and consequently, the iterative global-local formulation are affected.

This change in the kinematic assumption results in a modification of the constraint applied to the local shell element nodal displacements of the global-local model through the decomposition matrix $\mathbf{N}$. Previously, the matrix $\mathbf{N}$ did not contain displacement terms and was solely obtained from cross-sectional properties and interpolation functions. However, inclusion of the second-order displacement terms changes the decomposition matrix to

$$\mathbf{N}=\begin{bmatrix} \mathbf{L}^{\mathrm{T}} & -\bar{x}\dfrac{\mathrm{d}\mathbf{H}^{\mathrm{T}}}{\mathrm{d}\bar{z}} & -\bar{y}\dfrac{\mathrm{d}\mathbf{H}^{\mathrm{T}}}{\mathrm{d}\bar{z}} & -\bar{\omega}\dfrac{\mathrm{d}\mathbf{H}^{\mathrm{T}}}{\mathrm{d}\bar{z}}+\boxed{\left(-xv'+yu'\right)\mathbf{H}^{\mathrm{T}}} \\ \mathbf{0} & \mathbf{H}^{\mathrm{T}} & \mathbf{0} & -\left(\bar{y}-a_y\right)\mathbf{H}^{\mathrm{T}} \\ \mathbf{0} & \dfrac{\mathrm{d}\mathbf{H}^{\mathrm{T}}}{\mathrm{d}\bar{z}} & \mathbf{0} & -\left(\bar{y}-a_y\right)\dfrac{\mathrm{d}\mathbf{H}^{\mathrm{T}}}{\mathrm{d}\bar{z}} \\ \mathbf{0} & \mathbf{0} & \mathbf{H}^{\mathrm{T}} & \left(\bar{x}-a_x\right)\mathbf{H}^{\mathrm{T}} \\ \mathbf{0} & \mathbf{0} & -\dfrac{\mathrm{d}\mathbf{H}^{\mathrm{T}}}{\mathrm{d}\bar{z}} & -\left(\bar{x}-a_x\right)\dfrac{\mathrm{d}\mathbf{H}^{\mathrm{T}}}{\mathrm{d}\bar{z}} \\ \mathbf{0} & \mathbf{0} & \mathbf{0} & -\mathbf{H}^{\mathrm{T}} \end{bmatrix} \tag{2.113}$$

where the newly added term is placed in a box ($\boxed{\ }$). It should be noted that the new decomposition matrix includes displacement terms u' and v', and therefore, the variation of the decomposition matrix $\delta\mathbf{N}$ would no longer vanish. Consequently, the variation of the displacement vector of the local shell model $\delta\hat{\mathbf{d}}$ would change to

$$\delta\hat{\mathbf{d}} = \mathbf{N}\delta\bar{\mathbf{d}} + \delta\mathbf{d}' + \boxed{\bar{\mathbf{d}}\delta\mathbf{N}} \tag{2.114}$$

We define a matrix $\mathbf{A}$ such that $\mathbf{A}\delta\bar{\mathbf{d}} = \mathbf{N}\delta\bar{\mathbf{d}} + \bar{\mathbf{d}}\delta\mathbf{N}$, the derivation of which is shown explicitly in Appendix 2.B.

2.7.3. Applications

In order to ensure the accuracy of the proposed formulation for the analysis of a thin-walled beam undergoing non-uniform bending conditions, three numerical examples are prepared in this section. In all the cases, the results from the iterative global-local procedure are compared with those of the full shell-type model for verification purposes. The full shell-type model is prepared by modelling the whole domain of the structure by the shell elements discussed in Chapter 3. The finite element mesh is taken to be similar in size to the mesh used for the local shell region in the iterative global-local model.

In order to ensure that the beam-type analysis is kinematically equivalent to the shell model, the comparison with the constraint shell solution is also presented. The constraint shell model is obtained by applying multiple-point constraints on the nodal displacement of the shell model based on the decomposition matrix $\mathbf{N}$, which is developed based on the kinematics of the thin-walled beam theory. Comparing the results of the constraint shell model and the beam model we can verify that the

modelling of the structure is equivalent for the two (in terms of, for example loading and boundary conditions).

2.7.3.1. Lateral buckling analysis of a simply-supported I-beam under linear moment gradient

The lateral-torsional buckling of a simply-supported doubly-symmetric I-beam is analysed in this section. The geometry, loading and boundary conditions of the beam are shown in Figure 2.17.

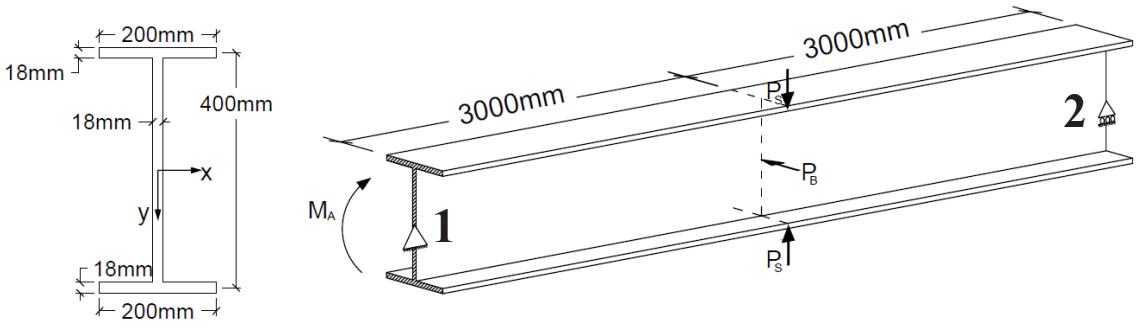

(a) Cross-section (b) Loading and boundary conditions

Figure 2.17: Layout of the simply-supported beam under moment gradient

The cross-sectional dimensions of the beam can be seen in Figure 2.17 (a). The beam has a span of $L = 6000mm$, and the material is structural steel $E = 200GPa$ and $G = 70GPa$.

The beam is analysed using the beam element, the shell element, the constraint shell model and the global-local model. The beam model is constructed by using elements with one meter length. The shell model is obtained by using two shell elements for the web and one element for each half flange, and dividing the axis of the beam into 30

pieces (Figure 2.18), which results in shell elements of $200mm \times 200mm$ and $100mm \times 200mm$ along the web and flanges, respectively.

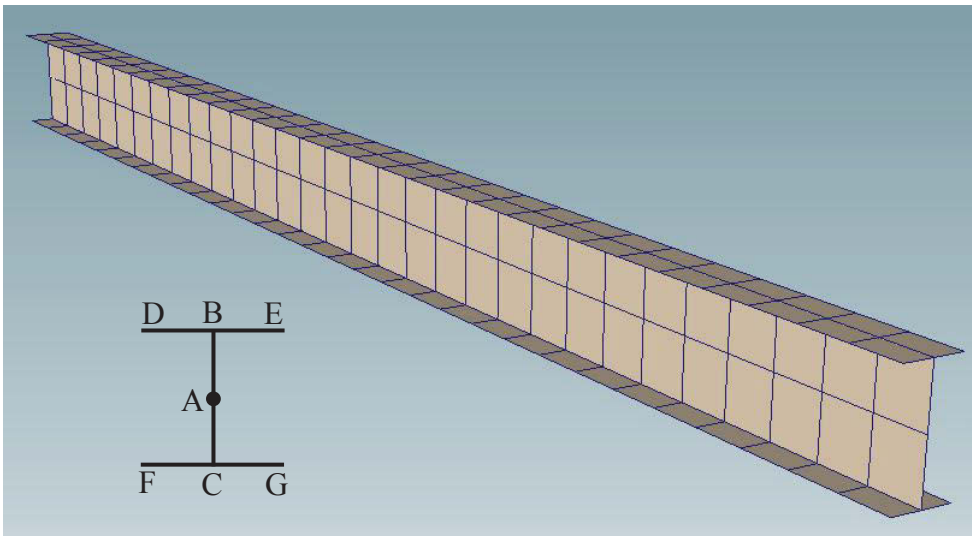

Figure 2.18: Finite element mesh of the shell model

In order to simulate the boundary conditions of Figure 2.17 in the beam model, the left-hand side end of the member (i.e. point 1) is restrained for translations along *x*, *y* and *z* directions and rotation around *z*-axis (twist), and the other end (i.e. point 2) is supported in *x* and *y* directions and twist rotation (i.e. $u_1 = v_1 = w_1 = \phi_1 = u_2 = v_2 = \phi_2 = 0$).

Equivalent boundary conditions are imposed on the shell model. In end 1, node A is fixed in the axial direction, nodes A, B and C are fixed in the lateral (*x* direction) and nodes A, D, E, F and G are fixed in the vertical direction, which is equivalent to $w_{1,A} = 0$, $u_{1,A} = u_{1,B} = u_{1,C} = 0$ and $v_{1,A} = v_{1,D} = v_{1,E} = v_{1,F} = v_{1,G} = 0$ (Figure 2.18). The fixities are the same at end 2 except for the axial direction where no node is fixed $(u_{2,A} = u_{2,B} = u_{2,C} = 0$, $v_{2,A} = v_{2,D} = v_{2,E} = v_{2,F} = v_{2,G} = 0)$.

The simply-supported beam is subjected to a concentrated bending moment at one end, resulting in a linear bending moment gradient. Since imperfections are not introduced to

the finite element model, the buckling can never occur under the applied bending moment only. In other word, the beam may pass the bifurcation point and follow the unstable equilibrium path because the geometry, loading and boundary conditions are ideal and exact. In order to overcome this problem, a buckling eigenvalue analysis is performed prior to the nonlinear analysis in order to obtain the critical buckling mode. The first mode, which is of lateral-torsional buckling type, is shown in Figure 2.19.

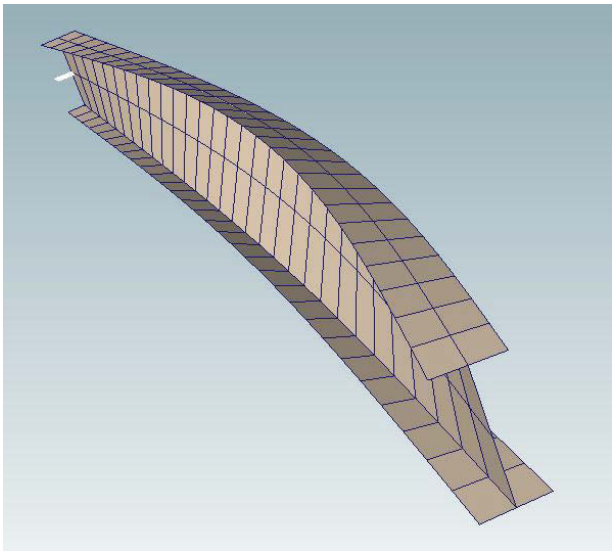

Figure 2.19: 1st buckling mode of the simply-supported thin-walled beam

In order to activate this buckling mode in the nonlinear analysis, a small horizontal load $P_B = 0.01kN$ (Figure 2.17) is applied at the mid-span of the beam. It should be noted that applying small loads for activation of buckling mode is commonplace in the literature (e.g. (Pi et al. 2007)).

At this stage, the load couple P_S in Figure 2.17 is not applied. The load-displacement curves are plotted in Figure 2.20 for lateral displacements at the bottom web-flange intersection at mid-span in the absence of a local deformation (i.e. $M_A = 875kNm$,

$P_B = 0.01kN$ and $P_S = 0$). It can be seen that there is an acceptable agreement between the different models at this stage.

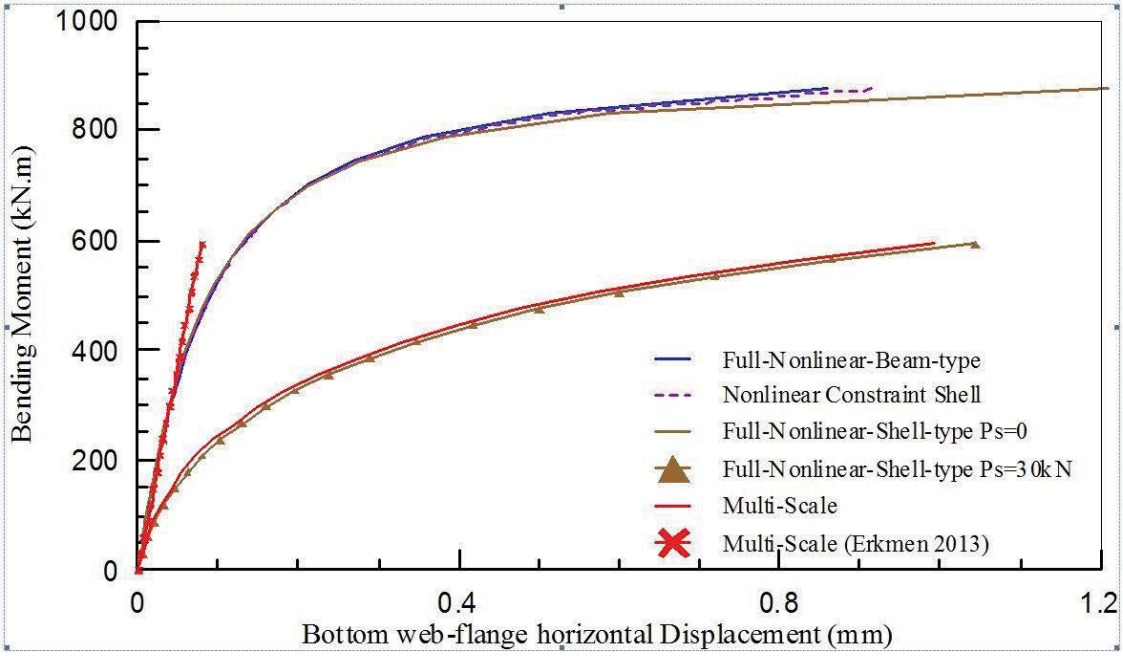

Figure 2.20: Load-deflection relations based on different modelling types

In the second stage, in order to illustrate the efficiency of the iterative global-local approach, local deformations are applied through a force couple at the tip of flanges at the mid-span in addition to the previous loadings (i.e. $M_A = 875kNm$, $P_B = 0.01kN$ and $P_S = 30kN$). This load couple has no resultant at the cross-sectional level and therefore, its effect cannot be captured by the beam element, which is formulated according to the rigid cross-sectional assumption. Consequently, the results of the beam and the constraint shell are not altered after the application of the load couple (Figure 2.20). However, the load couple has a significant effect on the result of the shell model. It causes a softening in the load-displacement curve and decreases the overall lateral torsional buckling load of the member.

The problem is also modelled by using the Iterative Global-local Method, in which the local shell is placed in the vicinity of the localized behaviour (from $z = 1400mm$ to $z = 4600mm$) as can be seen in Figure 2.21.

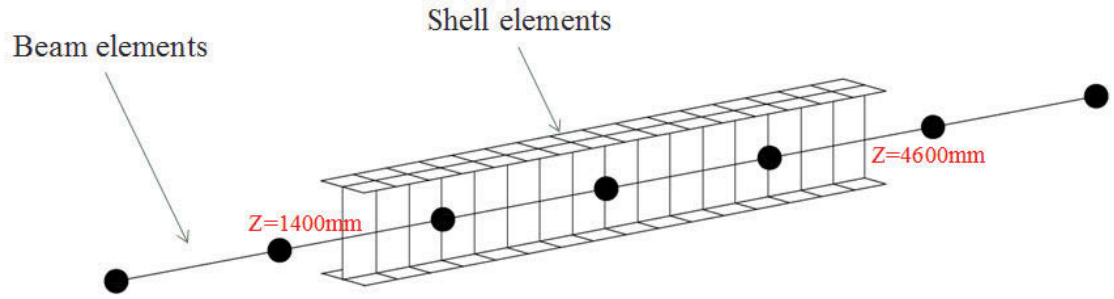

Figure 2.21: Schematic of the global-local model

It can be confirmed from Figure 2.20 that the proposed iterative global-local technique has been able to accurately capture the softening effect of the localized behaviour on the global response of the beam. It should be noted that the shell elements within the overlapping region include approximately half the shell elements used in the full-shell model, indicating the efficiency and the accuracy of the proposed method. It can also be seen that solution in Erkmen (2013) cannot accurately capture cases with moment gradient and thus, current modifications are required.

2.7.3.2. Lateral buckling analysis of a simply-supported I-beam under mid-span load

The same geometry, boundary conditions and material properties as the previous example are used in this model, only the concentrated moment is replaced by a concentrated vertical load at the mid-span. The finite elements used are also identical to the previous case.

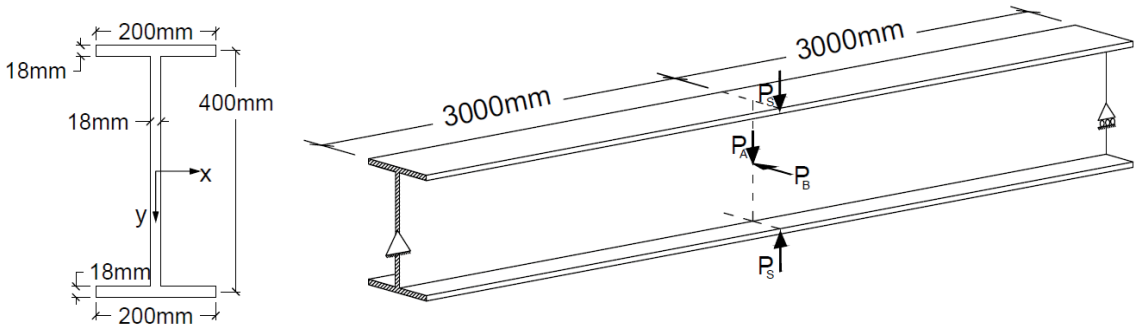

(a) Cross-section (b) Loading and boundary conditions

Figure 2.22: Layout of the simply-supported beam under mid-span point load

As in the previous example, the analyses are performed in two stages. Firstly, the vertical point load is applied with a small horizontal load to create a small imperfection, (i.e., $P_A = 434kNm,\ P_B = 0.1kN$ and $P_s = 0$). Similar to the previous example, an eigenvalue analysis is performed in order to determine the critical buckling mode of the beam and the imperfections are then introduced in line with that mode. Secondly, local deformations are introduced in terms of a load couple of $P_s = 70kN$ with opposite direction at the tip of the flanges at mid-span. As illustrated in Figure 2.23, there is a significant softening effect, captured by the shell model while the beam and the constraint shell remain unchanged.

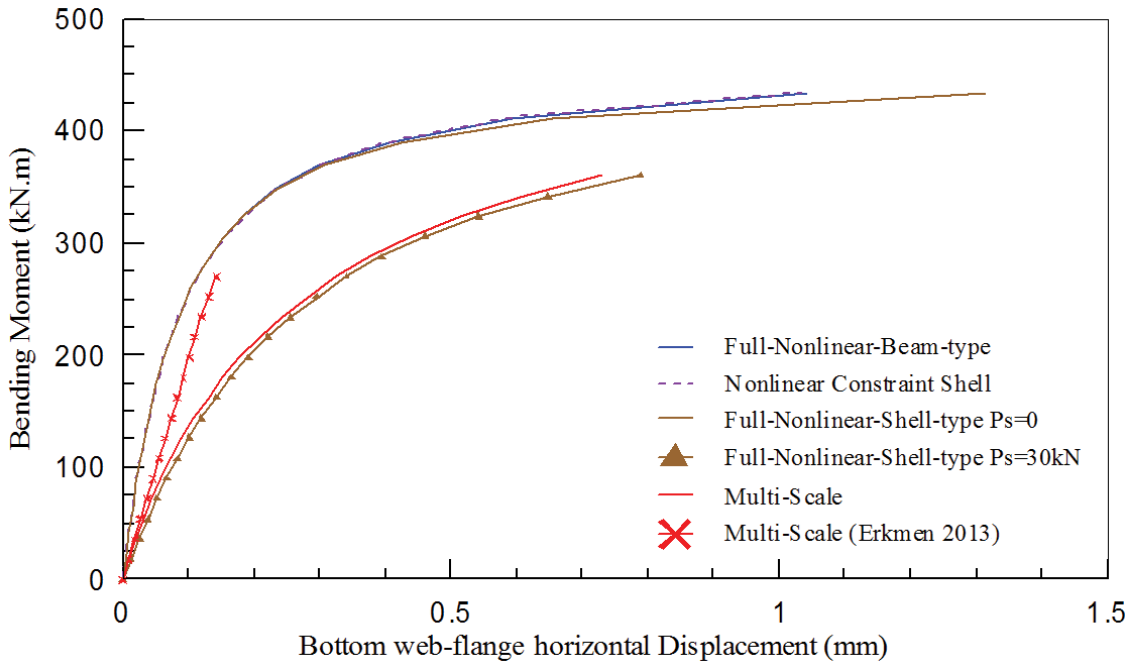

Figure 2.23: Load-deflection curves based on different modelling types

Again it can be observed that by approximately half the shell elements used in the shell model, the iterative global-local technique is capable of capturing the behaviour accurately. It should be noted that the overlapping region is from *z=1400mm* to *z=4600mm*. The answer obtained based on Erkmen (2013) is significantly different since the moment gradient effects were not included.

2.7.3.3. Lateral buckling analysis of a continuous beam

In this example a continuous beam with two spans is analysed, the spans, geometrical and boundary conditions of which are shown in Figure 2.24.

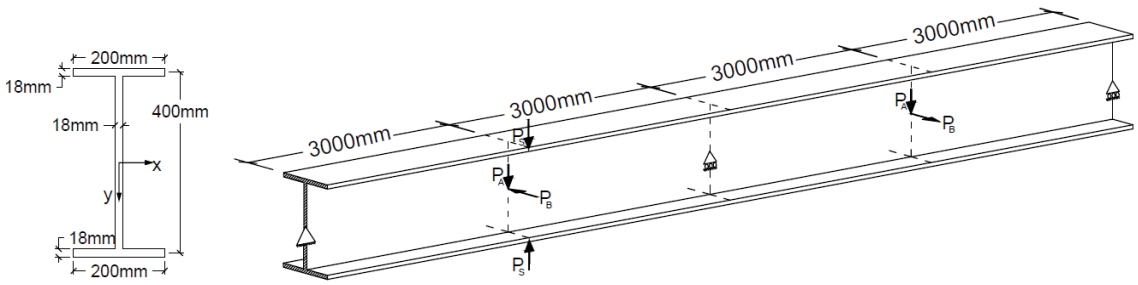

(a) Cross-section (b) Loading and boundary conditions

Figure 2.24: Layout of the continuous beam

The material and cross-sectional properties and the finite elements sizes are the same as the previous examples. Two vertical loads are applied at the middle of each of the spans along with two small horizontal loads that act as small imperfections in order to activate the lateral buckling behaviour. It can be observed from Figure 2.24 that this load couple are applied in opposite directions, which is based on the eigenvalue analysis that is performed prior to the nonlinear analysis. It was observed that the 1st buckling mode of the beam included lateral-torsional deflections of the two spans in opposite directions, and the buckling activator load couple are applied accordingly.

Similar to the previous examples, the analyses are performed in two stages: Firstly, the results are found according to the aforementioned loading ($P_A = 742kN$, $P_B = 0.1kN$ and $P_s = 0$). It can be observed from load-deformations curves (Figure 2.25) that there is a complete agreement between the beam, shell and constraint shell model at this stage. Secondly, local deformations are introduced in terms of a load couple applied at the tip of the flanges at the middle of one of the spans with a magnitude of *73.75kN*.

Since the load couple has no projection at the cross-sectional level, the results of the beam and constraint shell model are not affected by them. On the other hand, the behaviour of the beam changes significantly in the shell solution, which is captured by the global-local model accurately according to the load-deformation curves for the first and second span. It should be noted that even though the overlapping region is from $z=1400mm$ to $z=4600mm$ (i.e. at the vicinity of the local deformations only), the behaviour is captured accurately at the opposite span (i.e. $z=9000mm$) as well.

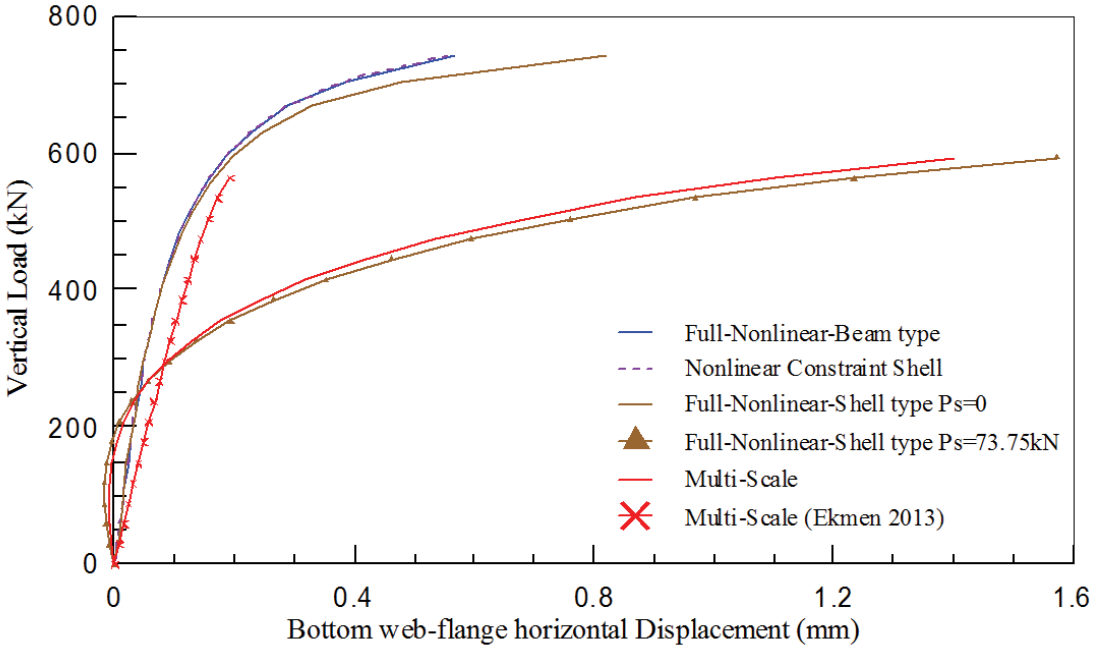

(a) Displacements at Z = 3000mm (the place of local deformations)

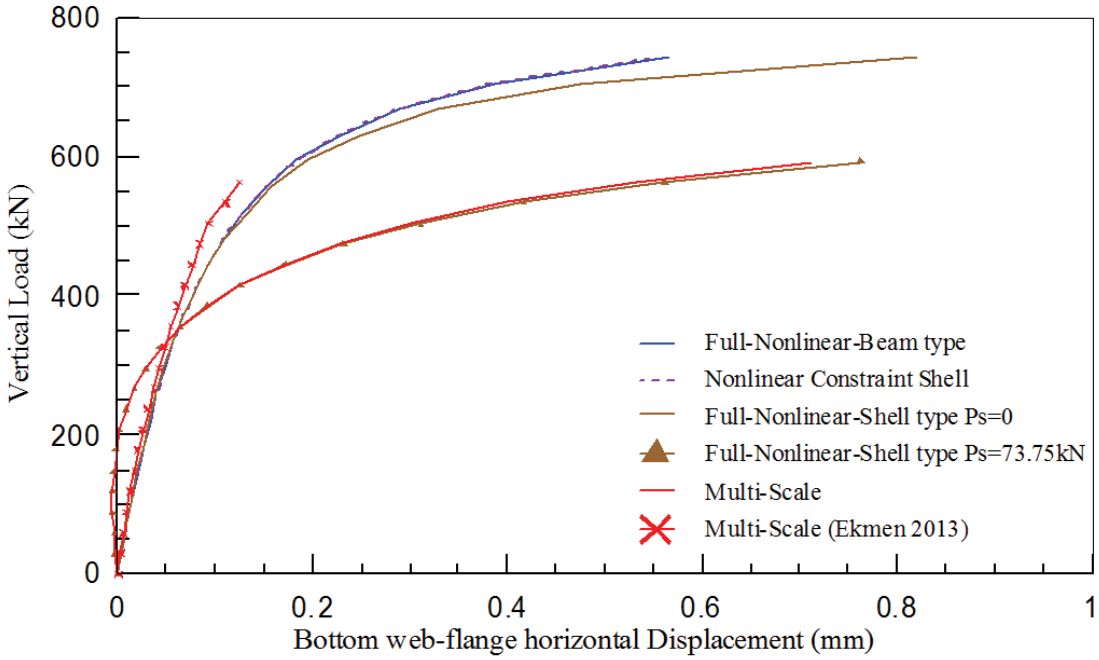

(b) Displacements at Z = 9000mm

Figure 2.25: Load-deflection curves based on different modelling types

In comparison to the previous examples, the current example clearly demonstrates the efficiency of the proposed Iterative Global-local Method when a localized behaviour is expected in a relatively large structure. In the present example, the effect of local deformation on the global response is captured accurately by placing approximately a quarter of the shell elements compared with the full-shell model. It can be argued that the efficiency of the proposed Iterative Global-local Method increases with the increase in the size of the structure. For instance, should a localized behaviour be expected in a particular element of a structural system with numerous members, the use of this method obviates the necessity of detailed modelling of the whole large structure and focuses solely on the critical regions.

Figure 2.25 (b) shows the load-displacement curves at $z=9000mm$, which is the span opposite the location of the local deformation. It can be observed that although the overlapping shell elements were placed where the localized behaviour existed (i.e. the 1st span), the effect of the local deformations is well captured in the 2nd span as well. It confirms that if a sufficiently large overlapping region in utilized, the effect on the other structural elements can be captured equally well.

2.8. Conclusions

In this chapter, the Iterative Global-local Method was introduced as a powerful tool in the analysis of thin-walled members. It is discussed that the method allows the consideration of the effect of localised behaviour on the global response of a thin-walled structural system without necessitating the use of computationally expensive finite elements throughout the structural domain. It is argued that the procedure is most advantageous when abrupt local/cross-sectional deformation exist in a relatively short

span of the element. The preliminaries of the method are discussed in detail and the solution algorithm is presented. It is then demonstrated that the original formulation of the Iterative Global-local Method was applicable for members under uniform internal moment actions, a limitation which is overcome herein by modifying the kinematical assumption of the adopted overlapping decomposition operator. Corresponding numerical examples are then presented in order to illustrate the accuracy of the modified formulation in the analysis of members under general loading conditions.

In the coming chapters, further modifications to the method will be suggested in order to make the Iterative Global-local Method applicable to a larger range of structural geometry and material behaviour.

2.9. References

Akhtar, M.N. 1987, 'Element stiffness of circular member', *Journal of structural engineering New York, N.Y.*, vol. 113, no. 4, pp. 867-72.

Allman, D.J. 1984, 'A compatible triangular element including vertex rotations for plane elasticity analysis', *Computers and Structures*, vol. 19, no. 1-2, pp. 1-8.

Argyris, J.H., Papadrakakis, M. & Karapitta, L. 2002, 'Elasto-plastic analysis of shells with the triangular element TRIC', *Computer Methods in Applied Mechanics and Engineering*, vol. 191, no. 33, pp. 3613-36.

Back, S.Y. & Will, K.M. 2008, 'Shear-flexible thin-walled element for composite I-beams', *Engineering Structures*, vol. 30, no. 5, pp. 1447-58.

Barbero, E.J. & Raftoyiannis, I.G. 1993, 'Local buckling of FRP beams and columns', *Journal of Materials in Civil Engineering*, vol. 5, no. 3, pp. 339-55.

Basler, K. & Kollbrunner, C.F. 1969, *Torsion in structures- An engineering approach*, Springer-Verlag, New York.

Bathe, K.J. & Almeida, C.A. 1980, 'Simple and effective pipe elbow element - linear analysis', *Journal of Applied Mechanics, Transactions ASME*, vol. 47, no. 1, pp. 93-100.

Bathe, K.J. & Almeida, C.A. 1982, 'Simple and effective pipe elbow element - interaction effects', *Journal of Applied Mechanics, Transactions ASME*, vol. 49, no. 1, pp. 165-71.

Batoz, J.L., Bathe, K.J. & Ho, L.W. 1980, 'Study of Three-node Triangular Plate Bending Elements', *International Journal for Numerical Methods in Engineering*, vol. 15, no. 12, pp. 1771-812.

Batoz, J.L. & Tahar, M.B. 1982, 'Evaluation of a new quadrilateral thin plate bending element', *INT J NUMER METHODS ENG*, vol. V 18, no. N 11, pp. 1655-77.

Bauld, N.R. & Tzeng, L.S. 1984, 'A Vlasov theory for fiber-reinforced beams with thin-walled open cross sections', *International Journal of Solids and Structures*, vol. 20, no. 3, pp. 277-97.

Bebiano, R., Silvestre, N. & Camotim, D. 2007, 'GBT formulation to analyze the buckling behavior of thin-walled members subjected to non-uniform bending', *International Journal of Structural Stability and Dynamics*, vol. 7, no. 1, pp. 23-54.

Bijlaard, P.P. & Fisher, G.P. 1953, *Column Strength of H-Sections and Square Tubes in Post-Buckling Range of Component Plates*, NACA, Washington, D.C, TN 2994.

Bleich, F. 1952, *Buckling Strength of Metal Structures*, McGraw-Hill, New York.

Boresi, A.P. & Sidebottom, O.M. 1985, *Advanced Mechanics of Materials*, Fourth edn, John Wiley & Sons, New York, USA.

Bradford, M.A. 1994, 'Buckling of post-tensioned composite beams', *Structural Engineering and Mechanics*, vol. 2, no. 1, pp. 113-23.

Bradford, M.A. & Ronagh, H.R. 1997, 'Generalized elastic buckling of restrained I-beams by FEM', *Journal of Structural Engineering*, vol. 123, no. 12, pp. 1631-7.

Bradford, M.A. & Trahair, N.S. 1981, 'Distortional buckling of I-beams', *ASCE J Struct Div*, vol. 107, no. 2, pp. 355-70.

Brookhart, G.C. 1967, 'Circular-arc I-type girders', *American Socienty for Civil Engineers*, vol. 93.

Bryan, G.H. 1891, 'On the Stability of Plane Plate under Thrust in its Own Plane with Applications on the Buckling of the Sides of a Ship', *London Mathematical Society*, vol. 22, p. 54.

Bulson, P.S. 1967, 'Local Stability and Strength of Structural Sections', *Thin-walled Structures*, pp. 153-207.

Cardoso, J.E.B., Benedito, N.M.B. & Valido, A.J.J. 2009, 'Finite element analysis of thin-walled composite laminated beams with geometrically nonlinear behavior including warping deformation', *Thin-Walled Structures*, vol. 47, no. 11, pp. 1363-72.

Carrera, E. & Petrolo, M. 2012, 'Refined beam elements with only displacement variables and plate/shell capabilities', *Meccanica*, vol. 47, no. 3, pp. 537-56.

Chajes, A. & Winter, G. 1965, 'Torsional Buckling of Thin-Walled Members', *Journal of Structural Division, ASCE*, vol. 91, no. ST4, pp. 103-25.

Cheung, Y.K. 1976, *Finite Strip Method in Structural Analysis*, Pregamon Press, New York.

Cook, R.D. 1986, 'On the allman triangle and a related quadrilateral element', *Computers and Structures*, vol. 22, no. 6, pp. 1065-7.

Cook, R.D. 1990, 'Simulating curved elements by offsets. Rationale and application to shells of revolution', *Engineering computations*, vol. 7, no. 1, pp. 79-80.

Cook, R.D., Malkus, D.S. & Plesha, M.E. 1989, *Concepts and applications of finite element analysis*, Wiley, New York.

Cook, R.D., Malkus, D.S., Plesha, M.E. & Witt, R.J. 2002, *Concepts and applications of finite element analysis*, fourth edn, John Wiley & Sons.

Crisfield, M.A. 1990, 'A consistent co-rotational formulation for non-linear, three-dimensional, beam-elements', *Computer Methods in Applied Mechanics and Engineering*, vol. 81, no. 2, pp. 131-50.

Crisfield, M.A. 1991, *Non-linear finite element analysis of solids and structures*, vol. 1, Wiley, New York.

Davids, A.J. & Hancock, G.J. 1987, 'Nonlinear elastic response of locally buckled thin-walled beam-columns', *Thin-Walled Structures*, vol. 5, no. 3, pp. 211-26.

Dekker, N.W. & Kemp, A.R. 1998, 'A simplified distortional buckling model for doubly symmetrical l-sections', *Canadian Journal of Civil Engineering*, vol. 25, no. 4, pp. 718-27.

DeWolf, J.T., Pekoz, T. & Winter, T. 1974, 'Local and overall buckling of cold-formed members', *ASCE J Struct Div*, vol. 100, no. 10, pp. 2017-36.

Dinis, P.B., Camotim, D. & Silvestre, N. 2006, 'GBT formulation to analyse the buckling behaviour of thin-walled members with arbitrarily 'branched' open cross-sections', *Thin-Walled Structures*, vol. 44, no. 1, pp. 20-38.

Eisenberger, M. 2003, 'An exact high order beam element', *Computers and Structures*, vol. 81, no. 3, pp. 147-52.

El-Amin, F.M. & Brotton, D.M. 1976, 'Horizontally curved beam finite element including warping', *International Journal for Numerical Methods in Engineering*, vol. 10, no. 6, pp. 1397-406.

El-Amin, F.M. & Kasem, M.A. 1978, 'Higher-order horizontally-curved beam finite element including warping for steel bridges', *International Journal for Numerical Methods in Engineering*, vol. 12, no. 1, pp. 159-67.

Erkmen, R.E. 2013, 'Bridging multi-scale approach to consider the effects of local deformations in the analysis of thin-walled members', *Computational Mechanics*, vol. 52, no. 1, pp. 65-79.

Erkmen, R.E. & Afnani, A. 2014, 'Bridging multi-scale method to consider the effects of local deformations in the analysis of composite thin-walled members', *11th World Congress on Computational Mechanics, WCCM 2014, 5th European Conference on Computational Mechanics, ECCM 2014 and 6th European Conference on Computational Fluid Dynamics, ECFD 2014*, pp. 3450-61.

Erkmen, R.E. & Bradford, M.A. 2009, 'Nonlinear elasto-dynamic analysis of I-beams curved in-plan', *International Journal of Structural Stability and Dynamics*, vol. 9, no. 2, pp. 213-41.

Fan, S.C. & Cheung, Y.K. 1983, 'Analysis of shallow shells by spline finite strip method', *Engineering Structures*, vol. 5, no. 4, pp. 255-63.

Feyel, F. 2003, 'A multilevel finite element method (FE2) to describe the response of highly non-linear structures using generalized continua', *Computer Methods in Applied Mechanics and Engineering*, vol. 192, no. 28–30, pp. 3233-44.

Fish, J., Markolefas, S., Guttal, R. & Nayak, P. 1994, 'On adaptive multilevel superposition of finite element meshes for linear elastostatics', *Applied Numerical Mathematics*, vol. 14, no. 1-3, pp. 135-64.

Fraternali, F. & Feo, L. 2000, 'On a moderate rotation theory of thin-walled composite beams', *Composites Part B: Engineering*, vol. 31, no. 2, pp. 141-58.

Frey, F. 1989, 'Shell finite elements with six degrees of freedom per node', *Presented at the Winter Annual Meeting of the ASME*, San Francisco, CA, USA, pp. 291-316.

Fukumoto, Y. & Nishida, S. 1981, 'Ultimate load behavior of curved I-beams', *ASCE J Eng Mech Div*, vol. 107, no. 2, pp. 367-85.

Geers, M.G.D., Kouznetsova, V.G. & Brekelmans, W.A.M. 2010, 'Multi-scale computational homogenization: Trends and challenges', *Journal of Computational and Applied Mathematics*, vol. 234, no. 7, pp. 2175-82.

Gendre, L., Allix, O., Gosselet, P. & Comte, F. 2009, 'Non-intrusive and exact global/local techniques for structural problems with local plasticity', *Computational Mechanics*, vol. 44, no. 2, pp. 233-45.

Grenier, R., Ofner, R. & Salzberger, G. 1999, 'Lateral torsional buckling of beam columns: Theoretical Background', *ECCS-Validation group,*, vol. report 5.

Hancock, G.J. 1981, 'Non-Linear Analysis of Thin Sections in Compression', *Journal of the Structural Division: Proceedings of the ASCE*, vol. 107, no. ST3, pp. 455-71.

Hancock, G.J., Bradford, M.A. & Trahair, N.S. 1980, 'Web distortion and flexural-torsional buckling', *ASCE J Struct Div*, vol. 106, no. 7, pp. 1557-71.

Hancock, G.J., Kwon, Y.B. & Stefan Bernard, E. 1994, 'Strength design curves for thin-walled sections undergoing distortional buckling', *Journal of Constructional Steel Research*, vol. 31, no. 2-3, pp. 169-86.

Hirai, I., Uchiyama, Y., Mizuta, Y. & Pilkey, W.D. 1985, 'An exact zooming method', *Finite Elements in Analysis and Design*, vol. 1, no. 1, pp. 61-9.

Hobbs, R.E. 1981, 'Pipeline buckling caused by axial loads', *Journal of Constructional Steel Research*, vol. 1, no. 2, pp. 2-10.

Houliara, S. & Karamanos, S.A. 2006, 'Buckling and post-buckling of long pressurized elastic thin-walled tubes under in-plane bending', *International Journal of Non-Linear Mechanics*, vol. 41, no. 4, pp. 491-511.

Houliara, S. & Karamanos, S.A. 2010, 'Stability of long transversely-isotropic elastic cylindrical shells under bending', *International Journal of Solids and Structures*, vol. 47, no. 1, pp. 10-24.

Hughes, T.J.R. & Brezzi, F. 1989, 'On drilling degrees of freedom', *Computer Methods in Applied Mechanics and Engineering*, vol. 72, no. 1, pp. 105-21.

Hughes, T.J.R. & Sangalli, G. 2007, 'Variational multiscale analysis: The fine-scale green's function, projection, optimization, localization, and stabilized methods', *SIAM Journal on Numerical Analysis*, vol. 45, no. 2, pp. 539-57.

Ibrahimbegovic, A., Taylor, R.L. & Wilson, E.L. 1990, 'Robust quadrilateral membrane finite element with drilling degrees of freedom', *International Journal for Numerical Methods in Engineering*, vol. 30, no. 3, pp. 445-57.

Iura, M. & Atluri, S.N. 1988, 'On a consistent theory, and variational formulation of finitely stretched and rotated 3-D space-curved beams', *Computational Mechanics*, vol. 4, no. 2, pp. 73-88.

Jin, L. 1994, 'Analysis and Evaluation of a Shell Finite Element with Drilling Degree of Freedom', Master thesis, University of Maryland at College Park.

Jones, R.M. 1975, *Mechanics of composite materials*, McGraw-Hill, New York.

Jönsson, J. 1999, 'Distortional theory of thin-walled beams', *Thin-Walled Structures*, vol. 33, no. 4, pp. 269-303.

Ju, G.T. & Kyriakides, S. 1992, 'Bifurcation and localization instabilities in cylindrical shells under bending-II. Predictions', *International Journal of Solids and Structures*, vol. 29, no. 9, pp. 1143-71.

Karamanos, S.A. 2002, 'Bending instabilities of elastic tubes', *International Journal of Solids and Structures*, vol. 39, no. 8, pp. 2059-85.

Karamanos, S.A. & Tassoulas, J.L. 1996, 'Tubular members. I: Stability analysis and preliminary results', *Journal of Engineering Mechanics*, vol. 122, no. 1, pp. 64-71.

Kim, N.I., Shin, D.K. & Kim, M.Y. 2007, 'Exact lateral buckling analysis for thin-walled composite beam under end moment', *Engineering Structures*, vol. 29, no. 8, pp. 1739-51.

Knight Jr, N.F., Ransom, J.B., Griffin Jr, O.H. & Thompson, D.M. 1991, 'Global/local methods research using a common structural analysis framework', *Finite Elements in Analysis and Design*, vol. 9, no. 2, pp. 91-112.

Koiter, W.T. 1984, 'Complementary energy, neutral equilibrium and buckling', *Meccanica*, vol. 19, no. 1 Supplement, pp. 52-6.

Krenk, S. 1994, 'A general format for curved and non-homogeneous beam elements', *Computers and Structures*, vol. 50, no. 4, pp. 449-54.

Kwon, Y.B. & Hancock, G.J. 1991, *Strength tests of cold-formed channel sections undergoing local and distortional buckling*.

Lau, S.C.W. & Hancock, G.J. 1986, 'Buckling of thin flat-walled structures by a spline finite strip method', *Thin-Walled Structures*, vol. 4, no. 4, pp. 269-94.

Lau, S.C.W. & Hancock, G.J. 1987, 'Distortional buckling formulas for channel columns', *Journal of structural engineering New York, N.Y.*, vol. 113, no. 5, pp. 1063-78.

Lee, D.J. 1978, 'Local buckling coefficient for orthotropic structural sections', *Aeronautical Journal*, vol. 82, no. 811, pp. 313-20.

Lee, J. 2006, 'Lateral buckling analysis of thin-walled laminated composite beams with monosymmetric sections', *Engineering Structures*, vol. 28, no. 14, pp. 1997-2009.

Lee, J., Kim, S.E. & Hong, K. 2002, 'Lateral buckling of I-section composite beams', *Engineering Structures*, vol. 24, no. 7, pp. 955-64.

Liew, R.J.Y., Thevendran, V., Shanmugam, N.E. & Tan, L.O. 1995, 'Behaviour and design of horizontally curved steel beams', *Journal of Constructional Steel Research*, vol. 32, no. 1, pp. 37-67.

Lim, N.H., Park, N.H., Kang, Y.J. & Sung, I.H. 2003, 'Elastic buckling of I-beams under linear moment gradient', *International Journal of Solids and Structures*, vol. 40, no. 21, pp. 5635-47.

Liu, W.K., Hao, S., Belytschko, T., Li, S. & Chang, C.T. 2000, 'Multi-scale methods', *International Journal for Numerical Methods in Engineering*, vol. 47, no. 7, pp. 1343-61.

Liu, W.K., Uras, R.A. & Chen, Y. 1997, 'Enrichment of the finite element method with the reproducing kernel particle method', *Journal of Applied Mechanics, Transactions ASME*, vol. 64, no. 4, pp. 861-70.

Liu, Y.J., Sun, Q. & Fan, X.L. 2014, 'A non-intrusive global/local algorithm with non-matching interface: Derivation and numerical validation', *Computer Methods in Applied Mechanics and Engineering*, vol. 277, pp. 81-103.

Love, A.E.H. 1944, *A Treatise on the Mathematical Theory of Elasticity*, 4th edn, Dover Publications Inc., New York.

Lundquist, E.E., Stowell, E.Z. & Schutte, E.H. 1943, *Principles of Moment Distribution Applied to Stability of Structures Composed of Bars or Plates*, 809, NACA.

Ma, M. & Hughes, O. 1996, 'Lateral distortional buckling of monosymmetric I-beams under distributed vertical load', *Thin-Walled Structures*, vol. 26, no. 2, pp. 123-43.

Machado, S.P. 2010, 'Interaction of combined loads on the lateral stability of thin-walled composite beams', *Engineering Structures*, vol. 32, no. 11, pp. 3516-27.

MacNeal, R.H. 1994, *Finite elements: Their Design and Performance*, Marcel Dekker, New York.

Mahendran, M. & Murray, N.W. 1986, 'Elastic buckling analysis of ideal thin-walled structures under combined loading using a finite strip method', *Thin-Walled Structures*, vol. 4, no. 5, pp. 329-62.

Marguerre, K. 1939, 'Zur Theorie der Gekrümmten Platte Grosser Formänderung', *Fifth International Congress on Applied Mechanics*, J. Wiley and sons, Cambridge, Massachusetts, pp. 93-101.

Marques, J.M.M.C. 1984, 'Stress computation in elastoplasticity', *Engineering Computations (Swansea, Wales)*, vol. 1, pp. 42-51.

Militello, C. & Huespe, A.E. 1988, 'A displacement-based pipe elbow element', *Computers and Structures*, vol. 29, no. 2, pp. 339-43.

Mittelstedt, C. 2007, 'Local buckling of wide-flange thin-walled anisotropic composite beams', *Archive of Applied Mechanics*, vol. 77, no. 7, pp. 439-52.

Mote, C. 1971, 'Global ‐ local finite element', *International Journal for Numerical Methods in Engineering*, vol. 3, no. 4, pp. 565-74.

Mottram, J.T. 1992, 'Lateral-torsional buckling of thin-walled composite I-beams by the finite difference method', *Composites Engineering*, vol. 2, no. 2, pp. 91-104.

Murakami, H. & Yamakawa, J. 1996, 'On approximate solutions for the deformation of plane anisotropic beams', *Composites Part B: Engineering*, vol. 27, no. 5, pp. 493-504.

Murray, N.W. 1984, *Introduction to the theory of thin-walled structures*, Claredon Press, Oxford, United Kingdom.

Noor, A.K. 1986, 'Global-local methodologies and their application to nonlinear analysis', *Finite Elements in Analysis and Design*, vol. 2, no. 4, pp. 333-46.

Noor, A.K. & Peters, J.M. 1983, 'Recent advances in reduction methods for instability analysis of structures', *Computers and Structures*, vol. 16, no. 1-4, pp. 67-80.

Nowzartash, F. & Mohareb, M. 2004, 'An elasto-plastic finite element for steel pipelines', *International Journal of Pressure Vessels and Piping*, vol. 81, no. 12, pp. 919-30.

Ozkan, I.F. & Mohareb, M. 2009, 'Testing and analysis of steel pipes under bending, tension, and internal pressure', *Journal of Structural Engineering*, vol. 135, no. 2, pp. 187-97.

Pandey, M.D., Kabir, M.Z. & Sherbourne, A.N. 1995, 'Flexural-torsional stability of thin-walled composite I-section beams', *Composites Engineering*, vol. 5, no. 3, pp. 321-42.

Pantazopoulou, S.J. 1992, 'Low-order interpolation functions for curved beams', *Journal of Engineering Mechanics*, vol. 118, no. 2, pp. 329-50.

Petrolito, J. 1995, 'Stiffness analysis of beams using a higher-order theory', *Computers and Structures*, vol. 55, no. 1, pp. 33-9.

Pi, Y.-L., Bradford, M.A. & Uy, B. 2005, 'Nonlinear analysis of members curved in space with warping and Wagner effects', *International Journal of Solids and Structures*, vol. 42, no. 11–12, pp. 3147-69.

Pi, Y.L., Bradford, M.A. & Uy, B. 2003, *Nonlinear analysis of members with open thin-walled cross-section curved in space*, University of New South Wales, School of Civil and Environmental Engineering, Sydney.

Pi, Y.L., Bradford, M.A. & Uy, B. 2007, 'A rational elasto-plastic spatially curved thin-walled beam element', *International Journal for Numerical Methods in Engineering*, vol. 70, no. 3, pp. 253-90.

Pi, Y.L. & Trahair, N.S. 1997, 'Nonlinear elastic behavior of I-beams curved in plan', *Journal of Structural Engineering*, vol. 123, no. 9, pp. 1201-9.

Plank, R.J. & Wittrick, W.H. 1974, 'Buckling inder combined loading of thin, flat-walled structures by a complex finite strip method', *International Journal for Numerical Methods in Engineering*, vol. 8, no. 2, pp. 323-39.

Poon, C.P. & Ronagh, H.R. 2004, 'Distortional Buckling of I-Beams by Finite Element Method', *Advances in Structural Engineering*, vol. 7, no. 1, pp. 71-80.

Przemieniecki, J.S. 1973, 'Finite Element Structural Analysis of Local Instability', *AIAA*, vol. 11, no. 1, pp. 33-9.

Qian, D., Wagner, G.J. & Liu, W.K. 2004, 'A Multi-scale projection method for the analysis of carbon nanotubes', *Computer Methods in Applied Mechanics and Engineering Computations (Swansea, Wales)*, vol. 193, pp. 1603-32.

Qiao, P., Davalos, J.F. & Wang, J. 2001, 'Local buckling of composite FRP shapes by discrete plate analysis', *Journal of structural engineering New York, N.Y.*, vol. 127, no. 3, pp. 245-55.

Rasmussen, K.J.R. 1997, 'Bifurcation of locally buckled members', *Thin-Walled Structures*, vol. 28, no. 2, pp. 117-54.

Reddy, J.N. 2004, *Mechanics of Laminated Composite Plates and Shells: Theory and Analysis*, 2nd edn, CRC Press, Boca Raton, Florida.

Rendek, S. & Baláž, I. 2004, 'Distortion of thin-walled beams', *Thin-Walled Structures*, vol. 42, no. 2, pp. 255-77.

Rhodes, J. & Harvey, J.M. 1971, 'Plates in uniaxial compression with various support conditions at the unloaded boundaries', *International Journal of Mechanical Sciences*, vol. 13, no. 9, pp. 787-802.

Roberts, T.M. 2002, 'Influence of shear deformation on buckling of pultruded fiber reinforced plastic profiles', *Journal of Composites for Construction*, vol. 6, no. 4, pp. 241-8.

Roberts, T.M. & Jhita, P.S. 1983, 'Lateral, local and distortional buckling of I-beams', *Thin-Walled Structures*, vol. 1, no. 4, pp. 289-308.

Roberts, T.M. & Masri, H.M.K.J.A.H. 2003, 'Section properties and buckling behavior of pultruded FRP profiles', *Journal of Reinforced Plastics and Composites*, vol. 22, no. 14, pp. 1305-17.

Rusch, A. & Lindner, J. 2001, 'Remarks to the Direct Strength Method', *Thin-Walled Structures*, vol. 39, no. 9, pp. 807-20.

Saint-Venant, M. 1883, *Discussion en Theorie de l'Elasticite des Corps Solides*, by Clebsch.

Salvadori, M.G. 1955, 'Lateral Buckling of I-beams', *ASCE Transactions, American Society of Civil Engineers,*, vol. 120, pp. 1165-77.

Sandhu, J.S., Stevens, K.A. & Davies, G.A.O. 1990, 'A 3-D, co-rotational, curved and twisted beam element', *Computers and Structures*, vol. 35, no. 1, pp. 69-79.

Sapkás, A. & Kollár, L.P. 2002, 'Lateral-torsional buckling of composite beams', *International Journal of Solids and Structures*, vol. 39, no. 11, pp. 2939-63.

Sawko, F. 1967, 'Computer analysis of grillages curved in plan', *International Association for Bridge and Structural Engineering*, vol. 8, pp. 151-70.

Schafer, B.W. & Pekoz, T. 1998, 'Direct Strength Prediction of Cold-Formed Steel Members using Numerical Elastic Buckling Solutions', *14th International Specialty Conference on Cold-Formed Steel Structures*, St. Louis, Missouri, pp. 69-76.

Schardt, R. 1994, 'Generalized beam theory-an adequate method for coupled stability problems', *Thin-Walled Structures*, vol. 19, no. 2-4, pp. 161-80.

Schardt, R.P. 1989, *Verallgemeinerte Technische Biegetheorie*, Springer, Berlin.

Serna, M.A., López, A., Puente, I. & Yong, D.J. 2006, 'Equivalent uniform moment factors for lateral-torsional buckling of steel members', *Journal of Constructional Steel Research*, vol. 62, no. 6, pp. 566-80.

Shanmugam, N.E., Thevendran, V., Liew, J.Y.R. & Tan, L.O. 1995, 'Experimental Study on Steel Beams Curved in Plan', *Journal of Structural Engineering*, vol. 121, no. 2, pp. 249-59.

Silvestre, N. 2007, 'Generalised beam theory to analyse the buckling behaviour of circular cylindrical shells and tubes', *Thin-Walled Structures*, vol. 45, no. 2, pp. 185-98.

Silvestre, N. & Camotim, D. 2003, 'Nonlinear generalized beam theory for cold-formed steel members', *International Journal of Structural Stability & Dynamics*, vol. 3, no. 4, pp. 461-90.

Simo, J.C. 1985, 'A finite strain beam formulation. The three-dimensional dynamic problem. Part I', *Computer Methods in Applied Mechanics and Engineering*, vol. 49, no. 1, pp. 55-70.

Simo, J.C. & Vu-Quoc, L. 1987, 'The role of non-linear theories in transient dynamic analysis of flexible structures', *Journal of Sound and Vibration*, vol. 119, no. 3, pp. 487-508.

Simo, J.C. & Vu-Quoc, L. 1991, 'A Geometrically-exact rod model incorporating shear and torsion-warping deformation', *International Journal of Solids and Structures*, vol. 27, no. 3, pp. 371-93.

Song, H.-W. & Tassoulas, J.L. 1993, 'Finite element analysis of propagating buckles', *International Journal for Numerical Methods in Engineering*, vol. 36, no. 20, pp. 3529-52.

Sun, C.T. & Mao, K.M. 1988, 'A global-local finite element method suitable for parallel computations', *Computers and Structures*, vol. 29, no. 2, pp. 309-15.

Szilard, R. 1985, 'Critical load and post-buckling analysis by FEM using energy balancing technique', *Computers & Structures*, vol. 20, no. 1, pp. 277-86.

Timoshenko, S.P. 1910, 'Einige Stabilitatsrobleme der Elastizitatsprobleme der Elastizitatstheorie', *Zeithschrift Fur Mathematik und Physik*, vol. 337.

Timoshenko, S.P. 1923, 'Bending Stresses in Curved Tubes of Rectangular Cross-Section', paper presented to the *ASME*, Montreal, Canada, 28 May, 1923.

Timoshenko, S.P. & Gere, J.M. 1961, *Theory of elastic stability*, 2nd edn, McGraw-Hil, New York.

Timoshenko, S.P. & Woinowsky-Krieger, S. 1959, *Theory of Plates and Shells*, 2nd edn, McGraw-Hill, New York.

Trahair, N.S. 1993, *Flexural-Torsional Buckling of Structures*, CRC Press, Boca Raton, FL, USA.

Trahair, N.S. 2003, *Flexural-Torsional Buckling of Structures*, Spon Press, London.

van der Neut, A. 1969, 'The interaction of Local Buckling and Column Failure of Thin-walled Compression Members', *12th International Congress on Applied Mechanics*, pp. 389-99.

Van Erp, G.M. & Menken, C.M. 1990, 'Spline finite-strip method in the buckling analyses of thin-walled structures', *Communications in Applied Numerical Methods*, vol. 6, no. 6, pp. 477-84.

Vlasov, V.Z. 1961, *Thin-walled elastic beams*, 2nd edn, Israel Program for Scientific Translations, Jerusalem, Israel.

von Kármán, T. 1910, *Festigkeitsprobleme im Maschinenbau*, Encyklopädie der mathematischen wissenschaften, Leipzig.

von Karman, T., Sechler, E.E. & Donnell, L.H. 1932, 'The Strength of Thin Plates in Compression', *ASME*, vol. 54, no. 5, pp. 53-70.

Wang, S.T. & Pao, H.Y. 1980, 'Torsional-flexural buckling of locally buckled columns', *Computers and Structures*, vol. 11, no. 1-2, pp. 127-36.

Wang, S.T., Yost, M.I. & Tien, Y.L. 1977, 'Lateral buckling of locally buckled beams using finite element techniques', *Computers and Structures*, vol. 7, no. 3, pp. 469-75.

Weicker, K., Salahifar, R. & Mohareb, M. 2010, 'Shell analysis of thin-walled pipes. Part II - Finite element formulation', *International Journal of Pressure Vessels and Piping*, vol. 87, no. 7, pp. 414-23.

Whitcomb, J.D. 1991, 'Iterative global/local finite element analysis', *Computers and Structures*, vol. 40, no. 4, pp. 1027-31.

Whitcomb, J.D. & Woo, K. 1993a, 'Application of iterative global/local finite-element analysis. Part 1: linear analysis', *Communications in Numerical Methods in Engineering*, vol. 9, no. 9, pp. 745-56.

Whitcomb, J.D. & Woo, K. 1993b, 'Application of iterative global/local finite-element analysis. Part 2: geometrically non-linear analysis', *Communications in Numerical Methods in Engineering*, vol. 9, no. 9, pp. 757-66.

Wong, E. & Driver, R.G. 2010, 'Critical evaluation of equivalent moment factor procedures for laterally unsupported beams', *Engineering Journal*, vol. 47, no. 1, pp. 1-20.

Yamao, T. & Sakimoto, T. 1986, 'Nonlinear analysis of thin-walled structures by a coupled finite element method', *Structural Engineering / Earthquake Engineering*, vol. 3, no. 2, pp. 225-35.

Yoo, C.H., Kang, Y.J. & Davidson, J.S. 1996, 'Buckling analysis of curved beams by finite-element discretization', *Journal of Engineering Mechanics*, vol. 122, no. 8, pp. 762-70.

Yoshida, H. & Maegawa, K. 1983, 'Ultimate strength analysis of curved I-beams', *Journal of Engineering Mechanics*, vol. 109, no. 1, pp. 192-214.

Young, B. & Rasmussen, K.J.R. 1997, 'Bifurcation of singly symmetric columns', *Thin-Walled Structures*, vol. 28, no. 2, pp. 155-77.

Young, M.C. 1969, 'Flexibility influence functions for curved beams', *American Society of Civil Engineers*, vol. 94.

Yu, C. & Schafer, B.W. 2003, 'Local buckling tests on cold-formed steel beams', *Journal of Structural Engineering*, vol. 129, no. 12, pp. 1596-606.

Zienkiewicz, O.C. 1977, *The Finite Element Method*, Third Expanded and Revised edn, McGraw-Hill, U.K.

Zienkiewicz, O.C. & Taylor, R.L. 2005, *The Finite Element Method for Solid and Structural Mechanics*, Sixth edn, Elsevier Butterworth-Heinemann, Oxford, United Kingdom.

Appendix 2.A

The interpolation matrix $\hat{\mathbf{X}}$ used in Eq. (2.78) can be written as

$$\hat{\mathbf{X}}=\left[\begin{array}{cccccc|c|c|c}
N_1 & 0 & N_1^x & 0 & 0 & 0 & N_2 \ldots N_2^x \ldots & N_3 \ldots N_3^x \ldots & N_4 \ldots N_4^x \ldots \\
0 & N_1 & N_1^y & 0 & 0 & 0 & \ldots N_2 \;\; N_2^y \ldots & \ldots N_3 \;\; N_3^y \ldots & \ldots N_4 \;\; N_4^y \ldots \\
0 & 0 & N_1 & 0 & 0 & 0 & \ldots N_2 \ldots & \ldots N_3 \ldots & \ldots N_4 \ldots \\
0 & 0 & 0 & N_1 & 0 & 0 & \ldots . N_2 . . & \ldots . N_3 . . & \ldots . N_4 . . \\
0 & 0 & 0 & H_1^x & H_2^x & H_3^x & \ldots H_4^x \;\; H_5^x \;\; H_6^x & \ldots H_7^x \;\; H_8^x \;\; H_9^x & \ldots H_{10}^x \;\; H_{11}^x \;\; H_{12}^x \\
0 & 0 & 0 & H_1^y & H_2^y & H_3^y & \ldots H_4^y \;\; H_5^y \;\; H_6^y & \ldots H_7^y \;\; H_8^y \;\; H_9^y & \ldots H_{10}^y \;\; H_{11}^y \;\; H_{12}^y
\end{array}\right] \tag{2.A.1}$$

where N_i is the standard bilinear interpolation functions defined as

$$N_i=\frac{1}{4}\left(1+\xi_i\xi\right)\left(1+\eta_i\eta\right),\ i=1,2,3,4 \tag{2.A.2}$$

in which ξ and η are natural coordinates defines as $\xi=x/a$ and $\eta=y/b$, in which a and b are the half length of the rectangular shell element in x and y directions, respectively. N_i^x and N_i^y are used to interpolate the membrane displacement components according to Allman-type interpolation as

$$N_i^x=\frac{1}{8}\left(\left(y_j-y_i\right)N_l-\left(y_k-y_i\right)N_m\right),\ i=1,2,3,4 \tag{2.A.3}$$

$$N_i^y=\frac{1}{8}\left(\left(x_j-x_i\right)N_l-\left(x_k-x_i\right)N_m\right),\ i=1,2,3,4 \tag{2.A.4}$$

where

$$N_m=\frac{1}{2}\left(1-\xi^2\right)\left(1+\eta_m\eta\right),\ m=8,5,6,7 \tag{2.A.5}$$

$$N_l=\frac{1}{2}\left(1+\xi_l\xi\right)\left(1-\eta^2\right),\ l=5,6,7,8 \tag{2.A.6}$$

The elements of the plate-bending component of interpolation functions are given explicitly in Eq. (2.A.7)

$$
\begin{array}{lll}
H_1^x = 1.5\left(a_5 N_5 - a_8 N_8\right) & H_2^x = -N_1 + c_5 N_5 + c_8 N_8 & H_3^x = b_5 N_5 + b_8 N_8 \\
H_4^x = 1.5\left(a_6 N_6 - a_5 N_5\right) & H_5^x = -N_2 + c_6 N_6 + c_5 N_5 & H_6^x = b_6 N_6 + b_5 N_5 \\
H_7^x = 1.5\left(a_7 N_7 - a_6 N_6\right) & H_8^x = -N_3 + c_7 N_7 + c_6 N_6 & H_9^x = b_7 N_7 + b_6 N_6 \\
H_{10}^x = 1.5\left(a_8 N_8 - a_7 N_7\right) & H_{11}^x = -N_4 + c_8 N_8 + c_7 N_7 & H_{12}^x = b_8 N_8 + b_7 N_7 \\
H_1^y = 1.5\left(d_5 N_5 - d_8 N_8\right) & H_2^y = b_5 N_5 + b_8 N_8 & H_3^y = -N_1 + e_5 N_5 + e_8 N_8 \\
H_4^y = 1.5\left(d_6 N_6 - d_5 N_5\right) & H_5^y = b_6 N_6 + b_5 N_5 & H_6^y = -N_2 + e_6 N_6 + e_5 N_5 \\
H_7^y = 1.5\left(d_7 N_7 - d_6 N_6\right) & H_8^y = b_7 N_7 + b_6 N_6 & H_9^y = -N_3 + e_7 N_7 + e_6 N_6 \\
H_{10}^y = 1.5\left(d_8 N_8 - d_7 N_7\right) & H_{11}^y = b_8 N_8 + b_7 N_7 & H_{12}^y = -N_4 + e_8 N_8 + e_7 N_7
\end{array}
\tag{2.A.7}
$$

in which $a_k = -\dfrac{x_{ij}}{l_{ij}^{\,2}}$, $b_k = \dfrac{3x_{ij}y_{ij}}{4l_{ij}^{\,2}}$, $c_k = \dfrac{\frac{1}{4}x_{ij}^{\,2} - \frac{1}{2}y_{ij}^{\,2}}{l_{ij}^{\,2}}$, $d_k = -\dfrac{y_{ij}}{l_{ij}^{\,2}}$, $e_k = \dfrac{-\frac{1}{2}x_{ij}^{\,2} + \frac{1}{4}y_{ij}^{\,2}}{l_{ij}^{\,2}}$

$(k = 5,6,7,8)$ $(i = 1,2,3,4)$, $(j = 2,3,4,1)$ and $(ij = 12,23,34,41)$.

Appendix 2.B

Due to the inclusion of the second-order displacement terms, the decomposition matrix $\mathbf{N}$ is modified to Eq. (2.113). Consequently, the variation of $\mathbf{N}$ is no longer equal to zero and has to be considered in the formulation. To this end, the last term in Eq. (2.114) is written explicitly as

$$\begin{aligned}\bar{\mathbf{d}}\delta\mathbf{N} &= \bar{\mathbf{d}}\begin{bmatrix} 0 & 0 & 0 & \left(-x\delta v' + y\delta u'\right)\mathbf{H}^{\mathrm{T}} \\ 0 & 0 & 0 & 0 \\ 0 & 0 & 0 & 0 \\ 0 & 0 & 0 & 0 \\ 0 & 0 & 0 & 0 \\ 0 & 0 & 0 & 0 \end{bmatrix} \\ &= \begin{Bmatrix} \left(-x\delta v' + y\delta u'\right)\mathbf{H}^{\mathrm{T}}\left\langle \phi_1 \quad \varphi_1 \quad \phi_2 \quad \varphi_2 \right\rangle^T \\ 0 \\ 0 \\ 0 \end{Bmatrix} == \begin{Bmatrix} \left(-x\delta v' + y\delta u'\right)\phi \\ 0 \\ 0 \\ 0 \end{Bmatrix}\end{aligned} \tag{2.B.1}$$

but

$$\delta u' = \frac{\mathrm{d}\mathbf{H}^{\mathrm{T}}}{\mathrm{d}\bar{z}}\left\langle u_1 \quad u_1' \quad u_2 \quad u_2' \right\rangle^T, \delta v' = \frac{\mathrm{d}\mathbf{H}^{\mathrm{T}}}{\mathrm{d}\bar{z}}\left\langle v_1 \quad v_1' \quad v_2 \quad v_2' \right\rangle^T \tag{2.B.2}$$

therefore, $\mathbf{A}$ can be written as

$$\mathbf{A}=\begin{bmatrix} \mathbf{L}^{\mathrm{T}} & -\bar{x}\dfrac{\mathrm{d}\mathbf{H}^{\mathrm{T}}}{\mathrm{d}\bar{z}}+\phi y\dfrac{\mathrm{d}\mathbf{H}^{\mathrm{T}}}{\mathrm{d}\bar{z}} & -\bar{y}\dfrac{\mathrm{d}\mathbf{H}^{\mathrm{T}}}{\mathrm{d}\bar{z}}-\phi x\dfrac{\mathrm{d}\mathbf{H}^{\mathrm{T}}}{\mathrm{d}\bar{z}} & -\bar{\omega}\dfrac{\mathrm{d}\mathbf{H}^{\mathrm{T}}}{\mathrm{d}\bar{z}}+\left(-xv'+yu'\right)\mathbf{H}^{\mathrm{T}} \\ \mathbf{0} & \mathbf{H}^{\mathrm{T}} & \mathbf{0} & -\left(\bar{y}-a_y\right)\mathbf{H}^{\mathrm{T}} \\ \mathbf{0} & \dfrac{\mathrm{d}\mathbf{H}^{\mathrm{T}}}{\mathrm{d}\bar{z}} & \mathbf{0} & -\left(\bar{y}-a_y\right)\dfrac{\mathrm{d}\mathbf{H}^{\mathrm{T}}}{\mathrm{d}\bar{z}} \\ \mathbf{0} & \mathbf{0} & \mathbf{H}^{\mathrm{T}} & \left(\bar{x}-a_x\right)\mathbf{H}^{\mathrm{T}} \\ \mathbf{0} & \mathbf{0} & -\dfrac{\mathrm{d}\mathbf{H}^{\mathrm{T}}}{\mathrm{d}\bar{z}} & -\left(\bar{x}-a_x\right)\dfrac{\mathrm{d}\mathbf{H}^{\mathrm{T}}}{\mathrm{d}\bar{z}} \\ \mathbf{0} & \mathbf{0} & \mathbf{0} & -\mathbf{H}^{\mathrm{T}} \end{bmatrix} \tag{2.B.3}$$

The contribution of $\bar{\mathbf{d}}\delta\mathbf{N}$ in matrix $\mathbf{A}$ is shown in grey in Eq. (2.B.3).

Chapter 2 list of symbols

The following symbols have been used in chapter 2.

A	=	cross-sectional area
A_p	=	sectorial pole (Figure 2.2)
a_x, a_y	=	coordinates of the thin-walled pole
D	=	flexural rigidity of a plate (Figure 2.3)
$\bar{\mathbf{d}}$	=	nodal displacement vector of the beam
$\hat{\mathbf{d}}$	=	nodal displacement vector of the shell
$\mathbf{d}'$	=	displacement difference term between the global and local models
$\hat{\mathbf{d}}_{i\&j}$	=	displacement values and the boundaries of the local shell
$\delta\hat{\mathbf{d}}_{IN}$	=	internal displacement values of the local shell
$\bar{\mathbf{E}}$	=	constitutive matrix of the beam element
$\hat{\mathbf{E}}$	=	constitutive matrix of the shell element
E	=	modulus of elasticity
$\bar{\mathbf{f}}$	=	external load vector of the beam element
$\hat{\mathbf{f}}_s$	=	portion of the external load vector in the local model

$\hat{\mathbf{f}}_{i\&j}$ = vector of tractions at the boundaries of the local shell model

$\Delta\bar{\mathbf{f}}_k$ = external load increment

$\mathbf{H}$ = vector of cubic interpolation functions

H = interpolation functions for plate bending

$\bar{\mathbf{K}}$ = stiffness matrix of the beam element

$\hat{\mathbf{K}}$ = stiffness matrix of the beam element

$\bar{\mathbf{K}}_k$ = tangent stiffness matrix of the beam model

$\mathbf{L}$ = vector of linear interpolation functions

L = length of the element

$\mathbf{N}$ = overlapping domain decomposition matrix

N = interpolation functions for the shell element

$\Delta\bar{\mathbf{R}}_k^n$ = unbalanced force vector

$\bar{\mathbf{S}}$ = matrix of cross-sectional coordinates

s = coordinate along the element sides

t = thickness of a plate (Figure 2.3)

$\bar{\mathbf{u}}_a$ = displacement vector of an arbitrary point in the beam element

$\hat{\mathbf{u}}$ = displacement field of the shell element

$\bar{u}, \bar{v}, \bar{w}$	=	displacement components of the beam element (Figure 2.8)
$\hat{u}, \hat{v}, \hat{w}$	=	displacement components of the shell element
u_t, u_n	=	tangential and normal displacement components along element sides
w	=	out of plane displacement of a plate (Figure 2.3)
$\bar{\mathbf{X}}_a$	=	beam interpolation matrix
$\hat{\mathbf{X}}$	=	shell interpolation matrix
$\mathbf{Y}$	=	matrix of thin-walled kinematical relations
x, y, z	=	coordinates in Cartesian system (Figure 2.3)
$\bar{x}, \bar{y}, \bar{z}$	=	Cartesian directions for beam element (Figure 2.8)
$\mathbf{Z}$	=	matrix of overlapping domain interpolations
$\bar{\varepsilon}_L, \bar{\gamma}_L, \bar{\varepsilon}_N, \bar{\gamma}_N$	=	strain components of the beam element
$\bar{\boldsymbol{\varepsilon}}, \bar{\boldsymbol{\varepsilon}}_L, \bar{\boldsymbol{\varepsilon}}_N$	=	strain vectors of the beam element
$\hat{\boldsymbol{\varepsilon}}, \hat{\boldsymbol{\varepsilon}}_b, \hat{\boldsymbol{\varepsilon}}_{mm}, \hat{\boldsymbol{\varepsilon}}_N$	=	strain vectors of the shell element
$\boldsymbol{\varepsilon}'$	=	strain difference term between local and global models
η	=	displacement in the tangential direction
η, ξ	=	natural coordinates

$\theta_x, \theta_y, \theta_z$ = rotation components

ν = Poisson's ratio

$\bar{\Pi}$ = total potential energy of the beam element

$\hat{\Pi}$ = total potential energy of the shell element

$\bar{\boldsymbol{\sigma}}$ = beam element stress vector

$\hat{\boldsymbol{\sigma}}$ = shell element stress vector

σ = normal stress (Figure 2.3)

$\bar{\sigma}, \bar{\tau}$ = normal and shear stress of the beam element

ϕ = twist rotation of the beam element (Figure 2.8)

$\bar{\boldsymbol{\chi}}_L, \bar{\boldsymbol{\chi}}_N$ = vectors of linear and nonlinear displacement derivatives

$\hat{\boldsymbol{\chi}}$ = curvature vector of the shell element

Ω = Drilling rotation

Ω_C = total structural domain (Figure 2.7)

Ω_m = overlapping local domain (Figure 2.7)

$\partial\Omega_S$ = boundary of global and local model (Figure 2.7)

$\bar{\omega}$ = sectorial coordinate

ω_i = vertex rotations

ψ_x, ψ_y = rotation components of a normal line to the undeformed plate

∇ = differential operator

Chapter 2 list of figures

Chapter 3: The Iterative global-local method for the analysis of composite thin-walled elements

3.1. Introduction

The Iterative Global-local Method was introduced in the previous chapter as an efficient tool for the analysis of thin-walled beams subjected to localized behaviour (e.g. local buckling and web crippling). The method is based on considering two levels of structural idealization based on the expected scales of deformation. For that purpose, two-dimensional beam-type finite elements were adopted as the global/coarse scale while two-dimensional shell elements were used as the local/fine scale. The two models would overlap at the areas affected by the local deformations, and the two models were synchronised by the introduction of a domain decomposition operator and iterations were introduced in order to minimise the unbalanced forces between the two models.

The application of the method proposed in the previous chapter was restricted to isotropic material. In this chapter, the Iterative Global-local Method is developed for fibre-reinforced polymer composite laminates. The proposed method can be used for composite polymer laminates with arbitrary fibre orientation directions in different layers of the material, and under various loading conditions. The material is assumed to be linear elastic in the current Chapter. Comparison with full shell-type finite element

analysis results are made in order to illustrate the efficiency and accuracy of the proposed technique.

3.2. Literature review

The use of fibre-reinforced polymer composite laminated plates as a construction material has increased in recent years. The primary reason for this increase is their non-corrosive nature and long term durability, high tensile strength-to-weight ratio, electromagnetic neutrality and resistance to chemical attack. Because of their high strength-to-weight ratios, slender structural components may be formed by using composite laminates, which can be used in building, bridge, aerospace and marine applications. Consequently, they are susceptible to buckling because of their slenderness and relatively low shear strength. FRP composite structural materials are often cast in beam-type shapes (i.e. large span in comparison to cross-sectional dimensions), for which they are commonly analysed by using beam-type elements.

A beam formulation was developed by Bauld & Tzeng (1984) to capture flexural and lateral-torsional buckling behaviour of thin-walled composite laminated members, and was later verified by Mottram (1992) using test results. Closed-form analytical solutions for buckling analysis based on beam-type formulations have been proposed by several researchers. Pandey et al. (1995) used the Galerkin method to solve the equilibrium equations and proposed a closed-form formulation for the lateral-torsional buckling of composite beams with I-shaped cross-section. Murakami & Yamakawa (1996) used Airy stress functions to determine the lateral buckling load of beams made of anisotropic materials. Sapkás & Kollár (2002) performed stability analysis of composite beams subjected to concentrated end-moments, end-forces and uniformly distributed

load. They solved the problem for simply-supported and cantilever beams with I-shaped cross-section. Similar studies are performed by Roberts (2002), Roberts & Masri (2003) and Kim et al. (2007). It should be noted that the above-mentioned closed form solutions are limited to certain boundary and loading conditions.

On the other hand, the finite element method can be used to obtain solutions that are applicable to general boundary conditions and loading cases. Several finite element formulations have been developed for the flexural-torsional buckling analysis of thin-walled composite beams. Omidvar & Ghorbanpoor (1996) developed a nonlinear finite element method based on the updated Lagragian formulation. Fraternali & Feo (2000) formulated a small strain and moderate rotation theory for laminated composite thin-walled beams, and developed a finite element based on their formulation. Lee et al. (2002) presented a finite element model for I-shaped cross-sections based on classical lamination theory to account for material coupling for laminates with different stacking sequence and arbitrary fibre alignment. Lee (2006) generalised the method for arbitrary mono-symmetric cross-sections. Using the first-order shear-deformable beam theory, Back & Will (2008) developed a shear-flexible element for composite doubly- and mono-symmetric cross-section. The developed element included both the transverse shear and the thin-walled warping-induced shear deformations. Cardoso et al. (2009) presented a finite element based on three-dimensional two-node Hermitean elements.

These types of elements are formulated based on the assumption that cross-sections remain rigid during the deformation, which limits their application to axis-related deformations only (i.e. flexural, torsional and flexural-torsional buckling), and hence they cannot capture local/cross-sectional deformations such as flange local buckling and web crippling. In order to account for the local buckling of orthotropic beams, Lee (1978) used deflection functions to obtain the buckling coefficients in terms of rigidities

of the plates composing the cross-section, and presented the buckling load in terms of flange-web ratio. Barbero & Raftoyiannis (1993) developed failure envelopes for box- and I- shape members, and introduced analytical models for various local buckling modes and buckling load values for axial and shear loading by considering the web-flange interaction. The analysis of local buckling of FRP members can also be performed by discrete plate analysis method (Qiao et al. 2001), in which each plate segment of the cross-section (i.e. web and flanges) are analysed separately, and the minimum buckling stress is reported as the critical buckling stress of the cross-section. Alternatively, shell-type elements have to be utilised for a detailed analysis of local buckling, e.g. (Yu & Schafer 2003).

Since modelling the whole structure by detailed shell elements is computationally expensive and practically impossible, the Iterative Global-local Method discussed in Chapter 2 is appealing for modelling of thin-walled composite elements where a local/cross-sectional deformation is expected in a relatively short span of the member, e.g. local buckling and locally-applied loads that can cause local buckling. In the following, the Iterative Global-local Method is developed for fibre-reinforced composite laminates by adopting a suitable beam-type element as the coarse-scale and a shell-type element as the fine-scale model. Numerical examples are then presented in order to justify the accuracy and efficiency of the proposed method.

3.3. Constitutive relations of an orthotropic plate

In order to obtain the stress-strain relationship of a laminate, we start from the basic mechanics of orthotropic materials (Jones 1975; Reddy 2004). Consider an orthotropic plate with moduli of elasticity E_1 and E_2 in parallel and perpendicular directions to its

fibres, respectively. If the loading of such a plate is either parallel or perpendicular to its fibres (Figure 3.1 a), it is considered "specially-orthotropic". Otherwise, it is regarded as "generally-orthotropic" (Figure 3.1 b).

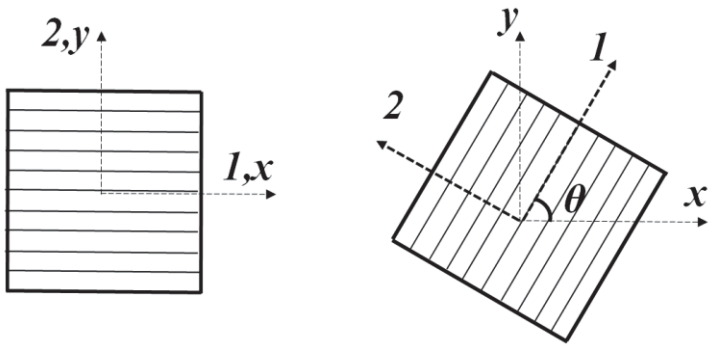

(a) specially-orthotropic plate (b) generally-orthotropic plate

Figure 3.1: Orthotropic plate (*1-2* fibre alignment, *x-y* load direction)

For a specially-orthotropic plate, the stress-strain relationship can be written as (Figure 3.1 a)

$$\begin{Bmatrix} \sigma_1 \\ \sigma_2 \\ \tau_{12} \end{Bmatrix} = \begin{bmatrix} Q_{11} & Q_{12} & 0 \\ Q_{12} & Q_{22} & 0 \\ 0 & 0 & Q_{66} \end{bmatrix} \begin{Bmatrix} \varepsilon_1 \\ \varepsilon_2 \\ \gamma_{12} \end{Bmatrix} \tag{3.1}$$

or in a more condensed form as

$$[\boldsymbol{\sigma}] = [\mathbf{Q}][\boldsymbol{\varepsilon}] \tag{3.2}$$

where

$$Q_{11} = \frac{E_1}{1 - \nu_{12}\nu_{21}}, \tag{3.3}$$

$$Q_{22} = \frac{E_2}{1-\nu_{12}\nu_{21}}, \tag{3.4}$$

$$Q_{12} = \frac{\nu_{12}E_2}{1-\nu_{12}\nu_{21}} = \frac{\nu_{21}E_1}{1-\nu_{12}\nu_{21}}, \tag{3.5}$$

$$Q_{66} = G_{12}. \tag{3.6}$$

in which ν_{12} and ν_{21} are Poisson's ratios for the two directions and G_{12} is the shear modulus. If the applied load has an angle different from 0^o or 90^o (i.e. generally-orthotropic plate, Figure 3.1 b), a transformation matrix has to be multiplied to both the stress and strain vectors, i.e.

$$[\boldsymbol{\sigma}] = [\mathbf{T}]^{-1}[\mathbf{Q}][\mathbf{T}][\boldsymbol{\varepsilon}] \tag{3.7}$$

where

$$\mathbf{T} = \begin{bmatrix} \cos^2\theta & \sin^2\theta & 2\sin\theta\cos\theta \\ \sin^2\theta & \cos^2\theta & -2\sin\theta\cos\theta \\ -\sin\theta\cos\theta & \sin\theta\cos\theta & \cos^2\theta - \sin^2\theta \end{bmatrix} \tag{3.8}$$

θ in Eq. (3.8) is the angle between the fibres and the coordinate in which the stress and strain values are calculated, as shown in Figure 3.1 b. The matrix $\bar{\mathbf{Q}}$ can be defined as

$$\bar{\mathbf{Q}} = [\mathbf{T}]^{-1}[\mathbf{Q}][\mathbf{T}] \tag{3.9}$$

$$\bar{\mathbf{Q}} = \begin{bmatrix} \bar{Q}_{11} & \bar{Q}_{12} & \bar{Q}_{16} \\ \bar{Q}_{12} & \bar{Q}_{22} & \bar{Q}_{26} \\ \bar{Q}_{16} & \bar{Q}_{26} & \bar{Q}_{66} \end{bmatrix} \tag{3.10}$$

Eq. (3.7) can be written as

$$[\boldsymbol{\sigma}] = \left[\bar{\mathbf{Q}}\right][\boldsymbol{\varepsilon}] \tag{3.11}$$

The components of $\bar{\mathbf{Q}}$ are written explicitly in the following.

$$\bar{Q}_{11} = Q_{11}\cos^4\theta + 2\left(Q_{12} + 2Q_{66}\right)\sin^2\theta\cos^2\theta + Q_{22}\sin^4\theta, \tag{3.12}$$

$$\bar{Q}_{12} = \left(Q_{11} + Q_{22} - 4Q_{66}\right)\sin^2\theta\cos^2\theta + Q_{12}\left(\sin^4\theta + \cos^4\theta\right), \tag{3.13}$$

$$\bar{Q}_{22} = Q_{11}\sin^4\theta + 2\left(Q_{12} + 2Q_{66}\right)\sin^2\theta\cos^2\theta + Q_{22}\cos^4\theta, \tag{3.14}$$

$$\bar{Q}_{16} = \left(Q_{11} - Q_{22} - 2Q_{66}\right)\sin\theta\cos^3\theta + \left(Q_{12} - Q_{22} + 2Q_{66}\right)\sin^3\theta\cos\theta, \tag{3.15}$$

$$\bar{Q}_{26} = \left(Q_{11} - Q_{22} - 2Q_{66}\right)\sin^3\theta\cos\theta + \left(Q_{12} - Q_{22} + 2Q_{66}\right)\sin\theta\cos^3\theta, \tag{3.16}$$

$$\bar{Q}_{66} = \left(Q_{11} + Q_{22} - 2Q_{12} - 2Q_{66}\right)\sin^2\theta\cos^2\theta + Q_{66}\left(\sin^4\theta + \cos^4\theta\right). \tag{3.17}$$

It should be noted that unless $\theta = 0^\circ$ or $\theta = 90^\circ$, $\bar{Q}_{16}$ and $\bar{Q}_{26}$ are nonzero. Therefore, normal strain would produce shear stresses and vice-versa. This phenomenon is called extension-shear coupling.

3.4. The global model

For the global/coarse-scale analysis, a thin-walled beam formulation based on second-order nonlinear thin-walled theory is used (Trahair 2003). The kinematic assumptions and the corresponding displacement and strain values of the beam are presented in detail in Chapter 2. The difference in the current formulation arises from the material behaviour, which is characterised by the modified constitutive relations.

The material is assumed to be composed of several laminated layers with different orientation of fibres in different layers. It is assumed that perfect interlaminar bond

exists between the lamina of the laminate. For a laminate composed of *n* orthotropic layers, the orientation of the local $\bar{s}_k\bar{z}_k$-plane with respect to the global $\bar{s}\bar{z}$-plane is determined by the angle about the $\bar{r}$-axis Φ (positive according to the opposite of the right hand rule) between $\bar{z}$ and $\bar{z}_k$ (Figure 3.2 b).

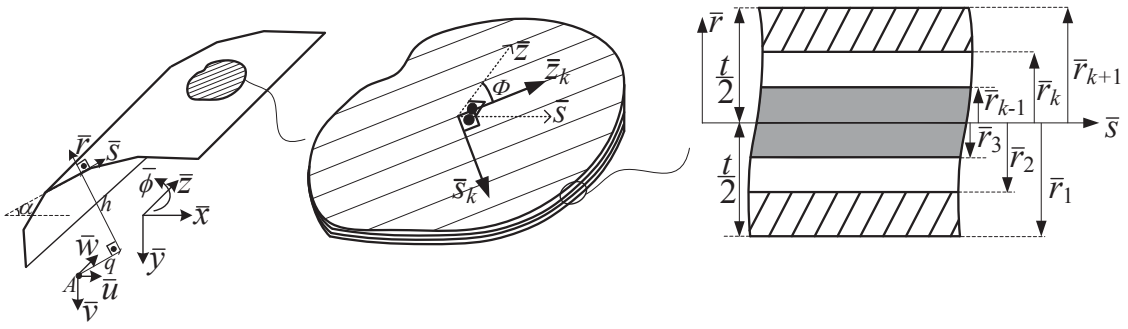

(a) Thin-walled beam (b) Fibre orientation (c) Laminates across the thickness

Figure 3.2: Thin-walled beam composed of fibre-reinforced laminates

Recalling from Chapter 2, the stress vector of the thin-walled beam includes normal stresses in the axial direction of the beam only, i.e. σ_2 in Eq. (3.1) vanishes. Consequently, from the second line of Eq. (3.11) we have

$$\sigma_y = \bar{Q}_{12}\varepsilon_x + \bar{Q}_{22}\varepsilon_y + \bar{Q}_{26}\gamma_{xy} = 0 \tag{3.18}$$

Therefore, ε_y can be calculated as

$$\varepsilon_y = -\frac{\bar{Q}_{12}}{\bar{Q}_{22}}\varepsilon_x - \frac{\bar{Q}_{26}}{\bar{Q}_{22}}\gamma_{xy} \tag{3.19}$$

Eq. (3.19) can be used to modify the $\bar{\mathbf{Q}}$ matrix such that the stresses can be obtained from ε_x and γ_{xy} only.

$$\begin{Bmatrix} \sigma_1 \\ \tau_{12} \end{Bmatrix} = \begin{bmatrix} \bar{Q}_{11}^* & \bar{Q}_{16}^* \\ \bar{Q}_{16}^* & \bar{Q}_{66}^* \end{bmatrix} \begin{Bmatrix} \varepsilon_1 \\ \gamma_{12} \end{Bmatrix} \tag{3.20}$$

where

$$\bar{Q}_{11}^* = \bar{Q}_{11} - \frac{\bar{Q}_{12}^2}{\bar{Q}_{22}} \tag{3.21}$$

$$\bar{Q}_{16}^* = \bar{Q}_{16} - \frac{\bar{Q}_{12}\bar{Q}_{26}}{\bar{Q}_{22}} \tag{3.22}$$

$$\bar{Q}_{66}^* = \bar{Q}_{66} - \frac{\bar{Q}_{26}^2}{\bar{Q}_{22}} \tag{3.23}$$

In order to be consistent with the dimensions of strain and stress vectors of the beam element in Chapter 2, the above equations can be written as

$$\bar{\boldsymbol{\sigma}}^{(k)} = \begin{Bmatrix} \bar{\sigma}_z^{(k)} \\ 0 \\ \bar{\tau}_{zs}^{(k)} \\ 0 \end{Bmatrix} = \bar{\mathbf{Q}}^{(k)} \bar{\boldsymbol{\varepsilon}} \tag{3.24}$$

in which

$$\bar{\mathbf{Q}}^{(k)} = \begin{bmatrix} \bar{Q}_{11}^{*(k)} & 0 & \bar{Q}_{16}^{*(k)} & 0 \\ 0 & 0 & 0 & 0 \\ \bar{Q}_{16}^{*(k)} & 0 & \bar{Q}_{66}^{*(k)} & 0 \\ 0 & 0 & 0 & 0 \end{bmatrix} \tag{3.25}$$

Superscript (k) in Eqs. (3.24) and (3.25) shows that the relationship is written for the k^{th} layer in the composite laminate.

3.5. The local model

The details of the shell element used as the fine-scale/local model are discussed in Chapter 2. Similar to the beam element, the only part of the formulation that requires modification is the constitutive relations. The coordinate systems used for the shell element are shown in Figure 3.3.

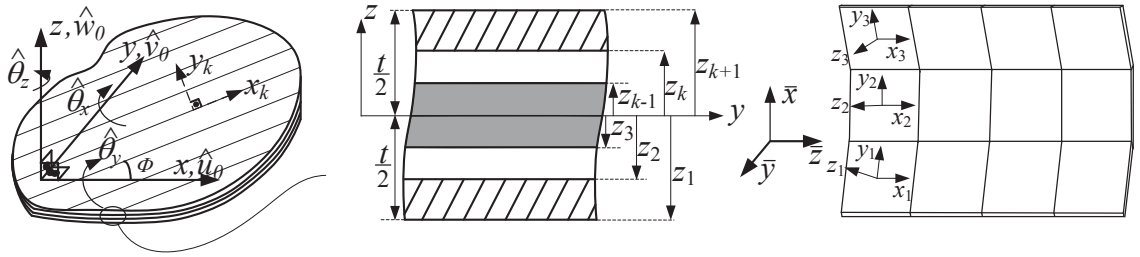

(a) Shell local coordinates (b) Laminates across thickness (c) Global & local coordinates

Figure 3.3: Deflections and coordinate system of the shell composed of fibre-reinforced laminates

For a laminate composed of n orthotropic layers, the orientation of the fibre attached $x_k y_k$-axes with respect to the plate's local x-y axes is determined by the angle Φ which is the angle about the plate's local z-axis (positive according to the right hand rule) between x and x_k (Figure 2(a)). In that case Φ is the same angle used in Section 3.4. Assuming that perfect interlaminar bond exists between the layers, the stress-strain relationship for the k^{th} layer according to the plate local axis directions can be written as (Reddy 2004)

$$\hat{\boldsymbol{\sigma}}^{(k)} = \begin{Bmatrix} \hat{\sigma}_x^{(k)} \\ \hat{\sigma}_y^{(k)} \\ \hat{\tau}_{xy}^{(k)} \\ \hline \hat{\tau}_m^{(k)} \end{Bmatrix} = \hat{\mathbf{Q}}^{(k)} \hat{\boldsymbol{\varepsilon}} \tag{3.26}$$

where

$$\hat{\mathbf{Q}}^{(k)} = \left[\begin{array}{ccc:c} \bar{Q}_{11}^{(k)} & \bar{Q}_{12}^{(k)} & \bar{Q}_{16}^{(k)} & 0 \\ \bar{Q}_{12}^{(k)} & \bar{Q}_{22}^{(k)} & \bar{Q}_{26}^{(k)} & 0 \\ \bar{Q}_{16}^{(k)} & \bar{Q}_{26}^{(k)} & \bar{Q}_{66}^{(k)} & 0 \\ \hdashline 0 & 0 & 0 & \bar{Q}_{66}^{(k)} \end{array}\right] \tag{3.27}$$

3.6. Numerical examples

As discussed previously, the Iterative Global-local Method is most advantageous when a limited portion of the member domain is affected by localized/cross-sectional deformations. Therefore, the accuracy and efficiency of the proposed iterative global-local procedure is verified through numerical examples in which local deformations cause a softening effect in the global behaviour of the structure. In all of the examples, the accuracy of the model is checked by comparing the results of the global-local model with that of a full shell element.

However, the accuracy of the developed shell element needs to be confirmed before being used as a benchmark. Consequently, the first three examples are presented to compare the buckling load obtained from the present model to the results from literature for various materials and loading conditions.

The critical load values reported in the first three examples are obtained from a nonlinear analysis and are defined as load level that minimizes the determinant of the tangential stiffness matrix of the structure as depicted in Figure 3.4 (Szilard 1985). It should be noted that the determinant of the stiffness matrix does not necessarily become zero especially in cases with stable post-buckling behaviour. Consequently, the minimum point in the determinant (i.e. the softest achievable configuration of the

structure) can be suitably defined as the critical load of the structure for practical purposes.

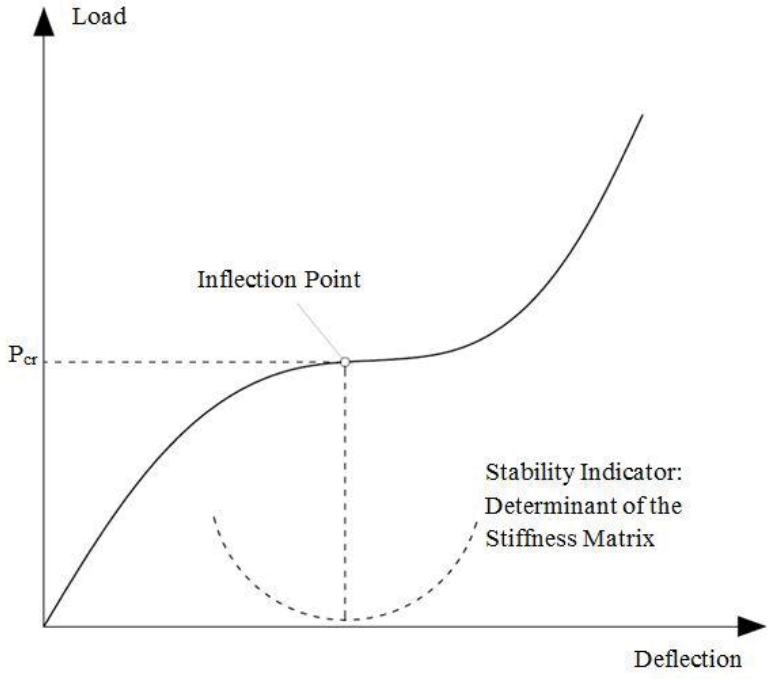

Figure 3.4: Definition of the buckling criteria in the nonlinear analysis

The rest of the examples are designed to express the accuracy and efficiency of the proposed global-local model. In the first example, an isotropic material (structural steel) is used while orthotropic graphite- and glass-epoxy composite laminates are used in the rest of the examples.

3.6.1. Verification of the shell element

3.6.1.1. Example 1: Isotropic simply supported I-beam

In order to verify the developed shell element, a simply supported I-beam made of isotropic material is analysed in example 1. Cross-sectional properties, loading and boundary conditions are shown in Figure 3.5. Geometrical dimensions of the I-section

are $b_f = 200mm$, $h = 195mm$, $t_f = 10mm$ and $t_w = 6.5mm$ and the length of the beam is $L = 6000mm$. Material properties corresponding to construction steel (i.e. $E = 200GPa$ and $\nu = 0.3$) is used, and the beam is simultaneously subjected to axial load and uniformly distributed lateral load (Figure 3.5).

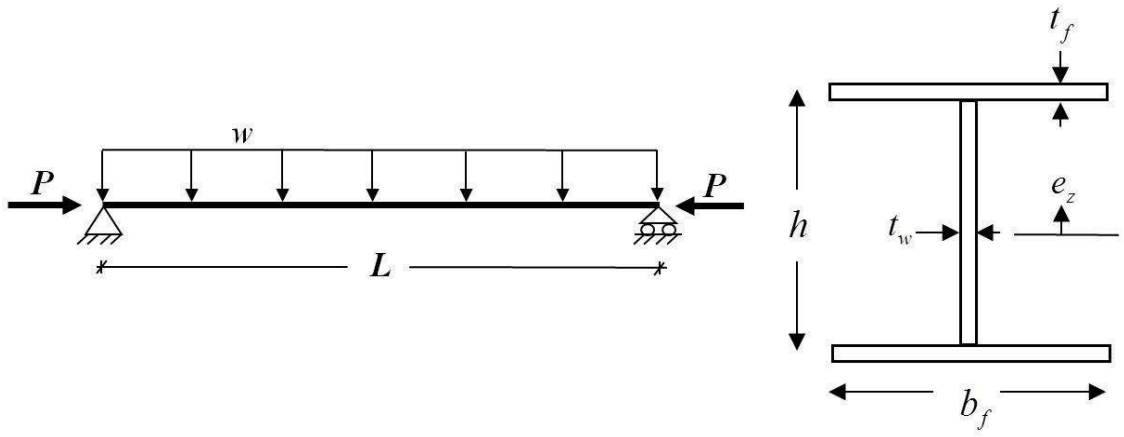

(a) Loading and boundary conditions (b) Cross-sectional dimensions

Figure 3.5: Simply-supported beam

Full nonlinear shell analysis is performed to obtain the buckling load as discussed previously, and the results are checked against the buckling results presented by Machado (2010). The buckling load is calculated for the simply supported beam subjected to axial and uniformly distributed lateral load. Two cases were analysed for the uniformly distributed load: firstly, the load was applied at the top flange and in a separate analysis, the load was applied on the bottom flange, which are denoted by $e_z = h/2$ and $e_z = -h/2$, respectively. The buckling loads are shown in Table 3.1, where for the lateral loads, the results are presented in terms of the corresponding maximum bending moment.

Table 3.1: Critical load and bending moment for isotropic simply supported beam

Load case	Machado (2010)	Present	Difference (%)
Axial	766.05 kN	771.75 kN	0.74
Lateral $e_z = h/2$	121.8 MNm	122.06 MNm	0.21
Lateral $e_z = -h/2$	240.4 MNm	244.10 MNm	1.52

The axial buckling load can also be calculated from the Euler formula $P_{cr} = \pi^2 EI / (L)^2$, where *L* is the length of the beam and EI is the flexural rigidity of the section about the minor principal axis. Using the properties of the member in this example, the Euler buckling load is calculated as 767.9 kN. It can be observed that the buckling load values obtained from the developed shell formulation are in good agreement with the results from the literature.

3.6.1.2. Example 2: Composite laminate simply-supported I-beam subjected to distributed load

The lateral-torsional buckling behaviour of a laminated simply-supported I-beam is investigated in this example. The beam length and the boundary conditions are the same as in the previous example, and the geometrical dimensions of the cross-section are: $b_f = 300mm$, $h = 600mm$ and $t_f = t_w = 30mm$ (Figure 3.5). The analysis is performed for two types of material; namely, graphite-epoxy and glass-epoxy composite laminates, the properties of which can be seen in Table 3.2.

Table 3.2: Material properties of composite laminates

Material	E_1	E_2	G_{12}	υ_{12}	υ_{21}
Graphite-epoxy	144 GPa	9.65 GPa	4.14 GPa	0.3	0.02
Glass-epoxy	48.3 GPa	19.8 GPa	8.96 GPa	0.27	0.11

The plates are made up of four layers of composite material, each of which have a thickness of $7.5mm$, with a stacking sequence of [0/0/0/0]. The uniformly distributed load is applied at three levels: the top flange, the shear centre and the bottom flange, which are depicted by $e_z = h/2$, $e_z = 0$ and $e_z = -h/2$, respectively. Similar to the previous example, the buckling load levels are obtained from the nonlinear shell analysis by drawing the lateral deflection versus the load level and considering the load level at which the tangential stiffness of the structures is a minimum, and the results are compared to the buckling loads reported by Machado (2010) for verification purposes. The results can be seen in Table 3.3 in terms of the values of the distributed load (in MN/m) causing the buckling behaviour.

Table 3.3: Buckling bending moment for composite simply-supported beam under distributed load

	Graphite/Epoxy		Glass/Epoxy	
Load level	Machado (2010)	Present	Machado (2010)	Present
$e_z = h/2$	0.25 MNm	0.25 MNm	0.12 MNm	0.12 MNm
$e_z = 0$	0.42 MNm	0.40 MNm	0.18 MNm	0.18 MNm
$e_z = -h/2$	0.67 MNm	0.63 MNm	0.26 MNm	0.24 MNm

Like the previous example, a good agreement can be confirmed between the results of the adopted shell model and results from the literature.

3.6.1.3. Example 3: Effect of fibre orientation on buckling behaviour of composite laminate columns

Simply-supported columns with various fibre orientation angles are analyzed in this example. The cross-section is a doubly-symmetric I with the following dimensions: $b_f = 80mm$, $h = 40mm$ and $t_f = t_w = 1mm$ (Figure 3.5). The length of the beam is $L = 240mm$, and the boundary conditions are similar to the previous examples. The column is composed of eight layers of graphite-epoxy composite laminates (Table 3.4) each $d = 0.125mm$ thick, with stacking sequence $[\theta/-\theta/\theta/-\theta]_S$. θ is the angle between the fibres and the axis of the beam, and is selected as 15°, 30°, 45°, 60°, 75° and 90°.

Table 3.4: Material properties for Example 3

Material	E_1	E_2	G_{12}	υ_{12}	υ_{21}
Graphite-epoxy	138 GPa	10 GPa	5 GPa	0.27	0.02

In order to obtain the buckling load of the column, a geometric nonlinear shell analysis is performed by adopting shell element of $20mm \times 20mm$ size. The results of the analysis in comparison with the buckling results presented by Mittelstedt (2007) can be observed in Table 3.5.

Table 3.5: Buckling load for simply-supported column, various fibre angles

θ	15°	30°	45°	60°	75°	90°
Present study	14.67	25.00	29.70	24.09	14.19	9.35
Mittelstedt [51	14.75	23.20	27.70	22.75	13.71	9.41

It can be observed from the results that the accuracy of the developed shell element for the analysis of composite laminates can be confirmed.

3.6.2. Verification of the proposed Iterative Global-local Method

In the following, numerical experiments are performed in order to demonstrate the accuracy and efficiency of the proposed global-local procedure in capturing the effect of localized behaviour. The results of the global-local method are compared with the beam and shell results for verification purposes. The material is taken as glass-epoxy, for which the material properties are provided in Table 3.6.

Table 3.6: Values of material properties used in Section 6.2

Material	E_1	E_2	G_{12}	υ_{12}	υ_{21}
Glass-epoxy	53.78 GPa	17.93 GPa	8.96 GPa	0.25	0.08

3.6.2.1. Flexural buckling of a C-shaped column

The Iterative Global-local Method is used to analyze the buckling behaviour of the composite column shown in Figure 3.6.

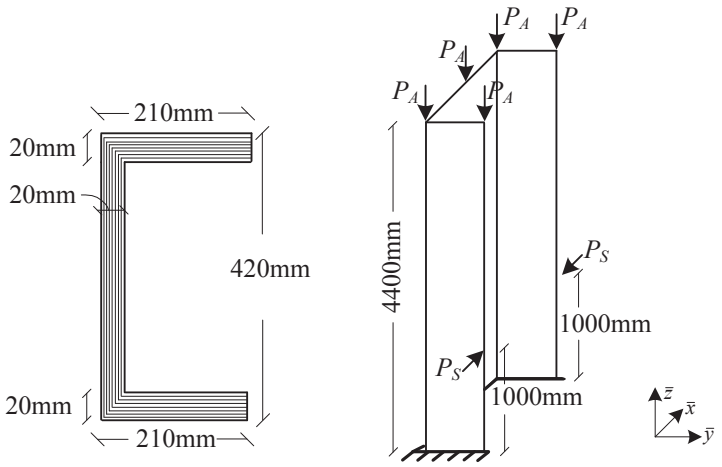

(a) Cross-sectional dimensions (b) Loading and boundary conditions

Figure 3.6: C-section composite column

The beam is composed of eight composite layers with equal thickness of *2.5mm* with a stacking sequence of $[0/-45/90/45]_S$. The analysis is performed using the beam-type element, the shell-type element and the global-local procedure. Apart from that, a constraint shell model is used to confirm that the beam-type analysis and the shell model are kinematically equivalent according to the kinematic assumptions of the thin-walled beam theory. It is obtained by applying multi-point constraints (MPCs) on the nodal displacements of the shell model in each cross-section according to the decomposition matrix $\mathbf{N}$. For beam analysis, 4 equal-span elements are used while the dimensions of the shell elements are approximately $200mm \times 200mm$.

The loading set presented in Figure 3.6 is applied at two stages; initially, the axial/vertical loads are applied (i.e. $P_s = 0$). The values of the buckling load are

calculated using the linearized buckling analysis corresponding to beam, constrain-shell and full-shell and are presented in Table 3.7. The close-form solution presented in the same table is the Euler buckling load, which is calculated from $N_{cr} = \pi^2 EI / (2L)^2$, where L is the length of the column, E is the Young's modulus and I is the second moment of area of the cross-section around the minor principal axis.

Table 3.7: Buckling load values for C-section column

Analysis	Beam	Constrain shell	shell	Closed-from (Euler)
Buckling load *(kN)*	52.19	52.12	53.48	51.93

Additionally, nonlinear analysis are performed using the aforementioned finite element models and the results are depicted in Table 3.7 in terms of horizontal deflection and rotation of the tip of the column versus the applied load. It can be observed that the results of all of the models match at this stage.

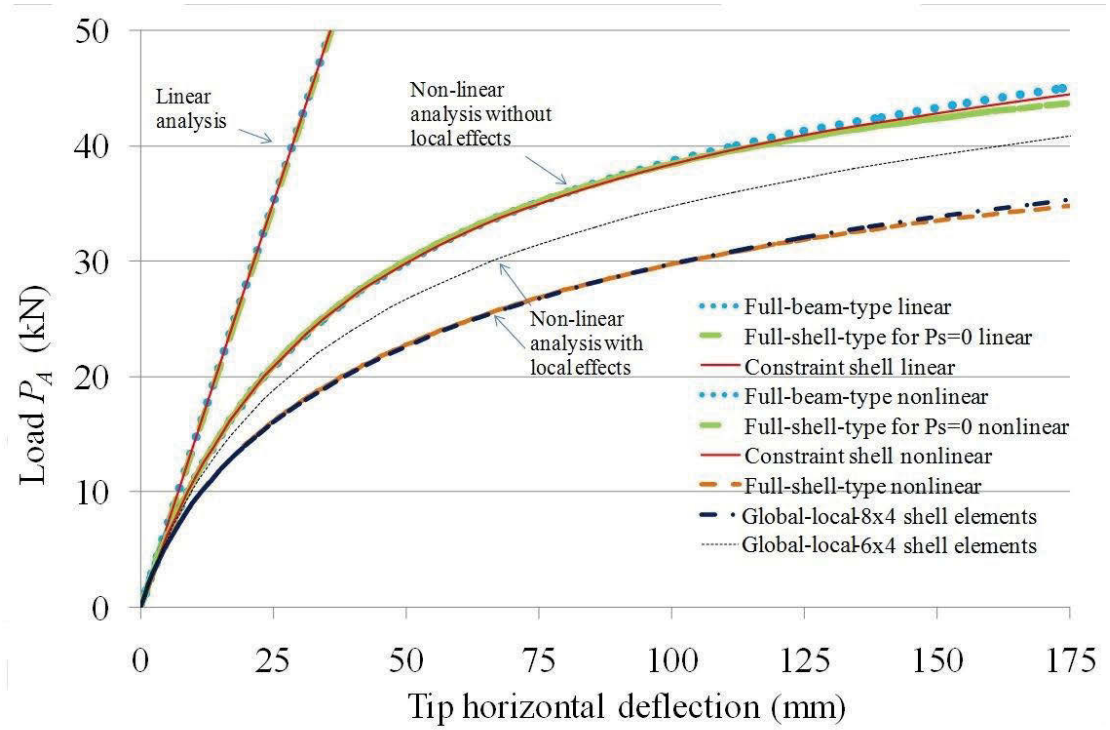

(a) Tip horizontal deflection

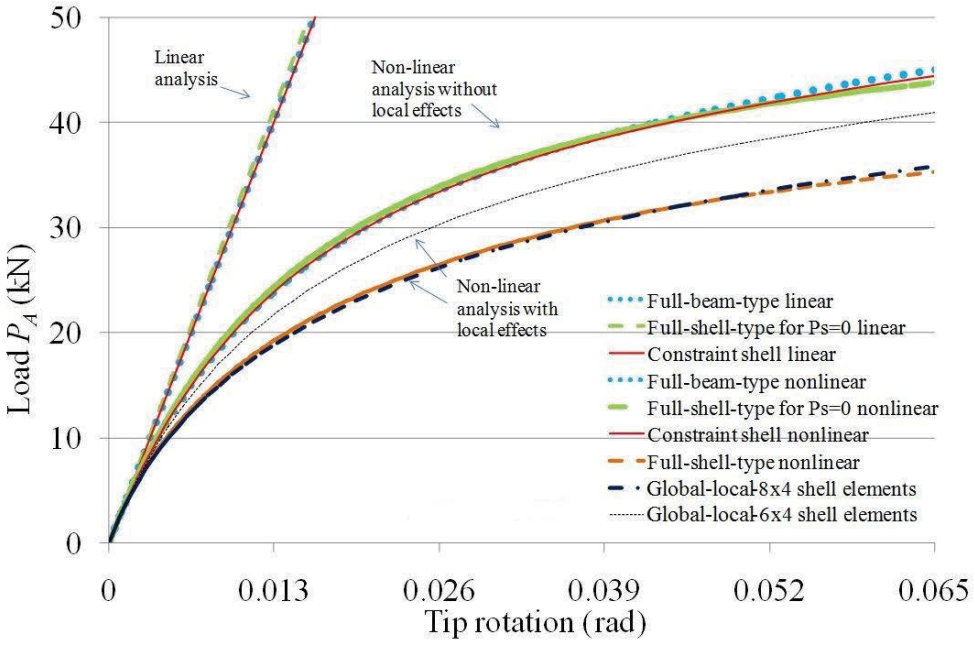

(b) Tip rotation

Figure 3.7: Load-displacement curves based on various finite element modeling

At a second stage, local/cross-sectional deformations are introduced to the model by assigning $P_s = 75kN$. It should be noted that the P_s load couple cancel the effect of each

other at cross-sectional level. Consequently, the beam-type finite element, which is formulated based on rigid cross-sectional assumption, fails to capture the effect of this load couple on the behaviour of the column. However, the softening effect of the local deformations is significant on the global response of the column, as shown by the curves obtained from the full shell model (Figure 3.7).

The above problem is also analyzed using the developed global-local model that is composed of beam and shell elements. The layout of the global-local model is shown in Figure 3.8.

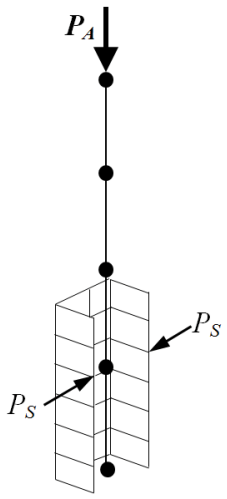

Figure 3.8: Layout of the global-local model

The model is analyzed by considering two values for the length of the overlapping region: initially it was considered between $z = 0$ and $z = 1200mm$ by using 6×4 shell elements, and then it was expanded to cover $z = 0$ and $z = 1600mm$ by using 8×4 elements.

The results of the global-local analysis are shown in Figure 3.7. It can be seen that the model with larger overlapping region (i.e. 8×4 elements) has been able to capture the effect of localized behaviour accurately and is matching well with the full shell model.

On the other hand, the model with smaller shell span is not able to fully capture the effect. It should be noted that even the model with larger shell span has a considerably smaller number of shell elements and therefore smaller number of degrees of freedom compared to the full shell model. Therefore, the accuracy and the efficiency of the proposed model can be verified herein. Care should be taken in choosing the overlapping region to ensure that it covers all the region affected by the localized behaviour.

3.6.2.2. Lateral-torsional buckling of an I-beam

The effect of a localized load couple on the lateral-torsional buckling resistance of a simply-supported I-beam is studied in this section. The geometry, boundary conditions and loading of the beam are shown in Figure 3.9.

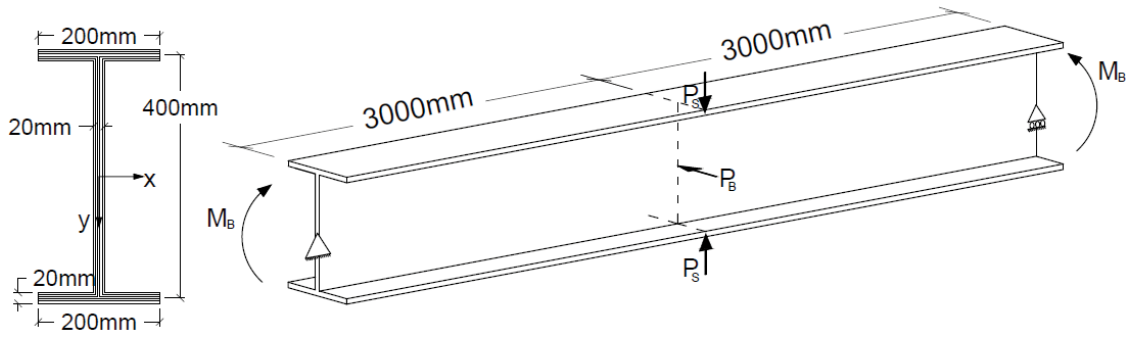

(a) Cross-sectional dimensions (b) Loading and boundary conditions

Figure 3.9: Properties of the simply supported I-beam

The flanges and the web of the beam is composed of 8 layers of glass-epoxy with angle-ply lay-ups of $[0/-45/90/45]_S$. Similar to the previous example, the beam is analysed using beam, shell and global-local models. 8 equal-span elements are used for the beam model while the shell elements have an approximate size of $200mm \times 200mm$. The loading is applied at two stages: firstly, only the global concentrated bending moments

are applied and secondly the load couple $P_S = 15kN$ are introduced to create the localized behaviour. Apart from that, a very small horizontal load ($P_B = 0.1kN$) is applied in order to initiate the lateral buckling behaviour in the first analysis. The global-local model is created by applying local shell elements in the vicinity of the local load couple (i.e. $z = 1400mm$ to $z = 4600mm$) by using 16×6 shell elements, as demonstrated in Figure 3.10.

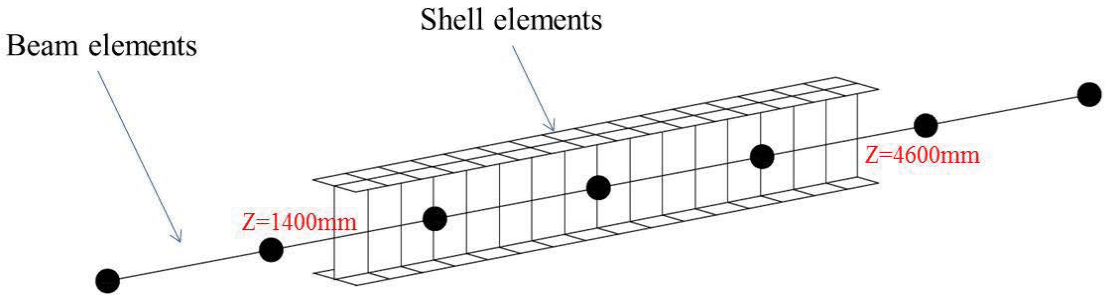

Figure 3.10: Schematic of the global-local model

The buckling behaviour is depicted using the lateral deflections of the beam mid-span (Figure 3.11). It can be observed that the reduction in the lateral buckling critical load, caused by the softening effect of the localized load couple, is captured accurately by the use of the global-local method.

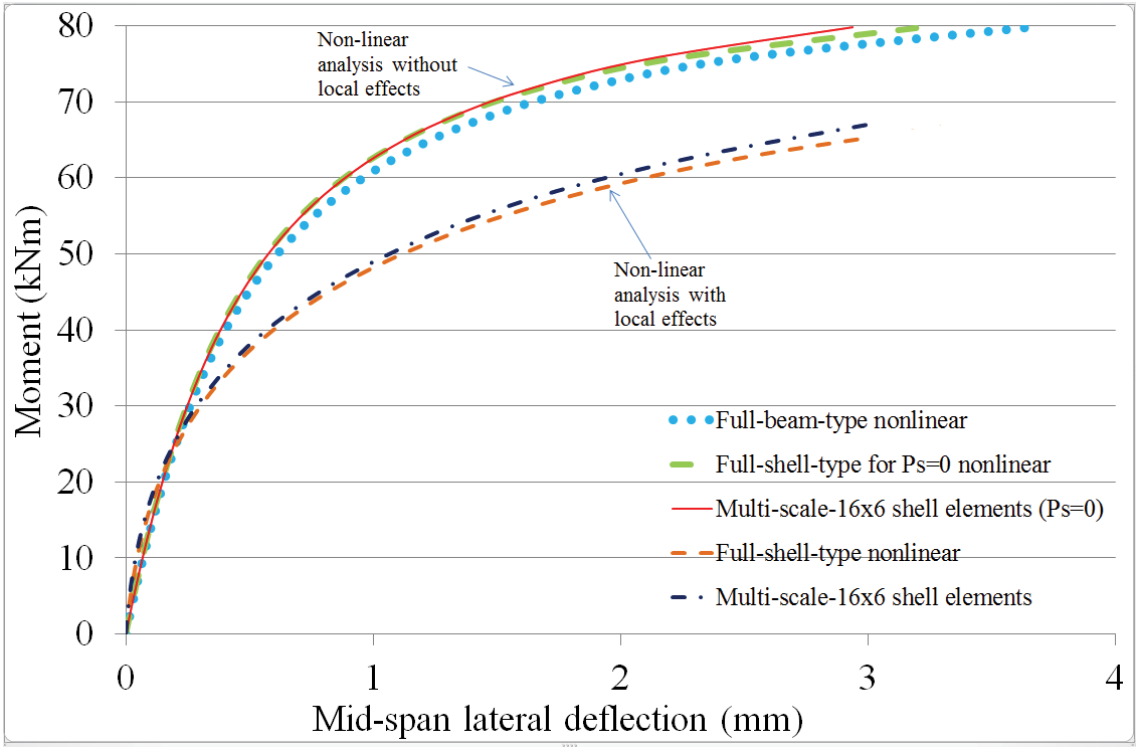

Figure 3.11: Load-deflection curve based on different modeling types

3.7. Conclusions

In this Chapter, a numerical method based on the Iterative Global-local Method was developed for the analysis of composite thin-walled members. A coarse-scale decomposition operator was proposed based on kinematic arguments, which associates the beam solution as the coarse-scale component of the shell solution. This decomposition allows for the method to incorporate the effects of local deformations on the global behaviour of the thin-walled member by using a shell model only within the region of local deformations. Thin-walled column and beam buckling cases were then analysed to show that the load carrying capacity can be influenced significantly by the local deformations, and the results of the multiscale procedure proposed herein were compared with those produced from full shell and beam-type analyses. In all cases, by selecting a sufficiently wide span of the local shell model in the global-local analyses, it

was confirmed that the behaviour according to the full shell-type analysis can be captured very accurately by using the global-local technique introduced in this chapter.

3.8. References

Back, S.Y. & Will, K.M. 2008, 'Shear-flexible thin-walled element for composite I-beams', *Engineering Structures*, vol. 30, no. 5, pp. 1447-58.

Barbero, E.J. & Raftoyiannis, I.G. 1993, 'Local buckling of FRP beams and columns', *Journal of Materials in Civil Engineering*, vol. 5, no. 3, pp. 339-55.

Bauld, N.R. & Tzeng, L.S. 1984, 'A Vlasov theory for fiber-reinforced beams with thin-walled open cross sections', *International Journal of Solids and Structures*, vol. 20, no. 3, pp. 277-97.

Cardoso, J.E.B., Benedito, N.M.B. & Valido, A.J.J. 2009, 'Finite element analysis of thin-walled composite laminated beams with geometrically nonlinear behavior including warping deformation', *Thin-Walled Structures*, vol. 47, no. 11, pp. 1363-72.

Fraternali, F. & Feo, L. 2000, 'On a moderate rotation theory of thin-walled composite beams', *Composites Part B: Engineering*, vol. 31, no. 2, pp. 141-58.

Jones, R.M. 1975, *Mechanics of composite materials*, McGraw-Hill, New York.

Kim, N.I., Shin, D.K. & Kim, M.Y. 2007, 'Exact lateral buckling analysis for thin-walled composite beam under end moment', *Engineering Structures*, vol. 29, no. 8, pp. 1739-51.

Lee, D.J. 1978, 'Local buckling coefficient for orthotropic structural sections', *Aeronautical Journal*, vol. 82, no. 811, pp. 313-20.

Lee, J. 2006, 'Lateral buckling analysis of thin-walled laminated composite beams with monosymmetric sections', *Engineering Structures*, vol. 28, no. 14, pp. 1997-2009.

Lee, J., Kim, S.E. & Hong, K. 2002, 'Lateral buckling of I-section composite beams', *Engineering Structures*, vol. 24, no. 7, pp. 955-64.

Machado, S.P. 2010, 'Interaction of combined loads on the lateral stability of thin-walled composite beams', *Engineering Structures*, vol. 32, no. 11, pp. 3516-27.

Mittelstedt, C. 2007, 'Local buckling of wide-flange thin-walled anisotropic composite beams', *Archive of Applied Mechanics*, vol. 77, no. 7, pp. 439-52.

Mottram, J.T. 1992, 'Lateral-torsional buckling of thin-walled composite I-beams by the finite difference method', *Composites Engineering*, vol. 2, no. 2, pp. 91-104.

Murakami, H. & Yamakawa, J. 1996, 'On approximate solutions for the deformation of plane anisotropic beams', *Composites Part B: Engineering*, vol. 27, no. 5, pp. 493-504.

Pandey, M.D., Kabir, M.Z. & Sherbourne, A.N. 1995, 'Flexural-torsional stability of thin-walled composite I-section beams', *Composites Engineering*, vol. 5, no. 3, pp. 321-42.

Qiao, P., Davalos, J.F. & Wang, J. 2001, 'Local buckling of composite FRP shapes by discrete plate analysis', *Journal of structural engineering New York, N.Y.*, vol. 127, no. 3, pp. 245-55.

Reddy, J.N. 2004, *Mechanics of Laminated Composite Plates and Shells: Theory and Analysis*, 2nd edn, CRC Press, Boca Raton, Florida.

Roberts, T.M. 2002, 'Influence of shear deformation on buckling of pultruded fiber reinforced plastic profiles', *Journal of Composites for Construction*, vol. 6, no. 4, pp. 241-8.

Roberts, T.M. & Masri, H.M.K.J.A.H. 2003, 'Section properties and buckling behavior of pultruded FRP profiles', *Journal of Reinforced Plastics and Composites*, vol. 22, no. 14, pp. 1305-17.

Sapkás, A. & Kollár, L.P. 2002, 'Lateral-torsional buckling of composite beams', *International Journal of Solids and Structures*, vol. 39, no. 11, pp. 2939-63.

Szilard, R. 1985, 'Critical load and post-buckling analysis by FEM using energy balancing technique', *Computers & Structures*, vol. 20, no. 1, pp. 277-86.

Trahair, N.S. 2003, *Flexural-Torsional Buckling of Structures*, Spon Press, London.

Yu, C. & Schafer, B.W. 2003, 'Local buckling tests on cold-formed steel beams', *Journal of Structural Engineering*, vol. 129, no. 12, pp. 1596-606.

Chapter 3 list of symbols

E_1, E_2	=	moduli of elasticity in two directions for orthotropic material
G_{12}	=	shear modulus
$\mathbf{Q}$	=	constitutive matrix for composite material
$Q_{ij}, \bar{Q}_{ij}$	=	components of constitutive matrix for composite material
$\bar{Q}^*_{ij}$	=	components of constitutive matrix for composite material in plane stress condition
$\mathbf{T}$	=	rotation matrix
$\boldsymbol{\varepsilon}$	=	strain vector
θ	=	angle between fibres and the axis of the beam
ν_{12}, ν_{21}	=	Poisson's ratios in two directions for orthotropic material
$\boldsymbol{\sigma}$	=	stress vector

Chapter 3 list of figures

Chapter 3 list of Tables

Chapter 4: The Iterative Global-local Method for the analysis of pipes

4.1. Abstract

The Iterative Global-local Method was presented in the previous chapters as a procedure to consider the effect of localized behaviour on the global response of thin-walled beams made of isotropic material and fibre reinforced laminates in chapters 2 and 3, respectively. In the current chapter, the Iterative Global-local Method is developed for the analysis of pipes. The material response, which was previously assumed as linear elastic, is generalised to include elasto plastic behaviour, which is common in pipelines.

Elevated pipelines are commonly encountered in petro-chemical and industrial applications. Within these applications, pipelines normally span hundreds of meters and are thus analysed using beam-type one-dimensional finite elements when the global behaviour of the pipeline is sought at a reasonably low computational cost. Standard beam-type elements, while computationally economic, are based on the assumption of rigid cross-section. Thus, they are unable to capture the effects of cross-sectional localized deformations. Such effects can be captured through shell-type finite element models. For long pipelines, shell models become prohibitively expensive. Within this context, the present chapter formulates an efficient numerical modelling which

effectively combines the efficiency of beam-type solutions while retaining the accuracy of shell-type solutions based on the Iterative Global-local Method. Solutions based on the present model are compared to those based on full shell-type analysis. The comparison demonstrates the accuracy and efficiency of the proposed method.

4.2. Introduction

Thin-walled pipes are widely used in industrial applications. Usually, they are susceptible to buckling and it is important to accurately predict their nonlinear response. Pipes usually span much larger distances in comparison to their cross-sectional dimensions. As such, beam-type elements are commonly adopted in their analysis. Standard beam-type elements, however, are based on the assumption of rigid cross-section and thus, cannot consider the deformations of the cross-section such as local buckling (Karamanos 2002) and only allow considerations of the global behaviour such as flexural-buckling (Hobbs 1981). In contrast, shell-type finite elements can capture local effects. The buckling response for long pipes under combinations of bending, axial force, and external pressure using shell analyses were investigated in (Houliara & Karamanos 2006, 2010; Karamanos & Tassoulas 1996). On the other hand shell elements are computationally more expensive and time consuming, and for typical pipeline networks spanning hundreds of meters, such shell analyses become impractical.

In pipe buckling behaviour, the interaction of local with global modes gives rise to multiple scales in the deformation fields. In order to capture the effect of local deformations, shell formulations have been utilised in the past e.g., (Ju & Kyriakides 1992; Ozkan & Mohareb 2009; Song & Tassoulas 1993; Weicker et al. 2010). Localized plasticity effects have also been incorporated into pipeline analysis through generalized plasticity models (Nowzartash & Mohareb 2004). In order to capture

ovalization in pipe elbows, efficient beam type formulations have been developed (Bathe & Almeida 1980, 1982; Militello & Huespe 1988).

In this chapter, the Iterative Global-local Method is extended for the elasto-plastic analysis of pipes. For that purpose, a beam-type element based on Euler-Bernoulli beam theory is adopted as the global/coarse-scale solution while a more-detailed elasto-plastic shell element is used as the local/fine-scale model. Similar to the previous chapters, the material behaviour of the global model is assumed to be linear elastic. However, elasto-plastic material response is considered for the local shell element. Comparisons with full shell- and beam-type models are provided in order to illustrate the efficiency of the proposed analysis.

4.3. Beam-type analysis

4.3.1. Kinematic assumptions, strains and stresses

In order to simplify the global analysis a beam formulation is used, which is based on the classical kinematic assumptions of the Euler-Bernoulli beam theory. These are: (a) plane section remains plane after deformation; (b) longitudinal axis of the pipe stays perpendicular to the cross-sectional plane after deformation; (c) contour of the cross-section does not deform in its plane; (d) normal stresses within the cross-sectional plane (hoop stresses) are zero. These assumptions imply that the nonzero strains in the pipe strain vector, i.e. $\bar{\boldsymbol{\varepsilon}}$ are due to the axial strains induced by membrane and bending actions, and shear strains induced by torsion only.

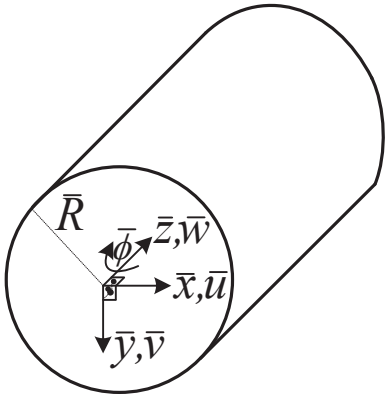

Figure 4.1: Deflections of the beam-type formulation

The beam element strain vector can be written in terms of linear and second order nonlinear terms, i.e. $\bar{\boldsymbol{\varepsilon}}=\bar{\boldsymbol{\varepsilon}}_L+\bar{\boldsymbol{\varepsilon}}_N$. The linear axial and shear strains $\bar{\varepsilon}_L$ and $\bar{\gamma}_L$, respectively can be obtained in terms of the derivatives of displacements $\bar{u},\bar{v},\bar{w}$ and the angle of twist $\bar{\phi}$ (Figure 4.1) as

$$\bar{\boldsymbol{\varepsilon}}_L=\left\langle \bar{\varepsilon}_L \quad 0 \quad \bar{\gamma}_L \quad 0 \right\rangle^{\mathrm{T}}=\bar{\mathbf{S}}\bar{\boldsymbol{\chi}}_L \tag{4.1}$$

which can be decomposed in terms of a matrix of cross-sectional coordinates, i.e.

$$\bar{\mathbf{S}}=\begin{bmatrix} 1 & -\bar{x} & -\bar{y} & 0 \\ 0 & 0 & 0 & 0 \\ 0 & 0 & 0 & \bar{R} \\ 0 & 0 & 0 & 0 \end{bmatrix} \tag{4.2}$$

and a vector of linear displacement derivatives, i.e.

$$\bar{\boldsymbol{\chi}}_L^{\mathrm{T}}=\left\langle \bar{w}' \quad \bar{u}'' \quad \bar{v}'' \quad \bar{\phi}' \right\rangle \tag{4.3}$$

In Eq. (4.2), $\bar{x}$ and $\bar{y}$ identifies coordinates of a point on the cross-section, and $\bar{R}$ is the radius of the pipe (Figure 4.1). In Eq. (4.3), prime denotes derivative with respect to the axial coordinate z, i.e. $()'=\mathrm{d}()/\mathrm{d}z$. The nonlinear strains can be written as

$$\bar{\boldsymbol{\varepsilon}}_N = \left\langle \bar{\varepsilon}_N \quad 0 \quad \bar{\gamma}_N \quad 0 \right\rangle^{\mathrm{T}} = \bar{\mathbf{S}}\bar{\boldsymbol{\chi}}_N \tag{4.4}$$

in which $\bar{\varepsilon}_N$ is the nonlinear axial strain and $\bar{\gamma}_N$ is considered to vanish. Similar to linear strains, the nonlinear strain vector in Eq. (4.4) can be expressed by using the same matrix of cross-sectional coordinates $\bar{\mathbf{S}}$ post-multiplied by a vector of second-order displacement derivatives, i.e.,

$$\bar{\boldsymbol{\chi}}_N{}^{\mathrm{T}} = \left\langle \frac{1}{2}\left(\bar{u}'^2+\bar{v}'^2\right) \quad 0 \quad 0 \quad 0 \quad 0 \right\rangle \tag{4.5}$$

4.3.2. Interpolation functions for the beam displacements

The element is developed by using linear interpolations for $\bar{w}$ and $\bar{\phi}$ and cubic interpolations for $\bar{u}$ and $\bar{v}$. Thus, the displacement vector of the beam axis is $\bar{\mathbf{u}}_a = \bar{\mathbf{X}}_a\bar{\mathbf{d}}$, in which

$$\bar{\mathbf{u}}_a = \left\langle \bar{w} \quad \bar{u} \quad \bar{v} \quad \bar{\phi} \right\rangle^{\mathrm{T}} \tag{4.6}$$

where the matrix of interpolation functions can be written as

$$\bar{\mathbf{X}}_a = \begin{bmatrix} \mathbf{L}^{\mathrm{T}} & \mathbf{0} & \mathbf{0} & \mathbf{0} \\ \mathbf{0} & \mathbf{H}^{\mathrm{T}} & \mathbf{0} & \mathbf{0} \\ \mathbf{0} & \mathbf{0} & \mathbf{H}^{\mathrm{T}} & \mathbf{0} \\ \mathbf{0} & \mathbf{0} & \mathbf{0} & \mathbf{L}^{\mathrm{T}} \end{bmatrix} \tag{4.7}$$

In Eq. **(4.7)**, vectors $\mathbf{L}$ and $\mathbf{H}$ are used for linear and cubic interpolation, respectively, i.e.,

$$\mathbf{L}=\left\langle 1-\frac{\bar{z}}{L} \quad \frac{\bar{z}}{L}\right\rangle^{\mathrm{T}} \tag{4.8}$$

and

$$\mathbf{H}=\left\langle 1-\frac{3\bar{z}^2}{L^2}+\frac{2\bar{z}^3}{L^3} \quad \bar{z}-\frac{2\bar{z}^2}{L}+\frac{\bar{z}^3}{L^2} \quad \frac{3\bar{z}^2}{L^2}-\frac{2\bar{z}^3}{L^3} \quad -\frac{\bar{z}^2}{L}+\frac{\bar{z}^3}{L^2}\right\rangle^{\mathrm{T}} \tag{4.9}$$

The nodal displacement vector $\bar{\mathbf{d}}$ of the beam type finite element can be written as

$$\bar{\mathbf{d}}=\left\langle \bar{w}_1 \quad \bar{w}_2 \;\vdots\; \bar{u}_1 \quad \bar{\theta}_{x1} \quad \bar{u}_2 \quad \bar{\theta}_{x2} \;\vdots\; \bar{v}_1 \quad \bar{\theta}_{y1} \quad \bar{v}_2 \quad \bar{\theta}_{y2} \;\vdots\; \bar{\phi}_1 \quad \bar{\phi}_2\right\rangle^{\mathrm{T}} \tag{4.10}$$

in which subscripts 1 and 2 refer to each of the two end nodes, $\bar{\theta}_x$ and $\bar{\theta}_y$ refer to bending rotations in $\bar{z}$–$\bar{x}$ and $\bar{z}$–$\bar{y}$ planes (Figure 4.1) respectively. Under the rigid sectional contour assumption of the beam theory, the displacement vector of a point α on the cross-section can be written as $\bar{\mathbf{u}}=\mathbf{N}\bar{\mathbf{d}}$ where

$$\bar{\mathbf{u}}=\left\langle \bar{w}_\alpha \quad \bar{u}_\alpha \quad \bar{u}'_\alpha \quad \bar{v}_\alpha \quad \bar{v}'_\alpha \quad \bar{\phi}_\alpha\right\rangle^{\mathrm{T}} \tag{4.11}$$

and $\mathbf{N}=\mathbf{YZ}$ in which $\mathbf{Z}$ is a matrix of interpolation functions, i.e.,

$$\mathbf{Z}=\left[\begin{array}{c|c|c|c} \mathbf{L}^{\mathrm{T}} & \mathbf{0} & \mathbf{0} & \mathbf{0} \\ \hline \mathbf{0} & \mathbf{H}^{\mathrm{T}} & \mathbf{0} & \mathbf{0} \\ \hline \mathbf{0} & \mathbf{0} & \mathbf{H}^{\mathrm{T}} & \mathbf{0} \\ \hline \mathbf{0} & \mathbf{0} & \mathbf{0} & \mathbf{L}^{\mathrm{T}} \\ \hline \mathbf{0} & \dfrac{\mathrm{d}\mathbf{H}^{\mathrm{T}}}{\mathrm{d}\bar{z}} & \mathbf{0} & \mathbf{0} \\ \hline \mathbf{0} & \mathbf{0} & \dfrac{\mathrm{d}\mathbf{H}^{\mathrm{T}}}{\mathrm{d}\bar{z}} & \mathbf{0} \\ \hline \mathbf{0} & \mathbf{0} & \mathbf{0} & \dfrac{\mathrm{d}\mathbf{L}^{\mathrm{T}}}{\mathrm{d}\bar{z}} \end{array}\right] \tag{4.12}$$

and $\mathbf{Y}$ is a matrix of cross-sectional coordinates, i.e.,

$$\mathbf{Y}=\begin{bmatrix} 1 & 0 & 0 & 0 & -\bar{x} & -\bar{y} & 0 \\ 0 & 1 & 0 & -\bar{y} & 0 & 0 & 0 \\ 0 & 0 & 0 & 0 & 1 & 0 & -\bar{y} \\ 0 & 0 & 1 & \bar{x} & 0 & 0 & 0 \\ 0 & 0 & 0 & 0 & 0 & -1 & -\bar{x} \\ 0 & 0 & 0 & -1 & 0 & 0 & 0 \end{bmatrix} \tag{4.13}$$

4.3.3. Variational formulation

The equilibrium equations for static analysis can be obtained in the variational form as

$$\delta\bar{\Pi}=\int_{L}\int_{A}\delta\bar{\boldsymbol{\varepsilon}}^{\mathrm{T}}\bar{\boldsymbol{\sigma}}\,\mathrm{d}A\,\mathrm{d}\bar{z}-\delta\bar{\mathbf{d}}^{\mathrm{T}}\bar{\mathbf{f}}=0 \tag{4.14}$$

in which A is the cross-sectional area, L is the beam span and $\bar{\mathbf{f}}$ is the external load vector. In this study, in the region where no local deformations occur, the material behaviour is assumed elastic. Thus, in Eq. (4.14), the beam stresses can be obtained directly from the strains using the linear stress-strain relationship for an isotropic material, i.e., $\bar{\boldsymbol{\sigma}}=\bar{\mathbf{E}}\bar{\boldsymbol{\varepsilon}}$, where the vector of beam stresses can be written as

$$\bar{\boldsymbol{\sigma}} = \left\langle \bar{\sigma} \quad 0 \quad \bar{\tau} \quad 0 \right\rangle^{\mathrm{T}} \tag{4.15}$$

and the beam constitutive matrix $\bar{\mathbf{E}}$ can be written as

$$\bar{\mathbf{E}} = \left[\begin{array}{ccc:c} E & 0 & 0 & 0 \\ 0 & 0 & 0 & 0 \\ 0 & 0 & \dfrac{E}{2(1+\nu)} & 0 \\ \hdashline 0 & 0 & 0 & 0 \end{array}\right] \tag{4.16}$$

The first variation of the strain vector for the beam element can be written as

$$\delta\bar{\boldsymbol{\varepsilon}} = \bar{\mathbf{S}}\bar{\mathbf{B}}\delta\bar{\mathbf{d}} \tag{4.17}$$

where $\bar{\mathbf{B}}$ can be written as

$$\bar{\mathbf{B}} = \begin{bmatrix} 1 & \bar{u}' & 0 & \bar{v}' & 0 & 0 & 0 \\ 0 & 0 & 1 & 0 & 0 & 0 & 0 \\ 0 & 0 & 0 & 0 & 1 & 0 & 0 \\ 0 & 0 & 0 & 0 & 0 & 0 & 1 \end{bmatrix} \nabla\bar{\mathbf{X}}_a \tag{4.18}$$

in which

$$\nabla = \begin{bmatrix} \dfrac{\mathrm{d}}{\mathrm{d}z} & 0 & 0 & 0 & 0 & 0 & 0 \\ 0 & \dfrac{\mathrm{d}}{\mathrm{d}z} & \dfrac{\mathrm{d}^2}{\mathrm{d}z^2} & 0 & 0 & 0 & 0 \\ 0 & 0 & 0 & \dfrac{\mathrm{d}}{\mathrm{d}z} & \dfrac{\mathrm{d}^2}{\mathrm{d}z^2} & 0 & 0 \\ 0 & 0 & 0 & 0 & 0 & 1 & \dfrac{\mathrm{d}}{\mathrm{d}z} \end{bmatrix}^{\mathrm{T}} \tag{4.19}$$

4.4. Shell-type analysis

4.4.1. Kinematic assumptions and strains

A schematic of the shell element and the adopted coordinate system is shown in Figure 4.2, in which the *x* and *y* axes define a plane tangential to the mid-surface of the shell and *z* axis is normal to the mid-surface.

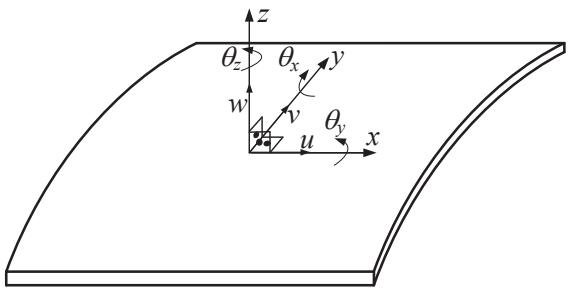

Figure 4.2: Deflections of the beam-type formulation

Strains of the shell-type analysis are composed of linear strains due to (a) membrane deformations $\hat{\boldsymbol{\varepsilon}}_{mm}$, (b) plate bending deformations $\hat{\boldsymbol{\varepsilon}}_{b}$, and (c) nonlinear components of strains due to membrane and plate bending action $\hat{\boldsymbol{\varepsilon}}_{N}$, i.e.,

$$\hat{\boldsymbol{\varepsilon}} = \hat{\boldsymbol{\varepsilon}}_{mm} + \hat{\boldsymbol{\varepsilon}}_{b} + \hat{\boldsymbol{\varepsilon}}_{N} = \left\langle \hat{\varepsilon}_{x} \quad \hat{\varepsilon}_{y} \quad \hat{\gamma}_{xy} \quad \hat{\gamma}_{m} \right\rangle^{\mathrm{T}} \tag{4.20}$$

The vector of linear components for the membrane strain $\hat{\boldsymbol{\varepsilon}}_{mm}$ can be written as

$$\hat{\boldsymbol{\varepsilon}}_{mm}^{T} = \left\langle \hat{\boldsymbol{\varepsilon}}_{m}^{\ T} \;\middle|\; \frac{1}{2}\left(\frac{\partial \hat{v}_0}{\partial x} - \frac{\partial \hat{u}_0}{\partial y}\right) - \hat{\theta}_z \right\rangle = \left\langle \frac{\partial \hat{u}_0}{\partial x} \quad \frac{\partial \hat{v}_0}{\partial y} + \frac{\partial f}{\partial r}\hat{\theta}_y \quad \frac{\partial \hat{u}_0}{\partial y} + \frac{\partial \hat{v}_0}{\partial x} \;\middle|\; \frac{1}{2}\left(\frac{\partial \hat{v}_0}{\partial x} - \frac{\partial \hat{u}_0}{\partial y}\right) - \hat{\theta}_z \right\rangle \tag{4.21}$$

in which $\hat{\theta}_x$ and $\hat{\theta}_y$ are rotations in local *x*-*z* and *y*-*z* planes respectively (Figure 4.2), $\hat{\theta}_z$ is the drilling rotation about the z axis, and $\hat{u}_0$ and $\hat{v}_0$ are the displacements of the mid-surface in the local *x*-*y* plane (Figure 4.2). In Eq. (4.21) the term $(\partial f/\partial r)\hat{\theta}_y$ is added according to Marguerre shallow shell theory (Cook 1990).

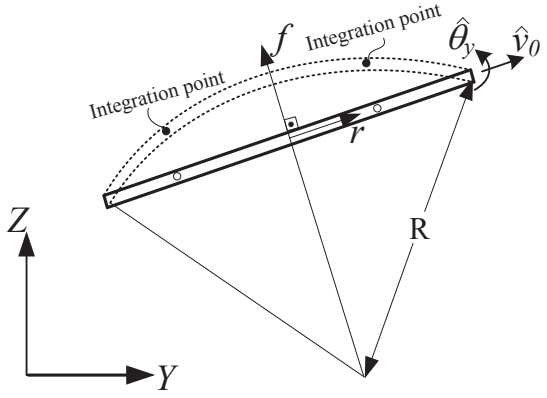

Figure 4.3: Arch elevation used in shell formulation

As shown in Figure 4.3, $f = f(r)$ is the expression for the elevation of the arch in Z-Y plane in terms of coordinate *r*. In calculating the element length and locations of the integration points, the arch length was considered.

For the membrane component of the shell-type element, the finite element of Ibrahimbegovic et al. (1990) employing drilling degrees of freedom is adopted herein. Adopting the membrane element with drilling degree of freedom is important because it allows easy assemblage when non-coplanar elements exist (Figure 4.4), which is the case for pipes.

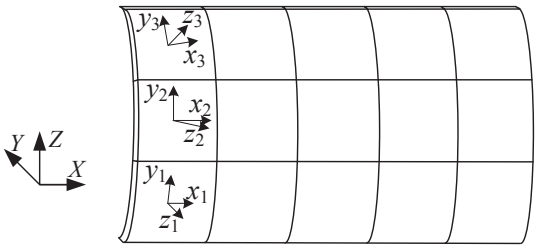

Figure 4.4: Global vs. local coordinate system in the shell element

The last entry in Eq. (4.21) contains the skew symmetric part of the membrane strains which is introduced into the potential energy functional related to a penalty term to avoid numerical instability when drilling rotations $\hat{\theta}_z$ are used with Allman-type interpolations (Hughes & Brezzi 1989), as discussed in Chapter 2. According to Mindlin-Reissner theory (Cook et al. 2002), the plate bending strains can be written as

$$\hat{\boldsymbol{\varepsilon}}_b = -z\left\langle \hat{\boldsymbol{\chi}} \;\vdots\; 0 \right\rangle^T = -z\left\langle \frac{\partial \hat{\theta}_x}{\partial x} \quad \frac{\partial \hat{\theta}_y}{\partial y} \quad \frac{\partial \hat{\theta}_x}{\partial y}+\frac{\partial \hat{\theta}_y}{\partial x} \;\vdots\; 0 \right\rangle^T \tag{4.22}$$

in which $\hat{\boldsymbol{\chi}}$ is the curvature vector. It is assumed that the second order longitudinal displacement derivatives, second order lateral strains and second order shear strains are negligibly small, i.e., $\frac{1}{2}\left[\left(\partial \hat{w}_0/\partial y\right)^2+\left(\partial \hat{u}_0/\partial y\right)^2\right] \approx 0$, $\left(\partial \hat{w}_0/\partial x\right)\left(\partial \hat{w}_0/\partial y\right) \approx 0$. Thus, the nonlinear strain component can be written as

$$\hat{\boldsymbol{\varepsilon}}_N \approx \left\langle \frac{1}{2}\left(\frac{\partial \hat{w}_0}{\partial x}\right)^2+\frac{1}{2}\left(\frac{\partial \hat{v}_0}{\partial x}\right)^2 \quad 0 \quad 0 \;\vdots\; 0 \right\rangle^T \tag{4.23}$$

in which $\hat{w}_0$ is the out of plane deflection of the mid-surface in the local z direction (Figure 4.2). It should be noted that the second order strain component is consistent with the second order strains of the beam formulation (Section 4.3), so that the beam solution can be considered as a special case of the shell solution.

4.4.2. Constitutive relations

The shell analysis is elasto-plastic. In this study, for convenience, we apply the one step forward Euler numerical procedure as described in Crisfield (1991). Initially, the vector of total stresses at any point within the shell is

$$\hat{\boldsymbol{\sigma}} = \left\langle \hat{\sigma}_x \quad \hat{\sigma}_y \quad \hat{\tau}_{xy} \;\vdots\; \hat{\tau}_m \right\rangle^{\mathrm{T}} \tag{4.24}$$

Assuming that the whole strain increment is elastic, the stress increment can be written as

$$\Delta\hat{\boldsymbol{\sigma}} = \hat{\mathbf{E}}\Delta\hat{\boldsymbol{\varepsilon}} \tag{4.25}$$

in which the matrix of elastic material properties of the shell element $\hat{\mathbf{E}}$ can be written as

$$\hat{\mathbf{E}} = \frac{E}{\left(1-\nu^2\right)} \left[\begin{array}{ccc:c} 1 & \nu & 0 & 0 \\ \nu & 1 & 0 & 0 \\ 0 & 0 & \dfrac{1-\nu}{2} & 0 \\ \hdashline 0 & 0 & 0 & \dfrac{(1-\nu)}{2} \end{array}\right] \tag{4.26}$$

in which E is Young's modulus and ν is the Poisson's ratio. The last diagonal term in Eq. (4.26) arises from the penalty term introduced into the potential energy functional (Hughes & Brezzi 1989). Within an incremental iterative solution, the trial stresses are obtained using stress increments. Under plane stress plasticity conditions, i.e. $\hat{\sigma}_z = \hat{\tau}_{yz} = \hat{\tau}_{zx} = 0$, the von Mises yield criterion is used to determine whether the trial

stresses are elastic. According to the forward Euler procedure (Crisfield 1991), since $\varepsilon_z \neq 0$, a four-dimensional yield surface f is assumed as

$$f = \sigma_{ef} - \sigma_Y \tag{4.27}$$

where $\sigma_{ef} = \left[\left(\hat{\sigma}_x - \sigma_y\right)^2 + \left(\hat{\sigma}_y - \sigma_z\right)^2 + \left(\hat{\sigma}_z - \sigma_x\right)^2 + 6\hat{\tau}_{xy}^{\,2} \right]^{1/2} \Big/ \sqrt{2}$ and σ_Y is the yield stress limit. When yielding occurs, the relation between the stress increment and the elastic strain increment is re-written in a four-dimensional context as

$$\Delta\hat{\boldsymbol{\sigma}}_a = \begin{Bmatrix} \Delta\hat{\sigma}_x \\ \Delta\hat{\sigma}_y \\ \Delta\hat{\sigma}_z \\ \Delta\hat{\tau}_{xy} \end{Bmatrix} = \frac{E}{(1+\nu)(1-2\nu)} \begin{bmatrix} (1-\nu) & \nu & \nu & 0 \\ \nu & (1-\nu) & \nu & 0 \\ \nu & \nu & (1-\nu) & 0 \\ 0 & 0 & 0 & \frac{1}{2}(1-2\nu) \end{bmatrix} \begin{Bmatrix} \Delta\hat{\varepsilon}_{ex} \\ \Delta\hat{\varepsilon}_{ey} \\ \Delta\hat{\varepsilon}_{ez} \\ \Delta\hat{\gamma}_{exy} \end{Bmatrix} = \mathbf{E}_a^{\,e} \Delta\boldsymbol{\varepsilon}_{ea} \tag{4.28}$$

The elastic part of the strain increment can be expressed as the plastic strain increment subtracted from the total strain, i.e., $\Delta\hat{\boldsymbol{\varepsilon}}_{ea} = \Delta\hat{\boldsymbol{\varepsilon}}_a - \hat{\boldsymbol{\varepsilon}}_{pa}$, where $\Delta\hat{\boldsymbol{\varepsilon}}_a^{\,\mathrm{T}} = \left\langle \Delta\hat{\varepsilon}_x \quad \Delta\hat{\varepsilon}_y \quad \Delta\hat{\varepsilon}_z \quad \Delta\hat{\gamma}_{xy} \right\rangle$. Strains $\Delta\hat{\varepsilon}_x$, $\Delta\hat{\varepsilon}_y$ and $\Delta\hat{\gamma}_{xy}$ are obtained from the displacement increments as given in Eqs. (4.21) to (4.23). Strain $\Delta\hat{\varepsilon}_z$ can be obtained by using the plane stress condition, i.e., $\Delta\sigma_z = 0$ in Eq. (4.28) while assuming incompressible plasticity (Marques 1984) yielding

$$\Delta\varepsilon_z = -\frac{\nu}{(1-\nu)}\left(\Delta\varepsilon_x + \Delta\varepsilon_y\right) - \frac{\Delta\lambda}{2\sigma_{ef}}\left(\sigma_x + \sigma_y\right)\frac{(1-2\nu)}{(1-\nu)} \tag{4.29}$$

From the Prandtl-Reuss flow rule for associative plasticity, the plastic strain increment vector $\Delta\boldsymbol{\varepsilon}_{pa}$ can be written as

$$\Delta\boldsymbol{\varepsilon}_{pa} = \Delta\lambda \frac{\partial f}{\partial \boldsymbol{\sigma}_a} \tag{4.30}$$

in which $\Delta\lambda = \dfrac{\mathbf{a}_a{}^{\mathrm{T}}\mathbf{E}_a{}^{\mathrm{e}}\Delta\boldsymbol{\varepsilon}_a}{\mathbf{a}_a{}^{\mathrm{T}}\mathbf{E}_a{}^{\mathrm{e}}\mathbf{a}_a}$. By setting $\sigma_z = 0$, one obtains $\mathbf{a}_a$ as

$$\mathbf{a}_a{}^{\mathrm{T}} = \frac{\partial f^{\mathrm{T}}}{\partial \boldsymbol{\sigma}} = \frac{1}{2\sigma_{ef}}\left\langle \left(2\sigma_x - \sigma_y\right) \quad \left(2\sigma_y - \sigma_x\right) \quad \left(-\sigma_x - \sigma_y\right) \quad 6\tau_{xy} \right\rangle \tag{4.31}$$

It should be noted that $\Delta\hat{\gamma}_m$ is assumed elastic. Updated stresses are collected in Eq. (4.24).

The interpolation functions of the shell element are similar to the ones used in Chapter 2 (Appendix 2.A.)

4.4.3. Variational formulation and consistent linearization

For the shell analysis, the equilibrium equations can be obtained in the variational form as

$$\delta\hat{\Pi} = \int_L \int_A \delta\hat{\boldsymbol{\varepsilon}}^{\mathrm{T}}\hat{\boldsymbol{\sigma}}\,\mathrm{d}A\,\mathrm{d}\bar{z} - \delta\hat{\mathbf{d}}^{\mathrm{T}}\hat{\mathbf{f}} = 0 \tag{4.32}$$

in which $\hat{\boldsymbol{\varepsilon}}$ represents the vector of strain components. The virtual work functional of the shell element is modified in order to avoid numerical stability issues with Allman type interpolations of the membrane component as suggested in (Ibrahimbegovic et al. 1990) and thus, the skew symmetric part of the membrane strains and associated drilling rotations are contained in the first term in Eq. (4.32). In the last term of Eq. (4.32), $\hat{\mathbf{f}}$ is the external load vector. The first variation of the strain field of the shell element can be expressed as

$$\delta\hat{\boldsymbol{\varepsilon}} = \hat{\mathbf{S}}\hat{\mathbf{B}}\delta\hat{\mathbf{d}} \tag{4.33}$$

where $\hat{\mathbf{B}}$ and $\hat{\mathbf{S}}$ for an element are explicitly given in Appendix 4.A. The incremental equilibrium equations for the shell formulation can be obtained by subtracting the first variation of the modified potential energy in Eq. (4.32) at two neighbouring equilibrium states and then linearizing the results by omitting the second- and higher-order terms, i.e.

$$\Delta\left(\delta\hat{\Pi}\right) \approx \delta\hat{\mathbf{d}}^{\mathrm{T}}\hat{\mathbf{K}}\Delta\hat{\mathbf{d}} - \delta\hat{\mathbf{d}}^{\mathrm{T}}\Delta\hat{\mathbf{f}} = 0 \tag{4.34}$$

where $\hat{\mathbf{K}}$ is the tangent stiffness matrix of the shell model, i.e.,

$$\hat{\mathbf{K}} = \int_L \int_A \hat{\mathbf{B}}^{\mathrm{T}}\hat{\mathbf{S}}^{\mathrm{T}}\hat{\mathbf{E}}_{ep}\hat{\mathbf{S}}\hat{\mathbf{B}}\mathrm{d}A\mathrm{d}\bar{z} + \int_L \hat{\mathbf{M}}_{\sigma}\mathrm{d}\bar{z} \tag{4.35}$$

where $\hat{\mathbf{M}}_{\sigma}\Delta\hat{\mathbf{d}} = \int_A \delta\hat{\mathbf{B}}^{\mathrm{T}}\hat{\mathbf{S}}^{\mathrm{T}}\hat{\boldsymbol{\sigma}}\mathrm{d}A$ and $\hat{\mathbf{E}}_{ep}$ is the elasto-plastic constitutive matrix.

4.5. Verification of the shell element

Before using iterative global-local developments in the present model, the elasto-plastic shell model implemented in Section 4.4 is verified. Towards this goal, a cylinder panel under point load was considered. As shown in Figure 4.5, the curve edge nodes of the panel are assumed to be free in all directions while the side nodes are fixed against translation in all three directions.

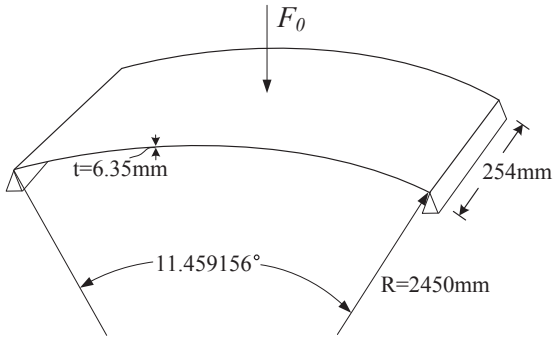

Figure 4.5: Geometry, loading and boundary conditions of the arch

The modulus of elasticity, the Poisson ratio and the yield stress is taken as 3.103kN/mm2, 0.3, and .001kN/mm2, respectively. The material is assumed to be elastic-perfectly plastic. The results are obtained by using 20x10 elements, i.e., 20 elements along the curved direction and 10 elements along the fixed edge direction, and compared with those obtained by the TRIC continuum formulation of Argyris et al. (2002) as shown in Figure 4.6. Acceptable agreement can be seen between the results considering the following two facts: a smaller number of elements are used in the current study (200 elements versus 800 elements used by Argyris et al. (2002)), and a shear deformable shell element based on Reissner-Mindlin plate theory is used by them as opposed to a Kirchhoff element of the current study.

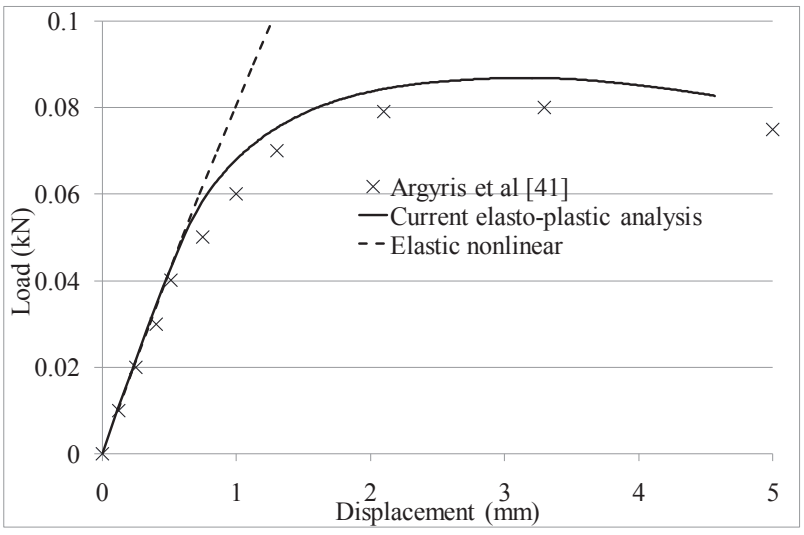

Figure 4.6: Load-deflection relations for the arch

4.6. Numerical examples

4.6.1. Cantilever pipe under compression, lateral force, and pinching forces

As shown in Figure 4.7.a, the pipe analysed has a 17.15m span, a 1m diameter and a 25mm wall thickness. The pipe is fixed at the bottom end and is subject to a compressive force up to $N=15000$kN acting at the top and a total lateral load up to 15 kN ($F_Y=7.5$kN).

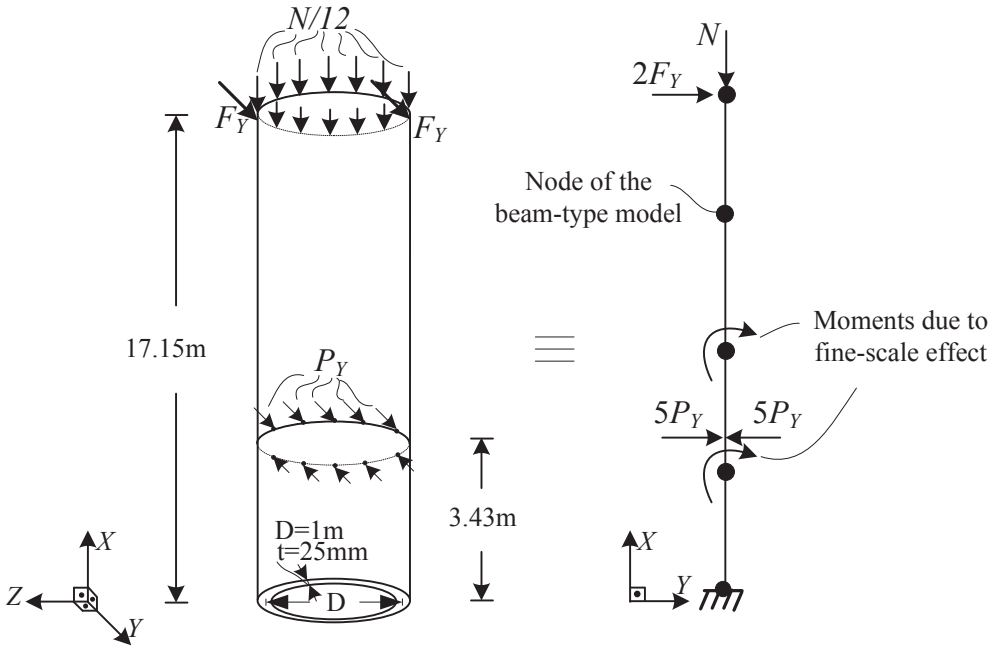

(a) Dimensions & loading of the pipe (shell model) (b) Equivalent global-local model

Figure 4.7: Description of the modelling of the pipe

The pipe is pinched at height z = 3430 mm through two equal and opposite sets of five forces 5Py as shown in Figure 4.7 (up to a value of P_Y = 1800 kN), in order to cause distortional deformations on the cross-section as well as plastic deformations. Modulus of elasticity and the Poisson's ratio used in this example and the next example are

$E = 200 \times 10^3$ MPA and ν=0.3, respectively. The yield stress was taken as 300MPa and no hardening was assumed.

For the beam-type and global-local analyses four equal-span elements were used. In the shell analysis, the cross-section was divided into 12 shell elements and the pipe span was sub-divided into 30 elements. The axial load was applied as a distributed load acting at the nodes of the cross-section of the shell model. In the global-local analysis the cross-section was again divided into 12 shell elements and span was sub-divided into 14 elements. In order to verify the validity of the beam-type analyses, we also present a comparison against the constrained shell solution which is obtained by applying multiple-point constraints on the nodal displacements of the shell model based on the decomposition matrix $\mathbf{N}$ and adopting the beam constitutive matrix $\overline{\mathbf{E}}$.

Firstly, a linearly elastic analysis was conducted. The applied loads were a compressive force (i.e., N=15000 kN) and a small lateral force, (F_Y=7.5 kN). The load versus tip horizontal deflection and tip rotation curves are plotted as shown in Figure 4.8 a, and b respectively.

Secondly, buckling loads based on a linearized buckling analysis corresponding to beam-type, constraint-shell-type and full-shell-type analysis are found as P_A=15,277kN, P_A=15,740kN and P_A=15,587kN, respectively, thus verifying the validity of the beam analysis model, and suggesting that ovalization in this case has a negligible effect on the results. In the shell analysis, it was verified that no plastic deformations have taken place in the case without local deformation while plasticity is experienced when local loads are applied to the model.

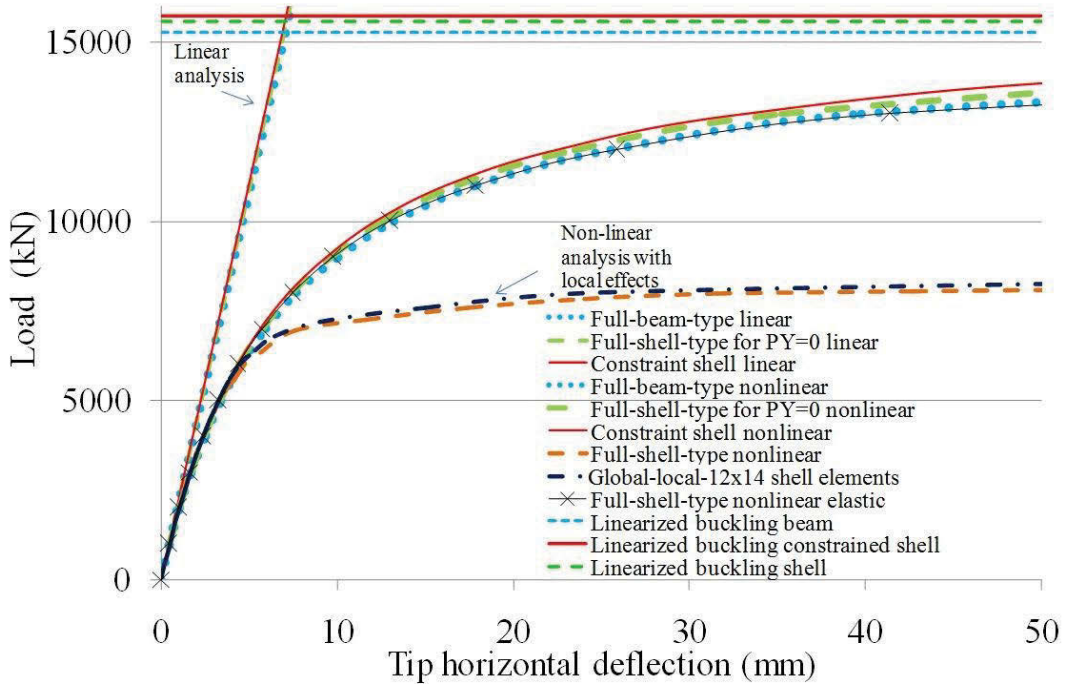

(a) Tip lateral deflection

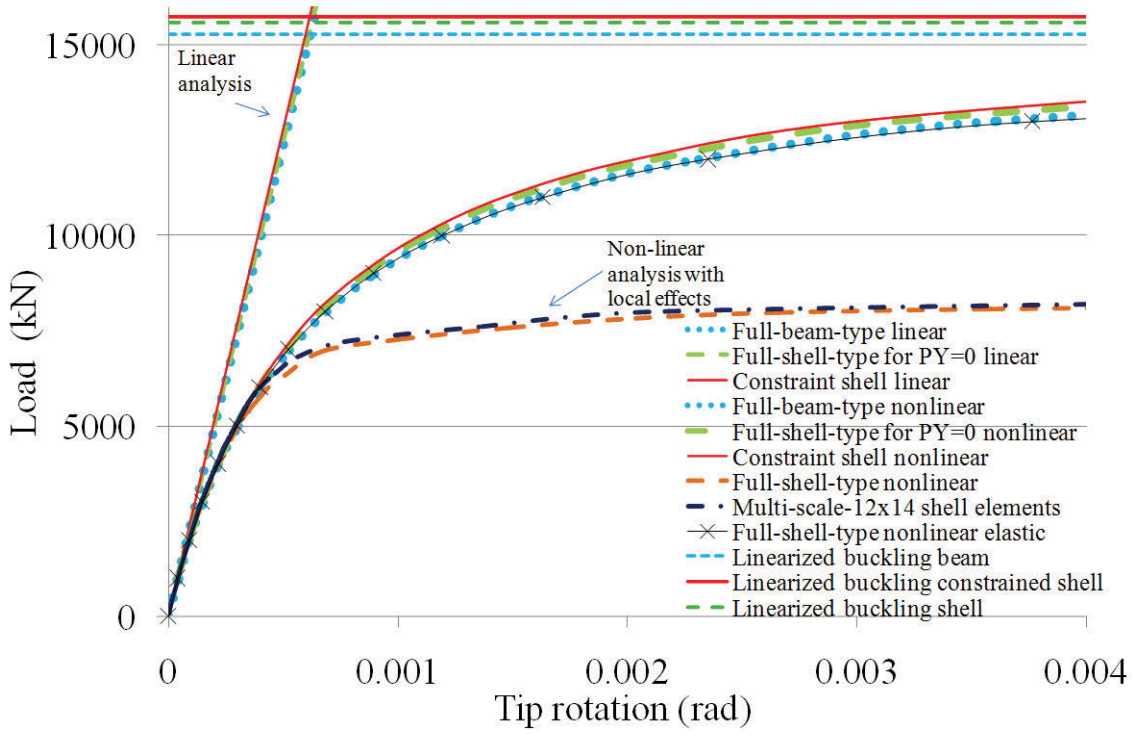

(b) Rotation at the tip

Figure 4.8: Load-deflection relations based on different modelling types

Thirdly, a nonlinear analysis was conducted, in which the loads were incremented from $N=0, F_y=0$ to a maximum of $N=15000$ kN, $F_Y=7.5$ kN without pinching loads (i.e., $P_Y=0$). As shown in Figure 4.8 a-b, excellent agreement is observed between the beam analysis and the shell analysis.

Fourthly, in addition to the applied compressive loads, pinching loads were incrementally applied from zero to $P_Y=1800$ kN in order to induce additional distortional deformations as well as plastic deformation. The corresponding load versus deflection curves are also shown in Figure 4.8. (a) and (b). It should be noted that comparison with fully elastic solution under local loads shows that plastic deformations are attained. The load versus deflection curves for the constrained shell and beam-type solutions are observed to be identical to those of the case where $P_Y=0$. On the other hand, when local deformations are introduced, the plastic deformations cause softening effect and increase the overall deflections of the full shell-type solution, which are not captured using the beam-type analysis given the rigid cross-section and elastic material response assumptions. In contrast, the global-local solution is very efficient in capturing the same behaviour as that predicted by the full shell-type analysis. In the global-local analysis, an overlapping region was considered between $\bar{z}=0$ and $\bar{z}=8003.33$ mm. The results are in very good agreement as can be verified from Figure 4.8. In Figure 4.9, the deformed shape and the stress contour for stresses in the longitudinal direction based on full shell-type analysis are shown for the loading of $N=7340$ kN, $F_Y=3.67$ kN and $P_Y=880.8$ kN.

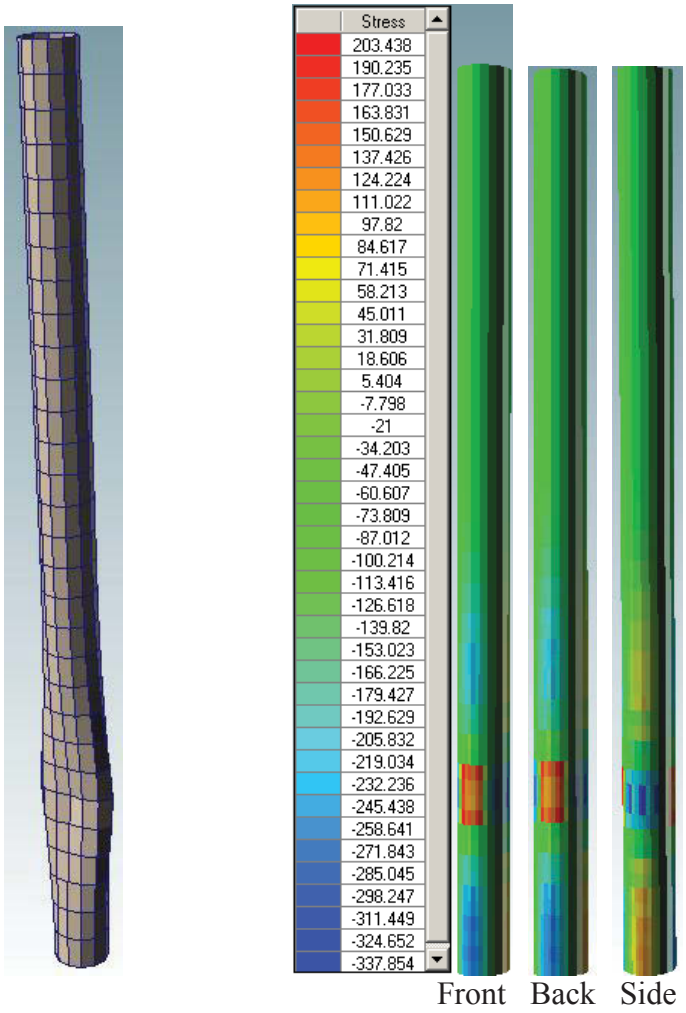

Figure 4.9: Deformed shape and contour stress in the longitudinal direction based on the shell-type nonlinear analysis (displacements scaled by a factor of 10)

In Figure 4.10, stresses in the longitudinal direction based on shell-type analysis are compared with those of the global-local solution.

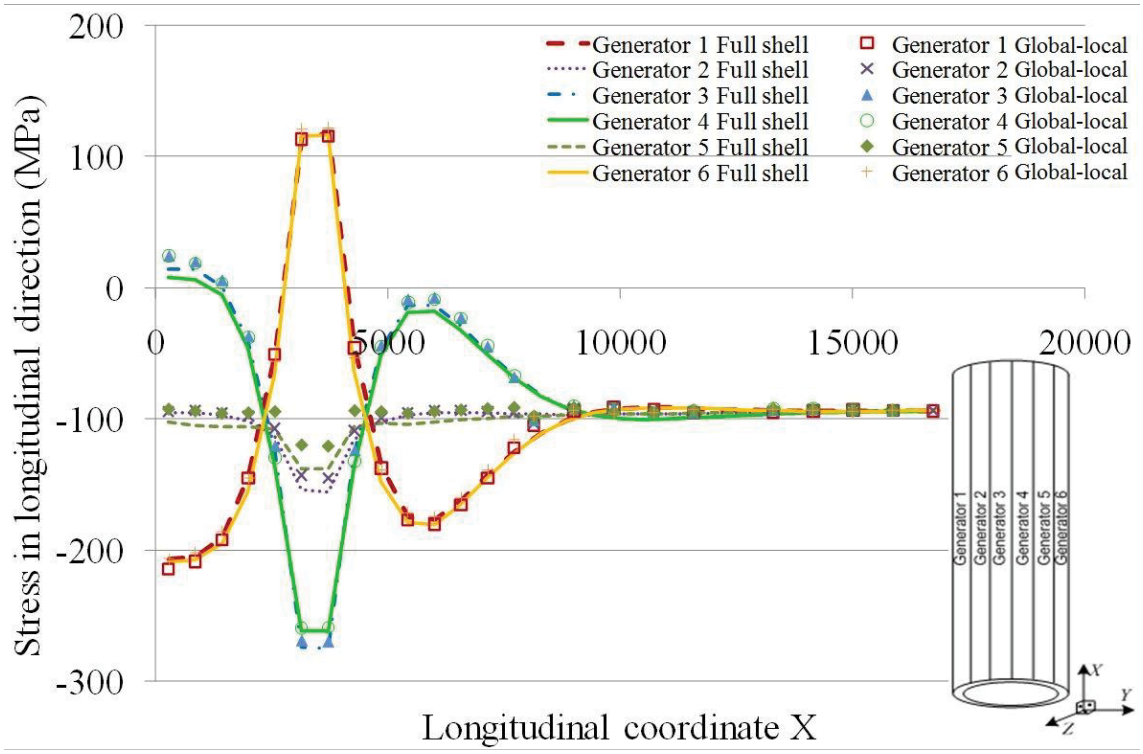

Figure 4.10: Deformed shape and contour stress in longitudinal direction based on the shell-type nonlinear analysis

The stresses are obtained at the middle of the elements by averaging the stresses at four integration points of the element. It can be verified that the global-local analysis results are very close to those of the shell analysis results.

4.6.2. Ovalization in a simply supported pipe

As shown in Figure 4.11, a 5m span simply supported horizontal pipe with a 200.25mm diameter and 3.25 wall thickness is analysed. The horizontal pipe is subject to a compressive force up to $N = 6000$ kN. Self –weight of the beam is also considered in the analysis.

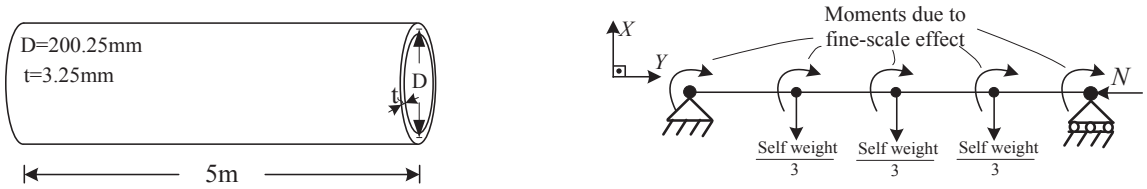

(a) Dimensions of the pipe (b) Equivalent global-local model

Figure 4.11: Description of the modelling of the pipe

In order to suppress inelastic behaviour, the yield stress was taken as 1450MPa. For the beam-type and global-local analyses, four equal-span elements are used. For the shell analysis the cross-section was divided into 12 elements and the span was divided into 16 elements. In the global-local analysis the cross-section is again divided into 12 shell elements and the span was sub-divided into 12 elements. Buckling loads based on the linearized buckling analysis corresponding to beam-type and full-shell-type analysis are P_A=6477kN and P_A=6022kN, respectively.

As shown in Figure 4.12, load versus mid-span deflection curves are plotted up to a compressive load of 6000kN. A comparison of the displacements at the top and side nodes suggests the model successfully captures ovalization induced by bending. Results based on the global-local analysis closely match those based on the shell solution and thus successfully capture the effects of ovalization.

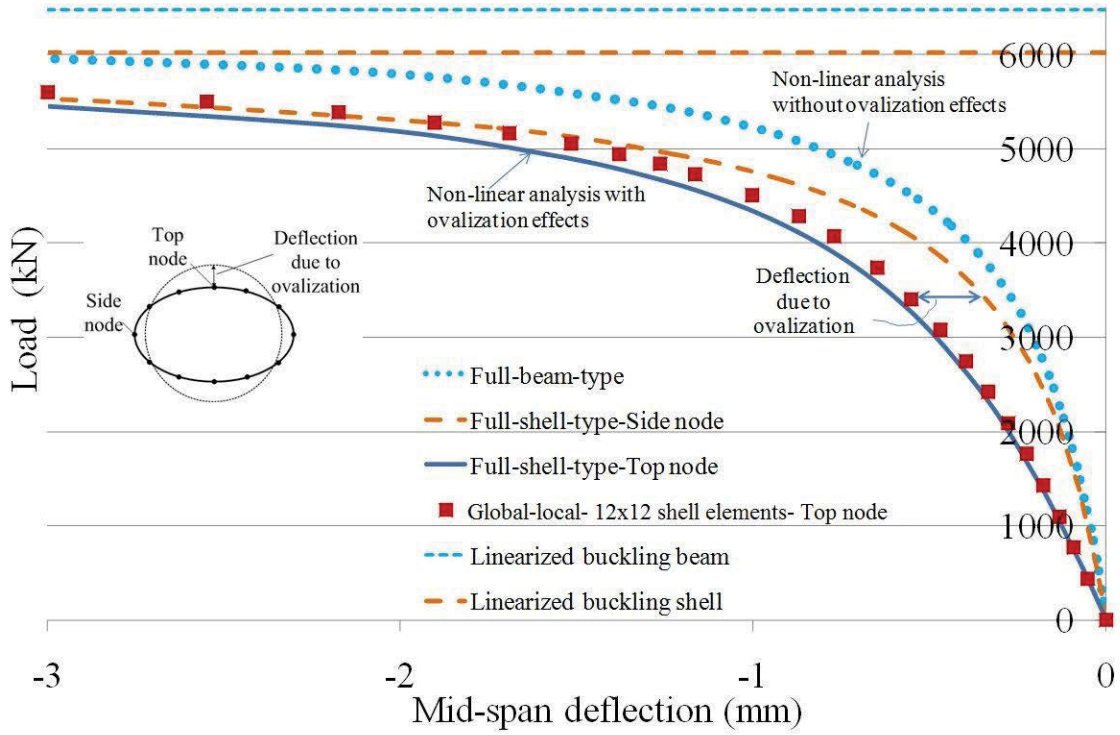

Figure 4.12: Load-deflection relations based on different modelling types

The deformed shape based on shell analysis is shown in Figure 4.13 and the stress contours based on full shell-type, full beam-type and global-local analyses are shown in Figure 4.14.

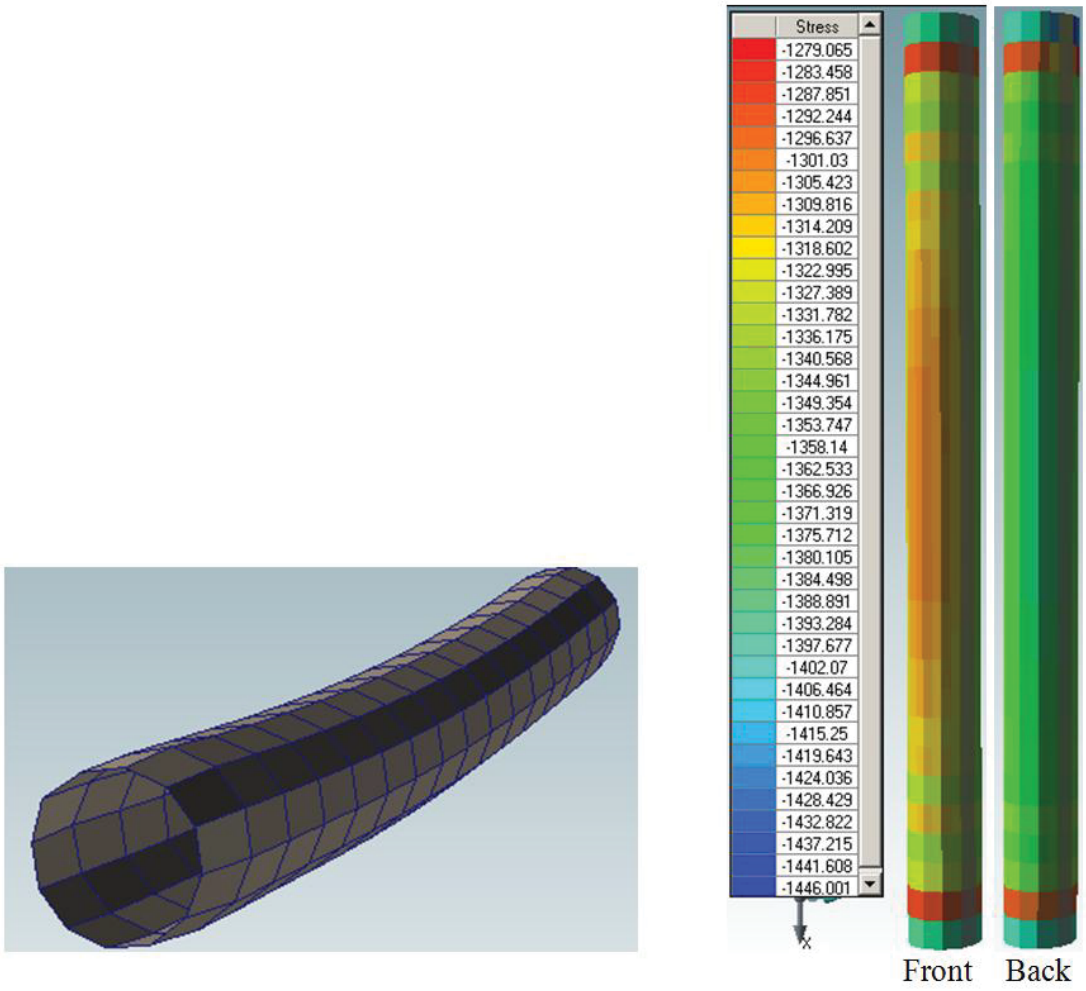

Figure 4.13: Deformed shape and stress contour based on shell-type nonlinear analysis (displacements scaled by a factor of 30)

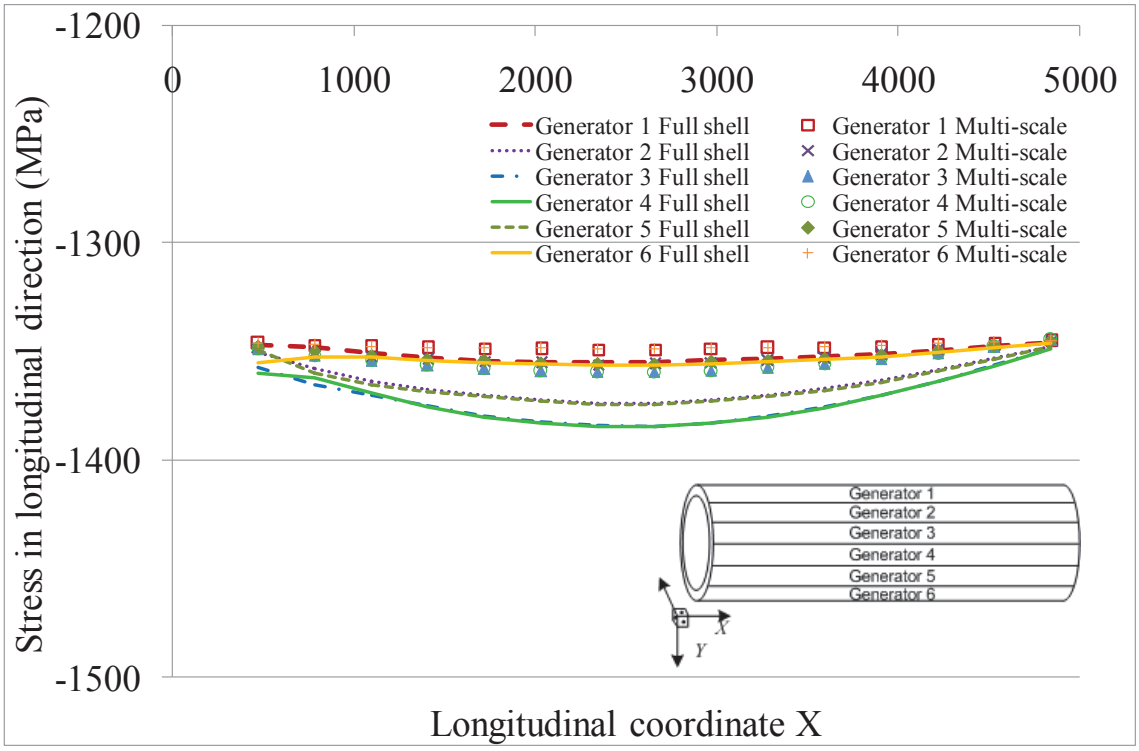

Figure 4.14: Stress in the longitudinal direction based on global-local and full shell-type analyses.

Very good agreement is also observed between the longitudinal stresses predicted by the shell model and those based on the global-local model.

4.7. Conclusions

In this chapter, an analysis method based on the iterative global-local approach was developed for the elasto-plastic analysis of pipes. The Iterative Global-local Method allows the method to incorporate the effects of local deformations on the global behaviour of the pipe by using a shell model only within the region of local deformations. A pipe buckling case was analysed and the results of the global-local procedure proposed herein were compared with those of the full shell- and beam-type analyses. It was shown that very accurate results are obtained using the proposed analysis procedure. Effect of ovalization on the behaviour of a thin-walled pipe is also illustrated and it was shown that the ovalization effect was successfully captured by using the global-local analysis procedure.

4.8. References

Argyris, J.H., Papadrakakis, M. & Karapitta, L. 2002, 'Elasto-plastic analysis of shells with the triangular element TRIC', *Computer Methods in Applied Mechanics and Engineering*, vol. 191, no. 33, pp. 3613-36.

Bathe, K.J. & Almeida, C.A. 1980, 'Simple and effective pipe elbow element - linear analysis', *Journal of Applied Mechanics, Transactions ASME*, vol. 47, no. 1, pp. 93-100.

Bathe, K.J. & Almeida, C.A. 1982, 'Simple and effective pipe elbow element - interaction effects', *Journal of Applied Mechanics, Transactions ASME*, vol. 49, no. 1, pp. 165-71.

Cook, R.D. 1990, 'Simulating curved elements by offsets. Rationale and application to shells of revolution', *Engineering computations*, vol. 7, no. 1, pp. 79-80.

Cook, R.D., Malkus, D.S., Plesha, M.E. & Witt, R.J. 2002, *Concepts and applications of finite element analysis*, fourth edn, John Wiley & Sons.

Crisfield, M.A. 1991, *Non-linear finite element analysis of solids and structures*, vol. 1, Wiley, New York.

Hobbs, R.E. 1981, 'Pipeline buckling caused by axial loads', *Journal of Constructional Steel Research*, vol. 1, no. 2, pp. 2-10.

Houliara, S. & Karamanos, S.A. 2006, 'Buckling and post-buckling of long pressurized elastic thin-walled tubes under in-plane bending', *International Journal of Non-Linear Mechanics*, vol. 41, no. 4, pp. 491-511.

Houliara, S. & Karamanos, S.A. 2010, 'Stability of long transversely-isotropic elastic cylindrical shells under bending', *International Journal of Solids and Structures*, vol. 47, no. 1, pp. 10-24.

Hughes, T.J.R. & Brezzi, F. 1989, 'On drilling degrees of freedom', *Computer Methods in Applied Mechanics and Engineering*, vol. 72, no. 1, pp. 105-21.

Ibrahimbegovic, A., Taylor, R.L. & Wilson, E.L. 1990, 'Robust quadrilateral membrane finite element with drilling degrees of freedom', *International Journal for Numerical Methods in Engineering*, vol. 30, no. 3, pp. 445-57.

Ju, G.T. & Kyriakides, S. 1992, 'Bifurcation and localization instabilities in cylindrical shells under bending-II. Predictions', *International Journal of Solids and Structures*, vol. 29, no. 9, pp. 1143-71.

Karamanos, S.A. 2002, 'Bending instabilities of elastic tubes', *International Journal of Solids and Structures*, vol. 39, no. 8, pp. 2059-85.

Karamanos, S.A. & Tassoulas, J.L. 1996, 'Tubular members. I: Stability analysis and preliminary results', *Journal of Engineering Mechanics*, vol. 122, no. 1, pp. 64-71.

Marques, J.M.M.C. 1984, 'Stress computation in elastoplasticity', *Engineering Computations (Swansea, Wales)*, vol. 1, pp. 42-51.

Militello, C. & Huespe, A.E. 1988, 'A displacement-based pipe elbow element', *Computers and Structures*, vol. 29, no. 2, pp. 339-43.

Nowzartash, F. & Mohareb, M. 2004, 'An elasto-plastic finite element for steel pipelines', *International Journal of Pressure Vessels and Piping*, vol. 81, no. 12, pp. 919-30.

Ozkan, I.F. & Mohareb, M. 2009, 'Testing and analysis of steel pipes under bending, tension, and internal pressure', *Journal of Structural Engineering*, vol. 135, no. 2, pp. 187-97.

Song, H.-W. & Tassoulas, J.L. 1993, 'Finite element analysis of propagating buckles', *International Journal for Numerical Methods in Engineering*, vol. 36, no. 20, pp. 3529-52.

Weicker, K., Salahifar, R. & Mohareb, M. 2010, 'Shell analysis of thin-walled pipes. Part II - Finite element formulation', *International Journal of Pressure Vessels and Piping*, vol. 87, no. 7, pp. 414-23.

Appendix 4.A

In Eq. (4.33), the incremental strains $\delta\hat{\boldsymbol{\varepsilon}}$ were expressed in terms of the incremental nodal displacements $\hat{\mathbf{d}}$ through $\delta\hat{\boldsymbol{\varepsilon}} = \hat{\mathbf{S}}\hat{\mathbf{B}}\delta\hat{\mathbf{d}}$ in which matrix $\hat{\mathbf{S}}$ can be written as

$$\hat{\mathbf{S}} = \left[\mathbf{I} \;\vdots\; -z\mathbf{I}\right] \tag{4.A.1}$$

in which $\mathbf{I}$ is a 4x4 unit matrix and matrix $\hat{\mathbf{B}}$ can be written as

$$\hat{\mathbf{B}} = \begin{bmatrix} \hat{\mathbf{B}}_m + \hat{\mathbf{B}}_{Nm} & \vdots & \hat{\mathbf{B}}_{Nb} \\ \cdots & \vdots & \cdots \\ \mathbf{0} & \vdots & \hat{\mathbf{B}}_b \end{bmatrix} \begin{Bmatrix} \mathfrak{I} \\ \cdots \\ \aleph \end{Bmatrix} \hat{\mathbf{X}} \tag{4.A.2}$$

and

$$\hat{\mathbf{B}}_m = \begin{bmatrix} 1 & 0 & 0 & 0 & 0 \\ 0 & 1 & 0 & 0 & 0 \\ 0 & 0 & 1 & 1 & 0 \\ 0 & 0 & -\frac{1}{2} & \frac{1}{2} & -1 \end{bmatrix} \tag{4.A.3}$$

$$\hat{\mathbf{B}}_b = \begin{bmatrix} 0 & 0 & 0 & 0 & 1 & 0 & 0 \\ 0 & 0 & 0 & 0 & 0 & 1 & 0 \\ 0 & 0 & 0 & 0 & 0 & 0 & 1 \\ 0 & 0 & 0 & 0 & 0 & 0 & 0 \end{bmatrix} \tag{4.A.4}$$

$$\hat{\mathbf{B}}_{Nm} = \begin{bmatrix} 0 & 0 & 0 & \frac{\partial \hat{v}_0}{\partial x} & 0 \\ 0 & 0 & 0 & 0 & 0 \\ 0 & 0 & 0 & 0 & 0 \\ 0 & 0 & 0 & 0 & 0 \end{bmatrix} \tag{4.A.5}$$

$$\widehat{\mathbf{B}}_{Nb} = \begin{bmatrix} \dfrac{\partial \hat{w}_0}{\partial x} & 0 & 0 & 0 & 0 & 0 & 0 \\ 0 & 0 & 0 & 0 & 0 & 0 & 0 \\ 0 & 0 & 0 & 0 & 0 & 0 & 0 \\ 0 & 0 & 0 & 0 & 0 & 0 & 0 \end{bmatrix} \tag{4.A.6}$$

and

$$\mathfrak{I} = \begin{bmatrix} \dfrac{\partial}{\partial x} & 0 & 0 & 0 & 0 & 0 \\ 0 & \dfrac{\partial}{\partial y} & 0 & 0 & \dfrac{\partial f}{\partial r} & 0 \\ \dfrac{\partial}{\partial y} & 0 & 0 & 0 & 0 & 0 \\ 0 & \dfrac{\partial}{\partial x} & 0 & 0 & 0 & 0 \\ 0 & 0 & 0 & 0 & 0 & 1 \end{bmatrix} \tag{4.A.7}$$

$$\aleph = \begin{bmatrix} 0 & 0 & 0 & \dfrac{\partial}{\partial x} & 0 & 0 \\ 0 & 0 & 0 & \dfrac{\partial}{\partial y} & 0 & 0 \\ 0 & 0 & 0 & 0 & 1 & 0 \\ 0 & 0 & 0 & 0 & 0 & 1 \\ 0 & 0 & 0 & 0 & \dfrac{\partial}{\partial x} & 0 \\ 0 & 0 & 0 & 0 & 0 & \dfrac{\partial}{\partial y} \\ 0 & 0 & 0 & \dfrac{\partial^2}{\partial x \partial y} & 0 & 0 \end{bmatrix} \tag{4.A.8}$$

Chapter 4 list of symbols

A	=	cross-sectional area
$\bar{\mathbf{d}}$	=	nodal displacement vector of the beam
$\bar{\mathbf{E}}$	=	constitutive matrix of the beam element
$\hat{\mathbf{E}}$	=	constitutive matrix of the shell element
$\bar{\mathbf{f}}$	=	external load vector of the beam element
$\hat{\mathbf{f}}$	=	shell element external load vector
f	=	expression for the elevation of the curved shell, yield surface
$\mathbf{H}$	=	vector of cubic interpolation functions
$\bar{\mathbf{K}}$	=	stiffness matrix of the beam element
$\hat{\mathbf{K}}$	=	stiffness matrix of the shell element
$\mathbf{L}$	=	vector of linear interpolation functions
$\mathbf{N}$	=	overlapping domain decomposition matrix
$\bar{R}$	=	radius of the pipe
$\bar{\mathbf{S}}$	=	matrix of cross-sectional coordinates
$\bar{u}, \bar{v}, \bar{w}$	=	displacement components of the beam element
$\bar{\mathbf{u}}$	=	displacement vector of an arbitrary point in the beam element

$\bar{\mathbf{X}}_a$ = beam interpolation matrix

$\mathbf{Y}$ = matrix of thin-walled kinematical relations

$\mathbf{Z}$ = matrix of overlapping domain interpolations

$\bar{\boldsymbol{\varepsilon}}, \bar{\boldsymbol{\varepsilon}}_L, \bar{\boldsymbol{\varepsilon}}_N$ = strain vectors of the beam element

$\hat{\boldsymbol{\varepsilon}}, \hat{\boldsymbol{\varepsilon}}_b, \hat{\boldsymbol{\varepsilon}}_{mm}, \hat{\boldsymbol{\varepsilon}}_N$ = strain vectors of the shell element

$\Delta\hat{\boldsymbol{\varepsilon}}_{ea}$ = elastic part of strain increment

$\Delta\hat{\boldsymbol{\varepsilon}}_a$ = total strain increment

$\hat{\boldsymbol{\varepsilon}}_{pa}$ = plastic strain increment

$\theta_x, \theta_y, \theta_z$ = rotation components

$\bar{\Pi}$ = total potential energy of the beam element

$\hat{\Pi}$ = total potential energy of the shell element

$\bar{\boldsymbol{\sigma}}$ = beam element stress vector

$\hat{\boldsymbol{\sigma}}$ = shell element stress vector

σ_{ef} = the effective stress (according to von Mises yield criterion)

σ_Y = yield stress limit of the material

ϕ = twist rotation of the beam element

$\bar{\chi}_L$ = vector of beam linear displacement derivatives

∇ = differential operator

Chapter 4 list of figures

Chapter 5: Thin-walled curved beam formulation

5.1. Introduction

Curved beams are extensively used as structural elements especially in highway interchanges and railway bridges. Due to the couplings that arise in a curved beam between the displacement fields, straight beam formulations cannot be used for the analysis of these types of members especially when large displacements exist. As shown in the following, existing methods are accurate for small values of initial curvature only, which necessitates the development of a more robust technique.

In this chapter, a finite element formulation is developed for the elastic analysis of thin-walled beams curved in a single plane. Using a second-order rotation tensor, the curvature values of the deformed configuration are calculated in terms of the displacement values and the initial curvature. The principle of virtual work is then used to obtain the nonlinear equilibrium equations, based on which, a finite element beam formulation is developed. The accuracy of the method is confirmed through comparison with test results and shell-type finite element formulation. It was observed that the current element is more accurate than the previous formulations, especially for large included angle per beam finite element.

5.2. Literature review

Curved members are extensively used in engineering structures such as highway interchanges and railway bridges. A horizontally curved member subjected to a vertical out-of-plane loading undergoes torsion, compression, and biaxial moments as primary actions. Apart from that, second order bending moments and torsional moments are generated by coupling between the angle of twist and the bending moment and between the vertical displacement and the torsional moment, respectively.

Timoshenko (1923) made the first effort to solve the problem of curved beams. He considered the curved beam shown in Figure 5.1, which is a portion of a circular ring fixed at one end with loading of a vertical out-of-plane point load applied at the free end. The deflections of the beam were considered as a combination of deflection in two perpendicular planes plus the twist of the section. He assumed that the cross-section remains rigid during deformations, and that warping deformations are negligible.

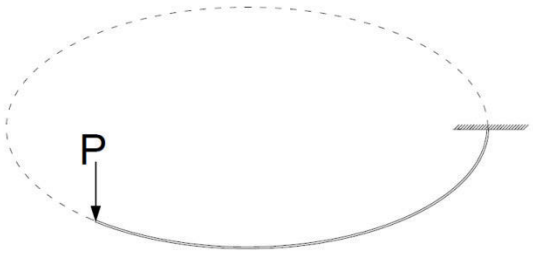

Figure 5.1: Layout of the curved beam analysed by Timoshenko (1923)

Based on these assumptions, Timoshenko found the potential energy functional based on bending in two directions and the torsion of the member, which were used to find the deflection of the bar.

Brookhart (1967) derived differential equations of a circular horizontally curved beam by extending Timoshenko's theory of torsion. However, numerical methods have gained much more popularity in the analysis of curved beams since solving the corresponding differential equations to obtain stresses and displacements in the curved beams are very complicated in most of the cases.

Traditionally, horizontally-curved beams were numerically analysed by a sequence of short straight beam elements. However, it was shown (Sawko 1967) that the straight idealisation error may be significant even for small included angle (in the order of 1˚). Consequently, several researchers proposed curved beam finite elements, starting from the late 1960s. Sawko (1967), Brookhart (1967) and Young (1969) proposed finite element models for beams curved in plan. El-Amin & Brotton (1976) included the warping restraint in the formulation of a displacement-based finite element. Later, El-Amin & Kasem (1978) improved the efficiency of the model by assigning higher order polynomials for the angle of twist: in the former both the vertical displacement and the angle of twist of the beam were interpolated by cubic polynomials. While the vertical displacement polynomial was unchanged, a 7^{th} order polynomial was utilized to model the angle of twist of the beam.

Akhtar (1987) obtained the stiffness matrix of a circular member using flexibility matrix. To this end, he considered a beam element consisting of a portion of a circle with end actions of shear force, axial force and a bending moment. The flexibility matrix was then obtained by differentiating the energy equation with respect to each of the actions. Flexibility matrix was inverted at last to find the stiffness matrix. Krenk (1994) derived the stiffness matrix for beam element by using the static equilibrium state along with the principle of stationary complementary energy. The method was applied to a circular beam. However, neither of the two finites elements discussed

herein is applicable to horizontally curved beams because the torsional actions are not considered in formulating the stiffness matrices. Therefore, these two methods can be used when the curvature of the beam is in the vertical plane as in arches.

Pantazopoulou (1992) proposed a displacement-based finite element for horizontally-curved beams. In order to prevent locking problems, he used lower order interpolation polynomials and adopted a selectively-reduced integration procedure.

All the aforementioned numerical models were based on the linear analysis of curved beams. However, the effect of geometric nonlinearity may be significant for curved members even under serviceability stage and therefore, several finite element formulations have been developed to capture the geometrically nonlinear behaviour. These works include those of Fukumoto & Nishida (1981) and Yoshida & Maegawa (1983) for the analysis of horizontally curved I-beams undergoing large displacements. The transfer matrix method was used to solve the differential equations in order to obtain the ultimate strength of the member. The transfer matrix method considers the second-order actions due to material and geometric nonlinearities as well as the residual stresses. Iura & Atluri (1988) developed a three dimensional beam element for elements curved in space. Liew et al. (1995) used triangular and quadrilateral shell elements in the finite element program ABAQUS to study the second order behaviour of horizontally curved I-beams by focusing on the effect of radius of curvature to span length and the residual stresses on the ultimate load capacity of the member. Based on the study, they proposed a design formula for predicting the ultimate load-carrying capacity of horizontally curved I-beams.

All the nonlinear studies discussed so far (Fukumoto & Nishida 1981; Liew et al. 1995; Yoshida & Maegawa 1983) are limited to beams with very small horizontal curvature.

Yoo et al. (1996) presented a finite element formulation by the principle of minimum potential energy. They included the effect of curvature in derivation of elastic and geometric stiffness matrices; therefore, the model was capable of analysing beams with higher initial curvature. Using the model, they studied the bifurcation buckling of horizontally curved beams, and presented relations to predict the ultimate load.

Several researchers have worked on developing finite elements based on the "geometrically exact beam theory". The motivation is that conventionally in developing the finite elements based on energy equations, strain-displacement relations are used to specify the strain based on the kinematic assumptions that relate the displacement at an arbitrary point on the cross-section to the displacement and rotations of the centre line. In order to separate the linear relations from the nonlinear part, approximations are normally made. However, it has been reported (Crisfield 1990; Simo & Vu-Quoc 1987) that this sort of approximation may result in the loss of some important terms in the strain-displacement relations, resulting in overly stiff nonlinear response. To solve the problem, the geometrically exact formulations have been proposed that are based on the resultants of the equilibrium equations. Simo (1985) developed the first finite element formulations based on the geometrically exact descriptions, without considering warping effects. Simo & Vu-Quoc (1991) added the torsional warping effect and the warping due to combined bending and torsion to the theory.

Sandhu et al. (1990) and Crisfield (1990) developed a co-rotational formulation for curved beams undergoing large deformations. In co-rotational formulations, the rigid body motion of the element is removed by assigning a local coordinate system attached to each finite element, which is capable of continuous translation and rotation with the element displacements during the loading.

Pi & Trahair (1997) studied the behaviour of horizontally curved beams under vertical loading and developed a curved finite element. They concluded that when the included curvature in the beam is small, the nonlinear behaviour of the beam becomes similar to straight beams (i.e. lateral-torsional buckling becomes the dominant mode of failure). However, when the included angle is relatively large, the coupling between the bending moment and the twisting moment become significant, and the nonlinear behaviour starts far before the lateral-torsional buckling load. Based on these observations, they stated that the term "Buckling load" may not have much significance in curved beams. Although mathematical values of the buckling load can be obtained from the nonlinear equilibrium equations, they don't have a physical significance and are the maxima and minima of the load-deformation curve.

Pi et al. (2005) stated that inclusion of Wagner moments and Wagner terms considerably increases the accuracy of the models dealing with cases with large torsional actions. As torsion is a primary action in horizontally-curved beam, they concluded that a sound finite element for such problems cannot ignore the Wagner effects. Consequently, based on the geometrically exact definition of kinematics of the deformations, a finite element was developed that included Wagner moments and Wagner terms in the finite strains to predict the torsional behaviour of the member more accurately. The model was made applicable for beams with initial curvatures in two directions as well as initial twist, and their interaction with large displacements.

Erkmen & Bradford (2009) extended the work of Pi & Trahair (1997) by developing a finite element formulation for the elastic dynamic analysis of horizontally curved I-beams. It was observed by the authors that the response of curved beams is considerably different when the initial curvature is medium to large. However, the formulation based

on Pi & Trahair (1997) is accurate when the initial curvature per the beam element is relatively small.

In this study, using a second-order rotation tensor, the curvature values of the deformed configuration are calculated in terms of the displacement values and the initial curvature. The principle of virtual work is then used to obtain the nonlinear equilibrium equations, based on which a finite element beam formulation is developed.

5.3. Assumptions and scope

The following assumptions are made in this study:

- The beam is assumed to be initially curved in a single plane.
- The cross-section is assumed to remain rigid throughout the deformation.
- The shear strains are considered to be negligible on the mid-surface.
- Rotations and deflections are large, but strains are assumed to be small.

5.4. Kinematics of the problem

5.4.1. Displacements

A schematic of a curved beam can be seen in Figure 5.2, where the undeformed and deformed configurations of the curved beam are shown by dashed and solid lines, respectively.

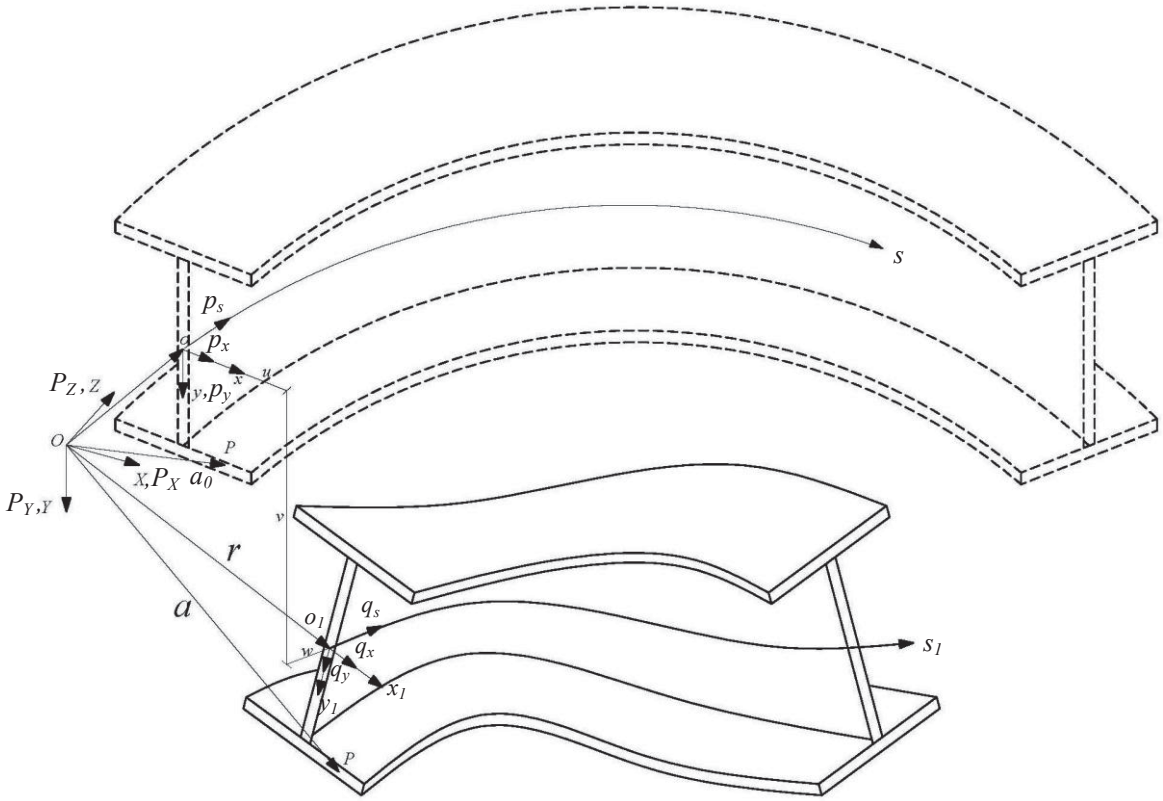

Figure 5.2: Schematic of the curved beam: Coordinate systems and displacements

In order to incorporate large deformations of the curved beam, we assign a fixed space and two sets of coordinate systems for undeformed and deformed configurations of the body. The fixed space axes $OXYZ$ are formed by the orthogonal basis provided by the triad $\mathbf{P}(\mathbf{P}_X, \mathbf{P}_Y, \mathbf{P}_Z)$. In order to demonstrate the undeformed configuration of the curved beam, a body-attached $oxys$ coordinate system is adopted, the origin of which is placed at the centroid of the cross-section. The axis os is tangent to the axis of the beam, while the axes ox and oy lie in the plane of the cross-section and pass through the principal axes. The three components of the triad $\mathbf{p}(\mathbf{p}_x, \mathbf{p}_y, \mathbf{p}_s)$ form an orthogonal basis of the system $oxys$ in the direction of the tangent of the axes ox, oy and os respectively as depicted in Figure 5.2. The deformed configuration of the curved beam is shown by another set of axes $o_1x_1y_1s_1$, which form a (Lagrangian) curvilinear coordinate system

that changes with the deformation of the member and coincides with $oxys$ in the undeformed state. Similar to the undeformed coordinate system, the axis o_1s_1 lies in the direction tangent to the axis of the deformed beam and the axes o_1x_1 and o_1y_1 lie in the cross-sectional plane of the deformed configuration. A triad $\mathbf{q}(\mathbf{q}_x, \mathbf{q}_y, \mathbf{q}_s)$ forms the orthogonal basis for the latter system, the components of which are in the tangent direction of o_1x_1, o_1y_1 and o_1s_1 respectively.

Based on the above definition, the position vectors of a point P on the cross-section before and after the deformation can be stated as

$$\mathbf{a}_0 = \mathbf{r}_0 + x\mathbf{p}_\mathbf{x} + y\mathbf{p}_\mathbf{y} \tag{5.1}$$

$$\mathbf{a} = \mathbf{r} + x\mathbf{q}_\mathbf{x} + y\mathbf{q}_\mathbf{y} - \omega(x,y)\,p(s)\mathbf{q}_\mathbf{s} \tag{5.2}$$

where $\mathbf{r}_0$ and $\mathbf{r}$ are the position vectors of the centroid o before and after the deformation respectively in the fixed axes $OXYZ$, $\omega(x,y)$ is the normalized section warping displacement function and $p(s)$ is the warping amplitude. The position vector of the deformed centroid can be obtained from the undeformed centroid and the displacement components as (Figure 5.2)

$$\mathbf{r} = \mathbf{r}_0 + u\mathbf{p}_x + v\mathbf{p}_y + w\mathbf{p}_s \tag{5.3}$$

The orientation of the triad $\mathbf{q}$ is determined by the use of a rotation tensor $\mathbf{R}$ multiplied by the triad $\mathbf{p}$ as

$$\mathbf{q} = \mathbf{R}\mathbf{p} \tag{5.4}$$

According to the orthogonality condition of the rotation tensor, i.e. $\mathbf{R}^T\mathbf{R}=\mathbf{I}$, only six out of the nine components of the rotation tensor are linearly independent. According to the Euler-Rodriguez formula (Koiter 1984), the rotation tensor can be calculated in term of the rotation components ϕ_1, ϕ_2 and ϕ_3 around the axes OX, OY and OZ, respectively, as

$$R_{ij}=\delta_{ij}\left(1-\tfrac{1}{2}\phi_k\phi_k\right)+\varepsilon_{ikj}\phi_k+\tfrac{1}{2}\phi_i\phi_j+o\left(\left|\phi\right|^3\right) \tag{5.5}$$

where δ_{ij} is the Kronecker delta, ε_{ikj} is the permutation symbol and $o\left(\left|\phi\right|^3\right)$ refers to terms higher than second order. The indices 1, 2 and 3 indicate the x, y and s axes, respectively. According to the right hand rule sign convention, the rotation components ϕ_i are related to the derivatives of the displacement of the beam centroid as

$$\phi_X=-v' \tag{5.6}$$

$$\phi_Y=\tilde{u}' \tag{5.7}$$

For a beam curved in plan, $\tilde{u}=u'+\kappa_0 w$ where u, v and w are displacement components in x, y and s directions respectively, and κ_0 is the initial curvature of the curved beam's centroidal locus about the Y axis. By neglecting rotation terms higher than the second order, the rotation matrix can be written as

$$\mathbf{R}=\begin{bmatrix} 1-\frac{1}{2}\left(\phi^2+\tilde{u}'^2\right) & -\phi-\frac{1}{2}\tilde{u}'v' & \tilde{u}'-\frac{1}{2}\phi v' \\ \phi-\frac{1}{2}\tilde{u}'v' & 1-\frac{1}{2}\left(\phi^2+v'^2\right) & v'+\frac{1}{2}\phi\tilde{u}' \\ -\tilde{u}'-\frac{1}{2}\phi v' & -v'+\frac{1}{2}\phi\tilde{u}' & 1-\frac{1}{2}\left(\tilde{u}'^2+v'^2\right) \end{bmatrix} \tag{5.8}$$

in which ϕ is the twist rotation of the cross-section, and the symbol $()'$ denotes the derivative with respect to the s coordinate.

5.4.2. Curvature values at deformed configuration

In the deformed configuration, the curvatures in x and y directions, i.e. κ_x and κ_y, and the twist can be obtained by Frenet-Serret formulae (Love 1944) using the aforementioned rotation matrix (Appendix 5.A) to be

$$\kappa_x = \left(1+\varepsilon\right)^{-1}\left[-v'' - \tfrac{1}{2}\tilde{u}'\phi' + \tfrac{1}{2}\tilde{u}''\phi + \kappa_0\left(\phi - \tfrac{1}{2}\tilde{u}'v'\right)\right] \tag{5.9}$$

$$\kappa_y = \left(1+\varepsilon\right)^{-1}\left[\tilde{u}'' - \tfrac{1}{2}v'\phi' + \tfrac{1}{2}v''\phi + \kappa_0\left(-\tfrac{1}{2}v'^2 - \tfrac{1}{2}\phi^2 + 1\right)\right] \tag{5.10}$$

$$\kappa_s = \left(1+\varepsilon\right)^{-1}\left[\phi' - \tfrac{1}{2}\tilde{u}'v'' + \tfrac{1}{2}\tilde{u}''v' + \kappa_0\left(v' + \tfrac{1}{2}\tilde{u}'\phi\right)\right] \tag{5.11}$$

where κ_0 is the initial curvature of the curved beam's centroidal locus about the Y axis, $\tilde{w}' = w' - \kappa_0 u$ and ε can be written as

$$\varepsilon \approx \tilde{w}' + \tfrac{1}{2}\tilde{u}'^2 + \tfrac{1}{2}v'^2 + \tfrac{1}{2}\tilde{w}'^2 \tag{5.12}$$

5.4.3. Strains

Using the right extensional strain definition we have

$$\mathbf{D} = \mathbf{RU} - \mathbf{I} \tag{5.13}$$

where $\mathbf{D}$ is the deformation gradient tensor, $\mathbf{R}$ is the rotation tensor, $\mathbf{I}$ is the identity matrix and $\mathbf{U}$ is the right stretch tensor, i.e. $\mathbf{U} = \mathbf{I} + \boldsymbol{\varepsilon}$. Pre-multiplying Eq. (5.13) by $\mathbf{R}^T$ we have

$$\mathbf{R}^T\mathbf{D} = \mathbf{I} + \boldsymbol{\varepsilon} - \mathbf{R}^T \tag{5.14}$$

The strain can be obtained from Eq. (5.14) as

$$\boldsymbol{\varepsilon} = \mathbf{R}^T\mathbf{D} - \mathbf{I} + \mathbf{R}^T \tag{5.15}$$

Matrix $\mathbf{D}$ is found by taking the gradient of the deformation vector with respect to x, y and s coordinates. The deformation can be considered as the difference between the initial and final position vectors $\mathbf{a}$ and $\mathbf{a}_0$

$$\mathbf{D} = \left(\frac{\partial(\mathbf{a}-\mathbf{a}_0)}{\partial x} \quad \frac{\partial(\mathbf{a}-\mathbf{a}_0)}{\partial y} \quad \frac{\partial(\mathbf{a}-\mathbf{a}_0)}{\partial s} \right) \tag{5.16}$$

Using the definitions of the position vector in Eq. (5.1), the deformation gradient tensor in calculated in terms of curvature components of the deformed configuration as

$$\mathbf{D} = \begin{bmatrix} 0 & 0 & (1+\varepsilon)\left(-y\kappa_s - \omega p \kappa_y\right) \\ 0 & 0 & (1+\varepsilon)\left(x\kappa_s + \omega p \kappa_x\right) \\ y - \dfrac{\partial \omega}{\partial x} p & x - \dfrac{\partial \omega}{\partial y} p & (1+\varepsilon)\left(1 - x\kappa_y + y\kappa_x - \omega p'\right) - \left(1 - x\kappa_0\right) \end{bmatrix} \tag{5.17}$$

By performing the calculations (Appendix 5.B), the normal strain can be written as

$$\begin{aligned} \varepsilon_{ss} &= w' + \tfrac{1}{2}w'^2 + \kappa_0\left(-u - uw'\right) + \tfrac{1}{2}\kappa_0{}^2 u^2 \\ &+ x\left[-u'' + \tfrac{3}{2}v'\phi' - \tfrac{1}{2}v''\phi + \kappa_0\left(-w' + \tfrac{3}{2}v'^2 + \tfrac{1}{2}\phi^2\right)\right] \\ &+ y\left[-v'' - \tfrac{3}{2}u'\phi' + \tfrac{1}{2}u''\phi + \kappa_0\left(\phi - \tfrac{3}{2}u'v' - \tfrac{3}{2}w\phi' + \tfrac{1}{2}w'\phi\right) - \tfrac{3}{2}\kappa_0{}^2 v'w\right] \\ &+ \omega\left[-\phi'' + \tfrac{1}{2}u'v''' - \tfrac{1}{2}u'''v' + \kappa_0\left(-v'' - \tfrac{1}{2}u''\phi - \tfrac{1}{2}u'\phi' + \tfrac{1}{2}v'''w - \tfrac{1}{2}v'w''\right) + \tfrac{1}{2}\kappa_0{}^2\left(-w'\phi - w\phi'\right)\right] \end{aligned} \tag{5.18}$$

The shear strain is calculated to be

$$\gamma_{sx} = \left(-y - \frac{\partial \omega}{\partial x} \right) (1+\varepsilon)^{-1} \left[\phi' - \tfrac{1}{2}\tilde{u}'v'' + \tfrac{1}{2}\tilde{u}''v' + \kappa_0 \left(v' + \tfrac{1}{2}\tilde{u}'\phi \right) \right] \tag{5.19}$$

$$\gamma_{sy} = \left(x - \frac{\partial \omega}{\partial x} \right) (1+\varepsilon)^{-1} \left[\phi' - \tfrac{1}{2}\tilde{u}'v'' + \tfrac{1}{2}\tilde{u}''v' + \kappa_0 \left(v' + \tfrac{1}{2}\tilde{u}'\phi \right) \right] \tag{5.20}$$

On the other hand, from the assumption of negligible shear strain on the mid-surface, the only non-zero shear strain is through the thickness t of the plate stiffness and can be approximated as

$$\gamma_p = -2r\kappa_s = -2r(1+\varepsilon)^{-1} \left[\phi' - \tfrac{1}{2}\tilde{u}'v'' + \tfrac{1}{2}\tilde{u}''v' + \kappa_0 \left(v' + \tfrac{1}{2}\tilde{u}'\phi \right) \right] \tag{5.21}$$

in which r is the normal distance from the mid-surface. It can be seen that the latter is compatible with Eqs. (5.19) and (5.20). Replacing $\tilde{u} = u' + \kappa_0 w$, the shear strain will be equal to

$$\gamma_p = -2r\kappa_s = -2r(1+\varepsilon)^{-1} \left[\phi' - \tfrac{1}{2}u'v'' + \tfrac{1}{2}u''v' + \kappa_0 \left(v' + \tfrac{1}{2}u'\phi - \tfrac{1}{2}v''w + \tfrac{1}{2}v'w' \right) + \tfrac{1}{2}\kappa_0{}^2 w\phi \right] \tag{5.22}$$

It should be noted that $2r = \sqrt{\left(-y - \frac{\partial \bar{\omega}}{\partial x} \right)^2 + \left(x - \frac{\partial \bar{\omega}}{\partial y} \right)^2}$ and $\gamma_p = \sqrt{\gamma_{sx}{}^2 + \gamma_{sy}{}^2}$ were used in Eq. (5.22), and $\bar{\omega}$ is approximated as the Vlasov warping function ω (Vlasov 1961), i.e. $\omega \approx \bar{\omega}$.

5.4.4. Variations of strains

The first variation of the normal and shear strain can be written as

$$\delta\boldsymbol{\varepsilon} = \left\langle \delta\varepsilon_p \quad \delta\gamma_p \right\rangle^T = \mathbf{SB}\delta\boldsymbol{\theta} = \mathbf{SBN}\delta\mathbf{u} \tag{5.23}$$

The matrix $\mathbf{S}$ in Eq. (5.23) contains geometrical characteristics of the point and can be shown explicitly as

$$\mathbf{S}=\begin{bmatrix}1 & x & y & \omega & 0\\ 0 & 0 & 0 & 0 & 2t_p\end{bmatrix} \tag{5.24}$$

The non-zero elements of matrix $\mathbf{B}$ are presented in Appendix 5.C, and vector $\boldsymbol{\theta}$ contains displacement components of a point in the body as

$$\boldsymbol{\theta}=\left\langle u \quad u' \quad u'' \quad u''' \quad v \quad v' \quad v'' \quad v''' \quad w \quad w' \quad w'' \quad \phi \quad \phi' \quad \phi''\right\rangle^T \tag{5.25}$$

$\mathbf{N}$ includes shape functions that are polynomial functions of s, and $\mathbf{u}$ is the nodal displacement vector (Appendix 5.E).

5.5. Stresses and Stress Resultants

In this study, linear-elastic material behaviour is assumed. Correspondingly, the constitutive relations can be of the form

$$\boldsymbol{\sigma}=\left\langle \sigma_p \quad \tau_p\right\rangle^T=\begin{bmatrix}E & 0\\ 0 & G\end{bmatrix}\begin{Bmatrix}\varepsilon_p\\ \gamma_p\end{Bmatrix}=\mathbf{E}\boldsymbol{\varepsilon} \tag{5.26}$$

where E and G are the Young's modulus and the shear modulus of the material, respectively. The stress resultants vector can be written as

$$\mathbf{R}=\left\langle N \quad M_x \quad M_y \quad B \quad T\right\rangle^T=\int_A \mathbf{S}^T\boldsymbol{\sigma}dA \tag{5.27}$$

where N, M_x, M_y, B and T are the axial normal force, bending moments about x and y axes, bimoment and the torque, respectively, which are shown explicitly as

$$N = \int_A \sigma_p dA, \tag{5.28}$$

$$M_x = \int_A \sigma_p y dA, \tag{5.29}$$

$$M_y = \int_A \sigma_p x dA, \tag{5.30}$$

$$B = \int_A \sigma_p \omega dA, \tag{5.31}$$

$$T = \int_A \tau_p \left(2t_p\right) dA. \tag{5.32}$$

The cross-sectional properties associated with the above stress resultants are

$$A = \int_A dA, \tag{5.33}$$

$$I_{xx} = \int_A y^2 dA, \tag{5.34}$$

$$I_{yy} = \int_A x^2 dA, \tag{5.35}$$

$$I_{\omega\omega} = \int_A \omega^2 dA, \tag{5.36}$$

while the torsional constant associated with the torque can be written as

$$J_d \approx \tfrac{1}{3} \sum_{i=1}^{n} b_i t_i^3 \tag{5.37}$$

where n is the number of plate sections in the cross-section and b_i and t_i are the width and thickness of the i^{th} segment, respectively.

5.6. Loading

The vector of the external loading is defined as

$$\mathbf{Q} = \left\langle Q_x \quad Q_y \quad Q_s \quad M_{ex} \quad M_{ey} \quad M_{es} \quad B_e \right\rangle^T, \tag{5.38}$$

in which Q_x, Q_y and Q_s are the concentrated force in the *X, Y* and *S* directions, respectively, M_{ex} and M_{ey} are the bending moments around *X* and *Y* axes, M_{es} is the external torque and B_e is the externally applied bimoment. The distributed external load vector can be written in the same fashion as

$$\mathbf{q} = \left\langle q_x \quad q_y \quad q_s \quad m_{ex} \quad m_{ey} \quad m_{es} \quad b_e \right\rangle^T, \tag{5.39}$$

The components of $\mathbf{q}$ are the counterparts of concentrated external loads of Eq. (5.38) distributed along the s-direction throughout the member. The concentrated and distributed loads are all applied at the centroid of the cross-section.

5.7. Principle of Virtual Work

5.7.1. Nonlinear equilibrium equations

According to the principle of virtual work, if a kinematically admissible virtual strain is applied to a structure in equilibrium, the sum of the work done by the external forces due to the virtual strain is equal to the work done internally by the stresses

$$\delta\Pi = \delta U - \delta V = 0 \tag{5.40}$$

where δU and δV are the variation of internal work and the variation of work done by external forces, respectively. The variation of the internal work can be written as

$$\delta U = \int_V \delta \boldsymbol{\varepsilon}^T \boldsymbol{\sigma} dV = \int_0^S \delta \mathbf{u}^T \mathbf{N}^T \mathbf{B}^T \left(\int_A \mathbf{S}^T \boldsymbol{\sigma} dA \right) ds = \int_0^S \delta \mathbf{u}^T \mathbf{N}^T \mathbf{B}^T \mathbf{R} ds. \tag{5.41}$$

The virtual work done by the external loads can be written as

$$\delta V = \int_0^S \delta \mathbf{u}_q{}^T \mathbf{q} ds + \sum_{i=1}^n \delta \mathbf{u}_i{}^T \mathbf{Q}_i = \int_0^S \delta \mathbf{u}_i{}^T \mathbf{N}_q{}^T \mathbf{A}^T \mathbf{q} ds + \sum_{i=1}^n \delta \mathbf{u}_i{}^T \mathbf{Q}_i = \delta \mathbf{u}^T \mathbf{F} \tag{5.42}$$

By the virtue of Eq. (5.40) we have

$$\delta \mathbf{u}^T \int_0^S \mathbf{N}^T \mathbf{B}^T \mathbf{R} ds = \delta \mathbf{u}^T \mathbf{F} \tag{5.43}$$

As the virtual displacement vector $\delta \mathbf{u}$ is arbitrary, the equilibrium equation can be written as

$$\int_0^S \mathbf{N}^T \mathbf{B}^T \mathbf{R} ds = \mathbf{F} \tag{5.44}$$

5.7.2. Consistent linearization

The incremental equilibrium equation is obtained by subtracting the expressions for virtual work at two neighbouring positions, i.e. $\delta\Pi(\mathbf{u}, \mathbf{q}, \mathbf{Q})$ and $\delta\Pi(\mathbf{u} + \delta\mathbf{u}, \mathbf{q} + \delta\mathbf{q}, \mathbf{Q} + \delta\mathbf{Q})$, and linearizing the results by omitting second and higher order terms. Using the Taylor expansion, the difference between the aforementioned virtual expressions can be approximated with the second variation of the potential as

$$\begin{aligned}\delta\Pi\left(\mathbf{u}+\delta\mathbf{u},\mathbf{q}+\delta\mathbf{q},\mathbf{Q}+\delta\mathbf{Q}\right)-\delta\Pi\left(\mathbf{u},\mathbf{q},\mathbf{Q}\right)&=\Delta\left(\delta\Pi\right)\approx\delta\left(\delta\Pi\right)\\&=\left(\frac{\partial\delta\Pi}{\partial\mathbf{u}^T}\right)\delta\mathbf{u}+\left(\frac{\partial\delta\Pi}{\partial\mathbf{q}^T}\right)\delta\mathbf{q}+\left(\frac{\partial\delta\Pi}{\partial\mathbf{Q}^T}\right)\delta\mathbf{Q}\end{aligned}\tag{5.45}$$

As matrices $\mathbf{B}$ and $\mathbf{R}$ in the equilibrium Eq. (5.44) are functions of the displacement vector $\mathbf{u}$, the first term of Eq. (5.45) can be written as

$$\left(\frac{\partial\delta\Pi}{\partial\mathbf{u}^T}\right)\delta\mathbf{u}=\int_0^S\delta\mathbf{u}^T\mathbf{N}^T\delta\mathbf{B}^T\mathbf{R}ds+\int_0^S\delta\mathbf{u}^T\mathbf{N}^T\mathbf{B}^T\delta\mathbf{R}ds\tag{5.46}$$

By noting that

$$\delta\mathbf{R}=\int_A\mathbf{S}^T\mathbf{E}\delta\boldsymbol{\varepsilon}dA=\int_A\mathbf{S}^T\mathbf{E}\mathbf{S}\mathbf{B}\mathbf{N}\delta\mathbf{u}dA\tag{5.47}$$

Eq. (5.46) can be written as

$$\left(\frac{\partial\delta\Pi}{\partial\mathbf{u}^T}\right)\delta\mathbf{u}=\int_0^S\delta\mathbf{u}^T\mathbf{N}^T\delta\mathbf{B}^T\mathbf{R}ds+\delta\mathbf{u}^T\mathbf{K}\delta\mathbf{u},\tag{5.48}$$

where $\mathbf{K}$ is the stiffness matrix

$$\mathbf{K}=\int_S\mathbf{N}^T\mathbf{B}^T\mathbf{D}\mathbf{B}\mathbf{N}ds\tag{5.49}$$

in which

$$\mathbf{D}=\int_A\mathbf{S}^T\mathbf{E}\mathbf{S}dA\tag{5.50}$$

is the elasticity matrix. The variation of the $\mathbf{B}$ matrix is handled by the introduction of a 14×14 matrix $\mathbf{M}_\sigma$ that satisfies the following equation

$$\delta \mathbf{B}^T \mathbf{R} = \mathbf{M}_\sigma \delta \boldsymbol{\theta} = \mathbf{M}_\sigma \mathbf{N} \delta \mathbf{u} \tag{5.51}$$

Consequently, Eq. (5.48) takes the form

$$\left(\frac{\partial \delta \Pi}{\partial \mathbf{u}^T} \right) \delta \mathbf{u} = \delta \mathbf{u}^T \int_0^S \mathbf{N}^T \mathbf{M}_\sigma \mathbf{N} \delta \mathbf{u} ds + \delta \mathbf{u}^T \mathbf{K} \delta \mathbf{u} = \delta \mathbf{u}^T \mathbf{K}_t \delta \mathbf{u} \tag{5.52}$$

Non-zero elements of the matrix $\mathbf{M}_\sigma$ are given explicitly in Appendix 5.D. The second terms of Eq. (5.45) can be written as

$$\left(\frac{\partial \delta \Pi}{\partial \mathbf{q}^T} \right) \delta \mathbf{q} = -\int_0^S \delta \mathbf{u}_i \mathbf{N}_q{}^T \mathbf{A}^T \delta \mathbf{q} ds, \tag{5.53}$$

and from the last term of Eq. (5.45),

$$\left(\frac{\partial \delta \Pi}{\partial \mathbf{Q}^T} \right) \delta \mathbf{Q} = -\sum_{i=1}^{n} \delta \mathbf{u}_i{}^T \delta \mathbf{Q}_i. \tag{5.54}$$

By the virtue of Eqs. (5.45), (5.52), (5.53) and (5.54), the incremental equilibrium equation can be expressed as

$$\mathbf{K}_t \delta \mathbf{u} - \delta \mathbf{F} = 0 \tag{5.55}$$

where $\delta \mathbf{u}$ is the incremental displacement vector and $\delta \mathbf{F}$ is the incremental load, which is shown explicitly in Eq. (5.56).

$$\delta \mathbf{F} = \delta \mathbf{Q} + \int_0^S \mathbf{N}_q{}^T \mathbf{A}^T \delta \mathbf{q} ds. \tag{5.56}$$

5.7.3. Finite element formulation

A finite element formulation is developed according to the abovementioned discussion, by assigning cubic interpolation for u, v and ϕ, and a linear interpolation for w.The shape function matrix **N** and the nodal displacement vector **u** are presented in Appendix 5.E.

5.8. Applications

The accuracy of the proposed model is verified in the following numerical examples by providing comparisons with results from the literature and a full shell-type finite element formulation.

The plate-bending component of the shell element is developed by using Discrete Kirchhoff Quadrilateral (Batoz & Tahar 1982) that omits the shear deformation effects to avoid shear locking in the analysis of thin plates. The finite element developed by Ibrahimbegovic et al. (1990) employing the drilling degree of freedom is used for the membrane component of the shell element. Using the Isoparametric formulation, a four-noded quadrilateral is developed with 6 degrees of freedom per node. The finite element is developed by adopting standard linear interpolation function for the out-of-plane displacement and Allman-type interpolation functions for the in-plane deflections. The drilling degree of freedom is interpolated using the standard bilinear functions.

5.8.1. Simply-supported horizontally-curved beam

In the first example, simply-supported curved beams tested by Shanmugam et al. (1995) are analysed using the proposed beam element for verification purposes. The beams

were made of hot-rolled I-section and were simply-supported spanning 5 meters, as shown in Figure 5.3. The loading consisted of a vertical load applied at a distance of $L_1 = 3.8m$ from the end of the beam.

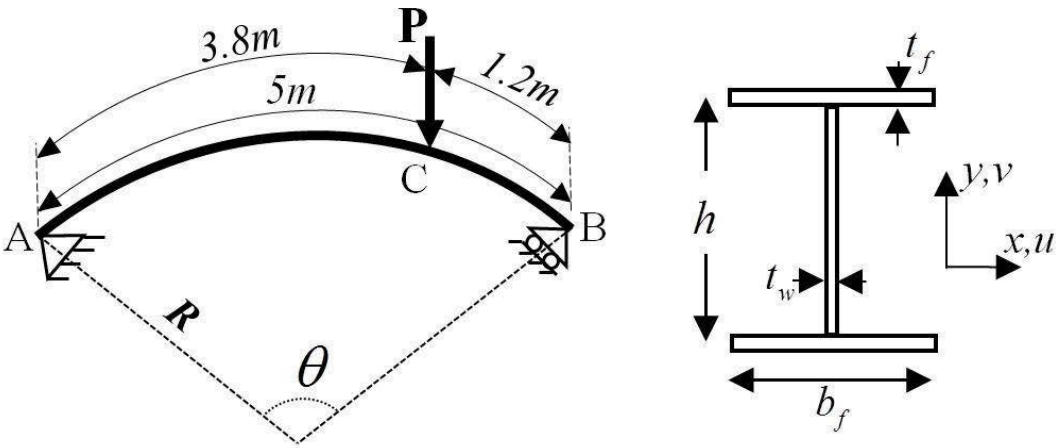

Figure 5.3: Cross-section, loading and boundary conditions of beams analysed in Example 1.

The lateral, vertical and twist displacement were restrained at both ends (i.e. $u_A = u_B = v_A = v_B = \phi_A = \phi_B = 0$) while two cases were introduced for lateral behaviour of the beam, namely "F" and "SS". The former indicates that the beam is laterally fixed (i.e. $u' = \phi' = 0$) while the latter denotes that only the above simply-supported boundary conditions are applied. The beams were also laterally fixed at load application point (i.e. $u_C = 0$. The dimensions, material properties and boundary conditions of the analysed beams are shown in Table 5.1.

Table 5.1: Properties of the beams analysed in Example 1.

Beam	$E(GPa)$	$h(mm)$	$b_f(mm)$	$t_f(mm)$	$t_w(mm)$	$R(m)$	θ°	Boundary
CB1	205.1	306.6	124.3	12.1	8.0	20	14.32	F/F
CB2	210.0					30	9.55	F/F
CB3	216.2					50	5.73	SS/F
CB4	206.7					75	3.82	SS/F
CB5	206.7					150	1.91	SS/F

Shanmugam et al. (1995) also performed a finite element modelling of the tested beam using ABAQUS (1985) curved shell elements, results of which are presented in the following figures as well. The proposed curved-beam element is used to model the behaviour of the tested curved beams using 10 beams elements. The results are then compared with the aforementioned experimental and ABAQUS results.

The vertical-displacement profile along the length of CB1 can be observed in Figure 5.4 for three load levels.

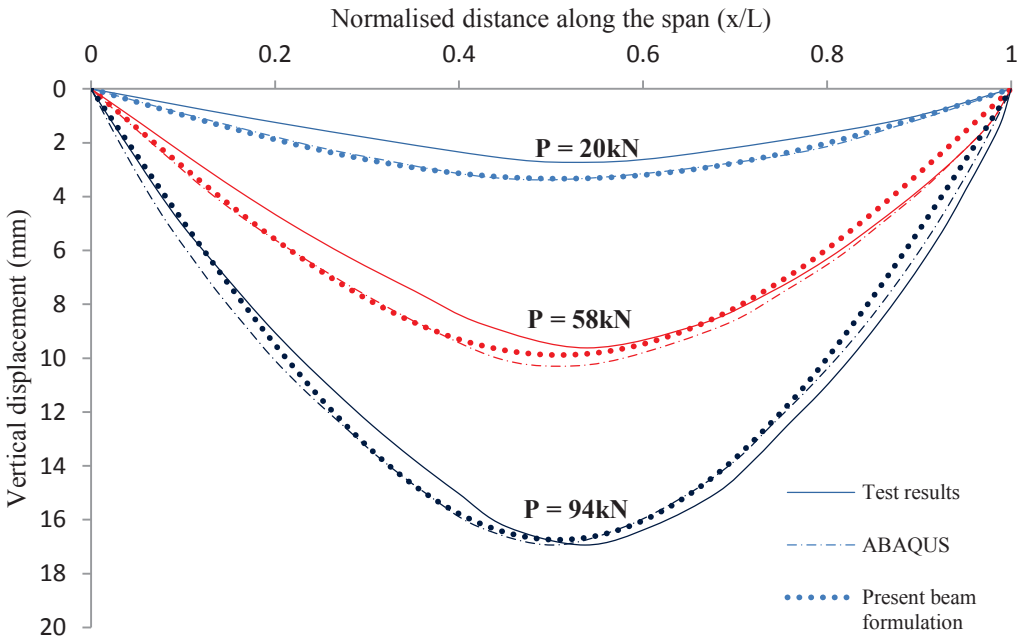

Figure 5.4: Displacement profile for CB1

It can be observed that the results of the proposed beam element formulation are in good agreement with the experimental and ABAQUS results. It should be noted that the ABAQUS results were obtained by using approximately 650 shell elements while in the current study only 10 beam elements are used.

The load-displacement curves for the mid-span of 5 CB beams can be seen in Figure 5.5. Very close agreement between the rest results and the results of the proposed beam element can be confirmed. It should be noted that since the material behaviour in the developed beam element is assumed to be elastic, the elastic portion of the test results is presented herein in order to make a comparison possible.

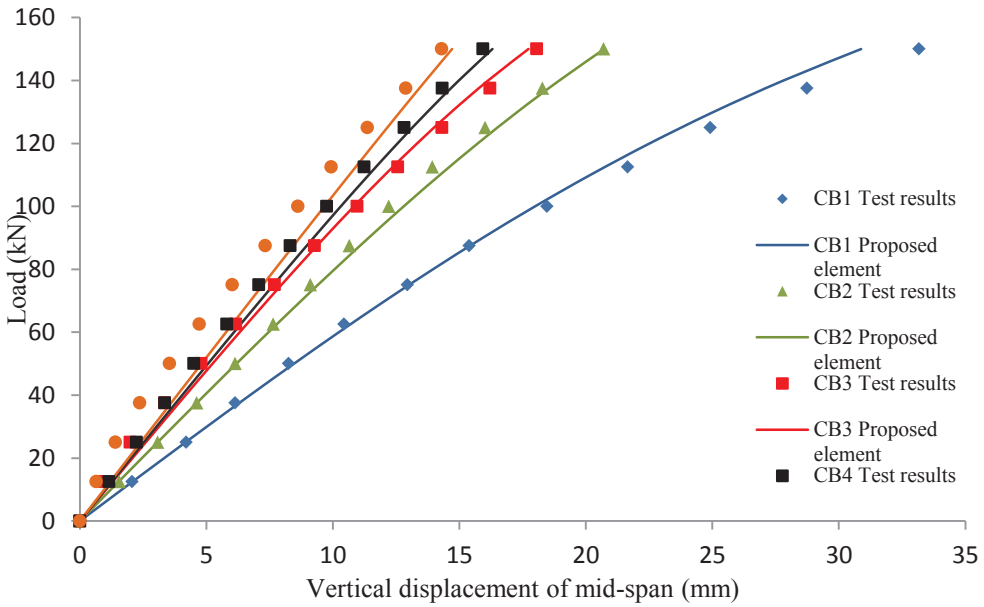

Figure 5.5: Load versus vertical displacement of mid-span

The load-displacement at the location of the point load *P* is drawn in Figure 5.6 for CB5. Comparing the results with the test data and ABAQUS results, the accuracy of the proposed model can be confirmed.

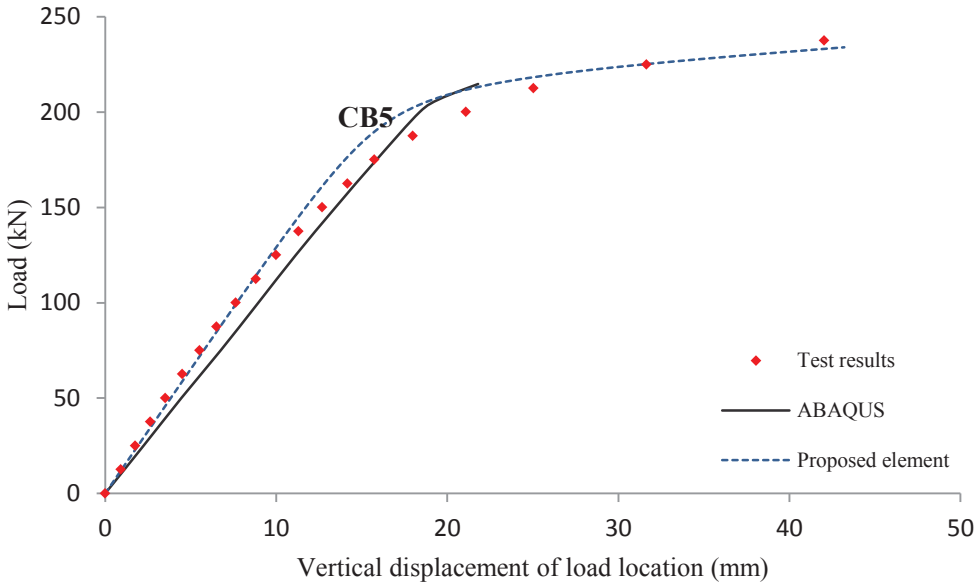

Figure 5.6: Load versus vertical displacement of load location for CB5

5.8.2. Cantilever curved beam

A cantilever curved beam with I-shape cross-section is analysed in this section. The material is construction steel, which has material properties of $E = 200GPa$, $\nu = 0.3$, and is assumed to behave elastically. The beam is subjected to vertical point load applied at the tip of the cantilever, perpendicular to the plane of curvature. Cross-sectional properties and a schematic of the beam loading and boundary conditions can be seen in Figure 5.7. Cross-sectional dimensions are $b_f = 200mm$, $h = 400mm$ and $t_f = t_w = 16mm$. The length of the beam is chosen as $L = 5000mm$.

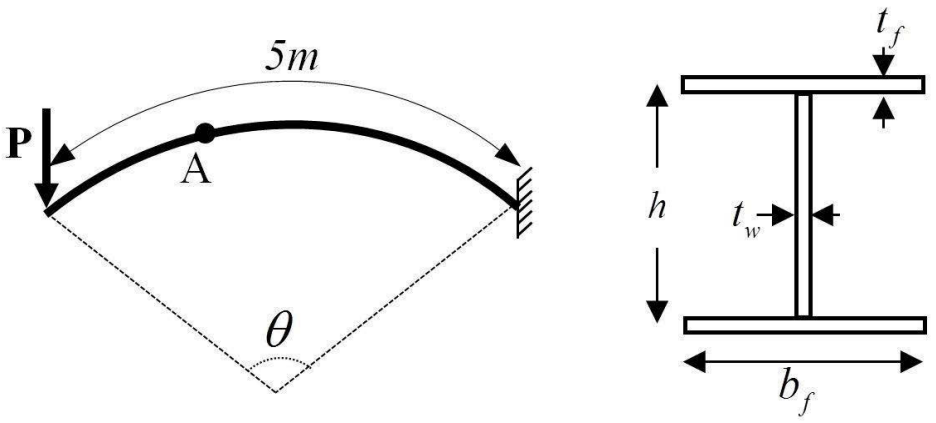

Figure 5.7: Schematic of cross-section, loading and boundary conditions for example 2

In order to demonstrate the accuracy of the present model in the analysis of highly-curved beams, the load factor versus vertical displacements are plotted for beams with different curvature values (i.e. various included angles) using the current curved-beam formulation, results obtained from the formulation of Pi et al. (2005) and the shell finite element. The vertical displacements are plotted for point A (Figure 5.7) located at 3/5 of the beam span from the support in order to exclude the local effects of point-load application in the shell analysis. The beam model is formed by using 10 elements of equal size while the shell elements used have dimensions of approximately $200\times200mm$. The shell finite element mesh used in the analysis can be observed in Figure 5.8.

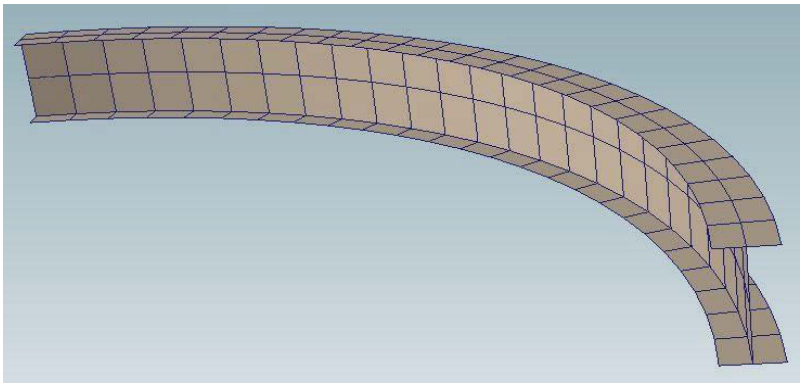

Figure 5.8: Finite element shell mesh for horizontally-curved beam

Analysis is performed for beams with 3 values of curvature, which are presented in Table 5.2 along with the corresponding radii and included angles.

Table 5.2: Properties of the arches analysed in Example 2.

Beam	*Curvature*$(1/mm)$	$R(mm)$	θ°
B1	1.00E-05	100000	2.86
B2	1.00E-04	10000	28.65
B3	3.14E-04	3184.7	89.95

Load versus vertical displacement curves obtained from the shell finite element, curved-beam finite element of Pi et al. (2005) and the proposed curved-beam element are compared in Figure 5.9 for 3 values of curvature and included angle. It can be observed that for small values of included angle, all the figures match. However, the results of the previous study diverges from shell results for larger values of included angle per element while the curved beam element developed herein is capable of capturing the behaviour of the beam accurately.

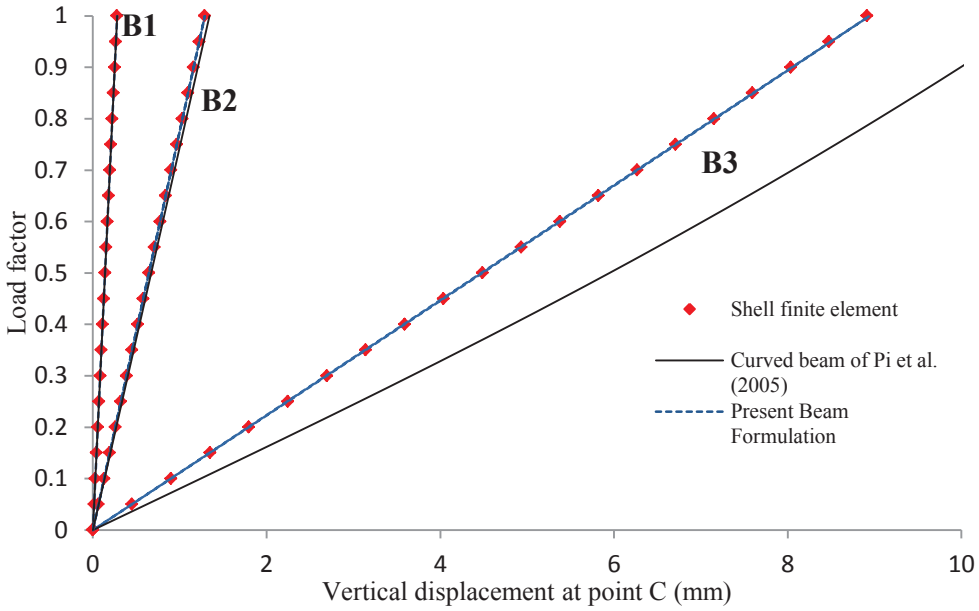

Figure 5.9: Load vs. vertical displacement for cantilever curved beam

5.9. Conclusions

An elastic curved-beam element is developed in this study for nonlinear analysis of thin-walled curved structures. The deformed configuration is obtained from the initial state using the Frenet-Serret formulae and a second-order rotation tensor. Right extensional strain definition is adopted to calculate the strain terms based on the translations and rotations of the cross-section. The Principle of virtual work is then used to obtain a finite element with 7 degrees of freedom per node. It is assumed that the beam is curved in one plane only resulting in examples of beams curved in plan.

The developed beam-element formulation was applied to various examples of beams curved-in-plan and arches, and the results were compared with experimental data and finite element results from the literature. The accuracy of the proposed element in the analysis of highly curved members is confirmed without necessitating the use of a large number of finite elements.

5.10. References

Akhtar, M.N. 1987, 'Element stiffness of circular member', *Journal of structural engineering New York, N.Y.*, vol. 113, no. 4, pp. 867-72.

Basler, K. & Kollbrunner, C.F. 1969, *Torsion in structures- An engineering approach*, Springer-Verlag, New York.

Batoz, J.L. & Tahar, M.B. 1982, 'Evaluation of a new quadrilateral thin plate bending element', *INT J NUMER METHODS ENG*, vol. V 18, no. N 11, pp. 1655-77.

Brookhart, G.C. 1967, 'Circular-arc I-type girders', *American Society for Civil Engineers*, vol. 93.

Crisfield, M.A. 1990, 'A consistent co-rotational formulation for non-linear, three-dimensional, beam-elements', *Computer Methods in Applied Mechanics and Engineering*, vol. 81, no. 2, pp. 131-50.

El-Amin, F.M. & Brotton, D.M. 1976, 'Horizontally curved beam finite element including warping', *International Journal for Numerical Methods in Engineering*, vol. 10, no. 6, pp. 1397-406.

El-Amin, F.M. & Kasem, M.A. 1978, 'Higher-order horizontally-curved beam finite element including warping for steel bridges', *International Journal for Numerical Methods in Engineering*, vol. 12, no. 1, pp. 159-67.

Erkmen, R.E. & Bradford, M.A. 2009, 'Nonlinear elasto-dynamic analysis of I-beams curved in-plan', *International Journal of Structural Stability and Dynamics*, vol. 9, no. 2, pp. 213-41.

Fukumoto, Y. & Nishida, S. 1981, 'Ultimate load behavior of curved I-beams', *ASCE J Eng Mech Div*, vol. 107, no. 2, pp. 367-85.

Ibrahimbegovic, A., Taylor, R.L. & Wilson, E.L. 1990, 'Robust quadrilateral membrane finite element with drilling degrees of freedom', *International Journal for Numerical Methods in Engineering*, vol. 30, no. 3, pp. 445-57.

Iura, M. & Atluri, S.N. 1988, 'On a consistent theory, and variational formulation of finitely stretched and rotated 3-D space-curved beams', *Computational Mechanics*, vol. 4, no. 2, pp. 73-88.

Koiter, W.T. 1984, 'Complementary energy, neutral equilibrium and buckling', *Meccanica*, vol. 19, no. 1 Supplement, pp. 52-6.

Krenk, S. 1994, 'A general format for curved and non-homogeneous beam elements', *Computers and Structures*, vol. 50, no. 4, pp. 449-54.

Liew, R.J.Y., Thevendran, V., Shanmugam, N.E. & Tan, L.O. 1995, 'Behaviour and design of horizontally curved steel beams', *Journal of Constructional Steel Research*, vol. 32, no. 1, pp. 37-67.

Love, A.E.H. 1944, *A Treatise on the Mathematical Theory of Elasticity*, 4th edn, Dover Publications Inc., New York.

Pantazopoulou, S.J. 1992, 'Low-order interpolation functions for curved beams', *Journal of Engineering Mechanics*, vol. 118, no. 2, pp. 329-50.

Pi, Y.-L., Bradford, M.A. & Uy, B. 2005, 'Nonlinear analysis of members curved in space with warping and Wagner effects', *International Journal of Solids and Structures*, vol. 42, no. 11–12, pp. 3147-69.

Pi, Y.L., Bradford, M.A. & Uy, B. 2003, *Nonlinear analysis of members with open thin-walled cross-section curved in space*, University of New South Wales, School of Civil and Environmental Engineering, Sydney.

Pi, Y.L. & Trahair, N.S. 1997, 'Nonlinear elastic behavior of I-beams curved in plan', *Journal of Structural Engineering*, vol. 123, no. 9, pp. 1201-9.

Sandhu, J.S., Stevens, K.A. & Davies, G.A.O. 1990, 'A 3-D, co-rotational, curved and twisted beam element', *Computers and Structures*, vol. 35, no. 1, pp. 69-79.

Sawko, F. 1967, 'Computer analysis of grillages curved in plan', *International Association for Bridge and Structural Engineering*, vol. 8, pp. 151-70.

Shanmugam, N.E., Thevendran, V., Liew, J.Y.R. & Tan, L.O. 1995, 'Experimental Study on Steel Beams Curved in Plan', *Journal of Structural Engineering*, vol. 121, no. 2, pp. 249-59.

Simo, J.C. 1985, 'A finite strain beam formulation. The three-dimensional dynamic problem. Part I', *Computer Methods in Applied Mechanics and Engineering*, vol. 49, no. 1, pp. 55-70.

Simo, J.C. & Vu-Quoc, L. 1987, 'The role of non-linear theories in transient dynamic analysis of flexible structures', *Journal of Sound and Vibration*, vol. 119, no. 3, pp. 487-508.

Simo, J.C. & Vu-Quoc, L. 1991, 'A Geometrically-exact rod model incorporating shear and torsion-warping deformation', *International Journal of Solids and Structures*, vol. 27, no. 3, pp. 371-93.

Timoshenko, S.P. 1923, 'Bending Stresses in Curved Tubes of Rectangular Cross-Section', paper presented to the *ASME*, Montreal, Canada, 28 May, 1923.

Vlasov, V.Z. 1961, *Thin-walled elastic beams*, 2nd edn, Israel Program for Scientific Translation, Jerusalem.

Yoo, C.H., Kang, Y.J. & Davidson, J.S. 1996, 'Buckling analysis of curved beams by finite-element discretization', *Journal of Engineering Mechanics*, vol. 122, no. 8, pp. 762-70.

Yoshida, H. & Maegawa, K. 1983, 'Ultimate strength analysis of curved I-beams', *Journal of Engineering Mechanics*, vol. 109, no. 1, pp. 192-214.

Young, M.C. 1969, 'Flexibility influence functions for curved beams', *American Society of Civil Engineers*, vol. 94.

Appendix 5.A

Eq. (5.4) can be used to obtain the deformed curvatures in terms of the initial curvature and displacement term. Differentiating this equation with respect to *s* yields

$$\frac{d\mathbf{q}}{ds} = \mathbf{R}\frac{d\mathbf{p}}{ds} + \frac{d\mathbf{R}}{ds}\mathbf{p} \tag{5.A.1}$$

where $\mathbf{q} = \begin{bmatrix} \mathbf{q}_x & \mathbf{q}_y & \mathbf{q}_s \end{bmatrix}^T$ and $\mathbf{p} = \begin{bmatrix} \mathbf{p}_x & \mathbf{p}_y & \mathbf{p}_s \end{bmatrix}^T$. We have (Pi et al. 2003)

$$\frac{d\mathbf{p}}{ds} = \mathbf{K}_0\mathbf{p} \tag{5.A.2}$$

$$\frac{d\mathbf{q}}{ds^*} = \mathbf{K}\mathbf{q} \tag{5.A.3}$$

where $\mathbf{K}_0$ and $\mathbf{K}$ are curvature matrices in the undeformed and deformed configurations, respectively, which are defined as

$$\mathbf{K}_0 = \begin{bmatrix} 0 & 0 & -\kappa_0 \\ 0 & 0 & 0 \\ \kappa_0 & 0 & 0 \end{bmatrix} \tag{5.A.4}$$

$$\mathbf{K} = \begin{bmatrix} 0 & \kappa_s & -\kappa_y \\ -\kappa_s & 0 & \kappa_x \\ \kappa_y & -\kappa_x & 0 \end{bmatrix} \tag{5.A.5}$$

where κ_0 is the initial curvature of the beam and κ_x, κ_y and κ_s are the curvature values after the deformations around *x, y* and *s* axes, respectively. It should be noted that it is assumed in the formulation that the initial curvature lies in one plane only resulting in the other terms of the initial curvature matrix vanishing. ds^* in Eq. (5.A.3) refers to the deformed length of the beam segment, for which the relation $ds^* = (1+\varepsilon)ds$ holds,

where ε is the normal strain at the centroid of the beam along the beam axis and ds is the undeformed length of the beam segment. Using the above definitions, the curvature matrix in the deformed configuration can be obtained as

$$(1+\varepsilon)\mathbf{K} = \mathbf{R}\mathbf{K}_0\mathbf{R}^T + \frac{d\mathbf{R}}{ds}\mathbf{R}^T \tag{5.A.6}$$

If the elements of the rotation matrix $\mathbf{R}$ are nominated as the following

$$\mathbf{R} = \begin{bmatrix} R_{11} & R_{12} & R_{13} \\ R_{21} & R_{22} & R_{23} \\ R_{31} & R_{32} & R_{33} \end{bmatrix} \tag{5.A.7}$$

the deformed curvature values can be obtained from the elements of the rotation matrix as

$$\kappa_x = \left(1+\varepsilon\right)^{-1}\left[\left(R_{13}R'_{12} + R_{23}R'_{22} + R_{33}R'_{32}\right) + \kappa_0\left(R_{32}R_{13} - R_{12}R_{33}\right)\right] \tag{5.A.8}$$

$$\kappa_y = \left(1+\varepsilon\right)^{-1}\left[\left(R_{11}R'_{13} + R_{21}R'_{23} + R_{31}R'_{33}\right) + \kappa_0\left(R_{33}R_{11} - R_{13}R_{31}\right)\right] \tag{5.A.9}$$

$$\kappa_s = \left(1+\varepsilon\right)^{-1}\left[\left(R_{12}R'_{11} + R_{22}R'_{21} + R_{32}R'_{31}\right) + \kappa_0\left(R_{31}R_{12} - R_{11}R_{32}\right)\right] \tag{5.A.10}$$

where $()'$ denotes derivative with respect to s. After performing the calculations and ignoring third and higher order terms, we obtain Eqs. (5.9) to (5.11) in terms of displacement components.

Appendix 5.B

The normal strain ε_p, which is the last diagonal term in strain matrix $\boldsymbol{\varepsilon}$, is obtained as

$$\begin{aligned}\varepsilon_{ss} &= \left(\tilde{u}' - \tfrac{1}{2}\phi v'\right)(1+\varepsilon)\left(-y\kappa_s - \omega p\kappa_y\right) + \left(v' + \tfrac{1}{2}\phi\tilde{u}'\right)(1+\varepsilon)\left(x\kappa_s + \omega p\kappa_x\right) + \\ &\left[1 - \tfrac{1}{2}\left(\tilde{u}'^2 + v'^2\right)\right]\left[(1+\varepsilon)\left(1 - x\kappa_y + y\kappa_x - \omega p'\right) - \left(1 - x\kappa_0\right)\right] - 1 + \left[1 - \tfrac{1}{2}\left(\tilde{u}'^2 + v'^2\right)\right] \\ &= A + B + C + D\end{aligned} \tag{5.B.1}$$

$p(s)$ is the warping amplitude function. For warping torsion it is approximated to be equal to the twist rate (Basler & Kollbrunner 1969; Pi et al. 2005; Vlasov 1961), which is the difference between the initial and final twist as

$$p(s) = \kappa_s - \kappa_{s0}, \tag{5.B.2}$$

and since the initial twist is assumed to be zero in this study, the warping amplitude is assumed to be equal to the final twist of the member (i.e. $p(s) = \kappa_s$). Consequently, the first term in Eq. (5.B.1) is calculated as

$$A = (1+\varepsilon)\left[y\kappa_s\left(-\tilde{u}' + \tfrac{1}{2}\phi v'\right) + \omega\kappa_s\kappa_y\left(-\tilde{u}' + \tfrac{1}{2}\phi v'\right)\right] = y\left[-u'\phi' + \kappa_0\left(-u'v' - w\phi'\right) - \kappa_0{}^2 v'w\right] \tag{5.B.3}$$

Similarly, the second term of Eq. (5.B.1) is equal to

$$B = (1+\varepsilon)\left[x\kappa_s\left(v' + \tfrac{1}{2}\phi\tilde{u}'\right) + \omega\kappa_s\kappa_x\left(v' + \tfrac{1}{2}\phi\tilde{u}'\right)\right] = x\left[v'\phi' + \kappa_0 v'^2\right] \tag{5.B.4}$$

The third term of Eq. (5.B.1) is re-written as

$$C = \left[1 - \tfrac{1}{2}\left(\tilde{u}'^2 + v'^2\right)\right]\left[(1+\varepsilon)\left(1 - x\kappa_y + y\kappa_x - \omega p'\right) - \left(1 - x\kappa_0\right)\right], \tag{5.B.5}$$

which is separated as

$$\begin{aligned} C &= \left[(1+\varepsilon)\left(1-x\kappa_y+y\kappa_x-\omega p'\right)-\left(1-x\kappa_0\right)\right] \\ &-\tfrac{1}{2}\left(\tilde{u}'^2+v'^2\right)\left[(1+\varepsilon)\left(1-x\kappa_y+y\kappa_x-\omega p'\right)-\left(1-x\kappa_0\right)\right] \\ &= E+F \end{aligned} \tag{5.B.6}$$

The elements of the first term of Eq. (5.B.6) are written explicitly as the following:

$$E_1=(1+\varepsilon)=1+\tilde{w}'+\tfrac{1}{2}\tilde{u}'^2+\tfrac{1}{2}v'^2+\tfrac{1}{2}\tilde{w}'^2 \tag{5.B.7}$$

$$E_2=x(1+\varepsilon)\left(\kappa_y-\kappa_0\right)=x\left[u''-\tfrac{1}{2}v'\phi'+\tfrac{1}{2}v''\phi+\kappa_0\left(w'-\tfrac{1}{2}v'^2-\tfrac{1}{2}\phi^2\right)\right] \tag{5.B.8}$$

$$E_3=y(1+\varepsilon)\kappa_x=y\left[-v''-\tfrac{1}{2}u'\phi'+\tfrac{1}{2}u''\phi+\kappa_0\left(\phi-\tfrac{1}{2}u'v'-\tfrac{1}{2}w\phi'+\tfrac{1}{2}w'\phi\right)-\tfrac{1}{2}\kappa_0{}^2v'w\right] \tag{5.B.9}$$

$$\begin{aligned} E_4 &= \omega(1+\varepsilon)\kappa_s{}' \\ &= \omega\left[\phi''-\tfrac{1}{2}u'v'''+\tfrac{1}{2}u'''v'+\kappa_0\left(v''+\tfrac{1}{2}u''\phi+\tfrac{1}{2}u'\phi'-\tfrac{1}{2}v'''w+\tfrac{1}{2}v'w''\right)+\tfrac{1}{2}\kappa_0{}^2\left(w'\phi+w\phi'\right)\right] \end{aligned} \tag{5.B.10}$$

The second term of Eq. (5.B.6) is calculated to be

$$F=-\tfrac{1}{2}\left(\tilde{u}'^2+v'^2\right)\left[(1+\varepsilon)\left(1-x\kappa_y+y\kappa_x-\omega p'\right)-\left(1-x\kappa_0\right)\right]=0 \tag{5.B.11}$$

It should be noted that the third and higher order terms are neglected in the above calculations. Using Eqs. (5.B.3) to (5.B.11), the normal strain can be written as

$$\begin{aligned} \varepsilon_{ss} &= w'+\tfrac{1}{2}w'^2+\kappa_0\left(-u-uw'\right)+\tfrac{1}{2}\kappa_0{}^2u^2 \\ &+x\left[-u''+\tfrac{3}{2}v'\phi'-\tfrac{1}{2}v''\phi+\kappa_0\left(-w'+\tfrac{3}{2}v'^2+\tfrac{1}{2}\phi^2\right)\right] \\ &+y\left[-v''-\tfrac{3}{2}u'\phi'+\tfrac{1}{2}u''\phi+\kappa_0\left(\phi-\tfrac{3}{2}u'v'-\tfrac{3}{2}w\phi'+\tfrac{1}{2}w'\phi\right)-\tfrac{3}{2}\kappa_0{}^2v'w\right] \\ &+\omega\left[-\phi''+\tfrac{1}{2}u'v'''-\tfrac{1}{2}u'''v'+\kappa_0\left(-v''-\tfrac{1}{2}u''\phi-\tfrac{1}{2}u'\phi'+\tfrac{1}{2}v'''w-\tfrac{1}{2}v'w''\right)+\tfrac{1}{2}\kappa_0{}^2\left(-w'\phi-w\phi'\right)\right] \end{aligned} \tag{5.B.12}$$

Appendix 5.C

$$
\begin{aligned}
&B_{11}=-\kappa_0-\kappa_0 w'+{\kappa_0}^2 u, && B_{1,10}=1+w'-\kappa_0 u, && B_{23}=-1,\\
&B_{26}=\tfrac{3}{2}\phi'+3\kappa_0 v', && B_{27}=-\tfrac{1}{2}\phi, && B_{2,10}=-\kappa_0,\\
&B_{2,12}=-\tfrac{1}{2}v''+\kappa_0\phi, && B_{2,13}=\tfrac{3}{2}v', && B_{32}=-\tfrac{3}{2}\phi'-\tfrac{3}{2}\kappa_0 v',\\
&B_{33}=\tfrac{1}{2}\phi, && B_{36}=-\tfrac{3}{2}\kappa_0 u'-\tfrac{3}{2}{\kappa_0}^2 w, && B_{37}=-1,\\
&B_{39}=-\tfrac{3}{2}\kappa_0\phi'-\tfrac{3}{2}{\kappa_0}^2 v', && B_{3,10}=\tfrac{1}{2}\kappa_0\phi, && B_{3,12}=\kappa_0+\tfrac{1}{2}u''+\tfrac{1}{2}\kappa_0 w',\\
&B_{3,13}=-\tfrac{3}{2}u'-\tfrac{3}{2}\kappa_0 w, && B_{42}=\tfrac{1}{2}v'''-\tfrac{1}{2}\kappa_0\phi', && B_{43}=-\tfrac{1}{2}\kappa_0\phi,\\
&B_{44}=-\tfrac{1}{2}v', && B_{46}=-\tfrac{1}{2}u'''-\tfrac{1}{2}\kappa_0 w'', && B_{47}=-\kappa_0,\\
&B_{48}=\tfrac{1}{2}u'+\tfrac{1}{2}\kappa_0 w, && B_{49}=\tfrac{1}{2}\kappa_0 v'''-\tfrac{1}{2}{\kappa_0}^2\phi', && B_{4,10}=-\tfrac{1}{2}{\kappa_0}^2\phi,\\
&B_{4,11}=-\tfrac{1}{2}\kappa_0 v', && B_{4,12}=-\tfrac{1}{2}\kappa_0 u''-\tfrac{1}{2}{\kappa_0}^2 w', && B_{4,13}=-\tfrac{1}{2}\kappa_0 u'-\tfrac{1}{2}{\kappa_0}^2 w,\\
&B_{4,14}=-1, && B_{52}=\tfrac{1}{2}v''-\tfrac{1}{2}\kappa_0\phi, && B_{53}=-\tfrac{1}{2}v',\\
&B_{56}=-\kappa_0-\tfrac{1}{2}u''-\tfrac{1}{2}\kappa_0 w', && B_{57}=\tfrac{1}{2}u'+\tfrac{1}{2}\kappa_0 w, && B_{59}=-\tfrac{1}{2}\kappa_0 v''-\tfrac{1}{2}{\kappa_0}^2\phi,\\
&B_{5,10}=-\tfrac{1}{2}\kappa_0 v', && B_{5,12}=-\tfrac{1}{2}\kappa_0 u'-\tfrac{1}{2}{\kappa_0}^2 w, && B_{5,13}=-1.
\end{aligned}
\tag{5.C.1}
$$

Appendix 5.D

$$
\begin{aligned}
&M_{11}=\kappa_0{}^2R_1, && M_{1,10}=\kappa_0R_1, && M_{26}=-\tfrac{3}{2}\kappa_0R_3,\\
&M_{27}=\tfrac{1}{2}R_5, && M_{28}=\tfrac{1}{2}R_4, && M_{2,12}=-\tfrac{1}{2}\kappa_0R_5,\\
&M_{2,13}=-\tfrac{3}{2}R_3-\tfrac{1}{2}\kappa_0R_4, && M_{36}=-\tfrac{1}{2}R_5, && M_{3,12}=\tfrac{1}{2}R_3-\tfrac{1}{2}\kappa_0R_4,\\
&M_{46}=-\tfrac{1}{2}R_4, && M_{62}=-\tfrac{3}{2}\kappa_0R_3, && M_{63}=-\tfrac{1}{2}R_5,\\
&M_{64}=-\tfrac{1}{2}R_4, && M_{66}=3\kappa_0R_2, && M_{69}=-\tfrac{3}{2}\kappa_0{}^2R_3,\\
&M_{6,10}=-\tfrac{1}{2}\kappa_0R_5, && M_{6,11}=-\tfrac{1}{2}\kappa_0R_4, && M_{6,13}=\tfrac{3}{2}R_2,\\
&M_{72}=\tfrac{1}{2}R_5, && M_{79}=\tfrac{1}{2}\kappa_0R_5, && M_{7,12}=-\tfrac{1}{2}R_2,\\
&M_{82}=\tfrac{1}{2}R_4, && M_{89}=\tfrac{1}{2}\kappa_0R_4, && M_{96}=-\tfrac{3}{2}\kappa_0{}^2R_3,\\
&M_{97}=\tfrac{1}{2}\kappa_0R_5, && M_{98}=\tfrac{1}{2}\kappa_0R_4, && M_{9,12}=-\tfrac{1}{2}\kappa_0{}^2R_5,\\
&M_{9,13}=-\tfrac{3}{2}\kappa_0R_3-\tfrac{1}{2}\kappa_0{}^2R_4, && M_{10,1}=-\kappa_0R_1, && M_{10,6}=-\tfrac{1}{2}\kappa_0R_5,\\
&M_{10,10}=R_1, && M_{10,12}=\tfrac{1}{2}\kappa_0R_3-\tfrac{1}{2}\kappa_0{}^2R_4, && M_{11,6}=-\tfrac{1}{2}\kappa_0R_4,\\
&M_{12,2}=-\tfrac{1}{2}\kappa_0R_5, && M_{12,3}=\tfrac{1}{2}R_3-\tfrac{1}{2}\kappa_0R_4, && M_{12,7}=-\tfrac{1}{2}R_2,\\
&M_{12,9}=-\tfrac{1}{2}\kappa_0{}^2R_5, && M_{12,10}=\tfrac{1}{2}\kappa_0R_3-\tfrac{1}{2}\kappa_0{}^2R_4, && M_{12,12}=\kappa_0R_2,\\
&M_{13,2}=-\tfrac{3}{2}R_3-\tfrac{1}{2}\kappa_0R_4, && M_{13,6}=\tfrac{3}{2}R_2, && M_{13,9}=-\tfrac{3}{2}\kappa_0R_3-\tfrac{1}{2}\kappa_0{}^2R_4,
\end{aligned}
\tag{5.D.1}
$$

where

$$
\mathbf{R}=\begin{Bmatrix}R_1 & R_2 & R_3 & R_4 & R_5\end{Bmatrix}^T \tag{5.D.2}
$$

Appendix 5.E

The nodal displacement vector used in the development of finite element formulation is

$$\mathbf{u}_{14\times1} = \langle w_1 \quad w_2 \quad u_1 \quad u_1' \quad u_2 \quad u_2' \quad v_1 \quad v_1' \quad v_2 \quad v_2' \quad \phi_1 \quad \phi_1' \quad \phi_2 \quad \phi_2' \rangle^T \tag{5.E.1}$$

The displacement field functions are obtained using cubic polynomials for u, v and ϕ, and a linear interpolation function for w:

$$u(s) = N_1 u_1 + N_2 u_1' + N_3 u_2 + N_4 u_2', \tag{5.E.2}$$

$$v(s) = N_1 v_1 + N_2 v_1' + N_3 v_2 + N_4 v_2', \tag{5.E.3}$$

$$\phi(s) = N_1 \phi_1 + N_2 \phi_1' + N_3 \phi_2 + N_4 \phi_2', \tag{5.E.4}$$

$$w(s) = M_1 w_1 + M_2 w_2, \tag{5.E.5}$$

where N_1, N_2, N_3, and N_4 are the Hermitian polynomials

$$N_1 = 1 - 3\xi^2 + 2\xi^3, \tag{5.E.6}$$

$$N_2 = S\left(\xi - 2\xi^2 + \xi^3\right), \tag{5.E.7}$$

$$N_3 = 3\xi^2 - 2\xi^3, \tag{5.E.8}$$

$$N_4 = S\left(-\xi^2 + \xi^3\right) \tag{5.E.9}$$

M_1 and M_2 are linear interpolations

$$M_1 = 1 - \xi, \tag{5.E.10}$$

$$M_2 = \xi, \tag{5.E.11}$$

where $\xi = s/S$ and S is the span of the member.

Chapter 5 list of symbols

The following symbols have been used in chapter 2.

A	=	cross-sectional area
$\mathbf{a}_0, \mathbf{a}$	=	position vector of an arbitrary point in undeformed and deformed configurations
B	=	Bimoment
$\mathbf{D}$	=	deformation gradient tensor, elasticity matrix
$\mathbf{E}$	=	matrix of constitutive relation
$\mathbf{F}$	=	load vector
$\mathbf{I}$	=	identity matrix
$I_{xx}, I_{yy}, I_{\omega\omega}$	=	cross-sectional moment of inertia
J_d	=	St. Venant torsional rigidity constant
$\mathbf{K}$	=	stiffness matrix of the curved element
M_x, M_y	=	bending moment about x and y axes
N	=	axial force
$\mathbf{P}_X, \mathbf{P}_Y, \mathbf{P}_Z$	=	global coordinate system
$\mathbf{p}_x, \mathbf{p}_y, \mathbf{p}_s$	=	orthogonal basis for undeformed configuration

p = warping amplitude

$\mathbf{Q}$ = vector of external nodal forces

$\mathbf{q}$ = vector of external member forces

$\mathbf{q}_x, \mathbf{q}_y, \mathbf{q}_s$ = orthogonal basis for deformed configuration

$\mathbf{R}$ = rotation tensor, vector of stress resultants

$\mathbf{r}_0, \mathbf{r}$ = position vectors of cross-sectional centroid in undeformed and deformed configurations

r = normal distance from the mid-surface

$\mathbf{S}$ = matrix of geometrical characteristics

T = torque

$\mathbf{U}$ = right stretch tensor

U = internal potential energy

V = external potential energy

u, v, w = displacement components along x, y and z coordinates

$\boldsymbol{\varepsilon}$ = strain vector

ε_{ikj} = permutation symbol

$\boldsymbol{\theta}$ = vector of displacement components of a point in the body

κ_0	=	initial curvature
$\kappa_x, \kappa_y, \kappa_s$	=	curvature components of the deformed beam
Π	=	total potential of the beam
$\boldsymbol{\sigma}$	=	stress vector
ϕ_i	=	rotation components
ω	=	normalized section warping displacement function

Chapter 5 list of figures

Chapter 6: The Iterative Global-local Method for the analysis of curved beams

6.1. Introduction

In this section, the Iterative Global-local Method (Erkmen 2013) is developed for horizontally curved beams. As discussed previously, a global-local model for thin-walled members consists of a one-dimensional beam-type finite element as the coarse-scale/global model and two-dimensional shell-type element as the fine-scale/local model. Consequently, the development of a curved global-local model consists of adopting appropriate elements for each scale and synchronizing them together by the use of an appropriate overlapping decomposition operator $\mathbf{N}$. For that purpose, the curved beam element developed in Chapter 5 is adopted as the coarse-scale model. Prior to that, its performance is enhanced by replacing the conventional interpolation functions with the direct result from the solution of the homogeneous governing differential equation obtained from the linear part of the strain definition. Then the required modifications are made in order to make the previously used shell element applicable for the analysis of thin-walled curved members, followed by the changes in the overlapping decomposition operator. Finally, numerical examples are presented in order to verify the accuracy of the proposed method.

6.2. The beam element for curved thin-walled members

The beam element used in this section is the one developed in Chapter 2. In order to enhance the performance of this element, the conventional polynomial interpolation functions are replaced from the exact solution to the governing differential equation. The governing differential equation is obtained from the weak form of equilibrium equation by considering the linear portion of the strain vector.

Conventionally, the displacement components of beam-type finite elements are interpolated independently over the domain of the element, as was done in Chapter 5. In other words, each of the components of the displacement field (e.g. u) are obtained solely from its nodal values (i.e. u_i, u_j, u_i' and u_j' for a cubic interpolation) without any reference to the other displacement components. However, unlike a straight beam, in curved beams couplings exist between the lateral displacement component u and the axial component w on the one hand, and the vertical displacement component v and torsional rotation φ on the other hand. Consequently, the element can be made more efficient by taking this fact into account and modifying the interpolation functions accordingly. For that purpose, we need to obtain the governing differential equation of the developed curved beam and solve it throughout the element.

6.2.1. Derivation of the homogeneous governing differential equation

In this section, the governing differential equation of the curved beam is obtained. This equation can be derived from the weak form of the equilibrium equation by integration by parts. The weak form of the equilibrium equation is obtained from the virtual work principle, for which only the linear portion of the strain vector is used in this study. Consequently, the displacement field derived from the solution of the differential

equation will be exact for a linear structural response. As a result, the finite element formulation based on that will be accurate in the linear analysis domain. In other words, using only one element will give exact nodal results as long as the structural behaviour is linear but will be approximate when nonlinearities exist, and finer element will be required in such situations.

Let a curved thin-walled member of length l be subjected to end tractions σ_i and τ_i at $s=0$, and σ_j and τ_j at $s=l$, along with the member tractions $\mathbf{p}=\left\langle p_x \quad p_y \quad p_s \right\rangle^T$. The equilibrium equations can be obtained from the principle of stationary potential energy as

$$\delta\Pi = \delta U - \delta V = 0 \tag{6.1}$$

in which $\delta\Pi$ is the first variation of the total potential energy of the element, and δU and δV are the internal and external virtual works, respectively. The internal virtual work can be written as

$$\delta U = \delta U_n + \delta U_s \tag{6.2}$$

where δU_n and δU_s are the internal virtual work corresponding to the normal and St. Venant strain components, respectively. The strain components of the curved beam were obtained in Chapter 5 as

$$\varepsilon_{ss} = w' + \tfrac{1}{2}w'^2 + \kappa_0\left(-u - uw'\right) + \tfrac{1}{2}\kappa_0{}^2u^2$$
$$+x\left[-u'' + \tfrac{3}{2}v'\phi' - \tfrac{1}{2}v''\phi + \kappa_0\left(-w' + \tfrac{3}{2}v'^2 + \tfrac{1}{2}\phi^2\right)\right]$$
$$+y\left[-v'' - \tfrac{3}{2}u'\phi' + \tfrac{1}{2}u''\phi + \kappa_0\left(\phi - \tfrac{3}{2}u'v' - \tfrac{3}{2}w\phi' + \tfrac{1}{2}w'\phi\right) - \tfrac{3}{2}\kappa_0{}^2v'w\right]$$
$$+\omega\left[-\phi'' + \tfrac{1}{2}u'v''' - \tfrac{1}{2}u'''v' + \kappa_0\left(-v'' - \tfrac{1}{2}u''\phi - \tfrac{1}{2}u'\phi' + \tfrac{1}{2}v'''w - \tfrac{1}{2}v'w''\right) + \tfrac{1}{2}\kappa_0{}^2\left(-w'\phi - w\phi'\right)\right] \tag{6.3}$$

$$\gamma_p = -2r\kappa_s = -2r\left(1+\varepsilon\right)^{-1}\left[\phi' - \tfrac{1}{2}u'v'' + \tfrac{1}{2}u''v' + \kappa_0\left(v' + \tfrac{1}{2}u'\phi - \tfrac{1}{2}v''w + \tfrac{1}{2}v'w'\right) + \tfrac{1}{2}\kappa_0{}^2w\phi\right] \tag{6.4}$$

By ignoring the 2nd and higher order terms, the linear part of the strain components can be written as

$$\varepsilon_{ss,l} = w' - \kappa_0 u + x\left(-u'' - \kappa_0 w'\right) + y\left(-v'' + \kappa_0\phi\right) + \omega\left(-\phi'' - \kappa_0 v''\right) \tag{6.5}$$

$$\gamma_{p,l} = -2r\left(1+\varepsilon\right)^{-1}\left(\phi' + \kappa_0 v'\right) \tag{6.6}$$

where the subscript l refers to the fact that only linear terms are considered. The first component of Eq. (6.2) can be written as

$$\delta U_{n,l} = \int_V \sigma_{ss,l}\delta\varepsilon_{ss,l}dV = E\int_0^L\int_A \delta\mathbf{u}^T\mathbf{x}\mathbf{x}^T\mathbf{u}dAds \tag{6.7}$$

where

$$\mathbf{x}^T = \langle 1 \quad -x \quad -y \quad -\omega \rangle \tag{6.8}$$

and E is the Young's modulus. By replacing the normal strain term from Eq. (6.5), the vector $\mathbf{u}$ can be obtained as

$$\mathbf{u}^T = \left\langle w' - \kappa_0 u \quad u'' + \kappa_0 w' \quad v'' - \kappa_0 \phi \quad \phi'' + \kappa_0 v'' \right\rangle \tag{6.9}$$

The cross-sectional matrix $\mathbf{D}$ can be defined such that

$$\mathbf{D} = \int_A \mathbf{x}\mathbf{x}^T dA = \begin{bmatrix} A & -S_y & -S_x & -S_\omega \\ -S_y & I_{yy} & I_{xy} & I_{\omega x} \\ -S_x & I_{xy} & I_{xx} & I_{\omega y} \\ -S_\omega & I_{\omega x} & I_{\omega y} & I_{\omega\omega} \end{bmatrix} \tag{6.10}$$

where the cross-sectional constants are defined as $A = \int_A dA$, $S_x = \int_A y dA$, $S_y = \int_A x dA$, $S_\omega = \int_A \omega dA$, $I_{xx} = \int_A y^2 dA$, $I_{yy} = \int_A x^2 dA$, $I_{xy} = \int_A xy dA$, $I_{\omega x} = \int_A \omega x dA$, $I_{\omega y} = \int_A \omega y dA$ and $I_{\omega\omega} = \int_A \omega^2 dA$. By selecting an orthogonal coordinate system placed at cross-sectional centre, and considering doubly-symmetric cross-section, the off-diagonal terms of **D** would vanish, resulting in the following cross-sectional matrix (Murray 1984; Vlasov 1961)

$$\mathbf{D} = \begin{bmatrix} A & 0 & 0 & 0 \\ 0 & I_{yy} & 0 & 0 \\ 0 & 0 & I_{xx} & 0 \\ 0 & 0 & 0 & I_{\omega\omega} \end{bmatrix} \tag{6.11}$$

By replacing Eqs. (6.9) and (6.11) in Eq. (6.7), the virtual work resulting from the normal strain component can be written as

$$\begin{aligned} \delta U_{n,l} = \int_0^L \{ & \delta w' \left(A w' - \kappa_0 A u + \kappa_0 I_{yy} u'' + \kappa_0^2 I_{yy} w' \right) + \delta u \left(-\kappa_0 A w' + \kappa_0^2 A u \right) \\ & + \delta u'' \left(I_{yy} u'' + I_{yy} \kappa_0 w' \right) + \delta v'' \left(I_{xx} v'' - I_{xx} \kappa_0 \phi + I_{\omega\omega} \kappa_0 \phi'' + I_{\omega\omega} \kappa_0^2 v'' \right) \\ & + \delta \phi \left(-I_{xx} \kappa_0 v'' + I_{xx} \kappa_0^2 \phi \right) + \delta \phi'' \left(I_{\omega\omega} \phi'' + I_{\omega\omega} \kappa_0 v'' \right) \} ds \end{aligned} \tag{6.12}$$

Similarly, the contribution of the shear strain due to St. Venant shear on the internal virtual work can be written as

$$\delta U_{s,l} = GJ_d \int_0^L \delta \boldsymbol{\psi}^T \boldsymbol{\psi} dz \tag{6.13}$$

in which G is the shear modulus of the material and J_d is the St. Venant torsional rigidity constant. For a thin-walled section consisting of n rectangular pieces with the width of b_i and thickness of t_i, $(i = 1,2,...,n)$, J_d can be calculated as (Boresi & Sidebottom 1985)

$$J_d \approx \sum_{i=1}^{n} \frac{b_i t_i^3}{3} \tag{6.14}$$

$\boldsymbol{\psi}$ in Eq. (6.13) can be written as

$$\boldsymbol{\psi} = \phi' + \kappa_0 v' \tag{6.15}$$

Substituting Equation (6.15) in (6.13), the internal virtual work of the shear strain component can be obtained as

$$\delta U_{s,l} = GJ_d \int_0^L \left[\delta\phi' \left(\phi' + \kappa_0 v' \right) + \delta v' \left(\kappa_0 \phi' + \kappa_0^2 v' \right) \right] ds \tag{6.16}$$

In order to obtain the homogeneous displacement field expressions, we can set the external load values equal to zero, and therefore the equilibrium equation can be written as

$$\delta U = \delta U_n + \delta U_s = 0 \tag{6.17}$$

In order to obtain the differential equations, the terms including $\delta w'$, $\delta v'$ and $\delta\phi'$ in Eqs. (6.12) and (6.16) are integrated once by part, and the ones including $\delta u''$, $\delta v''$ and $\delta\phi''$ are integrated twice by parts. Considering that the virtual displacement components δw, δu, δv and $\delta\phi$ are arbitrary, the following coupled differential equation can be obtained.

$$E\begin{bmatrix} \left(-A-\kappa_0{}^2 I_{yy}\right)D^2 & \kappa_0 AD-\kappa_0 I_{yy}D^3 & 0 & 0 \\ -\kappa_0 AD+\kappa_0 I_{yy}D^3 & I_{yy}D^4+\kappa_0{}^2 A & 0 & 0 \\ 0 & 0 & \left(I_{xx}+\kappa_0{}^2 I_{\omega\omega}\right)D^4-E^{-1}GJ_d\kappa_0{}^2D^2 & I_{\omega\omega}\kappa_0 D^4-\left(I_{xx}\kappa_0+E^{-1}GJ_d\kappa_0\right)D^2 \\ 0 & 0 & I_{\omega\omega}\kappa_0 D^4-\left(I_{xx}\kappa_0+E^{-1}GJ_d\kappa_0\right)D^2 & I_{\omega\omega}D^4-E^{-1}GJ_dD^2+\kappa_0{}^2 I_{xx} \end{bmatrix}\begin{Bmatrix} w \\ u \\ v \\ \phi \end{Bmatrix}=\mathbf{0} \tag{6.18}$$

where the differentiation operators $D=\dfrac{d}{ds}$, $D^2=\dfrac{d^2}{ds^2}$, $D^3=\dfrac{d^3}{ds^3}$ and $D^4=\dfrac{d^4}{ds^4}$ are defined.

6.2.2. Solution to the homogeneous differential equation

6.2.2.1. *w* and *u* displacement fields

From the first line of Eq. **(6.18)** we have

$$\left(A+\kappa_0{}^2 I_{yy}\right)w''=\kappa_0 Au'-\kappa_0 I_{yy}u^{(3)} \tag{6.19}$$

$$w''=\frac{\kappa_0}{A+\kappa_0{}^2 I_{yy}}\left(Au'-I_{yy}u^{(3)}\right) \tag{6.20}$$

The second line of Eq. (6.18) can be differentiated to obtain

$$-\kappa_0 Aw''+\kappa_0 I_{yy}w^{(4)}+I_{yy}u^{(5)}+\kappa_0{}^2 Au'=0 \tag{6.21}$$

Replacing w'' and its second derivative $w^{(4)}$ from Eq. (6.20) into Eq. (6.21) results in the following linear homogeneous differential equation

$$u^{(5)} + 2\kappa_0^2 u^{(3)} + \kappa_0^4 u' = 0 \tag{6.22}$$

It can be solved to obtain the displacement field $u(s)$.

$$u(s) = C_1 + C_2\cos(\kappa_0 s) + C_3\sin(\kappa_0 s) + C_4 s\cos(\kappa_0 s) + C_5 s\sin(\kappa_0 s) \tag{6.23}$$

In order to obtain the axial displacement component $w(s)$, we firstly integrate Eq. (6.20) once to obtain

$$w' = \frac{\kappa_0}{A + \kappa_0^2 I_{yy}}\left(Au - I_{yy}u''\right) + C \tag{6.24}$$

where C is an unknown integration constant. The displacement field $u(s)$ and its second derivative are replaced from Eq. (6.23) to obtain

$$\begin{aligned} w' &= C + \lambda A C_1 + C_2\kappa_0\cos(\kappa_0 s) + C_3\kappa_0\sin(\kappa_0 s) \\ &+ C_4\left[s\kappa_0\cos(\kappa_0 s) + 2I_{yy}\lambda\kappa_0\sin(\kappa_0 s)\right] + C_5\left[s\kappa_0\sin(\kappa_0 s) - 2I_{yy}\lambda\kappa_0\cos(\kappa_0 s)\right] \end{aligned} \tag{6.25}$$

where $\lambda = \dfrac{\kappa_0}{A + \kappa_0^2 I_{yy}}$. It should be noted that the two constants $\lambda A C_1$ and C can be combined in an unknown constant C_7. The resulting expression can then be integrated to obtain $w(s)$.

$$w(s)=C_7 s+C_2\sin(\kappa_0 s)-C_3\cos(\kappa_0 s)+C_4\left[s\sin(\kappa_0 s)+\frac{1}{\kappa_0}\cos(\kappa_0 s)-2I_{yy}\lambda\cos(\kappa_0 s)\right]$$
$$+C_5\left[-s\cos(\kappa_0 s)+\frac{1}{\kappa_0}\sin(\kappa_0 s)-2I_{yy}\lambda\sin(\kappa_0 s)\right]+C_6 \tag{6.26}$$

By replacing the expression for $w(s)$ from Eq. (6.26) in the second line of Eq. (6.18), we obtain $C_7=\kappa_0 C_1$.

$$w(s)=\kappa_0 C_1 s+C_2\sin(\kappa_0 s)-C_3\cos(\kappa_0 s)+C_4\left[s\sin(\kappa_0 s)+\frac{1}{\kappa_0}\cos(\kappa_0 s)-2I_{yy}\lambda\cos(\kappa_0 s)\right]$$
$$+C_5\left[-s\cos(\kappa_0 s)+\frac{1}{\kappa_0}\sin(\kappa_0 s)-2I_{yy}\lambda\sin(\kappa_0 s)\right]+C_6 \tag{6.27}$$

The unknowns C_1 to C_6 in Eqs. (6.23) and (6.27) can be obtained from the nodal values of w and u at the two ends of the beam element. Considering $u(0)=u_i$, $u'(0)=u'_i$, $u(L)=u_j$, $u'(L)=u'_j$, $w(0)=w_i$ and $w(L)=w_j$, the nodal displacement can be written in terms of the constants C_1 to C_6 as

$$\boldsymbol{\varsigma}=\boldsymbol{\Xi}\mathbf{C} \tag{6.28}$$

in which $\boldsymbol{\varsigma}$ represents the nodal displacements corresponding to u and w, and $\mathbf{C}$ includes the unknown constants, i.e.,

$$\boldsymbol{\varsigma}=\langle u_i \quad u'_i \quad u_j \quad u'_j \quad w_i \quad w_j\rangle^T \tag{6.29}$$

$$\mathbf{C}=\langle C_1 \quad C_2 \quad C_3 \quad C_4 \quad C_5 \quad C_6\rangle^T \tag{6.30}$$

The 6 by 6 matrix $\boldsymbol{\Xi}$ is given explicitly as

$$\boldsymbol{\Xi}=\begin{bmatrix} 1 & 1 & 0 & 0 & 0 & 0 \\ 0 & 0 & \kappa_0 & 1 & 0 & 0 \\ 1 & \cos(\kappa_0 L) & \sin(\kappa_0 L) & \mathrm{L}\cos(\kappa_0 L) & \mathrm{L}\sin(\kappa_0 L) & 0 \\ 0 & -\kappa_0 \sin(\kappa_0 L) & \kappa_0 \cos(\kappa_0 L) & \cos(\kappa_0 L)-\kappa_0 \mathrm{L}\sin(\kappa_0 L) & \sin(\kappa_0 L)+\kappa_0 \mathrm{L}\cos(\kappa_0 L) & 0 \\ 0 & 0 & -1 & \frac{1}{\kappa_0}-2I_{yy}\lambda & 0 & 1 \\ \kappa_0 L & \sin(\kappa_0 L) & -\cos(\kappa_0 L) & \mathrm{L}\sin(\kappa_0 L)+\left(\frac{1}{\kappa_0}-2I_{yy}\lambda\right)\cos(\kappa_0 L) & -\mathrm{L}\cos(\kappa_0 L)+\left(\frac{1}{\kappa_0}-2I_{yy}\lambda\right)\sin(\kappa_0 L) & 1 \end{bmatrix} \tag{6.31}$$

The constants $\mathbf{C}$ can be obtained from Eq. (6.28) by obtaining the inverse of the matrix $\boldsymbol{\Xi}$.

$$\mathbf{C}=\boldsymbol{\Xi}^{-1}\boldsymbol{\varsigma} \tag{6.32}$$

Consequently, the displacement fields $u(s)$ can be obtained as

$$u=\boldsymbol{\eta}^{\mathrm{T}}\mathbf{C}=\boldsymbol{\eta}^{\mathrm{T}}\boldsymbol{\Xi}^{-1}\boldsymbol{\varsigma} \tag{6.33}$$

where $\boldsymbol{\eta}=\langle 1 \quad \cos(\kappa_0 s) \quad \sin(\kappa_0 s) \quad s\cos(\kappa_0 s) \quad s\sin(\kappa_0 s) \quad 0\rangle^{\mathrm{T}}$. Similarly, the displacement field $w(s)$ can be obtained from the nodal values as

$$w=\boldsymbol{\omega}^{\mathrm{T}}\mathbf{C}=\boldsymbol{\omega}^{\mathrm{T}}\boldsymbol{\Xi}^{-1}\boldsymbol{\varsigma} \tag{6.34}$$

in which $\boldsymbol{\omega}$ can be written as

$$\boldsymbol{\omega}=\left\langle \kappa_0 s \quad \sin(\kappa_0 s) \quad -\cos(\kappa_0 s) \quad s\sin(\kappa_0 s)+\left(\frac{1}{\kappa_0}-2I_{yy}\lambda\right)\cos(\kappa_0 s) \quad -s\cos(\kappa_0 s)+\left(\frac{1}{\kappa_0}-2I_{yy}\lambda\right)\sin(\kappa_0 s) \quad 1 \right\rangle^{\mathrm{T}} \tag{6.35}$$

6.2.2.2. v and ϕ displacement fields

The 3rd and 4th line of the differential Eq. (6.18) can be written as

$$v^{(4)}\left(I_{xx}+\kappa_0{}^2 I_{\omega\omega}\right)+v''\left(-E^{-1}GJ_d\kappa_0{}^2\right)+\phi''\left(-\kappa_0 I_{xx}-E^{-1}GJ_d\kappa_0\right)+\phi^{(4)}\left(\kappa_0 I_{\omega\omega}\right)=0 \tag{6.36}$$

$$v^{(4)}\left(\kappa_0 I_{\omega\omega}\right)+v''\left(-\kappa_0 I_{xx}-E^{-1}GJ_d\kappa_0\right)+\phi^{(4)}\left(I_{\omega\omega}\right)+\phi''\left(-E^{-1}GJ_d\right)+\kappa_0{}^2 I_{xx}\phi=0 \tag{6.37}$$

In order to solve the set of differential Eqs. (6.36) and (6.37), the displacement fields v and ϕ are assumed to have the following form

$$v(s)=\kappa_0 R(s)+a\exp(\kappa_0 s)+b\exp(-\kappa_0 s) \tag{6.38}$$

$$\phi(s)=R''(s)+a\kappa_0\exp(\kappa_0 s)+b\kappa_0\exp(\kappa_0 s) \tag{6.39}$$

where R is a function of s, and is at least 6 times differentiable. By replacing the above values, both Eqs. (6.36) and (6.37) reduce to

$$R^{(6)}I_{\omega\omega}+R^{(4)}\left(\kappa_0{}^2 I_{\omega\omega}-E^{-1}GJ_d\right)+R''\left(-E^{-1}GJ_d\kappa_0{}^2\right)+aq\exp(\kappa_0 s)+bq\exp(-\kappa_0 s)=0 \tag{6.40}$$

where $q=2\kappa_0{}^6 I_{\omega\omega}-2\kappa_0{}^4 E^{-1}GJ_d$. For simplicity, the coefficients are renamed to obtain

$$\alpha R^{(6)}+\beta R^{(4)}+\gamma R''+aq\exp(\kappa_0 s)+bq\exp(-\kappa_0 s)=0 \tag{6.41}$$

Eq. (6.41) is solved to obtain

$$R(s) = C_1 + C_2 s + C_3 \exp(\psi s) + C_4 \exp(-\psi s) + C_5 \sin(\kappa_0 s) + C_6 \cos(\kappa_0 s) + m \exp(\kappa_0 s) + n \exp(-\kappa_0 s)$$

(6.42)

in which $\psi = \sqrt{-\frac{\beta - \sqrt{\beta^2 - 4\alpha\gamma}}{2\alpha}} = \sqrt{\frac{E^{-1}GJ_d}{I_{\omega\omega}}}$. The unknowns m and n are obtained in terms of a and b by replacing Eq. (6.42) in Eq. (6.43).

$$m = -aq \tag{6.43}$$

$$n = -bq \tag{6.44}$$

Using the expression for R, we can obtain the displacement values v and ϕ as

$$v = C_1\kappa_0 + C_2\kappa_0 s + C_3\kappa_0 \exp(\psi s) + C_4\kappa_0 \exp(-\psi s) + C_5\kappa_0 \sin(\kappa_0 s) + C_6\kappa_0 \cos(\kappa_0 s) + a(1 - q\kappa_0)\exp(\kappa_0 s) + b(1 - q\kappa_0)\exp(-\kappa_0 s)$$

(6.45)

$$\phi = C_3\psi^2 \exp(\psi s) + C_4\psi^2 \exp(-\psi s) - C_5\kappa_0{}^2 \sin(\kappa_0 s) - C_6\kappa_0{}^2 \cos(\kappa_0 s) + a\kappa_0(1 - q\kappa_0)\exp(\kappa_0 s) + b\kappa_0(1 - q\kappa_0)\exp(-\kappa_0 s) \tag{6.46}$$

By calling the constant $C_7 = a(1 - q\kappa_0)$ and $C_8 = b(1 - q\kappa_0)$, the displacement fields can be re-written as

$$v = C_1\kappa_0 + C_2\kappa_0 s + C_3\kappa_0 \exp(\psi s) + C_4\kappa_0 \exp(-\psi s) + C_5\kappa_0 \sin(\kappa_0 s) + C_6\kappa_0 \cos(\kappa_0 s) + C_7 \exp(\kappa_0 s) + C_8 \exp(-\kappa_0 s)$$

(6.47)

$$\phi = C_3\psi^2\exp(\psi s) + C_4\psi^2\exp(-\psi s) - C_5\kappa_0{}^2\sin(\kappa_0 s) - C_6\kappa_0{}^2\cos(\kappa_0 s) + C_7\kappa_0\exp(\kappa_0 s) + C_8\kappa_0\exp(-\kappa_0 s) \tag{6.48}$$

The unknown constants of Eqs. (6.47) and (6.48) can be obtained from the boundary conditions of the two ends of the beam element. Considering $v(0) = v_i$, $v'(0) = v_i'$, $v(L) = v_j$, $v'(L) = v_j'$, $\phi(0) = \phi_i$, $\phi'(0) = \phi_i'$, $\phi(L) = \phi_j$ and $\phi'(L) = \phi_j'$, the nodal displacement can be written in terms of the unknowns as

$$\boldsymbol{\zeta} = \mathbf{Q}\mathbf{C} \tag{6.49}$$

In which $\boldsymbol{\zeta}$ represents the nodal displacements corresponding to v and ϕ, and $\mathbf{C}$ includes the unknown constants, i.e.,

$$\mathbf{C} = \langle C_1 \quad C_2 \quad C_3 \quad C_4 \quad C_5 \quad C_6 \quad C_7 \quad C_8 \rangle^T \tag{6.50}$$

The 8 by 8 matrix $\mathbf{Q}$ is given explicitly as

$$\mathbf{Q} = \begin{bmatrix}
\kappa_0 & 0 & \kappa_0 & \kappa_0 & 0 & \kappa_0 & 1 & 1 \\
0 & \kappa_0 & \kappa_0\psi & -\kappa_0\psi & \kappa_0{}^2 & 0 & \kappa_0 & -\kappa_0 \\
\kappa_0 & \kappa_0 L & \kappa_0\exp(\psi L) & \kappa_0\exp(-\psi L) & \kappa_0\sin(\kappa_0 L) & \kappa_0\cos(\kappa_0 L) & \exp(\kappa_0 L) & \exp(-\kappa_0 L) \\
0 & \kappa_0 & \kappa_0\psi\exp(\psi L) & -\kappa_0\psi\exp(-\psi L) & \kappa_0{}^2\cos(\kappa_0 L) & -\kappa_0{}^2\sin(\kappa_0 L) & \kappa_0\exp(\kappa_0 L) & -\kappa_0\exp(-\kappa_0 L) \\
0 & 0 & \psi^2 & \psi^2 & 0 & -\kappa_0{}^2 & \kappa_0 & \kappa_0 \\
0 & 0 & \psi^3 & -\psi^3 & -\kappa_0{}^3 & 0 & \kappa_0{}^2 & -\kappa_0{}^2 \\
0 & 0 & \psi^2\exp(\psi L) & \psi^2\exp(-\psi L) & -\kappa_0{}^2\sin(\kappa_0 L) & -\kappa_0{}^2\cos(\kappa_0 L) & \kappa_0\exp(\kappa_0 L) & \kappa_0\exp(-\kappa_0 L) \\
0 & 0 & \psi^3\exp(\psi L) & -\psi^3\exp(-\psi L) & -\kappa_0{}^3\cos(\kappa_0 L) & \kappa_0{}^3\sin(\kappa_0 L) & \kappa_0{}^2\exp(\kappa_0 L) & -\kappa_0{}^2\exp(-\kappa_0 L)
\end{bmatrix} \tag{6.51}$$

The constants $\mathbf{C}$ can be obtained from Eq. (6.49) by obtaining the inverse of the matrix $\mathbf{Q}$.

$$\mathbf{C} = \mathbf{Q}^{-1}\boldsymbol{\zeta} \tag{6.52}$$

Consequently, the displacement fields $v(s)$ can be obtained as

$$v = \mathbf{r}^{\mathbf{T}}\mathbf{C} = \mathbf{r}^{\mathbf{T}}\mathbf{Q}^{-1}\boldsymbol{\zeta} \tag{6.53}$$

where

$$\mathbf{r} = \langle \kappa_0 \quad \kappa_0 s \quad \kappa_0 \exp(\psi s) \quad \kappa_0 \exp(-\psi s) \quad \kappa_0 \sin(\kappa_0 s) \quad \kappa_0 \cos(\kappa_0 s) \quad \exp(\kappa_0 s) \quad \exp(-\kappa_0 s) \rangle^{\mathbf{T}} \tag{6.54}$$

Similarly, the displacement field $\phi(s)$ can be obtained from the nodal values as

$$\phi = \mathbf{X}^{\mathbf{T}}\mathbf{C} = \mathbf{X}^{\mathbf{T}}\boldsymbol{\Psi}^{-1}\boldsymbol{\zeta} \tag{6.55}$$

in which $\mathbf{X}$ can be written as

$$\mathbf{X} = \langle 0 \quad 0 \quad \psi^2 \exp(\psi s) \quad \psi^2 \exp(-\psi s) \quad -\kappa_0^2 \sin(\kappa_0 s) \quad -\kappa_0^2 \cos(\kappa_0 s) \quad \kappa_0 \exp(\kappa_0 s) \quad \kappa_0 \exp(-\kappa_0 s) \rangle^{\mathbf{T}} \tag{6.56}$$

6.2.3. Verification

In order to verify the efficiency of the obtained interpolation functions, a cantilever beam subjected to a point load at different directions is analysed in this section. The displacement values are calculated along the beam using the interpolation functions obtained in this section from the governing differential equation and the polynomial interpolation functions used in Chapter 2.

The beam is I-shaped and is composed of construction steel ($E = 200GPa$, $\nu = 0.3$). Loading, boundary conditions and cross-sectional properties of the beam are shown in Figure 6.1. Cross-sectional dimensions are $b_f = 200mm$, $h = 400mm$ and $t_f = t_w = 16mm$, and the length of the beam is equal to $L = 5000mm$. The beam is excessively curved with a total included angle of $\theta = 286.5^\circ$. The initial curvature of the beam is equal to $\kappa_0 = 0.001$, and lies in the *x*-*s* plane.

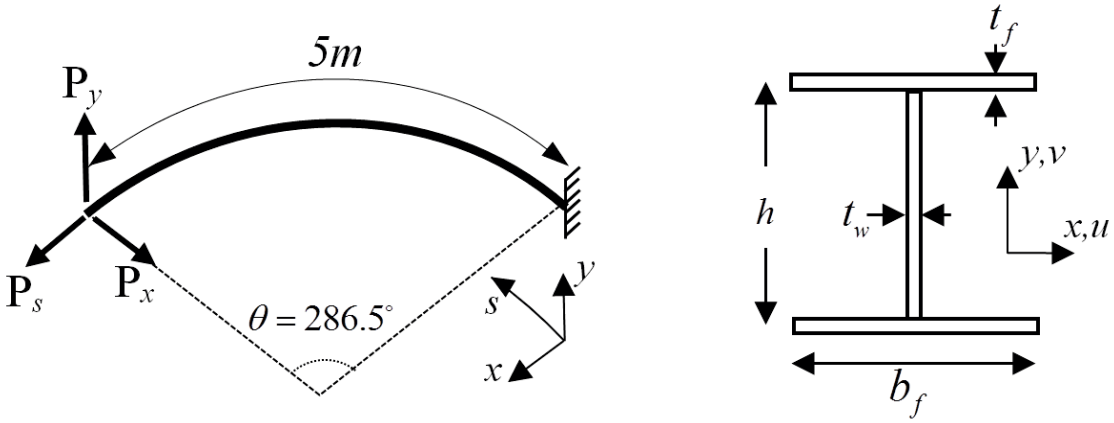

(a) Loading and boundary conditions (b) Cross-sectional dimensions

Figure 6.1: Cantilever curved beam used for verification of interpolations

The load vectors are applied separately, and for each case the corresponding displacement field is calculated along the beam using only one element of the newly developed interpolation functions and the results are compared with the results of conventional polynomial functions.

6.2.3.1. Curved-in-plan action

At this stage, only the load vector along the *y* axis (i.e. perpendicular to the plane of initial curvature) is applied, i.e. $\mathbf{P}_y = 1kN, \mathbf{P}_x = \mathbf{P}_s = 0$, corresponding to curved-in-plan beam action. The vertical displacement along the beam is shown in Figure 6.2, in which the results of the interpolation from the solution to the governing differential equation is

labelled as "new" while the results from polynomial interpolation functions (Chapter 2) are called "conventional".

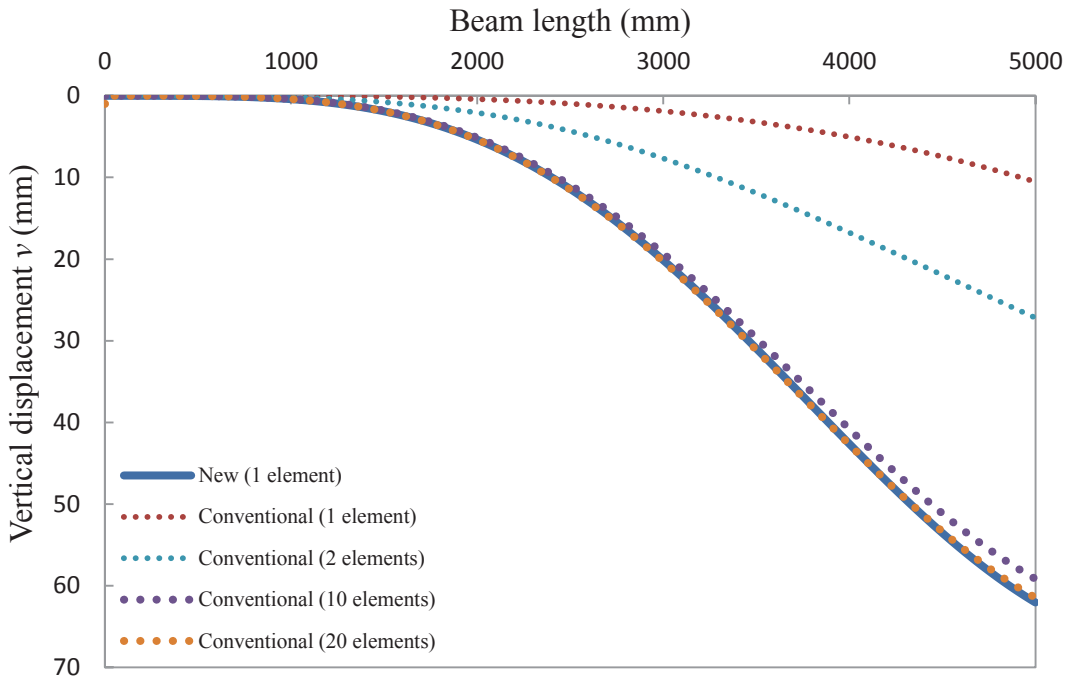

Figure 6.2: Vertical displacement along the beam

The exactness of the developed element can be confirmed from the figure. It can be seen that by using only one element, the "new" element is capable of capturing the out-of-plane displacement accurately. It can be observed that twenty finite elements are required for accurate modelling of the response of the beam in the element with conventional interpolation functions.

6.2.3.2. Arch action

In order to verify the exactness of the proposed element in arch action, point loads are applied in the plane of curvature. Firstly, a point load is applied in the axial direction of the beam, i.e. $\mathbf{P}_s = 1kN, \mathbf{P}_x = \mathbf{P}_y = 0$. The axial component of displacement w along the beam is shown in Figure 6.3 .

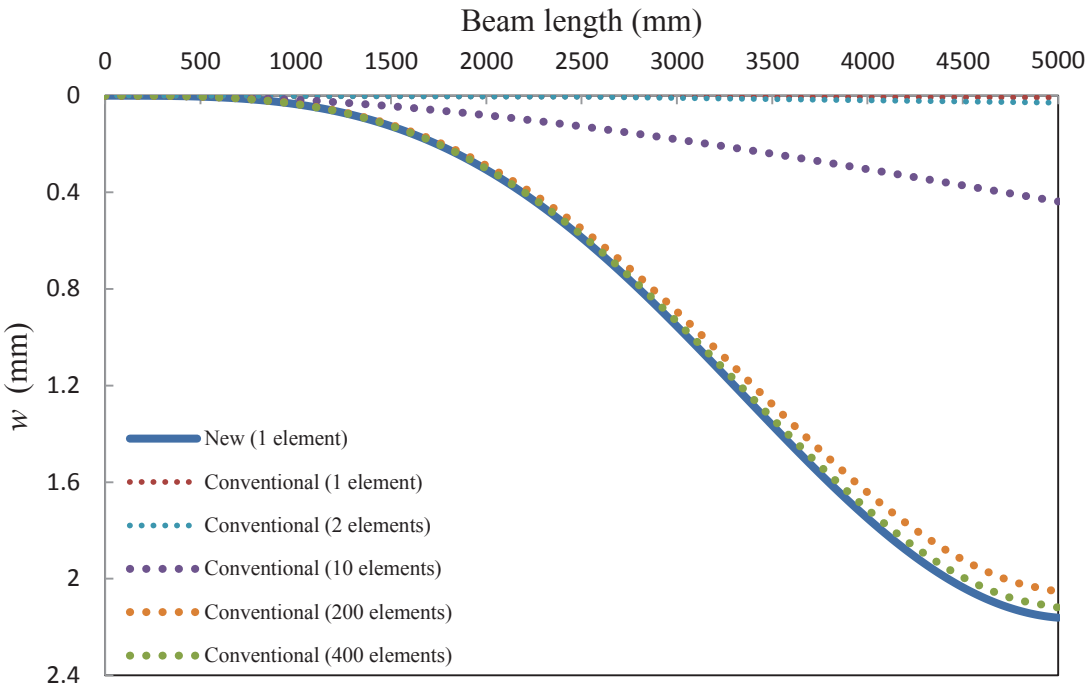

Figure 6.3: *w* component of displacement along the beam

It can be seen that around 400 elements of the conventional element are required in order to achieve a curve close to the figure obtained from only one element of the "new" element. It can be seen that the conventional element is less efficient in arch action in comparison with out-of-plane loading because the axial displacement in that element is interpolated linearly. Therefore, relatively more elements should be used in order to achieve the desired accuracy.

Similarly, a load is applied in the lateral direction of the cross-section to verify the arch action of the beam in the other direction, i.e. $\mathbf{P}_x = 1kN, \mathbf{P}_y = \mathbf{P}_s = 0$. The lateral component of the displacement, *u*, is depicted in Figure 6.4. Similar to the previous examples, it can be observed that the developed finite element is exact in obtaining the displacement field while a large number of elements are required to have acceptable results if the conventional element is used.

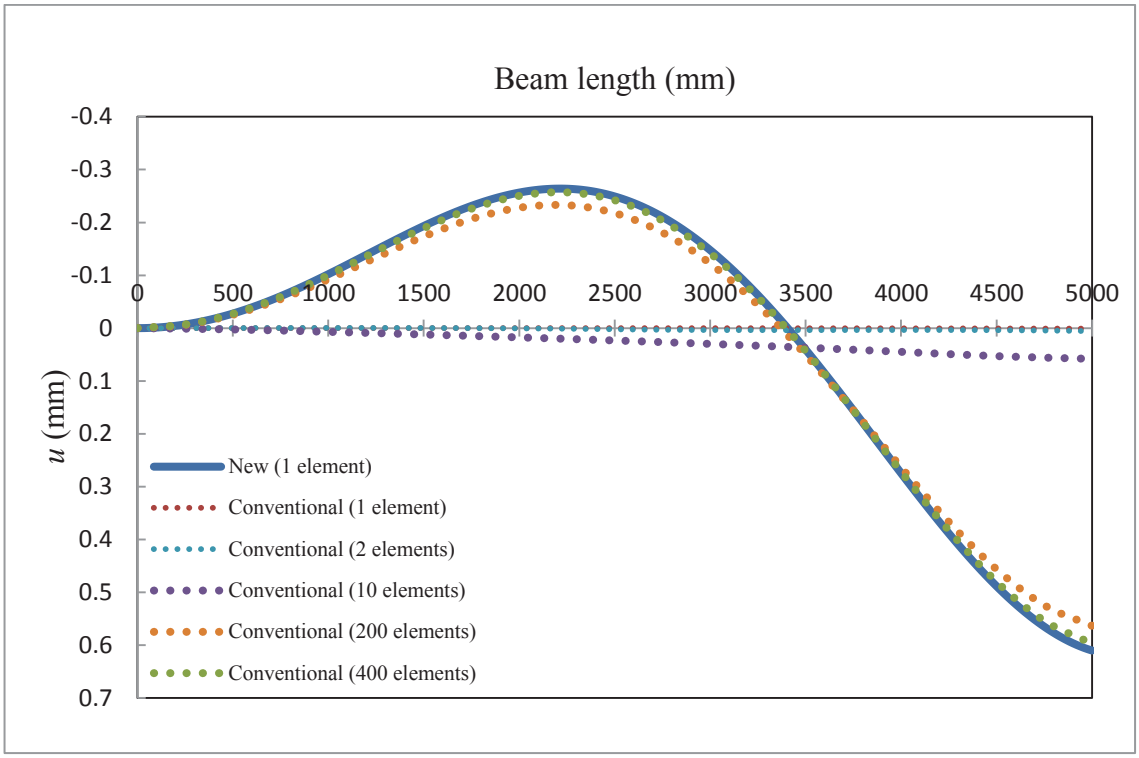

Figure 6.4: *u* component of displacement along the beam

6.3. The shell element for curved thin-walled members

The adopted shell element for straight thin-walled elements was presented in detail in Chapter 3. In order to utilize this element for the analysis of curved beams, we initially modify the mesh generation algorithm to organize the shell elements along a segment of a circle with a given radius of *r* instead of a straight line. Apart from that, two features of the shell element should be modified to match the new orientation, namely:

- The transformation matrix that was used to relate the local element and global coordinate systems was defined based on the assumption that all elements lie in the same direction along the axis of the beam.
- The elements had a rectangular geometry, which is suitable for a straight thin-walled member but has to be generalized to a quadrilateral to be able to model a curved beam accurately.

6.3.1. Transformation matrix

In order to develop a transformation matrix, we need to define a local coordinate system for each of the quadrilaterals. We can place the origin of this system on one of the corners of the element and the local *x*-axis along one of the sides, and define the *y*-axis so that the element lies in the *x*-*y* plane (Figure 6.5).

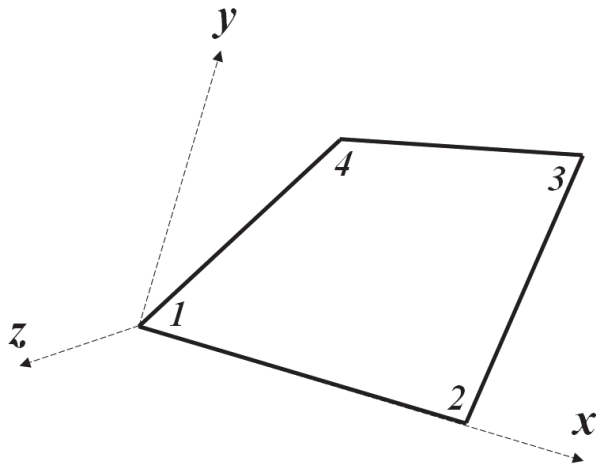

Figure 6.5: Load-deflection curves based on different modelling types

Since the coordinates of the corners in the global coordinate system are known, the vector $\mathbf{V}_{21}$ defining side 1-2 can be obtained as (Zienkiewicz & Taylor 2005)

$$\mathbf{V}_{21} = \begin{Bmatrix} x_2 - x_1 \\ y_2 - y_1 \\ z_2 - z_1 \end{Bmatrix} = \begin{Bmatrix} x_{21} \\ y_{21} \\ z_{21} \end{Bmatrix} \tag{6.57}$$

The direction cosines of $\mathbf{V}_{21}$ are calculated by dividing its components by its length

$$\boldsymbol{\lambda}_{21} = \boldsymbol{\lambda}_x = \begin{Bmatrix} \lambda_{xX} \\ \lambda_{xY} \\ \lambda_{xZ} \end{Bmatrix} = \frac{1}{l_{21}} \begin{Bmatrix} x_{21} \\ y_{21} \\ z_{21} \end{Bmatrix} \tag{6.58}$$

where $l_{21} = \sqrt{x_{21}^2 + y_{21}^2 + z_{21}^2}$, and *X*, *Y* and *Z* refer to the global coordinate axes. The vector in the *z* direction $\mathbf{V}_z$, which is normal to the plane of the quadrilateral, can be obtained from the cross-product of two vectors in that plane. Using the two sides of the quadrilateral connected to joint 1, we can write

$$\mathbf{V}_z = \mathbf{V}_{21} \times \mathbf{V}_{41} = \begin{Bmatrix} y_{21}z_{41} - z_{21}y_{41} \\ z_{21}x_{41} - x_{21}z_{41} \\ x_{21}y_{41} - y_{21}x_{41} \end{Bmatrix} \tag{6.59}$$

The direction cosines of $\mathbf{V}_z$ are obtained by dividing each of the components of this vector by its length.

$$\boldsymbol{\lambda}_z = \begin{Bmatrix} \lambda_{zX} \\ \lambda_{zY} \\ \lambda_{zZ} \end{Bmatrix} = \frac{1}{l_{Vz}} \begin{Bmatrix} x_z \\ y_z \\ z_z \end{Bmatrix} \tag{6.60}$$

where $l_{Vz} = \sqrt{x_z^2 + y_z^2 + z_z^2}$. Now that two of the three vectors of the local coordinate system are calculated, the remaining vector (i.e. $\boldsymbol{\lambda}_y$) can be determined by vector cross-product of $\boldsymbol{\lambda}_z$ and $\boldsymbol{\lambda}_x$ since it is normal to both of these vectors.

$$\boldsymbol{\lambda}_y = \boldsymbol{\lambda}_z \times \boldsymbol{\lambda}_x = \begin{Bmatrix} \lambda_{yX} \\ \lambda_{yY} \\ \lambda_{yZ} \end{Bmatrix} \tag{6.61}$$

It should be noted that we do not need to divide the components of $\boldsymbol{\lambda}_y$ by its length since it is a unit vector because both $\boldsymbol{\lambda}_z$ and $\boldsymbol{\lambda}_x$ are unit vectors.

6.3.2. Isoparametric formulation for quadrilateral element

The isoparametric formulation is required to model the geometry of an arbitrary quadrilateral. In isoparametric formulation, the geometry of the element is defined using the C^0 continuous interpolation functions which are used to create a mapping between the actual element (Figure 6.6 a) and a parent element in a natural coordinate space (Figure 6.6 b) (Cook et al. 1989; Zienkiewicz & Taylor 2005).

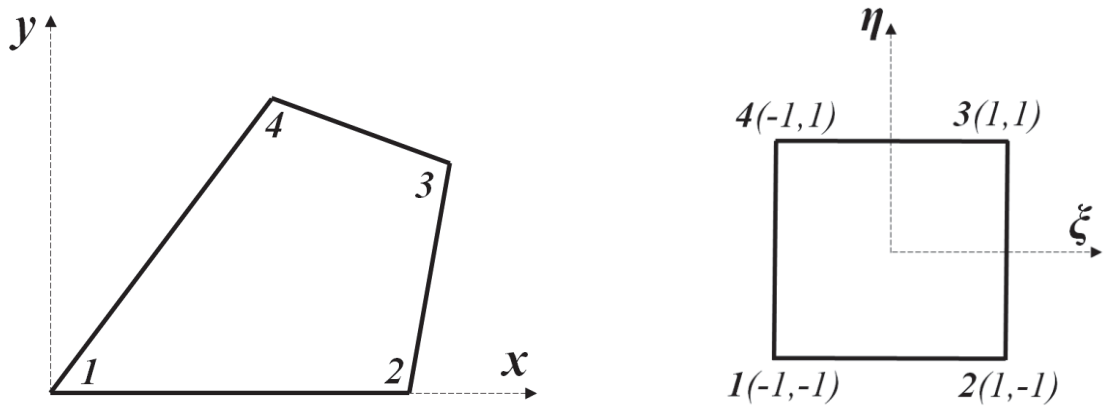

(a) Original element in Cartesian system (b) Parent element in natural coordinate system

Figure 6.6: Isoparametric transformation

The coordinate of any point inside the element can be written in terms of the nodal coordinates as

$$x = N_1 x_1 + N_2 x_2 + N_3 x_3 + N_4 x_4 \tag{6.62}$$

$$y = N_1 y_1 + N_2 y_2 + N_3 y_3 + N_4 y_4 \tag{6.63}$$

N_i s in Eqs. (6.62) and (6.63) are one-dimensional Lagrangian interpolation functions and are defined as

$$N_1 = \frac{1}{4}(1-\xi)(1-\eta) \tag{6.64}$$

$$N_2 = \frac{1}{4}(1+\xi)(1-\eta) \tag{6.65}$$

$$N_3 = \frac{1}{4}(1+\xi)(1+\eta) \tag{6.66}$$

$$N_4 = \frac{1}{4}(1-\xi)(1+\eta) \tag{6.67}$$

where $-1 \le \xi, \eta \le 1$. It is necessary to establish the derivatives of the variables with respect to the Cartesian coordinates. Using the chain rule,

$$\frac{\partial}{\partial x} = \frac{\partial}{\partial \xi}\frac{\partial \xi}{\partial x} + \frac{\partial}{\partial \eta}\frac{\partial \eta}{\partial x} \tag{6.68}$$

$$\frac{\partial}{\partial y} = \frac{\partial}{\partial \xi}\frac{\partial \xi}{\partial y} + \frac{\partial}{\partial \eta}\frac{\partial \eta}{\partial y} \tag{6.69}$$

Since the direct calculation of partial derivatives of the natural coordinates with respect to the global coordinates (e.g. $\frac{\partial \eta}{\partial x}$ or $\frac{\partial \xi}{\partial y}$) is difficult, the following method can be followed. We can write

$$\begin{Bmatrix} \frac{\partial}{\partial \xi} \\ \frac{\partial}{\partial \eta} \end{Bmatrix} = \begin{bmatrix} \frac{\partial x}{\partial \xi} & \frac{\partial y}{\partial \xi} \\ \frac{\partial x}{\partial \eta} & \frac{\partial y}{\partial \eta} \end{bmatrix} \begin{Bmatrix} \frac{\partial}{\partial x} \\ \frac{\partial}{\partial y} \end{Bmatrix} = [\mathbf{J}] \begin{Bmatrix} \frac{\partial}{\partial x} \\ \frac{\partial}{\partial y} \end{Bmatrix} \tag{6.70}$$

where **J** is the Jacobian matrix. Using Eq. (6.70), the derivatives with respect to the Cartesian coordinates can be found by calculating the inverse of the Jacobian matrix.

$$\begin{Bmatrix} \dfrac{\partial}{\partial x} \\ \dfrac{\partial}{\partial y} \end{Bmatrix} = [\mathbf{J}]^{-1} \begin{Bmatrix} \dfrac{\partial}{\partial \xi} \\ \dfrac{\partial}{\partial \eta} \end{Bmatrix} \tag{6.71}$$

Forming the Jacobian matrix is quite simple in this context since it just requires the differentiation of the interpolation functions, which are polynomials.

It should be noted that the shell element discussed in Chapter 3 requires interpolation functions for nodes in the middle of element sides as well (nodes 5 to 8 in Figure 6.7), which can be developed using the conventional Lagrangian interpolations.

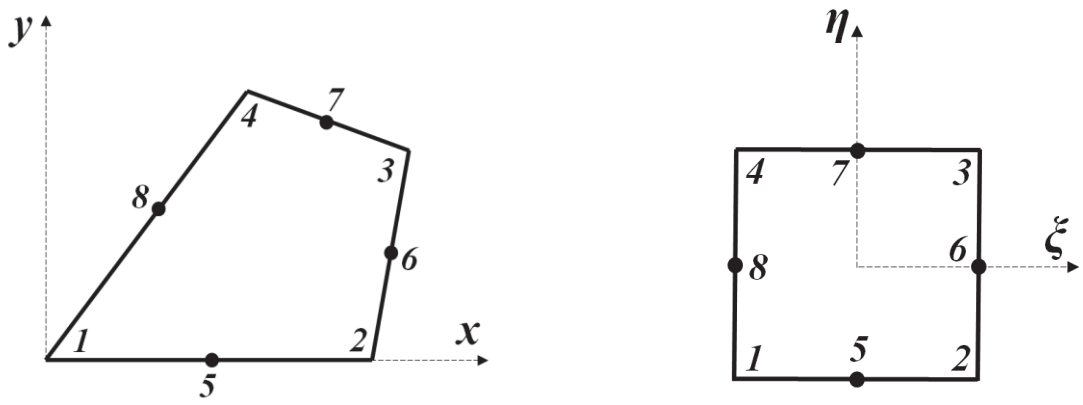

Figure 6.7: Isoparametric transformation for quadrilateral with middle nodes

$$N_5 = \frac{1}{2}\left(1-\xi^2\right)\left(1-\eta\right) \tag{6.72}$$

$$N_6 = \frac{1}{2}\left(1+\xi\right)\left(1-\eta^2\right) \tag{6.73}$$

$$N_7 = \frac{1}{2}\left(1-\xi^2\right)\left(1+\eta\right) \tag{6.74}$$

$$N_4 = \frac{1}{2}\left(1-\xi\right)\left(1-\eta^2\right) \tag{6.75}$$

6.4. The overlapping domain decomposition operator

The overlapping domain decomposition operator **N** was presented in Chapter 2 for a straight beam subjected to uniform bending and for general loading conditions. In this section, a rotation matrix is added to account for the curvature of the beam. A 2D view of the curved beam in its plane of curvature is shown in Figure 6.8.

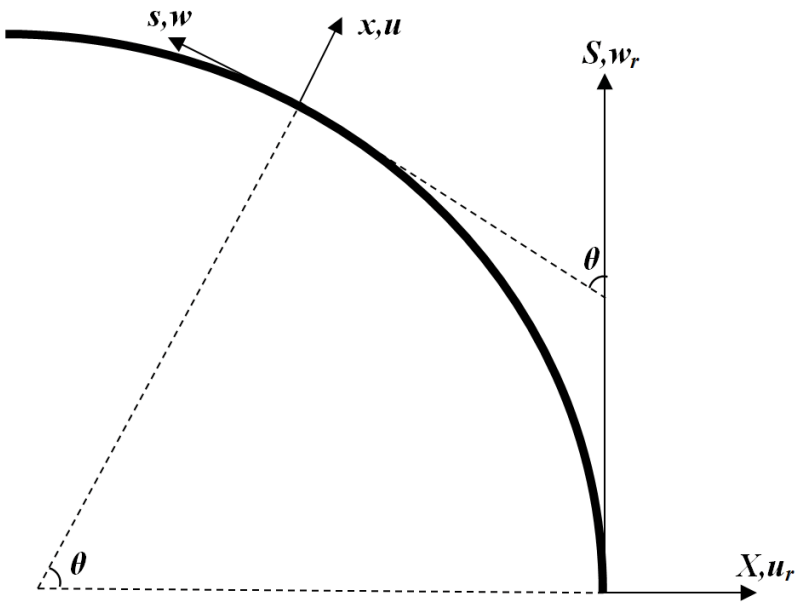

Figure 6.8: Schematic of the curved beam in its plane of curvature

The angle $\theta(s)$ is defined as the angle of the tangent to the beam at each cross-section to the tangent at $s=0$ (i.e. the starting point of the beam). As discussed previously, the decomposition operator imposes a constraint on the shell nodal displacement to obtain the equivalent nodal displacements of the beam element. It is easier to construct if it is thought of as an operator to apply to the nodal displacement of the beam element in order to obtain the nodal displacement of the shell. For that purpose, we can divide the development of the element into two stages:

Firstly, the appropriate interpolation functions are used to calculate the displacement of each of shell cross-section depending on its location relative to the beam elements.

$$\bar{\mathbf{d}}_C = \bar{\mathbf{Z}}\bar{\mathbf{d}} \tag{6.76}$$

where $\bar{\mathbf{d}}$ represents the nodal displacements of the two end of the beam element containing the desired shell node, i.e.

$$\bar{\mathbf{d}} = \left\langle \bar{w}_i \quad \bar{w}_j \quad \bar{u}_i \quad \bar{\theta}_{xi} \quad \bar{u}_j \quad \bar{\theta}_{xj} \quad \bar{v}_j \quad \bar{\theta}_{yj} \quad \bar{v}_j \quad \bar{\theta}_{yj} \quad \bar{\phi}_i \quad \bar{\varphi}_i \quad \bar{\phi}_j \quad \bar{\varphi}_j \right\rangle^{\mathrm{T}} \tag{6.77}$$

$\bar{\mathbf{d}}_C$ represents the beam displacement field at the centre of the cross-section containing the desired shell node $\bar{\mathbf{d}}_C = \left\langle \bar{w}_C \quad \bar{u}_C \quad \bar{v}_C \quad \bar{\phi}_C \quad \bar{u}_C' \quad \bar{v}_C' \quad \bar{\phi}_C' \right\rangle^{\mathrm{T}}$, and $\bar{\mathbf{Z}}$ contains interpolation functions as developed in Section 6.3.

Secondly, the displacements of each of the shell nodes on the cross-section are calculated from the central displacement vector $\bar{\mathbf{d}}_C$ according to the kinematics of the thin-walled theory.

$$\mathbf{u}_r = \mathbf{Y}\bar{\mathbf{d}}_C \tag{6.78}$$

where $\mathbf{u}_r$ refers to the displacement of the shell element, $\mathbf{u}_r = \left\langle \bar{w}_r \quad \bar{u}_r \quad \bar{u}_r' \quad \bar{v}_r \quad \bar{v}_r' \quad \bar{\phi}_r \right\rangle^{\mathrm{T}}$ and the matrix $\mathbf{Y}$ can be written as

$$\mathbf{Y}=\begin{bmatrix} 1 & 0 & 0 & -\left(\bar{x}\dfrac{\mathrm{d}\bar{v}}{\mathrm{d}\bar{z}}-\bar{y}\dfrac{\mathrm{d}\bar{u}}{\mathrm{d}\bar{z}}\right) & -\bar{x} & -\bar{y} & -\bar{\omega} \\ 0 & 1 & 0 & -\left(\bar{y}-a_y\right) & 0 & 0 & 0 \\ 0 & 0 & 0 & 0 & 1 & 0 & -\left(\bar{y}-a_y\right) \\ 0 & 0 & 1 & \left(\bar{x}-a_x\right) & 0 & 0 & 0 \\ 0 & 0 & 0 & 0 & 0 & -1 & -\left(\bar{x}-a_x\right) \\ 0 & 0 & 0 & -1 & 0 & 0 & 0 \end{bmatrix} \tag{6.79}$$

$\mathbf{u}_r$ in Eq. (6.78) is in the global coordinate system (i.e. *X*-*S* system in Figure 6.8) and needs to be transformed to the local coordinate system of the cross-section (*x*-*s*). For that purpose, the transformation matrix $\mathbf{R}$ is used.

$$\mathbf{u}=\mathbf{R}\mathbf{u}_r \tag{6.80}$$

in which $\mathbf{R}$ can be written as

$$\mathbf{R}=\begin{bmatrix} \cos\theta & -\sin\theta & 0 & 0 & 0 & 0 \\ \sin\theta & \cos\theta & 0 & 0 & 0 & 0 \\ 0 & 0 & 1 & 0 & 0 & 0 \\ 0 & 0 & 0 & 1 & 0 & 0 \\ 0 & 0 & 0 & 0 & \cos\theta & \sin\theta \\ 0 & 0 & 0 & 0 & -\sin\theta & \cos\theta \end{bmatrix} \tag{6.81}$$

It should be noted that the curvature lies in *X*-*S* plane and therefore the displacement components outside this plane (i.e. $\bar{u}_r'$ and $\bar{v}_r$) need not be rotated, which is why the number 1 is placed for the corresponding terms in the rotations matrix.

6.5. Numerical example

In order to verify the accuracy of the developed curved global-local model, a curved cantilever beam is analysed in this section. The geometry and boundary conditions of the analysed beam are shown in Figure 6.9.

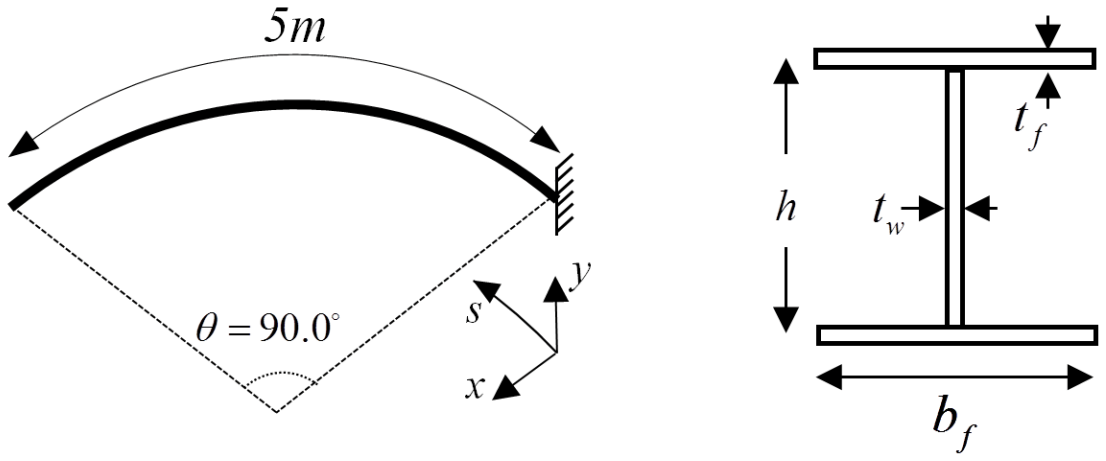

(a) Schematic of the curved beam (b) Cross-section of the curved beam

Figure 6.9: Geometry and boundary conditions of the cantilever curved beam

The beam is highly curved with the included angle of 90 degrees, and has a span of 5 meters. The material used in this example is structural steel, (i.e., $E = 200GPa$, $\nu = 0.3$ and $G = 70GPa$), and cross-sectional dimensions are $h = b_f = 400mm$ and $t_w = t_f = 10mm$. Loadings of the curved beam are shown in Figure 6.10.

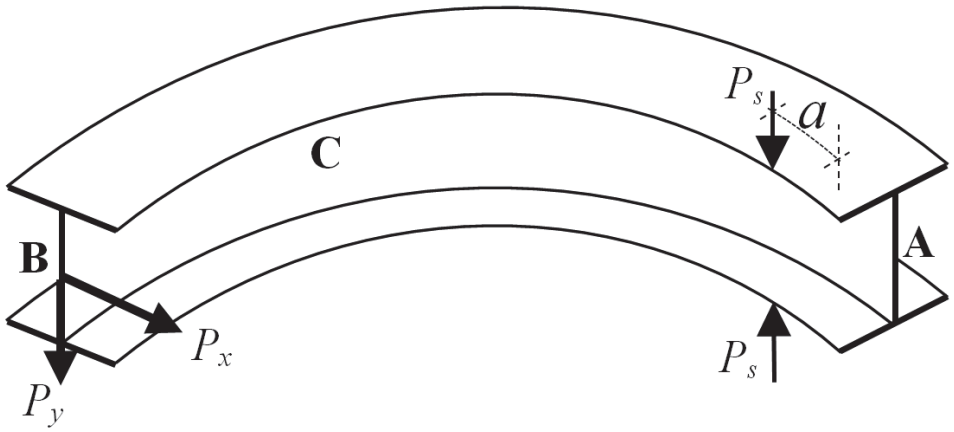

Figure 6.10: Loading of the cantilever curved beam

The beam is analysed using the developed Iterative Global-local Method and the full shell element. In the global-local model, 10 beam elements of equal size are used as the global model while shell elements with approximate size of $100mm \times 100mm$ are used in the overlapping region as the fine-scale/local model. The size of the shell elements in the full shell model is the same as the overlapping region in the global-local model.

The analysis is performed in two stages. Initially, the beam is subjected to concentrated loads at the free end of the beam only, (i.e. $P_y = 1500N$, $P_x = 150N$ and $P_S = 0$). Secondly, a load couple is added to the above loading in order to create cross-sectional deformations. It is applied at the tip of the top and bottom flanges at a distance of $a = 200mm$ from the support (Figure 6.10) and has a value of $P_S = 100kN$. It should be noted that since the two loads cancel the effect of each other at cross-sectional level, the global model of the iterative global-local solution, which is formulated based on rigid cross-sectional assumption, is not capable of capturing their effect. However, the softening effect of such local load on the global response of the curved beam is significant and can be seen from the result of the full shell model.

The overlapping region in the global-local model spans from the support up to 600mm from it, as show in Figure 6.11.

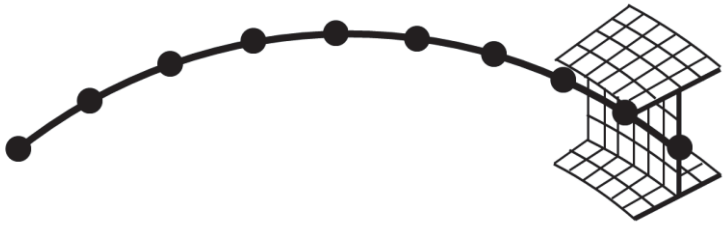

Figure 6.11: Layout of the global-local model

The analysis results are presented in Figure 6.12 in terms of the lateral displacement of a point C, located at a distance of *3000mm* from the support (Figure 6.10).

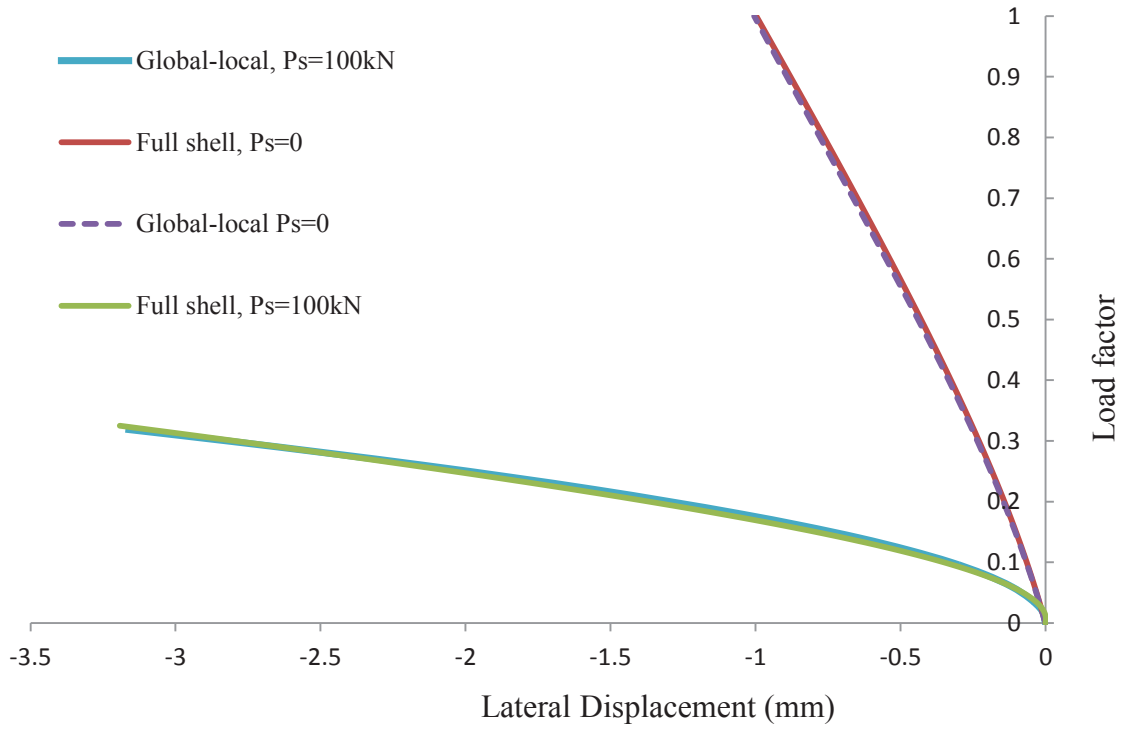

Figure 6.12: Load vs. lateral displacement of point C

It can be seen that the application of the local load couple P_s has a significant effect on the global response of the structure, which is denoted by considerable softening in the load-displacement curve of point C, far from the local loads. The accuracy of the proposed Iterative Global-local Method can be confirmed from the figure.

6.6. Conclusions

The Iterative Global-local Method was modified in this chapter to become applicable to curved thin-walled beams. To this end, the global/beam model was enhanced by replacing the conventional interpolation functions by the ones resulting from the solution to the linear differential equation, resulting in an exact beam formulation. The geometry and formulation of the shell model was also modified to become applicable to curved thin-walled members. Finally, the overlapping decomposition operator was changed by introducing a rotation matrix according to the location of the cross-section in the beam. Numerical examples were presented in order to verify the accuracy of the proposed model.

6.7. References

Boresi, A.P. & Sidebottom, O.M. 1985, *Advanced Mechanics of Materials*, Fourth edn, John Wiley & Sons, New York, USA.

Cook, R.D., Malkus, D.S. & Plesha, M.E. 1989, *Concepts and applications of finite element analysis*, Wiley, New York.

Erkmen, R.E. 2013, 'Bridging multi-scale approach to consider the effects of local deformations in the analysis of thin-walled members', *Computational Mechanics*, vol. 52, no. 1, pp. 65-79.

Murray, N.W. 1984, *Introduction to the theory of thin-walled structures*, Claredon Press, Oxford, United Kingdom.

Vlasov, V.Z. 1961, *Thin-walled elastic beams*, 2nd edn, Israel Program for Scientific Translations, Jerusalem, Israel.

Zienkiewicz, O.C. & Taylor, R.L. 2005, *The Finite Element Method for Solid and Structural Mechanics*, Sixth edn, Elsevier Butterworth-Heinemann, Oxford, United Kingdom.

Chapter 6 list of symbols

A	=	cross-sectional area
b_f	=	width of beam flange
$\mathbf{C}$	=	vector of unknown constants
C_i	=	unknown constants from the solution of differential equation
$\mathbf{D}$	=	cross-sectional matrix
D, D^2, D^3, D^4	=	differentiation operators
E	=	modulus of elasticity
G	=	shear modulus
h	=	height of the cross-section
$I_{xx}, I_{yy}, I_{\omega\omega}$	=	cross-sectional moment of inertia
$\mathbf{J}$	=	Jacobian Matrix
J_d	=	St. Venant torsional rigidity constant
$\mathbf{N}$	=	overlapping domain decomposition matrix
N_i	=	interpolation functions
$\mathbf{R}$	=	transformation matrix
R	=	6-times differentiable function used in the solution of DE

S_x, S_y, S_ω = first moment of area of the cross-section

t_f, t_w = thickness of flange and web

U = internal potential energy

U_n = internal potential energy due to normal strain

U_s = internal potential energy due to shear strain

$\mathbf{u}$ = displacement vector

u, v, w = displacement components along *x, y* and *z* coordinates

V = external potential energy

$\mathbf{V}_{ij}$ = vectors defining the local coordinate of the shell element

$\mathbf{Y}$ = matrix of thin-walled kinematical relations

$\mathbf{Z}$ = matrix of overlapping domain interpolations

γ_p = shear strain

$\gamma_{p,l}$ = linear part of the shear strain

ε_{ss} = normal strain

$\varepsilon_{ss,l}$ = linear part of the normal strain

$\boldsymbol{\zeta}$ = nodal displacement vector corresponding to v and ϕ

η, ξ = natural coordinates

θ = included angle of the beam

κ_0 = initial curvature

$\boldsymbol{\lambda}_x, \boldsymbol{\lambda}_y, \boldsymbol{\lambda}_z$ = direction cosines of the shell element

ν = Poisson's ratio

Π = total potential of the beam

$\boldsymbol{\varsigma}$ = nodal displacement vector corresponding to u and w

ϕ_i = rotation components

ω = sectorial coordinate

Chapter 6 list of figures

Chapter 7: Summary and recommendations

7.1. Summary

In this thesis, the Iterative Global-local Method (IGLM) is developed for the analysis of thin-walled members subjected to localised behaviour such as local buckling.

A literature review of the available methods for the analysis of thin-walled members was presented in Chapter 2, along with the justification for the requirement of a computationally efficient method in this area. The Iterative Global-local Method was then introduced as a powerful procedure to analyse local buckling deformations in thin-walled beams. The three main components of the method were presented afterwards, namely, the global model, the local model, and the overlapping decomposition operator which creates a mathematical link between the two. Later in Chapter 2, the kinematics of the Iterative Global-local Method were revisited and modified to make the method applicable to a beam with general loading conditions, i.e. non-uniform bending conditions. It should be noted that at this stage, the material is assumed to be isotropic linear elastic, and the structural element is assumed to be straight.

Chapter 3 was devoted to the development of the IGLM for open thin-walled members made of fibre-reinforced composite laminates. For that purpose, the constitutive relations in both the local and global models were modified to incorporate the behaviour

of composite laminates with arbitrary orientation of the fibres in different layers. Numerical examples were presented for validation of the method.

The IGLM was proposed in Chapter 4 to capture the ovalisation and local buckling behaviour of pipes. The pipe was assumed to experience inelastic material response in the local region. Therefore, the linear elastic local model was replaced by an elasto-plastic shell element. Apart from that, the global beam element, which had seven degrees of freedom in the previous chapters for warping deformations, is replaced by a two-node six degree-of-freedom per node element based on classical beam theory, suitable for closed circular thin-walled sections.

In an effort to introduce the IGLM for curved structural elements, a thin-walled curved-beam formulation was presented in Chapter 5. By assuming large deformations and small strains, the strains were calculated using the undeformed and deformed curvature values.

The Iterative Global-local Method was developed for curved members in Chapter 6. The beam element developed in the previous chapter was adopted as the global model, and the previously used shell element formulation was modified in this chapter to build the curved beam configurations. Furthermore, the decomposition operator has been amended to correctly relate the displacements of the local and global models of the curved beam.

It was observed that employing the Iterative Global-local Method can significantly reduce the size of the finite element model in cases with local buckling.

7.2. Recommendations for further research

a) As discussed previously, the IGLM is most advantageous in the presence of damage over a relatively short domain of the structure. As a result, the damage would create a difference between the internal stresses of the global and local models. This difference, which creates unbalanced forces, has to vanish. In cases where the damage is significant (e.g. plasticity, significant local buckling), the unbalanced force may be large in each solution step and a large number of iterations will be required to achieve convergence. Since the global model is not affected by the localised damage, the unbalanced forces can be accumulated and cause the convergence to become harder to be obtained.

A way to overcome this difficulty is to modify the stiffness matrix of the global model. Some efforts have been made in this area by the author and the supervisors.

b) Up to the present, the model is developed to deal with a known localised behaviour. In other words, it was assumed throughout the study that the place of local buckling is known a-priori. The method at its current capabilities is successful in capturing the effect of an existing defect in the global behaviour of the structure, but further research is required to automate the procedure of finding the critical regions and to apply the local models. Similarly, the method can be enhanced to become intelligent in assigning sufficient overlapping region to capture the effect of local deformations.

c) The Iterative Global-local Method developed in this thesis deals with thin-walled beams. However, it has the potential to be developed for other structural elements as well. Generally, the method is computationally advantageous in any case where a local deformation could have global consequences. For example, the initiation and

development of cracks in reinforced concrete members can be considered as a local deformation that can give rise to modifications in the global behaviour of the structure.